SZENT ISTVÁN UNIVERSITY
FACULTY OF MECHANICAL ENGINEERING
Gödöllő

R&D

MECHANICAL ENGINEERING LETTERS

2008

Research & Development

2008

Mechanical Engineering Letters, Szent István University

Annual Technical-Scientific Journal of the Mechanical Engineering Faculty,
Szent István University, Gödöllő, Hungary

Editor-in-Chief:
Dr. István SZABÓ

Editor:
Dr. Gábor KALÁCSKA

Executive Editorial Board:

Dr. István BARÓTFI	Dr. István HUSTI
Dr. János BEKE	Dr. Sándor MOLNÁR
Dr. István FARKAS	Dr. Péter SZENDRŐ
Dr. László FENYVESI	Dr. Zoltán VARGA

International Advisory Board:
Dr. Patrick DE BAETS (B)
Dr. Radu COTETIU (Ro)
Dr. Manuel GÁMEZ (Es)
Dr. Klaus GOTTSCHALK (D)
Dr. Yurii F. LACHUGA (Ru)
Dr. Elmar SCHLICH (D)

Cover design:
Dr. László ZSIDAI

HU ISSN 2060-3797

All Rights Reserved. No part of this publication may be reproduced, stored in a retrieval system or transmitted in any form or by any means, electronic, mechanical, photocopying, recording, scanning or otherwise without the written permission of Faculty.

Páter K. u. 1., Gödöllő, H-2103 Hungary
dekan@gek.szie.hu, www.gek.szie.hu,

Volume 1 (2008)

Anniversaries, 2008

Professor István HUSZÁR is 85!

István Huszár was born in Csurgó on the 8th of December, 1923. He obtained his diploma of merit in mechanical engineering at Budapest Technical University. Candidate of Technical Sciences (CSc academic degree) in 1954, Doctor of Technical Sciences (DSc academic degree) in 1971, Doctor Honoris Causa in 1999. From 1962 he became the head of the Structural Laboratory Department of Ganz Electrical Works. From 1st of July 1970 Professor and Head of Department of Mechanics at the Faculty of Engineering, Gödöllő University of Agricultural Sciences. Between 1972 and 1975 deputy dean, and from 1975 to 1981 dean of the Faculty. Professor Huszár retired in 1994 but as professor emeritus actively assists in both undergraduate and doctoral education. Due to his extensive domestic and foreign scientific relations he fulfils leading roles in several scientific organizations. His fruitful activity in engineering mechanics has been acknowledged several times.

Professor Pál SOÓS is 80!

He was born in Kassa, on the 6th of April, 1928. He obtained his diploma in mechanical engineering at Budapest Technical University in 1951. Candidate of Agricultural Sciences (CSc academic degree) in 1954. Budapest Technical and Economical University donated him Golden Diploma in 2001, and the Szent István University donated him a Doctor Honoris Causa title. He is professor from 1971 and professor Emeritus from 2000, but still a devoted and active participant of the education especially in the PhD training. As a Vice Dean he took part multiple times in the work of the first education schedule of the Faculty, and also in the modified version later in the ’60s. He is still an active participant of national scientific and industrial societies, his productive work in agricultural engineering was acknowledged by many prizes.

Professor József JANIK is 80!

He was born in Sárospatak on the 26th December, 1928. He was graduated as toolmaker in 1946. He obtained his diploma in mechanical engineering at Budapest Technical University in 1954. Candidate of Technical Sciences (CSc academic degree) in 1962, Doctor of Technical Sciences (DSc academic degree) in 1982. He directed the agricultural engineering college in Körmend between 1970 and 1977. From 1979 he is a Professor at the Department of Machine Repair at the Faculty of Engineering, Gödöllő University of Agricultural Sciences. His outstanding work in the field of Scientific Student Research (TDK) and PhD education has to be emphasized. As deputy dean and deputy rector he put great effort into the development of the Faculty. He is still an active professor emeritus in the field of maintenance of machinery and his work was acknowledged several times.

Dear Reader!

The Faculty of Mechanical Engineering at Szent István University has been known for its excellence among the Hungarian higher educational institutions for more than half of a century. Being one of the existing three mechanical engineering faculties in Hungary its general mission can be summarized as follows:

- Provision of quality undergraduate and graduate programs in four majors: mechanical engineering, agricultural and food industrial mechanical engineering, mechatronics, technical management.
- Integrating and supporting research teams for scientific collaboration with emphases on: bio-systems engineering, alternative and sustainable energy production, state of the art engineering design, material sciences and engineering applications of information and communication technologies.
- Supporting technology transfer initiatives with industrial partners, provision of R&D services and further training of engineers working at companies.

Each year staff members of the Faculty participate in various scientific programs, take part in international research projects and make contributions to several publications.

The primary objective of launching the first issue of the Mechanical Engineering Letters as an annual technical-scientific journal of the Faculty is to give some in-depth information on the scientific activities carried out by our colleagues. However in a separate chapter some invited presentations from our co-operative research partners are also included. Articles published are reviewed and selected by an international editorial board involving recognized scientists from partner institutions with emphases on providing wide spectrum of research results from the given year. According to our expectations the „Letters" will provide multidisciplinary scientific overview of resources and background we have in Gödöllő and also may attract professionals from other research organizations to publish or to review papers overlapping with the scope and theme of this Journal.

I do hope that the printed and digital versions of the Mechanical Engineering Letters will connect researchers and scientists of many institutions operating in the field of mechanical- and bio-systems engineering as well as mechatronics or engineering information and communication technologies and will provide a forum

for exploration of new ideas, innovation and engineering creativity. At the same time I believe that reviewing the articles published in the Journal experts may have a better understanding on technologies, procedures and methods in these highly interdisciplinary fields of engineering.

Dr. István SZABÓ
dean

Contens

Doctoral School of Engineering Sciences

Professor Dr. Péter SZENDRŐ
Immediate Past Director of the School

Professor Dr. István FARKAS
Director of the School

Dear Reader,
The Doctoral School of Engineering Sciences (DSES) offers research topics and postgraduate courses in the different fields of engineering connected to the topics of the Energetics in Agriculture, Environmental Engineering and the Agricultural Engineering. Generally saying it relates to the bio-systems engineering discipline.

The Doctoral School was established in 1993 by professor dr. Károly Kocsis and followed by professor dr. Péter Szendrő, who was the director of the School until 2008, when professor dr. István Farkas overtook the directorship. The School is working under the auspice of the PhD and Habilitation Committee of the Szent István University, Gödöllő (SIUG).

The DSES offers wide range of research activities. Just in the last academic year 29 research topics were offered to the potential PhD students. Individual research and educational plan is developed for every student according to the general credit rules of the PhD and Habilitation Committee of the University and ECT system. At the first three year of their studies the students has to finish courses connected to their topics beside doing their own research. A detailed working plan helps them with the timing of the work which is monitored permanently by the supervisors and checked yearly by the DSES.

Most of the students of the DSES are coming from the MSc students of the Mechanical Engineering Faculty at SIUG, were they generally proved their research abilities through the Students Scientific Program, but the School accepts numerous applications from nominees from other Universities as well, even from abroad.

At the moment the School has 85 students, 46 from them having courses at the first three year of their studies, the rest are „pre-doctors" finalizing their research. Between 1999 and 2007 years 49 students finished their studies and got PhD degree.

Beside the continuously developed educational program the conditions of the research are also developing. Just in the last academic year a new educational and research complex for the engineering informatics was inaugurated. Naturally, the students of the School can do their research activities not only at the University, but the industrial partners of the Faculty are available on this field in both Hungary and abroad. The PhD students have also opportunity to take part in a part-time education program abroad.

This first volume of Mechanical Engineering Letters highlights some research results that are strongly connected to our PhD study programs directed by our professors.

More details about the Doctoral School of Engineering Sciences are available at:

http://www.mtdi.szie.hu

Institute of Mathematics and Informatics

Professor Dr. Zoltán VARGA
Director of the Institute

Dear Reader,

Below we give a short summary of the research activity of our institute. The Institute of Mathematics and Informatics consists of two departments: Department of Mathematics (head: Zoltán Varga) and Department of Informatics (head: Sándor Molnár).

Both educational and research activities are divided among these units according to their names, with a reasonable collaboration among them.

In year 2008, the main results our research activity, by departments, have been the following:

Department of Mathematics: In the framework of a general research line concerning the applications of mathematical systems theory in population biology, the most important results of the year have been obtained on the observation problem of population genetics. Although mathematical systems theory has been developed for practical use in different fields of engineering, by the initiative of our department, the systems-theoretical studies of dynamical models of population biology have been developed over the last years. The achievements of this research are documented in a large number of papers authored in international cooperation, and published in high-ranked journals.

Our recent results concern the problem of observer design for evolutionary processes of sexual populations. In this context, the observation problem arises in a very natural way, since

it is natural to observe some macroscopic phenotypic characteristics of an evolving population, and we may be interested in recovering the underlying genetic process. Developing the corresponding mathematical tools, we succeeded in the construction of an observer system which enables us to recover the genetic process from phenotypic observation.

Department of Informatics: This year a main research topic was climate change mitigation.

The general research program is aimed at the analysis of greenhouse gas (GHG) emission reduction options (mitigation options) which would provide contribution to sustainable development, social welfare and the enhancement of the long term competitivity of the Hungarian economy. The objective of the research is the formulation of a uniform methodology and analytic software

model encompassing all sectors of the economy which would help quantify and assess the economically and technically feasible scenarios of emission reduction and provide foundation for the Hungarian strategy on GHG emissions abatement until 2025. A further objective is the integration of energy efficient technologies and renewable applications in the energy system for reducing GHG emissions.

Specific goals include model development and adaptation, GHG mitigation potential assessment by sectors, development of policies and measures by sectors, quantification of resulting emission reductions, macro-level costs assessment of the mitigation measures.

During the research the economic assessment of the mitigation measures would be concluded through economic analysis and feasibility assessment. In the research program nationwide package of policies and measures, and emission reduction scenarios would be developed and an impact assessment (direct and indirect economic impacts) would be undertaken.

The methodology strongly relies on internationally accepted and developed modeling background, the UN IPCC sectoral breakdown would be used in our analyses. The indirect impacts of GHG mitigation would also be thoroughly examined (efficiency improvements, sustainable economic development).

Observer Design for Genetic Processes*

Zoltán VARGA
Department of Mathematics, Institute of Mathematics and Informatics

Abstract

In the paper a single-locus sexual population is considered, where the phenotypic selection process is described by an evolutionary game. In general terms, the methodology of mathematical theory of nonlinear systems will be applied, which is a well-known tool of engineering practice. First, in order to recover the genetic process from different observations, observability is guaranteed by the linearization method developed in earlier papers of the author for systems with invariant manifold. Then, based on the results of Sundarapandian (2002), an observer system is constructed that makes it possible to asymptotically recover the solution of the original system from the observation. In the numerical illustrations the selection is described by a „rock-scissors-paper" type game widely studied in evolutionary game theory.

1. Introduction

In the engineering applications of mathematical systems theory, the reconstruction of the state process from available measurements is a major issue for several reasons. In biology, this problem naturally arises in relation with phenotypic observation of genetic processes. In static situation, in Garay and Garay (1998) biological conditions were given for the allele frequency – phenotype frequency correspondence to be one-to-one. In a dynamical situation, less restrictive conditions can guarantee that from the observation of time-dependent phenotypic characteristics the allele process can be uniquely recovered. In engineering practice, under the condition of observability and stability, for the effective approximate calculation of the state process from the observation, an auxiliary system, the so-called observer is constructed, the solution of which asymptotically produces the state process of the original system, in most cases with an exponential rate of convergence.

In earlier papers (López et al., 2007a, 2007b) observers have been constructed for different density-dependent population system models of *ecology*. In these models, for an observability analysis, it was enough to apply the classical sufficient condition of Lee and Markus (1971) for local observability. Since for frequency-dependent selection processes of *population genetics and evolutionary dynamics* the dynamic model has an invariant manifold, to

* Research partially supported by the Hungarian National Scientific Research Fund (OTKA 62 000 and 68187).

guarantee local observability, we need to apply the linearization method developed in Varga (1992) for systems with invariant manifold. (Related controllability results for such systems can be found in Varga, 1989, a general overview of our recent results in this research line can be found in Varga, 2008). In order to effectively recover the genetic process from the phenotypic observation, an observer system will be designed, applying the results of Sundarapandian (2002). In the present paper we shortly summarize a part of the results published with co-authors in López (2008). In the next section we recall some basic concepts and theorems of the above observability and observer design methodology. In Section 3 evolutionary dynamics for an evolving sexual population is set up. Section 4 is dedicated to the observer design for two different phenotypic observation situations in the considered evolutionary model.

2. Local observability and observer design

Definition 2.1. For given $n \in \mathbf{N}$ with $n > 1$, and $k \in \overline{1, n-1}$ a nonempty set $M \subset \mathbf{R}^n$ is called a *regular k-dimensional submanifold,* if there exist an open set $G \subset \mathbf{R}^n$ and a function $\phi \in C^1(G, \mathbf{R}^{n-k})$ such that, for all $x \in G$ and for the range of the derivative $\phi'(x)$, we have $R_{\phi'(x)} = \mathbf{R}^{n-k}$ and $M = \phi^{-1}(0)$.

For a continuously differentiable function $f : \mathbf{R}^n \to \mathbf{R}^n$, we consider the differential equation

$$\dot{x} = f(x). \tag{2.1}$$

Given a regular *k*-dimensional submanifold $M \subset \mathbf{R}^n$, let $x^* \in M$ be an equilibrium of system (2.1): $f(x^*) = 0$. Then there exists a neighbourhood of x^* and $T \in \mathbf{R}^+$ such that any solution of (2.1) starting from any point of this neighbourhood is defined at least in $[0,T]$.

For this section we suppose that M is locally positively invariant for system (2.1) at x^*, that is, any solution of (2.1) starting from any point of a neighbourhood of x^* in M, remains in M.

For a given $m \in \mathbf{N}$, let $h : \mathbf{R}^n \to \mathbf{R}^m$ be a continuously differentiable function with $h(x^*) = 0$. We define an *observation system* as

$$\begin{aligned} \dot{x} &= f(x) \\ y &= h \circ x \end{aligned} \tag{2.2}$$

where y is called the *observed function corresponding to solution* x.

Definition 2.2. We shall say that observation system (2.1)-(2.2) is *locally observable in* M *at* x^*, if there exists $\varepsilon \in \mathbf{R}^+$ with the property that conditions for $(i \in \overline{1,2})$ $z^i \in M$, $|z^i - x^*| < \varepsilon$,

$$\begin{aligned} &\dot{x}^i(t) = f(x^i(t)) \qquad (t \in [0,T]), \\ &x^i(0) = z^i, \\ &h(x^1(t)) = h(x^2(t)) \qquad (t \in [0,T]), \end{aligned}$$

imply

$z^1 = z^2$ (and consequently $x^1(t) = x^2(t) \quad (t \in [0,T])$).

Local observability M at x^* means that, if instead of the solution we can observe a transformation of it, then from this observed function we can recover the solution in a unique way, provided the solution starts at a point of *M* near the given equilibrium x^*.

To formulate a sufficient condition which guarantees the local observability of system (2.1)-(2.2), we linearize differential equation (2.2) at the equilibrium:

$$L := f'(x^*), \quad C := h'(x^*),$$

and define

$$Q := \begin{bmatrix} C \\ CL \\ \vdots \\ CL^{n-1} \end{bmatrix}.$$

Now we recall a theorem proved by Varga (1992), in which in „geometric" terms a sufficient condition is given for local observability.

Theorem 2.3. Suppose that

$$T_* \cap KerQ = \{0\}, \tag{2.3}$$

where T_* is the tangent space to M at x^*. Then system (2.1)-(2.2) is locally observable in M at x^*.

Now we adapt the standard concept of an observer to the case of an observation system with invariant manifold (2.1)-(2.2).

Definition 2.4. Given a continuously differentiable function $G : \mathbf{R}^n \times \mathbf{R}^m \to \mathbf{R}^n$, dynamical system

$$\dot{z} = G(z, y) \tag{2.4}$$

is called a local (exponential) observer for the observation system (2.1)-(2.2), if the composite system (2.1)-(2.2), (2.4) satisfies the following requirements:

- If $x(0) \in M$ and $z(0) = x(0)$, then $z(t) = x(t)$ for all $t \in \mathbf{R}^+$.
- There exists a neighbourhood V of the equilibrium x^* such that for all $x(0), z(0) \in V \cap M$, the estimation error $z(t) - x(t)$ tends to 0 (at exponential rate) as t tends to $+\infty$.

For the observer design we shall apply the following result (Sundarapandian, 2002):

Theorem 2.5. Suppose that observation system (2.1) is Lyapunov stable at equilibrium x^*, and there exists a matrix K (called gain matrix) such that matrix $L - KC$ is stable. Then system

$$\dot{z} = f(z) + K[y - h(z)] \tag{2.5}$$

is a local exponential observer for observation system (2.1)-(2.2).

3. Evolutionary dynamics for an evolving sexual population

Following Cressman et al. (1996), we shall consider a large panmictic diploid Mendelian population with alleles $A_1,\ldots, A_n$, at a single autosomal locus. By assumption, zygotes are produced according to the Hardy-Weinberg proportions. We consider N possible pure phenotypes or behaviour strategies identified with the vertices of the standard simplex of the phenotype vectors,

$$\Delta^N = \{(s_1,...,s_N) \in R^N \mid s_k \geq 0 \ \ (k \in \overline{1,N}, \sum_{k=1}^{N} s_k = 1\}.$$

We also suppose that the phenotype of a zygote is uniquely determined by its genotype: for each genotype A_iA_j let $S_{ij} \in \Delta^N$ be the phenotype of an A_iA_j zygote. (A mixed individual phenotype $s \in \Delta^N$ has the usual probabilistic interpretation: s_k is the probability for an individual to exhibit the pure phenotype e_k). For each allelic state vector $p \in \Delta^n$, the vector

$$S(p) := \sum_{i,j=1}^{n} p_i p_j S_{ij} \tag{3.1}$$

is the mean phenotype of the population. Given a payoff matrix $A \in \mathbf{R}^{N \times N}$, the fitness of an A_iA_j zygote of a population in allelic state $p \in \Delta^n$ is

$$S_{ij} \cdot AS(p) = \sum_{k,l=1}^{N} S_{ij,k} a_{kl} S_l(p),$$

where $\cdot$ stands for the scalar product of vectors, $S_{ij,k}$ and $S_l(p)$ are the k-th and the l-th components of the vectors S_{ij} and $S(p)$, respectively. Let now $p(t)$ be the allelic frequency vector in the zygote population at time t. Then the standard continuous-time evolutionary dynamics for the considered sexual population reads as follows:

$$\dot{p}_i = p_i \left(\sum_{j=1}^{n} p_i S_{ij} - \sum_{k,l=1}^{n} p_k p_l S_{kl} \right) \cdot A \sum_{k,l} p_k p_l S_{kl} \quad (i \in \overline{1,n}) \tag{3.2}$$

For any $p \in \Delta^n$, introducing the effective (or marginal) phenotype of allele A_i

$$S^i(p) := \sum_{j=1}^{n} p_j S_{ij}, \tag{3.3}$$

for the above dynamics we obtain the following compact form

$$\dot{p}_i = p_i \left(S^i(p) - S(p) \right) \cdot AS(p) \quad (i \in \overline{1,n}) \tag{3.4}$$

Remark 3.1. It is known that Δ^n and $\operatorname{int} \Delta^n$ are positively invariant for system (3.4), furthermore, if for some equilibrium $p^* \in \operatorname{int} \Delta^n$, $S(p^*)$ is an evolutionarily stable strategy (ESS), and effective phenotypes are linearly independent at p^*, then p^* is asymptotically stable, see Cressman et al. (1996) and also Gámez et al. (2003). For further details on this dynamics we refer to Garay and Varga (1998a), (1998b).

Now we consider a three-allele system with cyclic dominance $A_1 \succ A_2 \succ A_3 \succ A_1$, where the homozygotes exhibit pure phenotypes represented by the canonical basic vectors of $\mathbf{R}^3$:

$$S_{11} := e_1, \quad S_{22} := e_2, \quad S_{33} := e_3.$$

Then the dominance structure is represented by the hypermatrix

$$[S_{ij}] := \begin{bmatrix} e_1 & e_1 & e_3 \\ e_1 & e_2 & e_2 \\ e_3 & e_2 & e_3 \end{bmatrix}. \tag{3.5}$$

Consider now dynamics (3.4) with the following payoff matrix: fix an $\varepsilon \in \mathbf{R}$ and define

$$A(\varepsilon) := \begin{bmatrix} -\varepsilon & 1 & -1 \\ -1 & -\varepsilon & 1 \\ 1 & -1 & -\varepsilon \end{bmatrix}. \tag{3.6}$$

We remind that the payoff matrix $A(\varepsilon)$ defines a generalized „rock-scissors-paper" game in the sense that for $\varepsilon := 0$ it reduces to the payoff matrix of the standard „rock-scissors-paper" game well-known in evolutionary game theory (see e.g. Hofbauer and Sigmund, 1988).

Now the parametrized family of systems corresponding to (3.4) is

$$\dot{p}_i = p_i(S^i(p) - S(p)) \cdot A(\varepsilon)S(p) \qquad (i \in \overline{1,3}) \tag{3.7}$$

In López et al. (2008), reducing the model to a planar vector field, we have shown that the stability analysis results in a Hopf bifurcation with respect to the parameter ε of the matrix game. The asymptotic stability obtained for positive parameter values is also important for the observer design.

4. Phenotypic observation and observer design in an evolving sexual population

In this section we will see how to recover the genetic evolution from phenotypic observation, constructing an observer system for two observation situations.

Observation of the mean phenotype

First let us consider the general *n*-dimensional evolutionary dynamics (3.4)

$$\dot{p}_i = p_i\left(S^i(p) - S(p)\right) \cdot AS(p) \quad (i \in \overline{1,n}), \tag{4.1}$$

and assume we observe the mean phenotype of the population, which means that in terms of the notation of Section 2 we have

$$h(p) := S(p) - S(p^*). \tag{4.2}$$

(For technical reason the observed quantity is the deviation of the mean phenotype from its equilibrium value.) For the application of Theorem 2.3 we linearize observation system (4.1)-(4.2) at equilibrium. Denoting the right-hand side of system (3.4) by f, and using the notation of Section 2, for the linearization we obtain matrices

$$L := f'(p^*) \quad \text{and} \quad C := h'(p^*).$$

The observer we shall construct, will not only approximate the solution of the original system, but the solution of the observer is also a substitute of the latter in the sense that the interior of the simplex is long-term invariant for the observer system. We begin with this general statement on the observer constructed for the observation system (4.1)-(4.2). in López (2008) we have proved the following theorem, extending Theorem 2.5 to frequency-dependent observation systems.

Theorem 4.1. Considering the observation system (4.1)-(4.2), suppose that an interior equilibrium p^* is asymptotically stable for system (4.1), for a matrix $K \in \mathbf{R}^{n\times n}$ with some $k_0 \in \mathbf{R}$ for all $j \in \overline{1,n}$ $\sum_i k_{ij} = k_0$ holds, and $L - KC$ is a stable matrix. Then for any solution p of system (4.1), that is initially close enough to p^*, $\operatorname{int}\Delta^n$ is locally long-term invariant for the observer system

$$\dot{z} = f(z) + K[y - S(z)] \tag{4.3}$$

at equilibrium p^*. (The latter means that for any $z(0)$ from an appropriate neighbourhood of p^* in $\operatorname{int}\Delta^n$, there exists a $t_0 \in \mathbf{R}^+$ such that $z(t) \in \operatorname{int}\Delta^n$ for all $t \in]t_0, \infty[$.)

Example 4.2. Now we illustrate the observer design for the three-allele three-phenotype model of Section 4, namely, we consider the dynamic model of the evolution of a sexual population, given by equations (3.7). Since in this section we shall deal with a fixed value $\varepsilon \in \mathbf{R}^+$, in the notation the ε-dependence of the payoff matrix A can be suppressed:

$$(i \in \overline{1,3}) \tag{4.4}$$

with hypermatrix $[S_{ij}]$ defined in (3.5) and matrix A is given in (3.6). Let us fix $\varepsilon := 0.5$. From the previous section we know that this system has a positive equilibrium $p^* := (1/3, 1/3, 1/3)$. It is easy to check that for this game, the phenotypic image of equilibrium p^*, i.e., the mixed phenotype

$$S^* := S(p^*) = (1/3, 1/3, 1/3)$$

is an ESS, see, e.g. López, (2003). As an observation the three-dimensional version of (4.2) is considered:

$$h(p) := S(p) - S(p^*). \tag{4.5}$$

For the matrices of the linearization we obtain

$$L = \begin{bmatrix} -0.0185185 & 0.314815 & -0.12963 \\ -0.12963 & -0.0185185 & 0.314815 \\ 0.314815 & -0.12963 & -0.0185185 \end{bmatrix} \tag{4.6}$$

and

$$C = 2\begin{bmatrix} S^{*1} & S^{*2} & S^{*3} \end{bmatrix},$$

where S^{*1}, S^{*2}, S^{*3} are the marginal phenotypes at the equilibrium:

$$\begin{aligned} S^{*1} &= S^1(p^*) = (2/3, 0, 1/3), \\ S^{*2} &= S^2(p^*) = (1/3, 2/3, 0), \\ S^{*3} &= S^3(p^*) = (0, 1/3, 2/3), \end{aligned} \tag{4.7}$$

which are linearly independent vectors. Hence

$$C = \begin{bmatrix} 4/3 & 2/3 & 0 \\ 0 & 4/3 & 2/3 \\ 2/3 & 0 & 4/3 \end{bmatrix}.$$

From the linear independence of vectors (4.7), by Remark 3.1 we obtain that equilibrium $p^* = (1/3, 1/3, 1/3)$ is asymptotically stable.

Applying Theorem 2.3, in Gámez et al. (2003) it has been shown that (4.4)-(4.5) is locally observable in M at p^*. In other words, observing the "phenotypic evolution" of the population, in principle we can recover its "genetic evolution", i.e. the state process. For an effective (although approximate) calculation of this state process we apply the observer design method provided by Theorem 2.5.

For $K = \begin{bmatrix} 1 & 0 & 0 \\ 0 & 1 & 0 \\ 0 & 0 & 1 \end{bmatrix}$ we obtain that matrix $L - KC$ has eigenvalues with negative real parts. Therefore $L - KC$ is stable and from the linear independence of vectors (4.7), by Remark 3.1 we obtain that equilibrium $p^* = (1/3, 1/3, 1/3)$ is asymptotically stable. Hence by Theorem 2.5 we can construct a local exponential observer for observation system (4.4)-(4.5):

$$\dot{z}_i = z_i\left(S^i(z) - S(z)\right)AS(z) + K[S(p) - S(z)] \quad (i \in \overline{1,3}) \quad (4.8)$$

By the particular choice of the so-called gain matrix K, the conditions of Theorem 4.1 are also satisfied, implying that for any solution p of system (4.4), that is initially close enough to p^*, $\operatorname{int}\Delta^n$ is locally long-term invariant for the observer system (4.8).

Now we illustrate how the observer approximately provides the required solution from the observed function. Suppose that the initial condition is $p_0 = (0{,}3,\ 0{,}4,\ 0{,}3)$ for the original system (4.4) and $z_0 = (0{,}35,\ 0{,}35,\ 0{,}3)$ for the observer system (4.8). In Figure 1 it is shown (for brevity only considering the first coordinates) how solution z of the observer system practically ends up in solution p of the original system (4.4). Since p^* is asymptotically stable, if a solution p is initially close enough to p^*, the "unknown" solution p could also be asymptotically approximated by another solution w of system (4.4), with the same initial value as z. The coordinate w_1 of this solution is also represented in Figure1, showing that the observer performs much better.

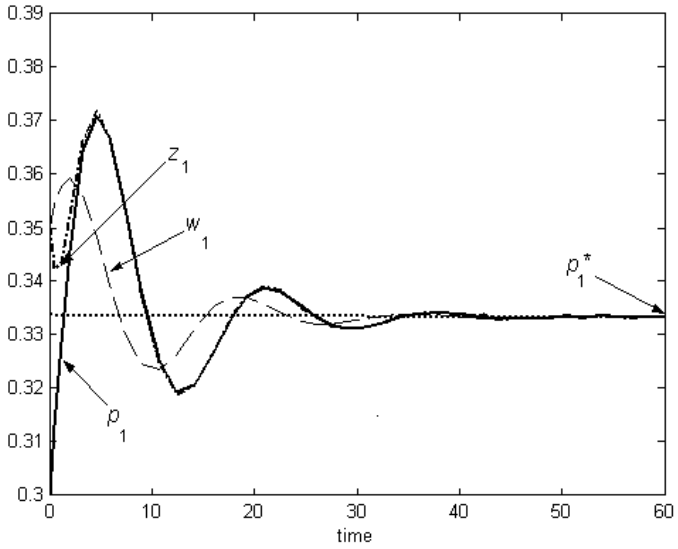

Figure 1. 1st coordinates of p, z and w.

Observation of a component of the mean phenotype

Since in Example 4.2, matrix C is invertible, by the inverse function theorem h is locally invertible at p^*. This means that near p^*, solution p can also be calculated from the observed function y by a point-wise inversion. In the

following example h is not invertible, so the observer design is the only real option.

Example 4.3 We consider again the evolutionary model (4.1), fixing again the value of ε at 0.5. Let us suppose now that we observe only the first coordinate of the mean phenotype:

$$h(p) := S_1(p) - S_1(p^*) . \tag{4.9}$$

The linearization matrix L is the same as in (4.6), but now

$$C := h'(p) = \begin{bmatrix} 4/3 & 2/3 & 0 \end{bmatrix}.$$

Again in Gámez et al. (2003), using transversality condition (2.3), the local observability of system has been proved. Now we also construct a corresponding observer. Choosing $K := \begin{bmatrix} 0 & 1 & 0 \end{bmatrix}$, we obtain that matrix $L - KC$ is stable. Applying Theorem 2.5 we obtain the observer system

$$\dot{z}_i = z_i \left(S^i(z) - S(z) \right) AS(z) + K[S_1(p) - S_1(z)] \quad (i \in \overline{1,3}) \tag{4.10}$$

Both for the original system (4.1) and for the observer (4.9) we set the same initial conditions as in Example 4.2, $p_0 = (0{,}3,\ 0{,}4,\ 0{,}3)$, and $z_0 = (0{,}35,\ 0{,}35,\ 0{,}3)$. In Figures 2 and 3 it is shown how the approximation of the third coordinate of p can be improved, by taking an appropriate gain matrix $K := \begin{bmatrix} 0 & 100 & 0 \end{bmatrix}$.

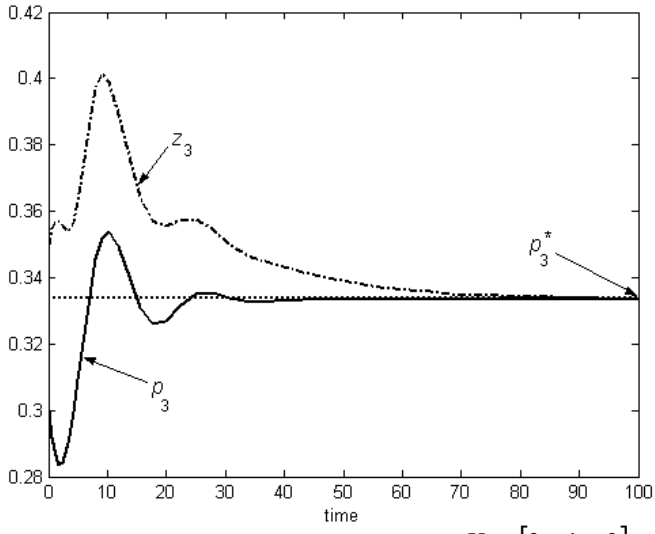

Figure 2. 3rd coordinates of p and z, for $K := \begin{bmatrix} 0 & 1 & 0 \end{bmatrix}$.

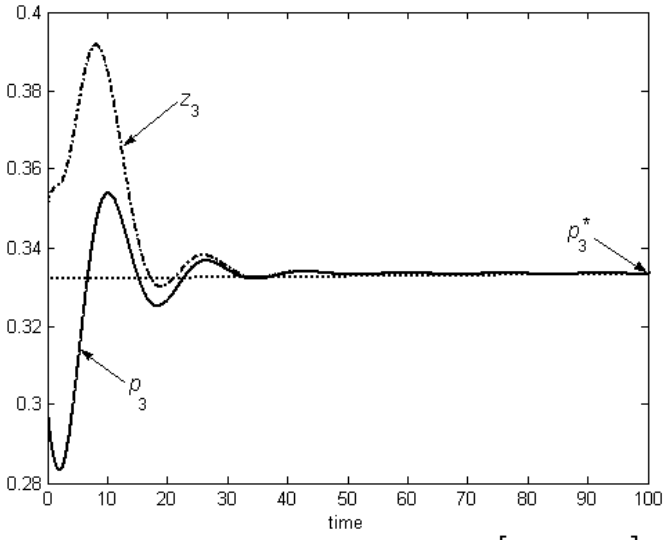

Figure 3. 3rd coordinates of p and z, for $K := \begin{bmatrix} 0 & 100 & 0 \end{bmatrix}$.

5. Discussion

The problem of reconstruction of the state process from an observed transform of it, in a natural way arises in the context of the evolution of a sexual population, where certain phenotypic characteristics are observed and the state of the population is described in terms of allele frequencies.

The application of an observer system seems to be an efficient tool for the approximation of an unknown solution, if the corresponding observation is known. In the considered dynamic evolutionary model, in a panmictic Mendelian population a particular type of evolutionary matrix game is played at phenotypic level.

In the case of three alleles and three pure phenotypes, numerical results also show how, by the appropriate choice of the gain matrix, the rate of convergence of the asymptotic approximation can be improved.

The applied observer design methodology may be also useful for the observation analysis and monitoring of different evolutionary and population system models (see e.g. Cressman et al. 2001, Cressman and Garay 2003a, Cressman and Garay 2003b, Garay and Varga 2000, Cressman, et al. 2004, Garay et al. 2003, Cressman and Garay 2006))

References

Cressman, R. Garay, J., Hofbauer, J. (2001) Evolutionary stability concepts for N- species frequency-dependent interactions. Journal of Theoretical Biology 211, 1-10

Cressman, R. and Garay, J. (2003a) Evolutionary stability in Lotka-Volterra systems. Journal of Theoretical Biology 222, 233-245

Cressman, R. and Garay, J. (2003b) Stability N-species coevolutionary systems. Theoretical Population Biology 64, 519-533

Cressman, R., Garay, J. (2006) A game–theoretical model for punctuated equilibrium: species invasion and stasis through coevolution. BioSystems 84, 1-14.

Cressman, R., Hofbauer, J. and Hines, W.G.S. (1996) Evolutionary stability in strategic models of single-locus frequency-dependent viability selection. Journal of Mathematical Biology 34, 707-733

Cressman, R., Krivan, V. and Garay, J. (2004) Ideal Free Distributions, Evolutionary Games and Population Dynamics in Multiple Species Environments, American Nauralist, 164, 473-489.

Gámez, M., Carreño, R., Kósa, A. and Varga, Z. (2003) Observability in strategic models of selection, Biosystems 71 (3), 249-255

Garay, J., Cressman, R. and Varga, Z. (2003) Optimal behaviour of honey bees based on imitation at fixed densities. Community Ecology 4 (2), 219-224

Garay, J. and Garay, M., B. (1998) Genetical reachability: When does a sexual population realize all phenotypic states? Journal of Mathematical Biology 37, 146-154

Garay, J. and Varga, Z. (1998a) Evolutionary stable allele distributions. Journal of Theoretical Biology 191, 163-172

Garay, J. and Varga, Z. (1998b) When will a sexual population evolve to an ESS? The Proceedings of the Royal Society. London Ser. B 265, 1007-1010

Garay, J., Varga, Z. (2000) Strict ESS for n-species systems. BioSystems 56: 131-137.

Hofbauer, J. and Sigmund, K. (1988) The Theory of Evolution and Dynamical System,. Cambridge University Press, Cambridge

Lee, E.B. and Markus, L., (1971). Foundations of Optimal Control Theory. Wiley, New York-London-Sydney

López, I. (2003) Observabilidad y controlabilidad en modelos de evolución. Servicio de Publicaciones de la Universidad de Almería, Spain (PhD Thesis in Spanish, ISBN: 84-8240-683-3)

López, I., Gámez, M., Garay, J. and Varga, Z. (2007a) Monitoring in a Lotka-Volterra model, BioSystems 87 (1), 68-74.

López, I., Gámez, M., Molnar, S. (2007b) Observability and observers in a food web, Appied Mathematics Letters 20 (8), 951-957

López, I., Gámez, M., and Varga, Z. (2008) Observer design for phenotypic observation of genetic processes, Nonlinear Analysis: Real World Applications 9, 290–302.

Sundarapandian, V. (2002) Local observer design for nonlinear systems, Mathematical Computer Modelling 35, 25-36.

Varga, Z. (1992) On Observability of Fisher's model of selection, Pure Mathematics and Applications. Ser. B., 3 (1), 15-25.

Varga, Z. (1989) On controllability of Fisher's model of selection. In „Differential Equations" (Eds. Dafermos, C. M., Ladas, G., Papanicolau, G.), Marcel Dekker, New York 717-723.

Varga, Z. (2008) Applications of mathematical systems theory in population biology.Periodica Mathematica Hungarica, 56 (1), 157-168.

The Influence of External Costs on Power System Expansion Planning*

Sándor MOLNÁR
Department of Informatics, Institute of Mathematics and Informatics

Abstract

This paper is based on cooperative research between Croatia and Hungary. External costs of electricity represent the monetary value of the environmental damage caused by electricity generation. They are here calculated applying the impact pathway methodology on Croatian specific conditions. This paper as a case study for Croatia estimates the external costs of coal and gas fired power plants determined as main candidates for Croatian power system expansion till 2030. It is analyzed how the estimated external costs, when incorporated into total production costs, would affect the competitiveness of fossil-fired plants compared to other electricity generation options, i.e. how they influence the optimal expansion strategy of the Croatian power system.

1. Introduction

External costs of electricity are the costs imposed on society and the environment that are not accounted for by the producers and consumers of electricity, i.e. that are not included in its market price. External costs should reflect the price of the environmental damage caused by electricity generation chain. They include damage to the natural and built environment, such as effects of air pollution on health, buildings, crops, forests and global warming; occupational disease and accidents; and reduced amenity from visual intrusion of plant or emissions of noise. Electricity generation chain embraces activities such as construction of new power plant, fuel extraction, fuel transport and processing, power generation, waste disposal and electricity transmission. The largest external costs within that cycle are those attributable to the power generation itself, i.e. at the power plant location, and thus are given highest priority.

2. Method Description

Impact assessment and valuation are performed using the 'damage function' or 'impact pathway' approach, which relates to a sequence of links between the burden and its impact. This approach assesses impacts in a logical and transparent manner, going stepwise as shown in Figure 1.

* R was partially supported by TéT Croatian-Hungarian cooperation.

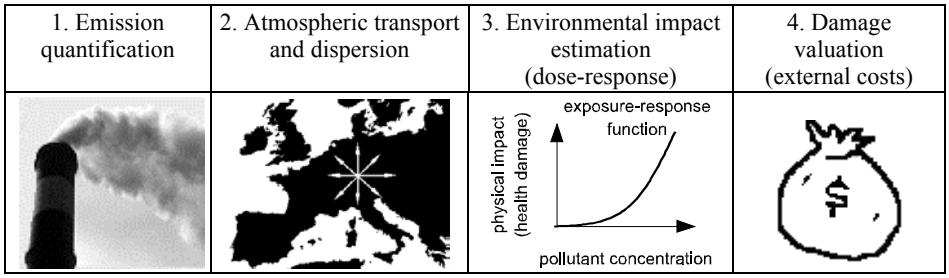

Figure 1. Impact pathway methodology, [1]

The impact pathway methodology consists of the following steps: (I) quantification of emissions, (II) calculation of the associated ambient concentration increase by means of atmospheric dispersion and transport models, (III) estimation of physical impacts using various exposure-response functions, and (IV) finally monetary evaluation of damages. In this analysis, the EcoSense model was used to assess damage costs caused by emissions from fossil-fired power plants in Croatia. It has to be stressed that environmental damage does not necessarily constitute in its entirety an external effect, so external cost might be different from the calculated damage cost.

Impact pathway method requires a detailed description of the reference environment, which in this case includes meteorological conditions affecting dispersion and chemistry of atmospheric pollutants, functions linking exposure to a particular pollutant (i.e. pollutant ambient concentration) with the health effect it causes, population density and age structure in the observed area (locally and for the whole of Europe), and costs of the estimated health effects. Each of these steps inevitably incorporates a dose of uncertainty, due to atmospheric model imperfections, transferability of data from one context to another (e.g. extrapolation of exposure-response functions from the laboratory to the field and from one geographical location to another, transferability of monetary values from one country to another), the fact that some impacts cannot be quantified or monetized at all, etc. However, there is a consensus among experts that transference of input parameters and results is to be preferred to ignoring some impact categories.

Focus of this analysis has been put on the effects of ambient air pollution on human health, as one of the priority impacts of electricity generation. Since the impact pathway methodology yields rather site-specific results, the analysis was conducted for the most representative power plant locations and most probable generation technologies. For locations this means choosing flat urban areas in the continental part of the country, while for technologies it assumes the best available ones that comply with environmental standards in Croatia and are considered to be candidates for future construction. The analyzed burdens relate only to routine emissions, while accidents are not taken into account. Since air pollutants are transported over large distances crossing national borders, their impacts are quantified not only on the local level, i.e. within 50 km from the source, but also for the whole of Europe.

3. The EcoSense Software

The software used here for calculation of externalities associated with electricity generation is EcoSense, developed within the European Community project ExternE. EcoSense was developed to support the assessment of priority impacts resulting from the exposure to airborne pollutants. It constitutes of several databases: technology, exposure-response and reference environment databases. The reference technology database holds a small set of technical data describing the emission source (power plant) that are mainly related to air quality modeling, including e.g. emission factors, flue gas characteristics, stack geometry and the geographic coordinates of the site. The impact assessment module calculates the physical impacts and the resulting damage costs by applying the exposure-response functions, based on receptor distribution and concentration levels of air pollutants from the reference environment database.

EcoSense also provides two air transport models (local and regional), to cover different pollutants and different scales. One is The Industrial Source Complex Model (ISC, developed by the US-EPA), which is a Gaussian plume model used for transport modeling of primary air pollutants (SO_2, NO_x, particulates) on a local scale. The other is The Windrose Trajectory Model (WTM, developed in Harwell Laboratory, UK) used to estimate the concentration and deposition of acid species on a European-wide scale.

4. Emissions

The most important pollutants emitted from fossil-fuelled power plants are carbon dioxide (CO_2), particulate matter (specially relevant for health effects are fine particles less than 10 and 2,5 microns in diameter respectively, so called PM_{10} and $PM_{2,5}$), sulfur dioxide (SO_2) and nitric oxides (NO_x, i.e. mainly NO later oxidized to NO_2). Apart from that, SO_2 and NO_x are subject to chemical transformations in the atmosphere, forming the so-called secondary pollutants: sulfuric and nitric acid (H_2SO_4 and HNO_3), sulfate and nitrate aerosols and tropospheric ozone (O_3). Both primary and secondary pollutants cause certain health effects, but here are considered only those for which the atmospheric modeling and the exposure-response functions are provided. Since modeling of ozone formation involves considerable complexity in both plume dynamics and chemistry, health effects associated with ozone are not quantified here. Impacts of global warming are not covered either because of the very different mechanism and global nature of impact.

5. Atmospheric Dispersion And Transport Models

On the local scale, i.e. within 50 km from the source, chemical transformations of pollutants can be neglected and thus their concentrations predicted using

Gaussian plume dispersion models. These models assume source emissions are carried in a straight line by the wind, mixing with the surrounding air to produce pollutant concentrations with a Gaussian spatial distribution. One of them, used in EcoSense, is the Industrial Source Complex Short-Term model, version 2 (ISCST2) developed by the U.S. EPA. The area analyzed in the local dispersion is represented by 10 x 10 grid of quadratic cells each 100 km^2 in size, with the power plant positioned in the grid center. The model calculates hourly concentration values of SO_2, NO_x and particulate matter averaged over one year at the center of each cell. Gaussian models require detailed description of meteorological data at the plant location provided by the user. They are valid up to 50 km from the plant.

However, pollutant transport extends over much greater distances, when chemical reactions and formation of secondary pollutants can no longer be neglected. Therefore, different models are required for assessing long-range (regional) transport of pollutants, the most common are the Lagrangian trajectory models. Receptor-oriented trajectory model examines incoming trajectories of air parcels arriving from different directions to the receptor point (which is characterized by its mean annual windrose), moving at a representative wind speed and constant mixing height. European-wide transport of pollution is in the EcoSense software handled by the Windrose Trajectory Model. Europe is represented by a 42 x 27 matrix of large cells, each 10000 km^2. The outputs from the model are atmospheric concentrations and deposition of emitted species and secondary pollutants in each grid cell. All input data required to run the Windrose Trajectory Model are provided by the EcoSense database.

6. Public Health Effects

Combustion processes cause an increase in the concentration of certain atmospheric pollutants that might be causing adverse health effects within the general public. There is now a broad-based body of evidence showing small but definite increases in risks associated with increases in air pollution, with no convincing evidence of threshold. Acute health effects, which occur on the same day as increases in air pollution or very soon thereafter, should be distinguished from the chronic or delayed effects of possible long-term exposure. There are less exposure-response functions for chronic effects since they are more difficult to estimate than the acute ones. It should be stressed that the acute mortality effects occur predominantly in older people, almost certainly with serious pre-existing health problems, though the precise mechanism of action is not yet resolved. Length of life lost in those who die prematurely following higher pollution days is also unknown, but is likely to be short – a few weeks or months. Averaged reduced life expectancy among those who die prematurely from chronic effects of air pollution is likely to be much greater and is measured in years.

The incremental air pollution attributable to power generation is a mixture of pollutants emitted from a power plant and those formed subsequently in atmospheric chemical reactions. Complex studies were made to disaggregate that mixture and determine separate exposure-response functions for each pollutant (particles, SO_2, NO_x and ozone). Most of the exposure-response functions used in the EcoSense model are chosen from studies which showed statistically significant relationship between pollutant and health endpoint and which eliminated possible confounding factors due to other pollutants. The strength of these studies is that relationships, expressed as percentage change in health effect per unit exposure, seem remarkably invariant to changes in population, location and pollution mixtures. For ease of implementation, the exposure-response functions are linearized, assuming independence of background levels and no threshold existence. Extrapolation of exposure-response functions to very low pollution increments, particularly at distances far away from source, without a threshold, may lead to an overestimation of effects.

Table 1. Summary of exposure-response functions and monetary values used here [1]

Impact Category	Monetary value (EURO)(1)	Pollutant	e-r slope (2)
Receptor: Total population			
Acute mortality(3)	155.000	PM_{10} and nitrates	0,040%
		$PM_{2,5}$ and sulfates	0,068%
		SO_2	0,072%
		NO_x	0,034%
Chronic mortality(3)	83.000	PM_{10} and nitrates	0,390%
		$PM_{2,5}$ and sulfates	0,640%
Hospital admissions respiratory	7.870	PM_{10} and nitrates	$2,07\times10^{-6}$
		$PM_{2,5}$ and sulfates	$3,46\times10^{-6}$
		SO_2	$2,04\times10^{-6}$
		NO_x	$2,34\times10^{-6}$
Hospital admissions cerebrovascular	7.870	PM_{10} and nitrates	$5,04\times10^{-6}$
		$PM_{2,5}$ and sulfates	$8,04\times10^{-6}$
Emergency room visits for asthma and COPD	223	PM_{10} and nitrates	$13,7\times10^{-6}$
		$PM_{2,5}$ and sulfates	$22,8\times10^{-6}$
Receptor: Adults(4)			
Restricted activity days	75	PM_{10} and nitrates	0,025
		$PM_{2,5}$ and sulfates	0,042

Remarks to the above table:

(1) mortality values given at a discount rate of 3%, based on YOLL.

(2) slope of the exposure-response function is expressed in percentage change in annual mortality rate per unit of pollutant concentration increase (% change per $\mu g/m^3$) for mortality, while in number of events per person per $\mu g/m^3$ for morbidity.

(3) baseline mortality in Croatia is 0,11%.

(4) (age group 14-65), in Croatia 68% of total population.

Quantitative relationships have been established linking air pollution with a number of health endpoints. Health impacts are divided into three categories: mortality, morbidity and accidents. Only first two categories are observed here since they refer to normal operation of a power plant. It is dealt with premature mortality (acute and chronic), restricted activity days, hospital admissions due to respiratory and cerebrovascular problems, as well as emergency room visits due to exacerbation of asthma and chronic obstructive pulmonary disease (COPD).

Here is how additional mortality and restricted activity days due to air pollution can be calculated, based on the given exposure-response functions:

Mortality (number of cases) = exposure-response slope/100 × baseline mortality × population of the observed area × pollutant concentration increase ($\mu g/m^3$).

Restricted activity days (number of days) = exposure-response slope/100 × population of the observed area × percentage of adults × pollutant concentration increase ($\mu g/m^3$).

7. Monetary Valuation Of Health Effects

Health impacts are generally valued more highly than the conventional economic approach would suggest. Mortality impacts can be valued based on the willingness to pay (WTP) for reduction of the risk of death, or on the willingness to accept compensation (WTA) for an increase in risk. WTP or WTA is converted into the value of statistical life (VSL) dividing it by the change in risk. For example, if the estimated WTP is EURO 100 for a reduction in the risk of death of 10^{-4}, the value of statistical life is estimated at 1 million EURO. However, increased air pollution can not actually cause 'additional' deaths – it can only reduce life expectancy slightly. For deaths arising from illnesses linked to air pollution it is recommended to use years of life lost (YOLL) calculation, while VSL approach only for valuing fatal accidents and cases where general population is affected and not only risk groups. Value of one year of life lost (v_{YOLL}) can be determined from the VSL estimate, applying the formula below, if one knows the age of the reference group and the discount rate to be applied to present vs. future years of life.

$$VSL = \sum_{t=0}^{T_l} \frac{v_{YOLL}}{(1+r)^t},$$

where:
r – discount rate (usually 3%),
T_l – number of years of life lost.

If e.g. life expectancy for a prime age male is assumed 37 years and if VSL equals 3,1 million EURO, value of YOLL turns out around 100.000 EURO with zero discount rate, i.e. 134.000 EURO with discount rate of 3%.

Morbidity impacts valuation is based on the cost of illness, that comprises the value of time lost due to the illness (valued through lost wages), the value of the lost utility because of pain and suffering and the costs of any expenditures on averting and mitigating consequences of illness.

8. Application Of The Impact Pathway Methodology On Croatian Power System

The aim of the analysis made here is to estimate costs of health damages through air pollution caused by electricity generation in Croatia. Two types of fossil-fired power plants are observed, one coal and one natural gas fired facility, since they are among candidates for future power system expansion. Both power plants are assumed to comply with domestic and European Union's emission standards, so the emission rates equal the upper emission limits. Basic technical end environmental data are given in Table 2.

Table 2. Technical data and emission rates of the analyzed power plants

	Coal facility		Natural gas facility	
Gross/net capacity	380/350 MW		370/350 MW	
Hours on full load	6570 h/yr		6570 h/yr	
Flue gas volume	1,2E+6 m^3/h		2,1E+6 m^3/h	
Flue gas temperature	403 K		403 K	
Stack height	200 m		200 m	
Stack diameter	6 m		6 m	
Emissions	mg/m^3	g/kWh	mg/m^3	g/kWh
Particulates	50	0,168	0	0
SO_2	400	1,343	0	0
NO_x	650	2,182	100	0,6
CO_2	2,45E+5	822,9	0,43E+5	258,55

Both facilities are assumed to be located in the densely populated urban area of Zagreb, the Croatian capital. Geographical coordinates of the site are 16° E and 45,8° N. Impact analysis on the local level, i.e. within 50 km from the source, displays a local (so called fine) grid with 100 km^2 large cells, the average pollutant increment ($\mu g/m^3$) in each cell and the total number of health events in the whole local grid. To calculate atmospheric dispersion on the local level, hourly meteorological data for the plant site are required, while for estimation of health impact population density in each cell of the local grid is needed.

The basic meteorological data for Zagreb – monthly temperature extremes and frequency of wind speeds and wind directions (so called windrose) in the 15-year sequence – are obtained from the Croatian State Meteorological and

Hydrological Service. Since no continuous measurements of wind and temperature were available, and because some additional parameters describing atmospheric conditions are needed for local dispersion modeling, meteorological data set had to be constructed before imported into the EcoSense. Average annual windrose for Zagreb and an approximation of daily temperature curve for each season are given in Figure 2.

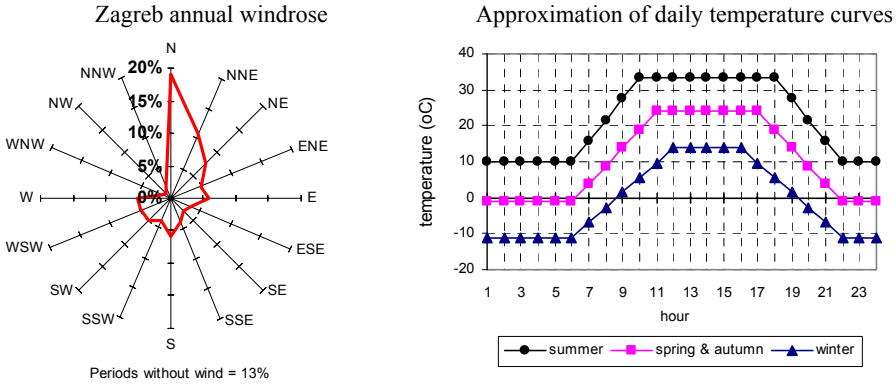

Figure 2. Annual windrose and approximated temperature daily flow at Zagreb site

Zagreb is not a very windy area, which can be concluded from rather high frequency of calms (13%). The prevailing winds are from north (19%) and northeast (11%). The largest average wind speeds, occurring in northeasterly and southwesterly directions, do not exceed 3 m/s (at 10 m above ground). According to the demographic data for Zagreb and Croatia, population density in the outer city area (comprising 4 cells around the plant, altogether 400 km^2) is set to 3000 people/km^2, while in the remaining 96 cells to 100 people/km^2. Average population density in Croatia equals 85 inhabitants/km^2.

9. Estimation Of External Costs Due To Operation Of The Analyzed Power Plants

Local analysis

Based on power plants' emission rates and local meteorological data, average annual concentrations of SO_2, NO_x and particulates on the local level were calculated, using the ISCST2 local dispersion model, incorporated in EcoSense. Spatial distributions of pollutant increments within 50 km of the coal power plant are shown in the figures below. The highest concentrations occur in the very grid cell where the plant is situated and in cells downwind the stack, i.e. southwest from the plant. The highest concentration of particulate matter amounts to 0,083 μg/m^3, the highest NO_x is 1,1 μg/m^3 while SO_2 0,7 μg/m^3.

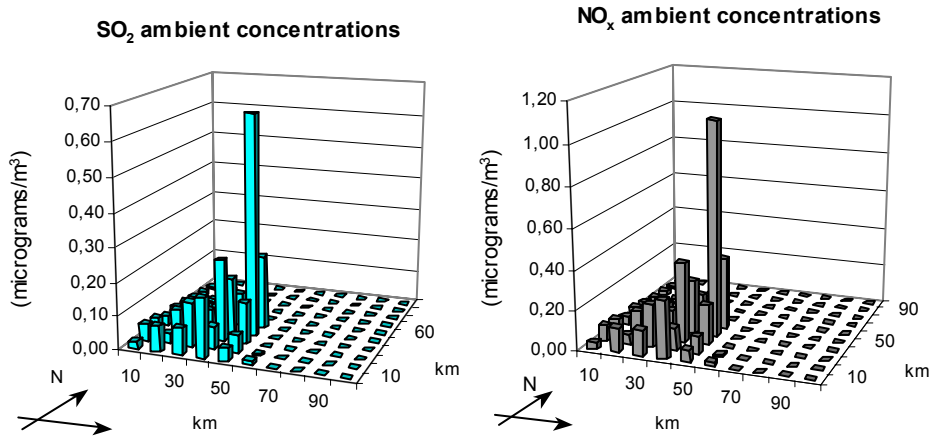

Figure 3. Ambient concentration increase of SO_2 and NO_x due to coal power plant

To calculate health impacts in the analyzed area, the concentration field for each pollutant has to be multiplied by the population field and the appropriate exposure-response coefficient. Health impacts have no common measure, mortality is expressed either in number of cases or in years of life lost, while morbidity in number of events or number of days. To sum them all up in a single number, health effects should be monetized, i.e. multiplied by their monetary values. Spatial distribution of the monetized health damage due to particulates-caused pollution, per unit of electricity generated in the power plant, is shown on the right-hand side of Figure 4. Mortality impacts are here valued using YOLL.

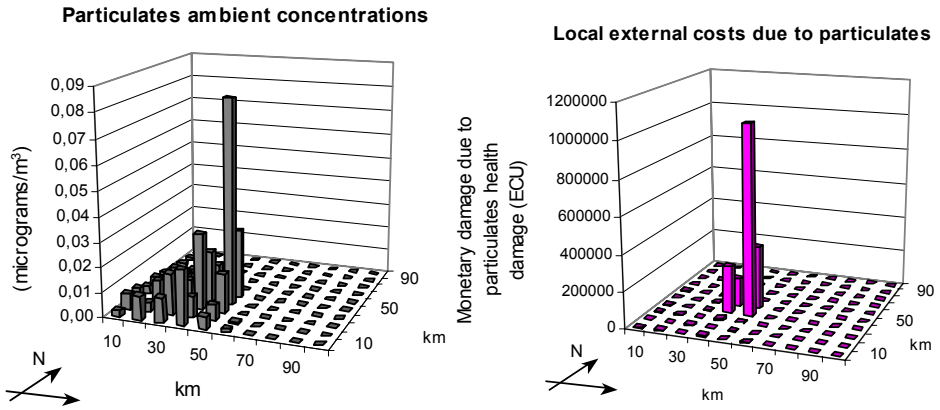

Figure 4. Spatial distribution of particulates concentration and monetized health damages

The level of health effects decisively depends on the number of people affected. Here the largest health damages occur in the four grid cells around the

power plant, where the population density is 3000 persons/km^2 (densely populated urban area). Health damages in other grid cells are almost negligible, due to 30 times lower population density and lower pollution increments at larger distances from source. Health damages also much depend on the way mortality is valued – if calculated via VSL damages are several times higher than via YOLL. The largest portion of damage costs, over 90%, account for mortality endpoints, specially if calculated via VSL.

Table 3. Damage costs of air pollution caused by electricity generation *

	VSL	YOLL	VSL	YOLL
	(mEURO/kWh)		(EURO/t)	
Coal local scale				
Particulates	2,08	0,84	12.414	5.003
SO_2	3,88	0,15	2.889	110
NO_x	2,97	0,12	1.362	53
Total local costs	8,94	1,10		
Coal regional scale				
Particulates [(a)]	0,64	1,69	3.825	10.082
SO_2	8,38	0,32	6.237	235
NO_x	4,35	0,16	1.993	75
Sulfates [(a)]	3,73	10,16	2.777 [(b)]	7.568 [(b)]
Nitrates [(a)]	6,77	17,98	3.101 [(b)]	8.240 [(b)]
Total regional costs	23,86	30,32		
Gas local scale				
NO_x	0,50	0,02	835	33
Total local costs	0,50	0,02		
Gas regional scale				
NO_x	1,15	0,05	1.915	76
Nitrates [(a)]	2,03	5,38	3.383 [(b)]	8.962 [(b)]
Total regional costs	3,18	5,42		

* health damage due to tropospheric ozone and global warming is not included.

[(a)] VSL-based chronic mortality due to regional-level particulates, sulfates and nitrates is not quantified in EcoSense, so the YOLL value is larger.

[(b)] sulfates are expressed per ton of SO_2, while nitrates per ton of NO_x.

Table 3 gives local damage (external) costs per unit of electricity produced and of pollutant emitted from a coal and a gas fired power plant. Total local costs due to air pollution (particulates, SO_2 and NO_x), amount to around 9 mEURO/kWh via VSL, i.e. 1,1 mEURO/kWh via YOLL. If the population density in the whole observed area equaled the average value for Croatia (85/km^2), the damage costs would be only 0,61 mEURO/kWh (VSL) i.e. 0,08 mEURO/kWh (YOLL). Health impacts of the gas-fired power plant originate only from NO_x emissions. Total health damages on the local level amount to

only 0,5 mEURO/kWh (VSL), i.e. 0,02 mEURO/kWh (YOLL). With the average population density of 85 inhab/km^2, health impacts and the associated damage costs would be only 0,03 mEURO/kWh.

Regional analysis

Regional analysis of health impacts caused by operation of the two analyzed power plants was conducted for the region of Europe. Since meteorological and population data for the whole of Europe are incorporated in the EcoSense model, the only necessary input data for the regional analysis were power plant's latitude and longitude and emission rates.

Table 4. Maximal regional concentrations (μg/m^3)

	Coal	Natural gas
Particulates	0,007	-
SO_2	0,052	-
NO_x	0,069	0,019
Sulfates	0,008	-
Nitrates	0,028	0,008

According to the European-wide atmospheric transport and distribution, there is an increase in ambient concentrations predominantly in the north and northeast from Croatia (Austria, Hungary, Slovakia). Maximal pollutant increments are given in Table 4. Health impact distribution depends on the population density, and is similar to the concentration field. Health damage costs on the European level, due to operation of the analyzed power plants, are given in Table 3. They are much larger than local damage costs, due to more people affected. Since VSL-based chronic mortality is not quantified on the regional level, YOLL-based mortality (and therefore total damage costs) is larger. Total regional health damage amounts to 30,3 mEURO/kWh for the coal power plant, and 5,4 mEURO/kWh for the gas power plant.

It has to be stressed the figures in Table 3 include neither NO_x damage through ozone nor CO_2 damage through global warming. There are suggestions to set the average ozone damage for the whole Europe to 1500 EURO/t NO_2, [3]. The range of suggested CO_2 damage cost is very broad (3,8-139 EURO/t CO_2), with the geometric mean estimate of 29 EURO/t.

10. Incorporating damage costs in power system expansion planning

Although the calculated damage costs do not necessarily constitute externalities in their entirety, they can be used as good indicators of external costs. External costs can serve as an additional criterion for the evaluation of different energy scenarios, thus introducing the environmental aspects into the social cost

optimization process. Only the air pollution → health impact pathway was observed here, i.e. only impacts of coal and natural gas combustion. Other fuel cycle steps and externalities of nuclear and hydro facilities are not taken into account. After having external costs estimated for two more or less representative power plants (reference technologies and rather a representative location), an attempt has been made to extrapolate them to the whole electricity sector and include in the planning process. Of course, it is a rather hypothetical exercise intended to give only a rough insight in what the consequences of external cost internalization might be.

Two extreme scenarios of Croatian power system expansion are observed: one with unlimited and the other one with very limited availability of natural gas, those two spanning the expansion options range. The question is how to meet the forecasted electricity demand at lowest possible cost, i.e. what kind of new units and in what dynamics should be built in the next 30 years. Candidate power plants are coal, gas, nuclear and hydro facilities, with annualized production costs given in Figure 5. Since the gas fired power plants are the cheapest, they are the first to enter the optimal capacity mix, so if gas availability is unconstrained the optimal expansion plan will constitute of gas fired units only (Figure 6, fist bar on the left). If on the other hand only a small part (20% in the scenario gas-min) of the total capacity needs can be gas fuelled, the rest has to be met by coal and nuclear units (almost 40% each, as shown in the fourth bar from the left). That optimization result is based on traditional, i.e. private costs of electricity, which include investment cost, fuel cost, operation and maintenance costs and costs of unserved energy.

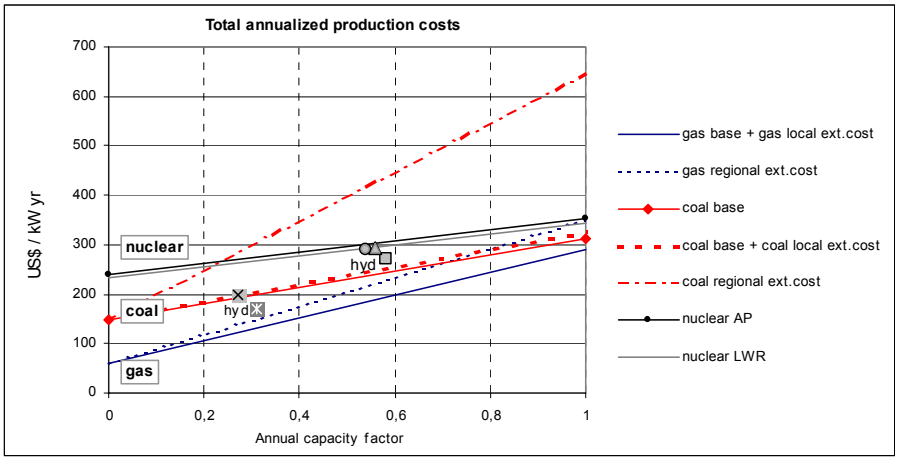

Figure 5. Annualized production costs with and without external costs added

What happens if external costs are added to private costs? Since external costs are proportional to emissions, they should be added to variable component of the

production costs, which is reflected through lifting up the right-hand side of the cost curve. Because only the air pollution damages were quantified here, fossil fired power plants are the only ones to experience increase in costs. If local external costs are added, following the values in Table 3, cost increase is almost negligible. The capacity structure in both scenarios remains practically unchanged with respect to the base case, except for the slight increase in hydro capacity. (Base case refers to private cost only). That can be seen comparing the first two bars, i.e. the fourth and fifth bar in Figure 6.

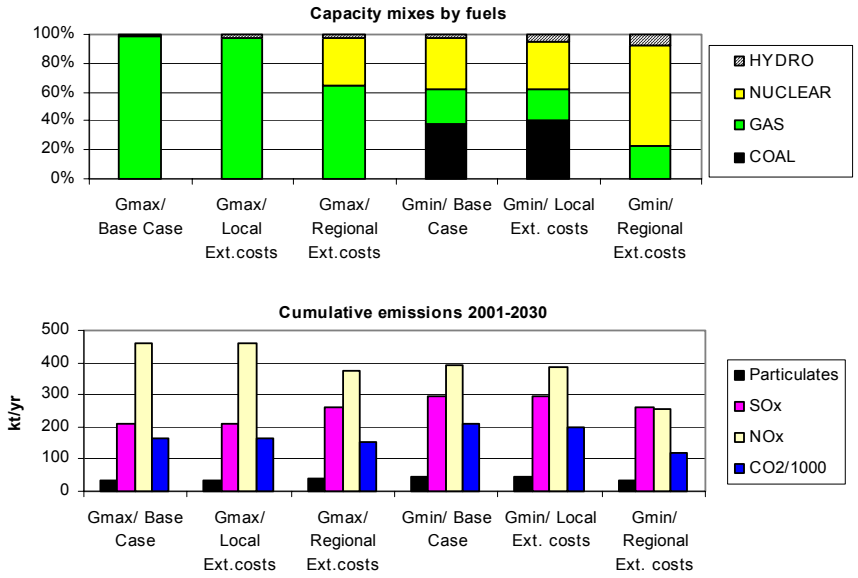

Figure 6. Optimal capacity mixes and cumulative emissions in the analyzed scenarios

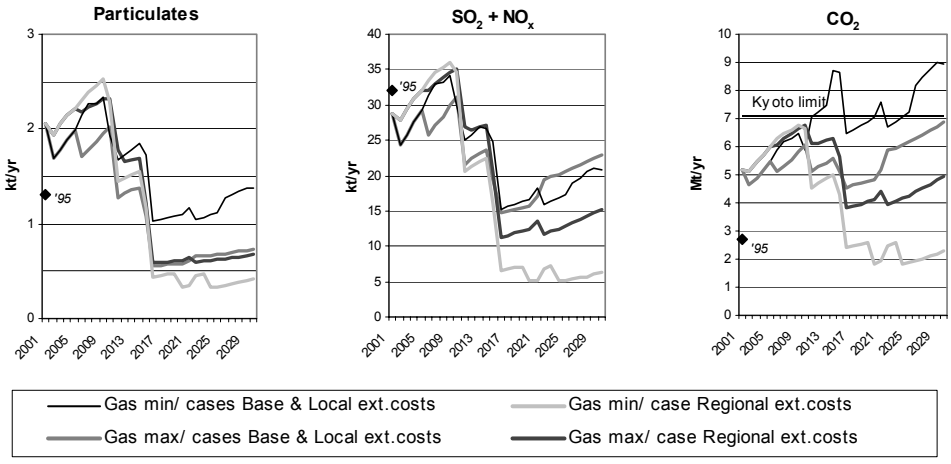

Figure 7. Emissions in the analyzed scenarios

However, if regional external costs are added, costs of coal units dramatically rise (at full load they get more than doubled), that having large consequences on the optimal capacity structure. The absolute advantage of gas units is also shaken – even with unlimited natural gas supply, two nuclear units enter the optimal expansion plan. If natural gas is limited, as much as four nuclear units are added to the system (almost 70% of total capacity).

Emission curves for three gas-max cases and three gas-min cases are given in Figure 6. The base case and the case with local external costs have the same emission curves, while the one with regional external costs included sits much lower. Optimal solution is much more affected by external costs if there is a limited quantity of natural gas, i.e. competition existing only between coal and nuclear facilities. Having the regional external costs included in the planning process leads once to four times lower emissions (that if natural gas is limited), and another time to only 30% lower emissions (that if natural gas is unconstrained).

11. Conclusion

External costs of electricity represent the monetary value of the environmental damage caused by electricity generation. Evaluation of externalities, better say damages, using the impact pathway approach is the most comprehensive but also a very site-specific routine. Since this paper is one of the first attempts to evaluate electricity externalities in Croatian power system, the focus was put on priority impacts for Croatia. Those are health effects of air pollution caused by coal and gas fired facilities, which are candidates for construction in the following 30 years. Damages linked to coal power plants are much larger than those linked to gas fired facilities, since the latter are responsible only for NO_x emission and nitrates. The largest share in the damage costs accounts for mortality effects. The highest damages are attributable to particulate matter, on local level directly while on the regional level in the form of sulfates and nitrates. Health damages highly depend on the number of people affected – that is why local damages (within 50 km from the source) are much lower than on the European scale.

When incorporated into electricity system expansion planning, the local external costs do not significantly influence the optimal capacity mix, but the regional external costs do so in a great deal. With regional external costs added, competitiveness of coal units gets largely reduced, so they lose battle with nuclear units. Even the absolute priority of gas units is disturbed and some room in the optimal capacity mix opens for nuclear power. It has to be stressed that external costs of coal power plants can be lowered by further reducing their emissions, i.e. by applying more efficient abatement technologies already available on the market. Of course, that would induce some additional direct costs.

A particularly important question here is the selection of spatial boundaries within which the external costs should be internalized and imposed on the

polluter. Numerous analyses proved it is due to pollutants' nature necessary to capture impacts as fully as possible. However, it is very important to define geographical scope within which those impacts should be taken into account, since that can seriously influence decision making in the country of emissions' origin.

References

ExternE – Externalities of Energy, EC EUR 16521 EN, DG XII, Brussels, 1995.

EcoSense, Version 2.0, IER, Stuttgart, 1997.

ExternE – Externalities of Energy, EC EUR 16523 EN, DG XII, Brussels, 1998.

D. Feretic, Z. Tomsic, T. Kovacevic, M. Bozicevic: Croatia MESPO Report, research study prepared for the IAEA Wienna, Faculty of electrical engineering and computing, Zagreb, 1999.

S. Molnár, N. Debrecin, T. Kovacevic, M. Molnár: The Impact Pathway Method for Estimating External Costs of Electricity Generation, Hungarian Agricultural Engineering, 20/2007, Gödöllő, pp. 70-72, 2007

Institute of Process Engineering

Professor Dr. János BEKE
Director of the Institute

Dear Reader,

On behalf of my colleagues in Institute of Process Engineering I would like to introduce briefly the operational structure of the institute as well as our most significant educational and scientific activities.

Due to the re-organization of the School of Mechanical Engineering the Institute of Process Engineering was founded in 2005 as integrations of two earlier independent departments (Department of Automotive and Thermal Technologies and Department of Energetics and Food Industry). The current institute consists of three professional working areas as follows:

- Department of Automotive Technology
- Department of Energetics
- Department of Measurement Technology

The main educational and scientific goals of the institute are to research and spread knowledge, needed to meet the expectations of qualified environmental-conscious activities in development as well as establishments of engineering systems, processes, technologies and equipment.

In fulfilling our purposes we pay special respects to the following topics:

- Basic technical knowledge forming the appropriate engineering approach,
- Engineering thermodynamics, electrotechnics and electronics,
- Basic and applied knowledge of energy conversion, energy utilization and energy economy,

- Special technical knowledge for development of environmental industry and utilization of alternative energy sources,
- Disciplines of measurement technology and process engineering needed to control, regulate and automate different engineering processes,
- Environmental- and market-conscious development of production and processing technologies.

Within the institutional activities Department of Energetics is willing to teach and research such caloric, hydraulic energetic and food-industrial operation disciplines which give theoretical as well as practical knowledge to create, develop or derive sustainable environment-industrial technologies and utilization processes of different energy carriers.

The basic aim of Department of Automotive Technology is to assist the institutional purposes by educating and researching different questions related to vehicle constructions, off-road technologies automotive mechatronics.

Department of Measurement Technology conduces to the institutional objectives by teaching and developing knowledge of electrotechnics, electronics as well as metrological technologies and equipment.

More details and other information can be found:

www.fomi.gek.szie.hu

Improvement of Maize Seed Drying Process by Using Semi-empirical Model and Special Thermal Analysis

János BEKE and Zoltán KURJÁK
Department of Energetics, Institute of Process Engineering

Abstract

One of the main conflicts of seed drying technology is to optimize the cross effects between the quality and energetic aspects. To solve the raised problem it should be known the detailed heat a and mass transport process taking place in the bulk and inside the ear as well as many versions of dehydration process should be investigated in order to find the best drying technology. Carrying out an industrial-scale experiment it was found, that the change of the moisture distribution in corn-cob and in corn-kernels differs during the drying time. However, both depend on the sort of seed and on the established drying technology. Moisture loss of corn-kernels is quite uniform along the layer depth, and it changes uniformly during the drying time while corn-cobs show different features from this point of view. The inlet and outlet drying air velocity and drying air temperature maps manly influence the dominant factors of the drying process. Furthermore, some local technological parameters (e.g. local density of drying material, distance between the fan and the drying chamber, local shrinkage behaviour, etc.) significantly modify the impact of drying air on the dehydration process. An appropriate modelling method was developed to describe and to predict the characteristic energy and mass transfer processes that take place inside the corncobs and in the bulk. On the basis of the experiment results and a special thermal analysis a modified drying routine was worked out. By applying the modified technology it resulted significantly less energy consumption while the original quality criteria were kept.

1. Theoretical Background

Development of seed drying process in a hybrid plant is one of the most crucial elements of the corn production technology. As it is widely known in the seed drying technology the long residence time increases the energy consumption (and the costs) most significantly. In order to reduce the energy costs while the product quality criteria are kept we must calculate the expecting drying time as exactly as possible. For this aim a semi-empirical process simulation which is based on an industrial scale experiment seems an appropriate tool.

Drying seeds together with corn-cobs usually can be considered as deep bed dehydration process of non-homogeneous materials. Some deep-bed drying models, which are based on heat- and mass balance equations assume the existence of an equilibrium state between the dried material and the drying

medium. Hence, they utilize the equilibrium moisture equation of the material to solve the problem. However, equilibrium exists only by slow drying at a low medium temperature and a low air-change ratio. The other type of simulation, the co-called MOREY'S BTM model takes the re-hydration effect into consideration, which occurs at the beginning of the drying process. Using the validity area of slow drying, low medium temperature, and low air-change ratio, this method, however, is not much different from the classical theoretical models: it is complicated and hardly usable in the practice.

The well known Hukill-method seems more practicable for describing the deep bed drying. Hukill assumed, that in the case of convective drying the heat demand of the dewatering process equals to the change of enthalpy of the drying medium. He used a semi-empirical model with which it was easy to calculate, but his model ignored the effect of the changes in the inlet drying medium properties as well as the role the moisture change in the drying medium played during the drying process.

$$MR = \frac{2^{\Delta}}{2^{\Delta} + 2^{\Gamma} - 1} \tag{1}$$

However, Equation (1) does not take the potentional local rewetting into consideration and this inadequacy causes an non-ignorable mistake in predicting the drying time. According to the existing equation [$MR=(X-X_e)/(X_0-X_e)$], kinetic curves can be determined. In order to make the classical Hukill-model more precise the dimensionless pressure (Π) must be introduced that helps us to count with the potential local or initial rewetting as follows:

$$\Pi = 1 - \frac{p_{s_{in}} - p_{out}}{p_{s_{in}} - p_{in}} \tag{2}$$

The original Hukill-equation will be valid if Π converges to zero, so (p_{in}-p_{out})$\rightarrow$0, as well. As for generalizing the Hukill-equation, the instantaneous value of the moisture ratio must be determined in order to simulate the re-watering at the beginning of the drying process:

$$MR = \frac{2^{\Delta} + 2^{\Pi} - 1}{2^{\Delta} + 2^{\Gamma} - 1} \tag{3}$$

By applying Equation (3) a more precise model can be derived and the topical moisture ratios in the bulk and the needed drying time can be predicted more accurately in spite of that it is rather easy formula.

2. The Measuring System

A novel industrial corncob drying technology was investigated. The operating scheme of the dryer can be seen in Figure 1. Actually it is a special dryer of twenty-four drying chambers with a triple air entering system. As the figure shows there is a central air distributing room and there are aeration windows inside and outside. In this way we could establish different aeration system.

Figure 1. The scheme of investigated dryer

Usually the residence time was divided into two intervals and between these intervals the airflow direction was reversed.

The drying chambers of numerous corn-cob dryers have trapezoid shapes (Figure 2., A-A section) with aeration grids (windows) at its bottom and top as well as sideward.

The top view of scheme in Figure 1 shows the offset arrangement of the sampling mines. Only three sampling mines were installed in one drying chamber to avoid disturbing the normal drying process.

Aeration settings can be seen at the bottom right corner of Figure 2. There were two basic solutions to aerate the drying chamber: The drying air with medium temperature level comes from the bottom grid up to the top of the batch (Figure 2., setup A.; black grid: closed; white grid: opened), which carry away the main moisture mass from the drying material. After a given period of time the settings are reversed between setups A and B, hence the drying air with high temperature level comes from sideward grid down to the bottom of the batch (Figure 2., setup B. ; black grid: closed; white grid: opened) make the drying material achieve the aimed moisture content.

An expediently developed data acquisition equipment (Eltek RX250AL with GENII radio data logging system, Darca Plus software) was applied to collect the information of the sensors. Being the circumstances of the measurement very special, radio wave sensors were used and installed into the deep of the sampling mines. Figure 3 shows measuring ports which were inserted into the walls of measuring mines at different layer levels where the air, the bulk and the ear component temperature were recorded. Moreover, we took samples to measure the moisture content of components of the drying material.

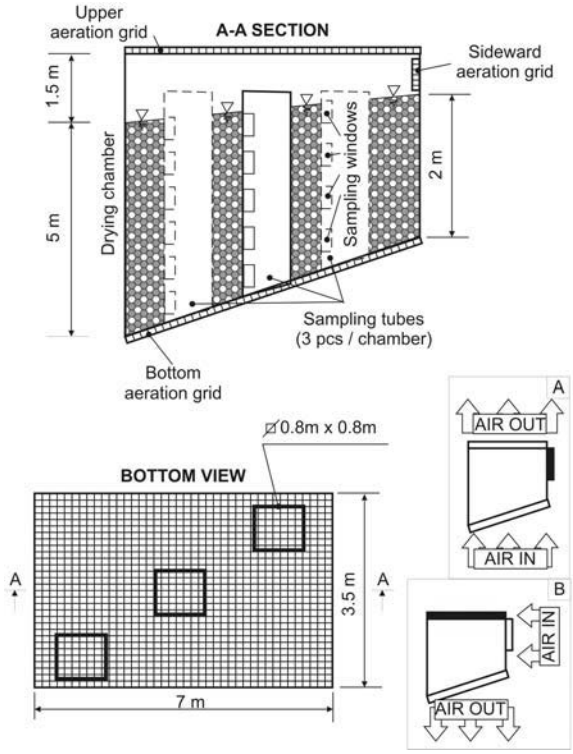

Figure 2. Structure of the drying chamber
(A: 1st setup of aeration; B: 2nd setup of aeration)

Figure 3. Assembly of the measuring ports for measuring the temperature and humidity of drying air and the temperature of material

An average drying period was about 72 hours, consequently sampling time of 15 minutes was adequately precise for this measurement.

The velocity of drying air was measured at each opened aeration window; the measurement points were the same like that of the coupled air temperature and humidity measurement points. Other velocity measurement points coincide with the installation place of the coupled sensors.

3. Results and Discussions

Figure 4 shows the typical change of the moisture content of corn-cobs as functions of the drying time and the layer depth. It can be determined, that, the bottom layer of the batch began to dry more rapidly that the top indeed at start the initial moisture content varied slightly along the depth of the batch. Firstly aeration setup A. (Figure 2.) was used, then after about 30 hours of drying aeration setup B. (Figure 2.) was chosen and applied. After reversion the moisture content of the bottom layer of the drying batch stayed at a constant level, but the moisture content of the upper layer began to decrease rapidly.

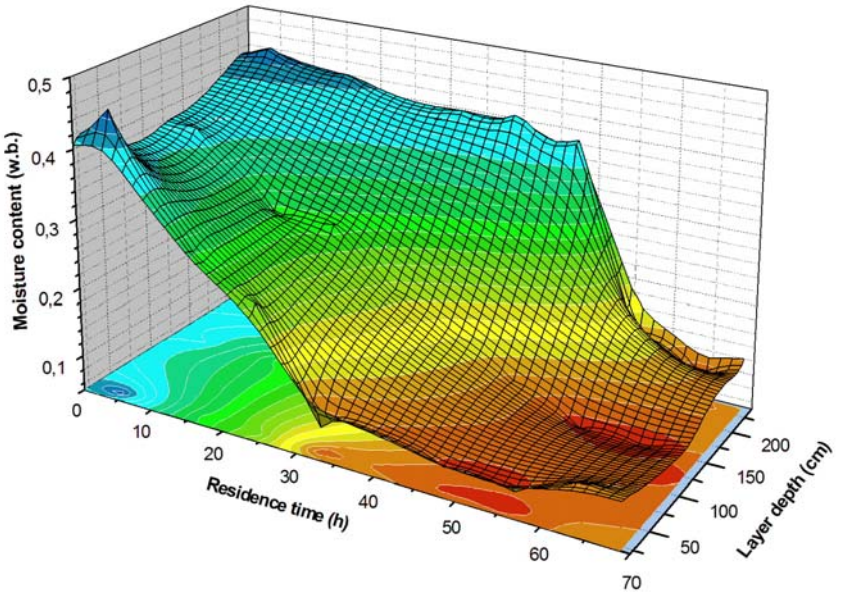

Figure 4. Typical integrated moisture content of the corn-cob as functions of the drying time and layer depth

The moisture distribution in the corn kernels (Figure 5.) differs significantly from that of the corn-cob (Figure 4.). Firstly the initial moisture content, and secondly the shape of the diagram is conspicuous. The initial moisture content of the corn-cob is

much higher then that of the corn-kernels, so it is obviously, that in case of the corn-cob and corn-kernels system the main water reservoir unit is the corn-cob, which results a definite water movement from the cob to the kernels. The further prominent difference is, that at the beginning of the drying process and after reversing the air flow direction a definite rewetting phenomena can be observed. And the other thing is that the moisture distribution of kernels as a function of layer depth is not as homogenous as it was in the case of corncobs even at the end of drying process. But similarly to the cob drying process – coming to the end of the residence time – the kernels that located in the upper half of bulk become overdried.

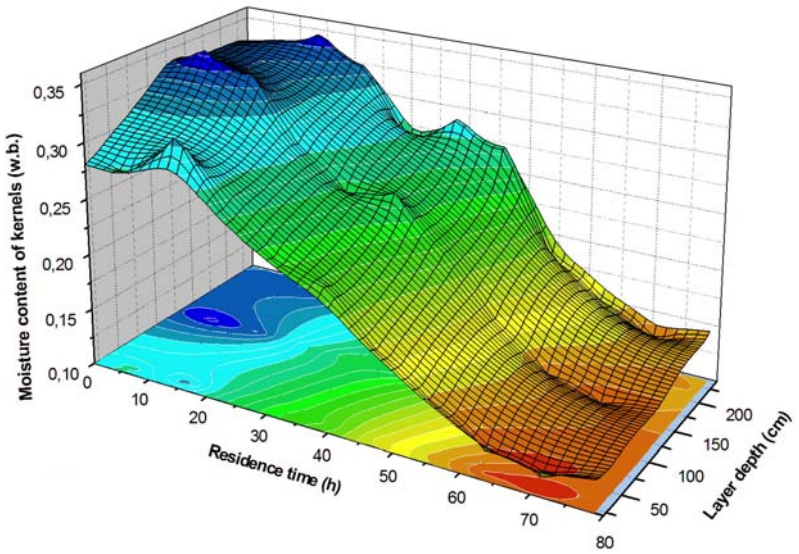

Figure 5. Typical integrated moisture content of corn-kernels as functions of the drying time and the layer depth

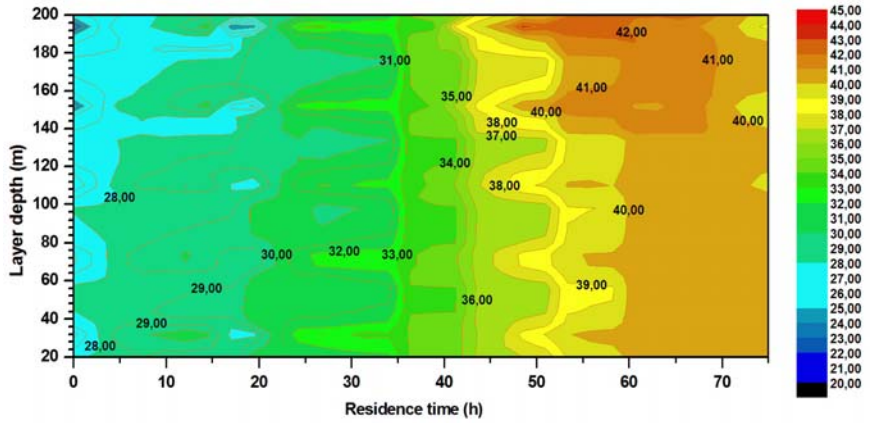

Figure 6. Characteristic temperature map of the corn-cob as functions of the layer depth and the drying time

The typical temperature field of corn-cob can be seen in Figure 6. As the picture shows the batch between the 160 cm and 220 cm warms up more slowly then the other part of that. The hottest part is the bottom layer until, in this way the temperature difference within the batch could hit the 5°C.

The temperature field of the bulk shows more uniform distribution (Figure 7.), but the bottom part of the batch seems to be up to 5°C colder then the other part of that.

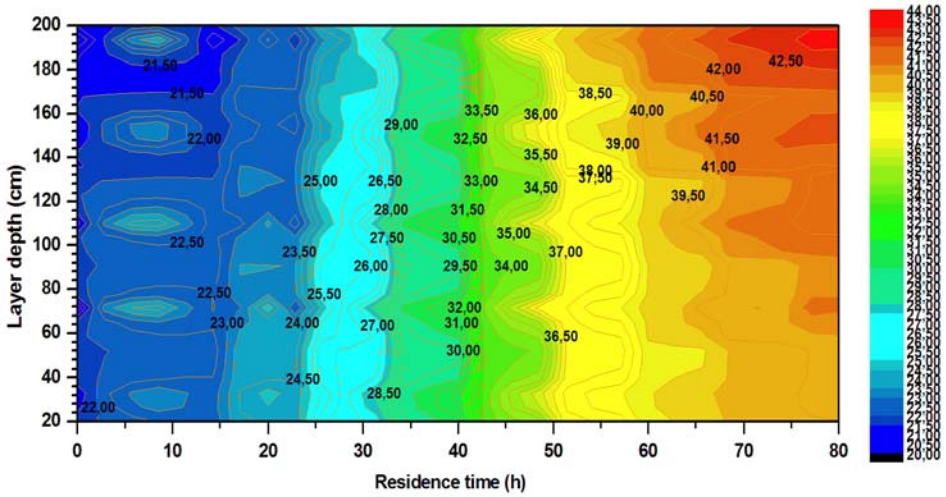

Figure 7. Temperature of the bulk as functions of the layer depth and the drying time

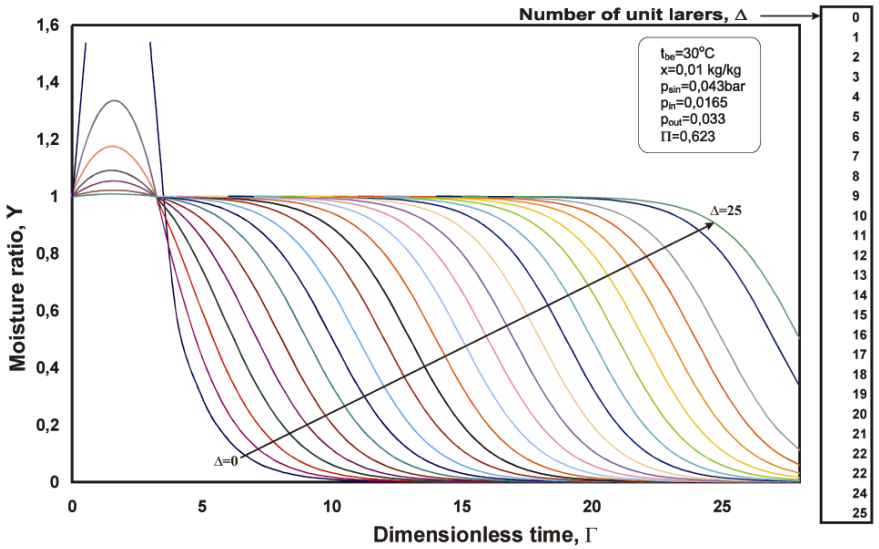

Figure 8. Modified Hukill-curves based on the seed-corncob drying conditions without changing the drying air direction

On the basis of the accumulated data the modified Hukill-curves can be drawn that obviously show the rewetting process at the beginning of drying (Figure 8.). After that the Figure 4. can be interpreted much easier, taking into consideration that the drying air direction – as the part of the applied technology – was changed 40 hours after the drying process started.

By taking in account all the measuring Figure 9 demonstrates a good example for energy loss of the established drying process.

If the desired final moisture content of the drying material is set to 12% we can observe that about 70 % of the material is overdried (Figure 9.), and this definitely causes redundant energy consumption.

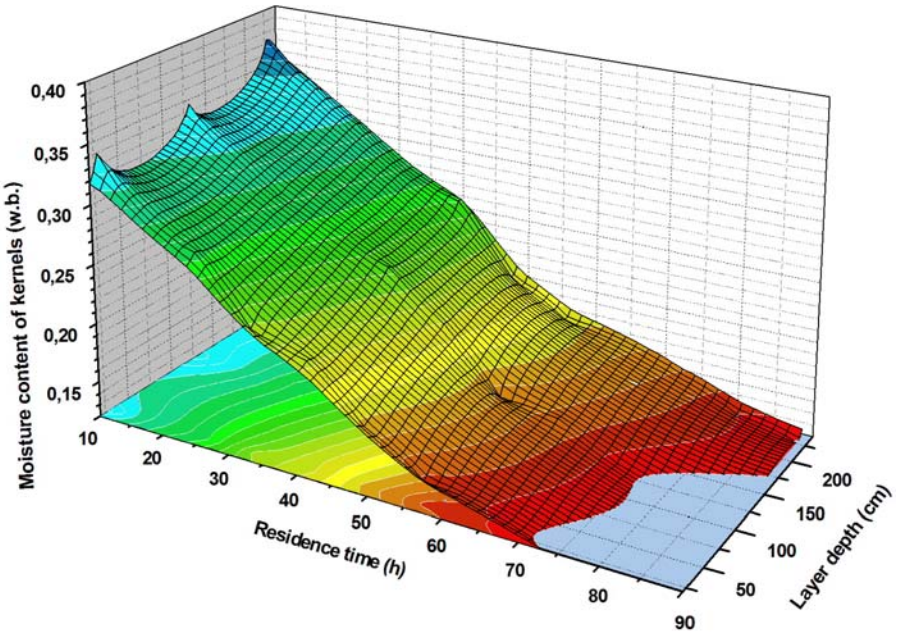

Figure 9. The local overdrying as the influence of the delayed change of drying air direction

There are some possibilities to avoid overdrying and reduce energy consumption. First of all to prevent the rewetting phenomena we should increase the airflow rate to an appropriate level, in our case we recommended by fifteen percent (15 %) at the beginning of the drying process and just after reversing the airflow direction. In this way the drying air will not be saturated. Secondly, we should choose the right time-point for reversing the drying air direction. The appropriate moment for this reversal is when the moisture contents of corn ear components are equals to each other (Figure 10.).

By taking the bulk and corn cob temperature distribution into consideration we can determine a well applicable operating diagram as functions of material moisture content and drying air temperature (Figure 11.). By using this diagram

we can find the optimal coherent temperature and moisture content pair and can optimize the process from energetical point of view considering the quality requirements.

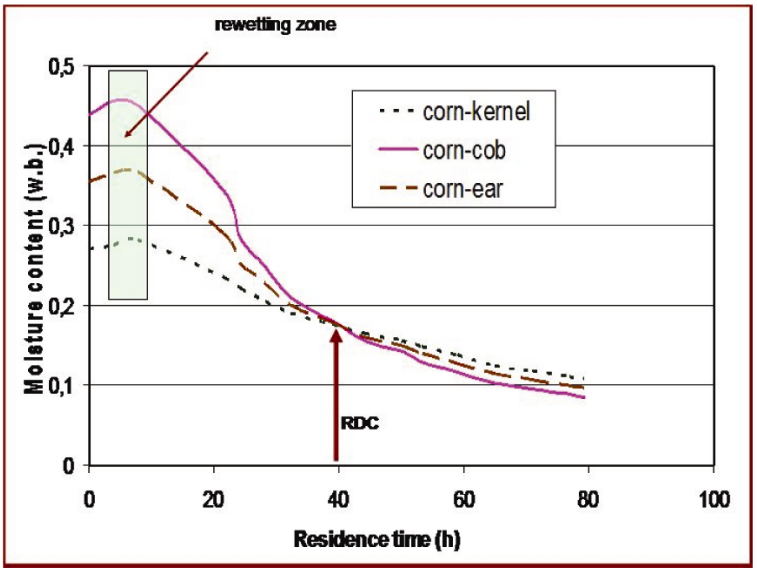

Figure 10. Desired change of air direction

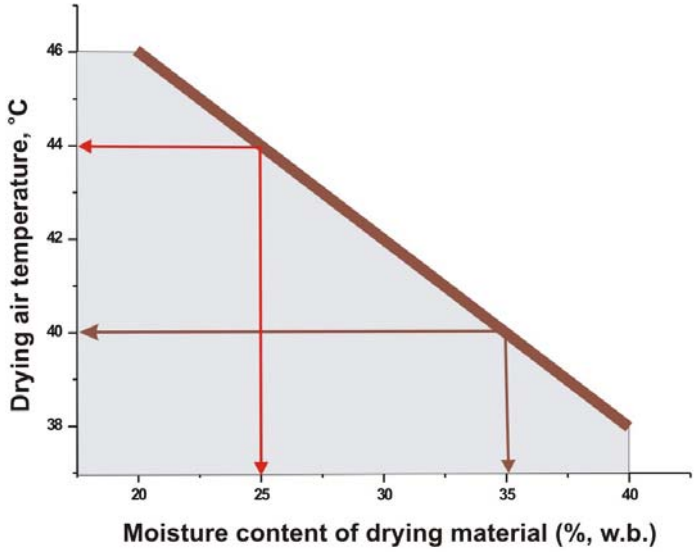

Figure 11. Coherent temperature and moisture content data in the appropriate drying process of maize ears

4. Conclusions

The change of moisture content of the corn-cob and that of the corn-kernels differ during the drying process. Moisture loss of corn-cobs is quite uniform while the corn-kernels dry irregularly, depending on numerous local considerations.

By an appropriate changing the drying air direction the overdrying and by increasing the drying air the local rewetting can be avoided.

The appropriate time for changing the air direction is the moment when the moisture contents of ear components are equal to each other.

The modified Hukill-model is an appropriate tool to describe the dewatering process of hybrid seeds in ears and predict precisely the expecting drying time depending on the drying conditions.

The increase of airflow at the beginning of the drying process and just after the changing of air direction helps to prevent the rewetting phenomena and gives a good chance to reduce the residence time.

Acknowledgement

The authors are grateful to the OTKA Foundation (K61480) and to Syngenta Ltd Hungary for their financial supports.

Nomenclature

Δ:	Number of uniform layers
Γ:	dimensionless time
k:	drying coefficient
p:	partial vapor pressure [Pa]
Π:	dimensionless pressure
τ:	time [h]
t:	temperature [^{o}C]
X:	material moisture content [kg/kg, d.b.]
x, y, z	length [m]

7. Indexes

0:	initial value
a:	drying air
e:	equilibrium
in:	inlet
out:	outlet
s:	saturated

v: vapor
w: water

References

Boyce, D.S. 1966. Heat and moisture transfer in ventilated grain, Journal of Agricultural Engineering Research, 11: 255-265.

Morey, R.V. – Cloud, H.A. – Gustafson, R.J.– Petersen, D.W. 1979. Evaluation of Feasibility of Solar Energy Grain Drying, Transactions of the ASAE, 22: 409-417.

Hukill, W.V. 1954. Grain dying in storage of cereal grains and their products (Ed. Anderson, J.A. and Alcock, A.W.), In: American Association of Cereal Chemistry, St. Paul: Minnesota

Bihercz, G .– Beke, J.: Semi-empirical Model of Convective Drying with Wide Range Layer Depth Validity, Drying Technology, 2006. 24: 1165-1172. p.

Bihercz, G .– Beke, J.– Kurjak, Z.: Simulation of drying process of corn kernels during microwave and convective treatment. Asia-Pacific Journal of Chemical Engineering Volume 2, Issue 2 , Pages75 – 82. Copyright © 2007 Curtin University of Technology and John Wiley & Sons Ltd.

Institute for Environmental Systems

Professor Dr. István BARÓTFI
Director of the Institute

Dear Reader,

The expectation towards the environment can be fulfilled only with an industrial scale activity today. The environmental industry is looking for solutions to the most emerging problems of today and therefore this is the most growth industry. For solving the problems the ability in any field of the industrial tasks/activities itself is not sufficient but there is a need of knowledge about the relation between technics and environment and the consequences of the human intervention.

For forming and developing different systems a wide spectrum of natural sciences and engineering knowledge is needed in order to establish technologies and products which enable to sustain the long term balance between humans and their environment due to analyzing and modeling the processes. The Institute have courses to the engineer level knowledge of the environmental systems like the basics in physics, energy management dealing with the relation between the humans and the environment, in building services, which gives an overview about the comfort in the direct environment of the humans, and also subjects in logistics, energy management, process control in the industrial activities, and subjects connected to designing, maintaining and operating of systems which ensure the protection and utilization of natural elements and resources and research and development as well in these fields.

The Institute's departments are as follows:

- Department of Environmental and Building Engineering
- Department of Physics and Process Control
- Department of Logistics

The departments of the Institute had been established according to the previous scheme of the Faculty of Mechanical Engineering, however they have a lot of interrelation between them. The research and development performed in each particular field build on each other, have interrelations and contribute to the exploration of the technical solutions which suit to the environmental requirements and to the needs of comprehensive way of thinking. The guarantee for sustainable developing is the economic-ecological uniform/common approach. This is a key issue also in the institute's research.

The main research activities in the institute in 2008:

- Development of energy efficiency performance of buildings, analysis of facility/building energetic, energy efficiency in buildings – in the built environment
- Energy and environment, emission reduction options of fossil energy sources
- Technical and technological questions of energetic utilization of biomass
- Development of thermal and photovoltaic use of solar energy
- Modelling of drying processes, solar drying, greenhouse operations
- Modelling, simulation and process control
- Waste management and recycling (and construction materials)
- LCA
- Household /domestic appliances

Significant part of the institutes research work is in international projects which gives the opportunity to distribute the latest results to abroad and the continuous maintaining of contacts and networks between the researcher. This is especially important for expansion of the view of our young researchers and also for the scientific carrier of our fellows.

Combustion Technologic Analysis of the Szarvas1 Energy-Grass

István BARÓTFI and Márta SZABÓ
Department of Environmental and Building Engineering, Institute for Environmental Systems

Introduction

The information about the combustion technologic characteristics of the material is a basic requirement for the utilisation of the biomass with burning. The combustion technologic analysis of the Szarvas 1 energy-grass has been carried out in a form of grass/plant and pellet. The analysis covered the following steps:

- Elementary composition of the grass and the pellet
- Determination of the Heat Value (Combustion heat) and the lower heat value (LHV) (net calorific value)
- Analysis of the burning characteristics of the pellet
- Analysis of the residuals (slag).

Because of the big variety of the analysis and the availability of the required modern tools the measurements had to be carried out parallel and complementary beside in the laboratories of the Szent Istvan University (SZIE) also in the laboratories of the Budapest Technical University, Miskolc University and the Eötvös Loránt University (ELTE).

1. Determination of the basic compounds of the energy grass and the pellet

During the examination of the biogenic combustion materials the following basic compounds has to be defined: C, H, O, N, S, Cl, and K. The analyses have been parallel carried out in the laboratory of the SZIE and ELTE.

The measurement method for the analysis of the C, H, and N has been performed with the element analyzer type Vario EL produced by Elementaranalyse. The principle of the method is: the material will be completely pyrolysed and the coal content will be transformed to CO_2, the hydrogen to water and the nitrogen to nitrogen gas. After the splitting these elements will be measured with thermal conductivity detector.

The result from this micro method appears in milligrams. It follows from that after the pulverization these samples still do not meet the homogeneity requirements, which is needed to this method. The inorganic content will be measured by direct burning, the chlorine content will be transformed into chloride with using the Schöninger method and will be determined in titrimetric way.

2. Definition of the net calorific value of the pellet

The net calorific value will be determined from the measured value of the combustion heat in view of the measured value of the combustible hydrogen

content and the moisture content. The analysis has been parallel carried out in the combustion technology laboratory of the SZIE and in the Laboratory of the Department of combustion technology of the ME.

Hydroscopic moisture content
The measurement was carried out according the MSZ KGST 751-77: drying the air-dry, raw granulate until reaching the constant mass in an electronic drying oven at the temperature tsz=105 °C .

Combustion heat
The measurement has been carried out according the standards MSZ 12000/5-68, MSZ/4-7017500: burning the air-dry samples in a Berthelot-Mahler Calorimeter filled with oxygen with 30-bar pressure.

The combustion heat of the pellet at the measured moisture content is 17120 kJ/kg.

Analysis of the burning characteristics of the pellet
The most comprehensive way for presenting the behaviour of the pellet during the burning can be made with thermo gravimetric (thermo analytic) analysis, in the course of this the quantitative parameters of the material will be measured at the different material-temperature.

3. Thermo analytic analysis

The thermo analytic analysis has been carried out with the TA 2960 STA equipment produced by TA Industrial Company (successor of the firm DuPont). This instrument measures at the same time the mass change of the sample caused by the heating and the temperature difference between the sample and the reference-material during the heating program.

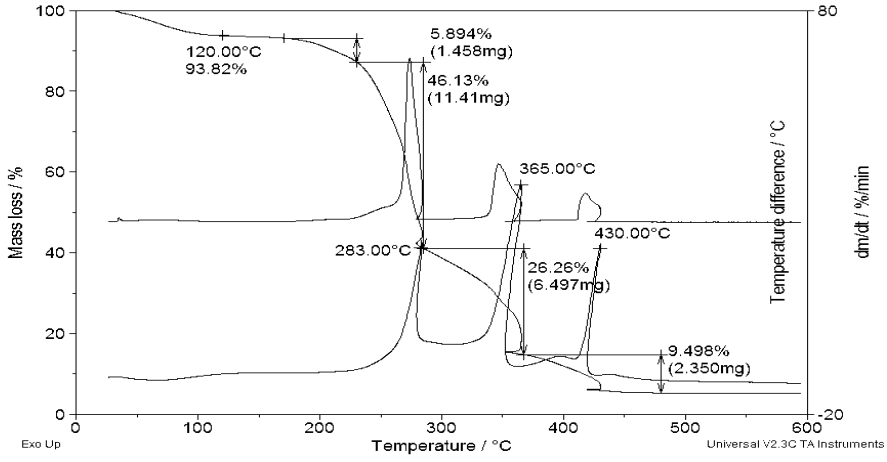

Figure 1. Thermo analytic curves of the energy grass samples (5 °C/min, air atmosphere)

Experimental parameters:

- Calibration: ca. 20-25 mg
- Heating speed: 5 °C/min
- Flushing gas: air, 10 l/h volume flow rate
- Measuring range: from room temperature – 600 °C.

The produced curves by the equipment are the mass change (TG), its derivative with respect to time (DTG) and the differential thermo analytic curve (DTA) (Figure 1.)

At the beginning phase of the heating (between air temperature and 120 °C) 6,2 % mass loss was measured, this was caused by the exit of the water abounded in the sample. After this the material dissolves in three main steps (these can be divided to further sub phases according the DTG curve). The temperature differences and mass losses of the main steps are the following:

a) app. 180 – 280 ^{O}C, $\Delta m = 52.0$ %,

b) app. 280 – 370 ^{O}C, $\Delta m = 26.3$ %

c) app. 370 – 470 ^{O}C, $\Delta m = 9.5$ %,

over 470 °C further mass change cannot be detected, the slag content abstracted from the whole measurement is 5,3 %.

According to the thermo analytic curves it can be stated that the material inflames during the steps A-C in the given experimental circumstances, consequently dissolves in an exothermic way.

Taking into account that the sample can be considered as an organic material, the main departing decomposition product is the carbon dioxide.

The advantage of the thermo analysis is that it is quick, reliable, can be well reproduced and does not need necessarily any sample preparation however does not give any information about the composition of the departing decomposition product.

To avoid this the thermo analyzers are connected with infrared spectrometer and mass spectrometer respectively so that the arisen gases and vapours can be transported through a heated capillary into the room of the other two instruments. With such an arrangement of the measuring equipment the composition of the developing gases and vapours - often with some limitation - can be given. Such an arrangement of the instruments is called literally as a coupled technique. The thermo scale was connected with a Balzers Thermostar GSD 300 T quadrupol mass spectrometer.

The mass spectrometer works in two modes:

- cyclic and
- serial measurement.

Starting with an arbitrarily chosen specific mass value between 0-300 amu[1] the ion flow rate at each specific mass unit will be measured in a chosen specific observation width and observing period. So we arrive to the two dimensional mass spectrum shown in the Figure 2.

[1] atomic mass unit, $1\ u = 1/N_A\ g = 1/(1000\ N_A)\ kg$ (N_A Avogadro Number) $1\ u \approx 1.66053886 \times 10^{-27}$ kg

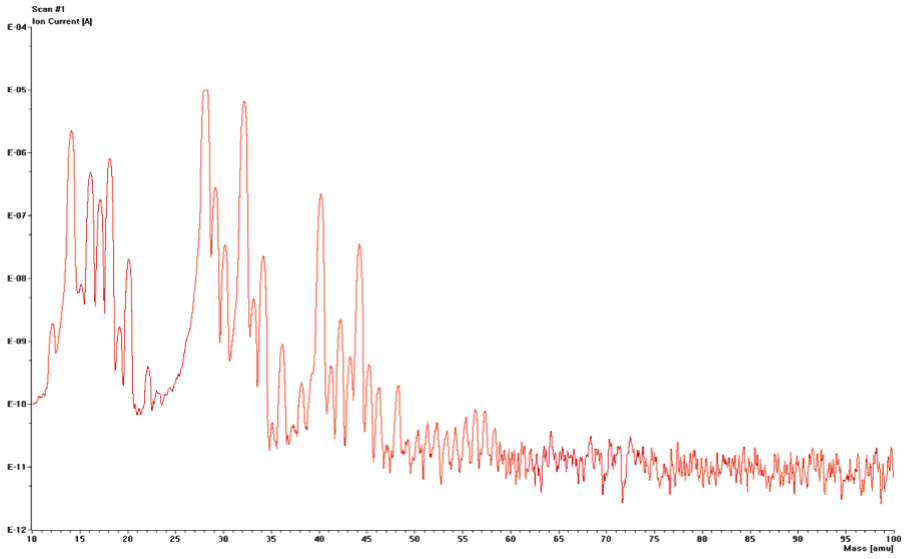

Figure 2. The two-dimensional mass spectrum of the energy grass

The experimental unit as it is showed in the Figure 2. is called like a „cycle/period" and its length and time duration depends from the observed specific mass range and from the observation time.

The chosen set measuring parameters:

- starting specific mass: 10 amu
- specific observation width: 90 amu
- observation time duration: 0,2 sec/channel.

After taking one of the mass spectrums the program goes back to the first set specific mass value and starts the measuring of the ion flow from the beginning.

The mass spectrum curves present a three dimensional picture, the X-axis show the masses, the Y ones the ion flow and the Z ones the number of the set cycles. This last one is proportional with the time, and through this with the temperature of the sample if we know the speed of the thermo analytical measurement.

Although this mass spectrum contains all of the information, it is hardly manageable and can hardly interpret. That is why these curves can be divided into freely chosen ranges of the specific mass with an available data analyser program.

It is also possible to convert the 3D mass spectrum so that on the X axes shows the elapsed time. This is already directly proportional with the temperature. The disadvantage of this is – first of all by the presentation of the whole mass spectrum – that certain peaks cannot be seen because they are covered by the other curves. (In these cases it is necessary to make a better resolution of the spectrum. This increases the numbers of the figures and worsens their manageability and transparency.)

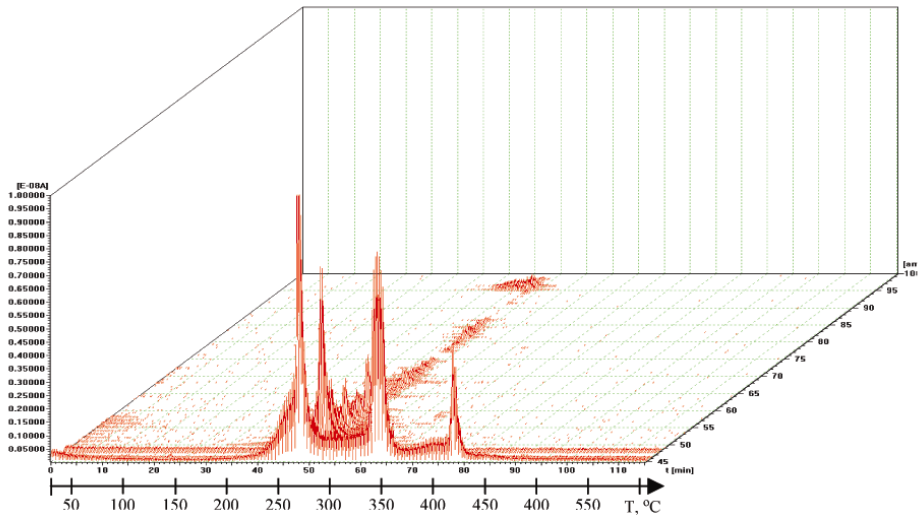

Figure 3. The three dimensional mass spectrum of an energy grass sample (45-100 amu)

The Figure 3 presents an example of the mass spectrum of the energy grass between the ranges of 45-100 amu. It can be seen that in the first decomposition step the more volatile and in hydrogen more rich components burn out. In the second and third phase there is a further oxidation of the components arisen from the primary and secondary decomposition with very low hydrogen content, this oxidation takes place with the formation of CO_2 and water.

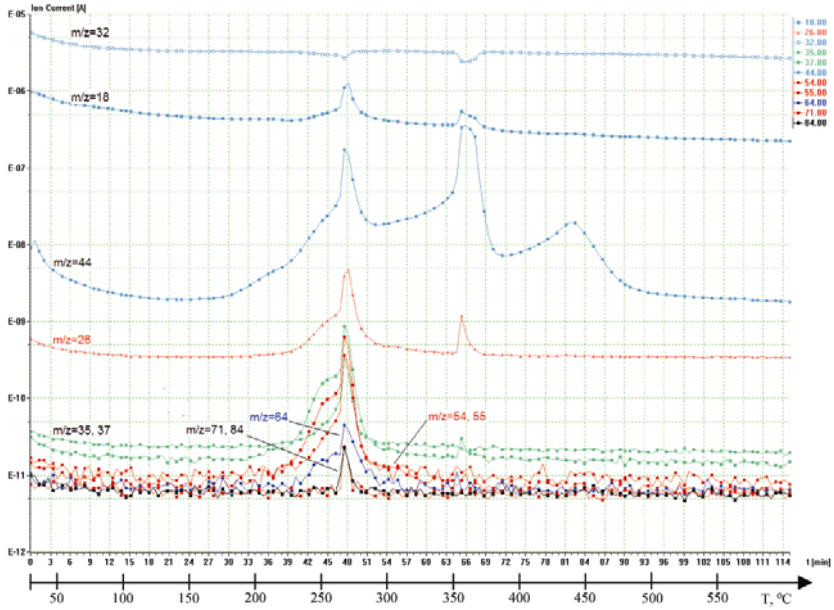

Figure 4 The MID curves of the energy grass sample

The mass spectrometry monitoring can work in two modes as it was mentioned earlier. The difficulties of the continuous measuring in the range of higher specific mass can be avoided with the so called "multiple ion detection" MID method. In this method the desirable specific mass values and their detecting time can be arbitrarily set. So the result is two-dimensional which is more transparent and simplifies the evaluation. The MID curves of the sample are presented in the Figure 4.

In the figure the development of the CO_2 and the water and also the quantitative change of the oxygen needed for the combustion in the working room of the oven can bee seen (curves of m/z = 18, 44 and 32).

The curves m/z=26, 54 and 55 indicate the evolution of different fragments coming from the first two phases of the oxidative decomposition.

The curves m/z=71 and 84 run parallel. The mass difference between these curves is 13 units, which corresponds to one –CH group, so it can be assumed that the fragments are arisen from the decomposition of the same component.

In the figure the blue m/z=64 curve appears mostly in the first decomposition step but it appears with a small intensity also around 350 °C. This can be a sign also for SO_2 forming.

It can be seen that the m/z = 35 and 37 curves are different. This confirms the earlier assumption that the arise of chlorine cannot be excluded however mainly at the specific mass volume of m/z = 37 beside the chlorine isotope other organic components can be also arisen.

The analysis of the volatile content was carried out according the MSZ 24000/10-83: glowing the dried samples for 7 minutes in a closed pot, in an oven electrically heated to 850 °C in a reductive (charcoal) atmosphere.

The residuals (slag/cinder) were analyzed in three points of view:

- quantity
- composition
- characteristics.

The analysis of the composition of the residuals was carried out in the Laboratory of the Department of combustion technology of the ME.

The slag/cinder content was carried out according to the MSZ ISO 1171: after drying on 105 °C until reaching the constant mass the sample was burned at 850 °C in an electronic oven in air atmosphere.

The measurement of the softening temperature of the cinder from the Szarvas1 energy grass was carried out with the registration of the height decrease of the dried cinder samples with a diameter of 12 mm, height of 12 mm during glowing in a reductive atmosphere in Bunte-Baum softening analyzer oven.

From the softening measurements it can be summarized concluded that the

- starting temperature of the sintering: 650÷680 °C;
- starting of softening: 750÷780 °C;
- starting of the intensive melting: 800÷820 °C.

These temperatures are by 300-400 °C lower than the characteristic temperature of the ashes from wood, and by 600-700 °C than from brown coal.

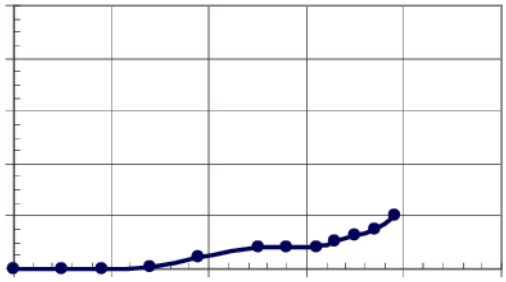

Figure 5. The softening diagram of the ash

The analysis of the chemical composition of slag of the energy grass has been determined with the DX4 EDAX EDS micro analyser of the AMRAY 1830 I type scanning Electro-microscope. The reason of the low softening temperature of ash is the presence of a relatively big amount of K_2O, Na_2O, P_2O_5 and Fe_2O_3 which have a strong liquefying effect on the SiO_2.

4. Summary and conclusions

After the analysis the combustion technical characteristics of the Szarva1 energy grass are the following:

Elementary composition in mass percentage

The analysed material	C	N	H	O	inorganic	Cl
Szarvas 1	41,0	0.9	5.69	45,8	6.45	<1
Szarvas 1 pellet	42.5	0.42	5.78	44,6	5.4	<1

Heating value: 17356 kJ/kg

Net calorific value (at the moisture content of the pressed material): 17 120 kJ/kg

Volatile content: 67,86 %

Slag content: 4,4-6,4 %

Characteristics of the slag:

- starting temperature of the sintering: 650÷680 °C;
- starting of softening: 750÷780 °C;
- starting of the intensive melting: 800÷820 °C.

Composition of slag:

Component	Mass percentage, %	Component	Mass percentage, %
Na_2O	6.53	Fe_2O_3	3.65
K_2O	13.37	Al_2O_3	2.34
SiO_2	60.72	MgO	3.13
P_2O_5	5.19	CaO	5.07

The characteristics of the Szarvas1 energy grass can be well perceptible if the measured parameters can be compared with parameters of other biogenic fuels. This is in general very interesting but especially compared with agricultural products or other similar dedicated energy plants.

After evaluating the measured combustion technical parameters of the Szarvas1 energy grass it can be summarised concluded that in energy content and in combustion technical characteristic point of view it is similar to other biogenic fuels. Of course some of the characteristics which are similar to the ones of different straws and grasses differ from the combustion technical characteristics of the woods. The main biggest difference is the softening temperature of slag: it is lower by 300-400 °C of the slag of wood. This low softening temperature of slag does not mean any insolvable problem with an adequate design of the combustion chamber in the furnaces.

References

Barótfi I. – Szabó M. – Szemmelweisz Tné – Szűcs I. : Szarvas 1 energiafű tüzeléstechnikai vizsgálata – 1. rész. Energiagazdálkodás 2006. 47. évf. 1. sz. p. 3-7.

Barótfi I. – Szabó M. – Szemmelweisz Tné – Szűcs I. Szarvas 1 energiafű tüzeléstechnikai vizsgálata. 2. rész; Energiagazdálkodás 2006. 47. évf. 2. sz. p.15-19.

Barótfi I.: Biomass combustion technologies. (Társszerzőkkel) In: FAO/CNRE Guideline. No. 1. 1988. (Ormea 1986 okt. 17-19) p. 84.

Operational Experiences with Small-Scale Grid-Connected PV System

István FARKAS and István SERES
Department of Physics and Process Control, Institute for Environmental Systems

Abstract

In the framework of the PV Enlargement Project of the European Union, a 10 kWp photovoltaic system was constructed on the campus of the Szent István University, Gödöllő, Hungary. This set-up is one of biggest the PV installations in Hungary. Beside the energy production it serves also as a demonstration and educational centre. Partly for the education and research aims two different PV technologies are installed (multi-crystalline and amorphous silicon technologies).

The entire system consists of three different subsystems, two identical parts of 3,1 kWp from amorphous silicon DS40 modules, and a 3,4 kWp part of ASE100 modules from multi-crystalline PV technology. Every subsystem uses a separate inverter, through which the produced energy is converted to the 230 V, 50 Hz electrical grid.

Together with the energy production system a PC based data logger was installed to measure the important properties as follows: irradiation, temperature, PV array (DC) voltage, current and power, AC voltage, current and power supplied to the electrical grid. Beside the PC based data logger for measuring the energy fed to the electrical grid (AC side) an authorized energy meter was installed, as a control unit of the data logger.

Together with the energy production of the total system, the working of the subsystems was also studied. The energy productions of the subsystems are measured continually as all the subsystems are measured separately. From the daily power distribution data it can be seen, that the two DS40 subsystems are working almost identically, but the power of the ASE subsystem is higher.

From these data the comparison of the energy production of the different module technologies under different meteorological conditions were investigated. As a seasonal effect, it can be seen from the measured data, the rate of the polycrystalline and the amorphous subsystems energy production during the winter period is about 25% higher than in the summer period. This fact is investigated by comparing the meteorological (temperature and radiation) conditions. For the better understanding the effect, the normalized energy production (the energy production of a 1 kWp system) of the different technologies were also compared.

1. Introduction

In the framework of the PV Enlargement Project (supported by the European Union) an about 10 kWp photovoltaic system was installed at the Gödöllő

campus of the Szent István University, Hungary. Beside the energy production the system is used for demonstrational, educational and research tasks, as well.

The PV system in Gödöllő is structured into 3 subsystems (fields). One subsystem has ASE-100 type modules (polycrystalline technology, RWE Solar Gmbh), and the remaining two identical subsystems has been constructed from DS40 (amorphous silicon technology, Dunasolar Ltd) type of modules. Each subsystem has its own inverter (Sunpower SP3100/600 and SP2800/550). The total power of the system is 9,6 kWp (Farkas et al, 2005).

The two and half year of operation (the system was switched on in 8th October, 2005) produced fairly enough data for the comparison of the subsystems. From the literature it can be known, that the modules with different technologies are working in different way under various meteorological (mainly on radiation and temperature) conditions. The aim of this work is to recognize this alternate behaviour of our system from the measured operational data.

2. System description

The PV system is structured into 3 subsystems (fields). One field has 32 pieces of ASE-100 type modules (RWE Solar Gmbh) and, the remaining two identical ones consist of 77 pieces of DS40 (Dunasolar Rt) type of modules each. The total power of the system is 9,6 kWp. The principal components and data of the systems are presented in Table 1.

Table 1. The main properties of the investigated PV system

	Sub-system 1	Sub-system 2	Sub-system 3
Nom. Power; [kWp]	3,4	3,1	3,1
Total System power; [kWp]	9,6		
PV module supplier	RWE Solar	DunaSolar	DunaSolar
Module type	ASE-100 GT-FT	DS40	DS40
PV cell technology	EFG	a-Si	a-Si
P_{stc}, PV module power at STC, [W]	105	40	40
Total number of modules	32	77	77
No. of modules in series (per string)	16	7	7
No. of strings in parallel (per inverter)	2	11	11
Inverter type (Sunpower):	SP3100/600	SP2800/550	SP2800/550
No. of inverters within the Sub-system	1	1	1
Total module area; [m^2]	28	65	65

The system is installed on the flat roof of a student hostel building of the campus. The azimuth angle is 5° to East and the tilt angle is 30°, which is a good

yearly average value for the site. In Fig. 1 the picture of the two used technologies can be seen.

Figure 1. The two PV module types of system
(DS40 in the front, ASE-100 in the background)

3. The data acquisition system

As the system serves also demonstrational and research purposes, the measurement of the key quantities was carried out by a PC based data logging system. The quantities measured by the data logging system are as follows:

- Irradiation (in the panel plane by a silicon reference sensor, and the total radiation by a pyranometer)
- Temperature (environmental and module temp, for each type, Pt100 sensors)
- PV array (DC) voltage, current and power
- AC voltage, current and power supplied to the electrical grid

The connection of the analog input channels with the description of the measured quantities are shown in Fig. 2.

As the data logger computer is relatively far from the measurement points (inverter room and sensor connection boxes), signal converters were installed to the system to serve as an amplifier. The signal converters (ISC – isolated signal converter) converts all different output signals of the sensors (e.g. different voltage levels) to 4-20 mA signal, what is sent to the AD converter unit of the data logger PC.

Beside the installed own designed data logger, an authorized two way electrical meter was installed as a control unit for the energy data. The unit can store the measured data of a three month period and the data can be read out through a telephone modem (Landys Gyr, 2005).

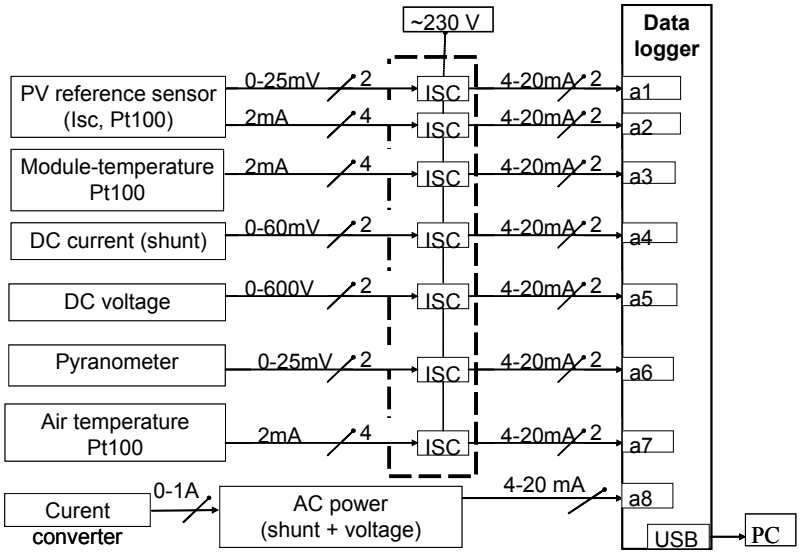

Figure 2. The input quantities of the data logger system

4. The energy production of the system

After a bit more then two years of operation some conclusions can be drawn about the energy production of the system. It can be concluded that the energy production is almost the same as it was predicted from the modelling (Seres et al., 2006). Some data are presented about this agreement in Table 2.

Table 2. Comparison of the measured and modelled energy production (in kWh)

Time period	Model, kWh	Measured, kWh
2005 oct-dec	1216	1383
2006 jan-dec	10260	10053
2007 jan-dec	10260	10325
2008 jan-jun	5 396	5 122
2005.10.08 - 2008.06. 30	27132	26883

The seasonal dependence of the energy production of the system can be seen from Fig. 3. In the figure the cumulative AC energy fed to the electrical grid by the studied system is graphed against the date.

From the figure the seasonal change of the energy curve can be seen very well, the parts with high slope (high derivative value) show the summer time with high energy production and the low slope parts the low energy productive winter times, as it can be seen from the dates.

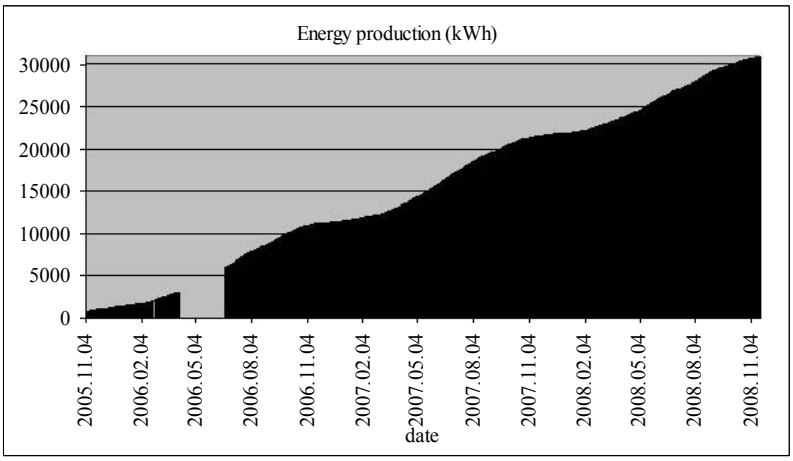

Figure 3. The cumulative AC energy production of the studied system

5. Operational consequences

As an overall notice, we can say, that the working of the system is very stable, from 8th of October, 2005 until 31 July, 2008 the the system was working through 1015 day without any problem. During the operation only two problems were noticed:

- DAS problem:
  because of an over-voltage from the grid (a lightning hit the power line somewhere out) the AD converter of the DAS went wrong.
- A fuse melted down and two subsystems went off. The cause for the fuse melting was that the minus lines of the two DS subsystems were common (Fig. 4.), and so the fuse was on its limit. (The Dc voltage is about 400 V=, the common DC power of the two DS subsystems about 6,2 kW, so the DC current is about 15,5 Amps on a fuse with a nominal current: 16 Amps. The problem was solved by replacing the fuse with a 25 Amps one.

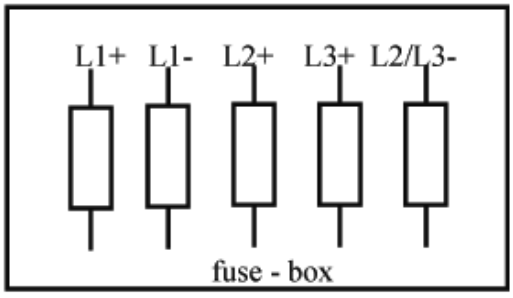

Figure 4. The scheme of the Dc fuse box

6. Comparison of the subsystems

As the system has three (but two identical) subsystems, an important question was how the system energy production is shared among the different subsystems (Seres et al., 2007). As it was described during the introduction the nominal power of the polycrystalline subsystem (Subsystem 1) is about 10 percent higher than the two other ones. The differences between the energy productions of the subsystems are measured continuously as all the subsystems are measured separately. From the data it can be seen, that subsystems 2 and 3 are working almost exactly the same way, and the power of subsystem 1 is obviously higher.

Fairly good comparison can be obtained from a long time analysis of the energy production of the subsystems. Such kinds of data are graphed in monthly distribution for the ASE and the two DS40 parts in Fig. 5.

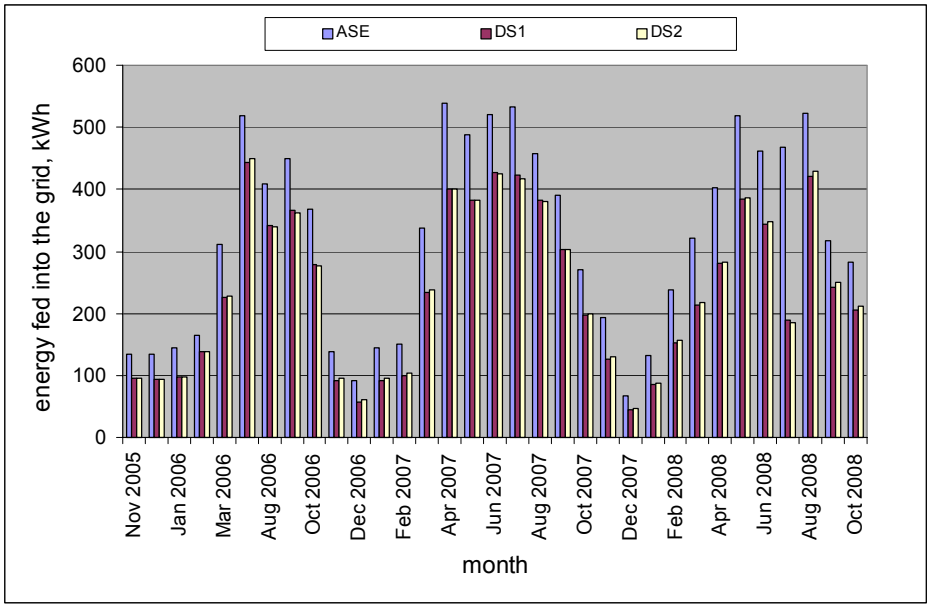

Figure 5. Comparison of the energy production of the subsystems

It can be seen from Fig 5 that each DS40 module fields are producing almost exactly the same energy, as it was planned but for the better comparison of the two DS subsystems a graph was drawn to shown the rate of their energy production (Fig. 6). From this figure a maximum 4% difference can be seen, but what is interesting, that this difference has a seasonal profile. The cause for this effect is under investigation yet, and it is thought to have some practical reasons (bigger shading for one DS40 subsystem during winter, when low radiation inclination angle occurs), as the DS40 modules showed quite homogenous behaviour during the producer test.

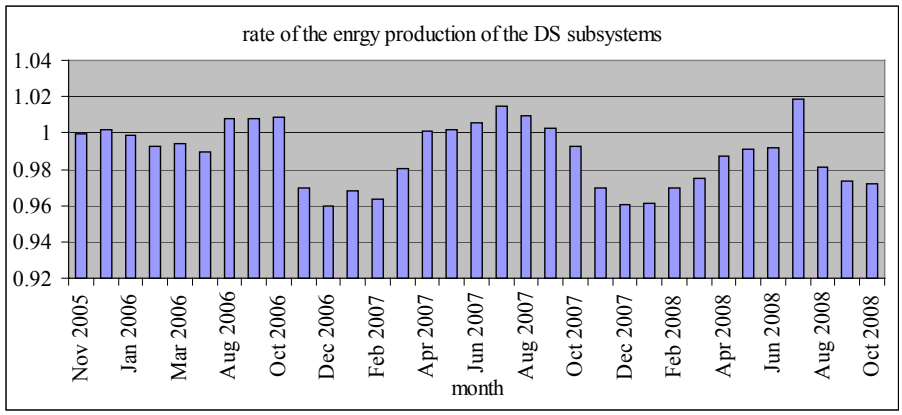

Figure 6. The comparison of the energy production of the DS subsystems

The rate of the energy production of the ASE and DS subsystems is graphed in Fig 7. From the figure it can be seen, that the ASE subsystem produced about 30% more energy than the DS, and the difference is higher in the winter time and lower in the summer time.

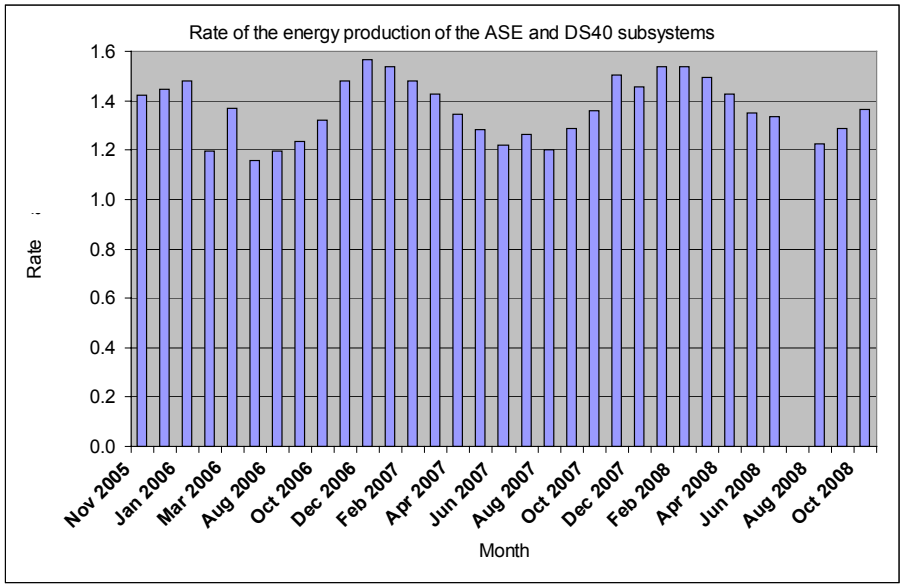

Figure 7. Energy production of ASE and a DS subsystems

6.1. Normalized energy production

As the difference in the energy production of the subsystems is partly coming from the different nominal power, a normalized energy production rate was

determined, too. In this case the normalized energy production is used as the energy production of 1 kWp nominal power part of the subsystems, so it was calculated by dividing the energy production with the nominal power of the given subsystem. The rate of the normalized energy production can be seen in Fig. 8.

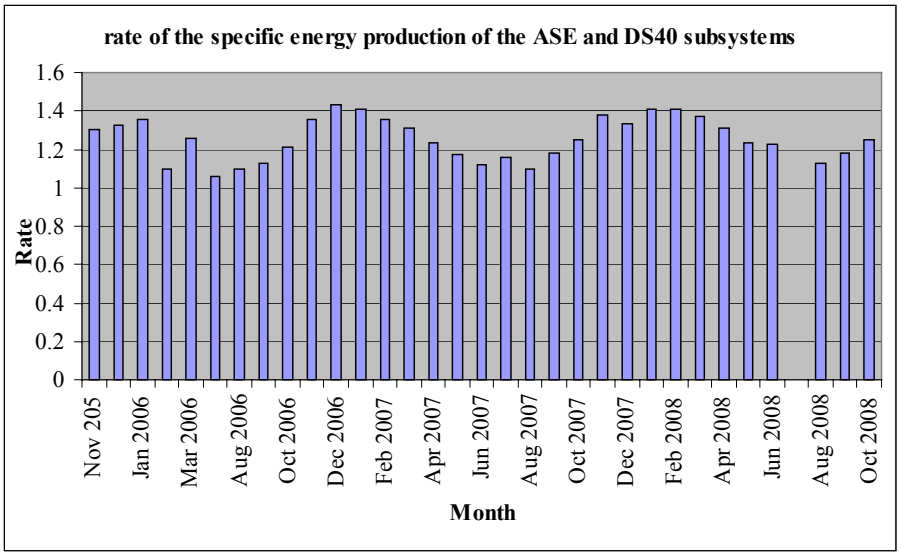

Figure 8. The rate of the normalized energy production

From the graph it can be seen, that there is a seasonal change in the energy production of the different technologies due to the different radiation conditions. The difference is smaller during the summer months (15-20%) and higher during winter time (upto 40%).

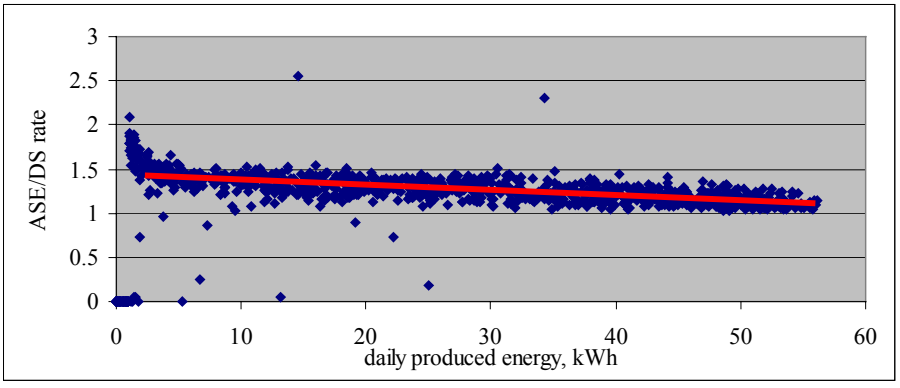

Figure 9. The dependence of the normalized energy production on the energy income

Fig. 9 shows how the rate of normalized energy production is depending on the incoming energy which was identified as the total energy production of the system.

7. Conclusions

Coincidently with the previous expectations the energy production of the two amorphous (DS) subsystems has a very slight difference (maximum difference is less then 4 percent), but the difference is systematic, showing seasonal effect. The reason of this effect is not clear yet, although there is some guess, it needs more investigations.

As it was expected the rate of the energy production of the different installed technologies (polycrystalline and amorphous silicon) shows much bigger dependence on the environmental properties (mainly on temperature) and radiation, which reflects in the seasonal production values. As the installed nominal power is different for the two technologies, the normalized energy production were used for the analysis. From the measured data of 931 days it can be concluded that during the days of low energy income the rate of the normalized energy production of the crystalline modules compared to the amorphous ones is about 10 percent higher, then for the days with higher energy income.

Acknowledgements

The research was carried out in the framework of the PV Enlargement (EC, NNE5-2001-00736) with the support of OTKA K 69094 and TE RO-9/05 projects.

References

Farkas,I., Seres,I. and Kocsis,L.: A 10 kWp photovoltaic grid connected system – Planning and checking the system components, Proceedings of ISES Solar World Congress 2005, Orlando, Florida, August 8-12, 2005, p. 6.

Landis+Gyr, MAP110 User Manual (H 71 0200 0332 c en), Lanndys+Gyr AG, 2005, Zug, Switzerland

Seres,I. - Farkas,I. - Kocsis,L.: Development of a 10 kWp photovoltaic system – installation and operational results, CD-ROM Proceedings, EuroSun 2006, 2006, Glasgow, UK, p. 6.

Seres,I. and Farkas,I.: Development of a 10 kWp photovoltaic system – efficiency analysis, Proceedings of ISES Solar World Congress 2007, Beijing, China, September 18-21, 2007, pp. 1652-1656.

Theoretical Fundaments of Crimped Closures

János BENKŐ[*], Gyula VINCZE[*] and Zsolt MAGYARY-KOSSA[**]
[*]Department of Logistics, Institute for Environmental Systems, [**]Sure Torque Európa Kft

Abstract

The control of the crimped closures sealing is a serious problem for the quality control of the producers using such closures. The sealing of this closure is ensured by the pressure of a seal-ring between the container and the crimped closure. The sealing quality depends on the applied materials, crimped force on the crimping machines and other settings. However the closing force on the sealing can not be controlled directly, just in an indirect way by measuring the torque of the crimped closures. During the research we have specified the connection between the crimp force, the remaining closing force after the relaxation and the measurable torque, and we have also developed the right instrumentation for the quality control of crimped closures.

1. Introduction

Crimped closure is primarily used for airtight closing of pharmaceutical and cosmetic industry products packaged in bottles (e.g. ampoules). Airtight closure is provided by the rubber seal placed in the filled bottle, which is usually tightened to the opening of the bottle by an easily deformable aluminium plate. A special tool, a so-called crimping head is used for crimping. The tool compresses the rubber plug and bends the aluminium lid on the lower brim of the bottle mouth. Airtight closure is provided by the compression stress remaining in the rubber plug.

2. Fundamental theory

Based on those written in the introduction, the sealing is formed between the bottle and the polymer surfaces, therefore let us introduce the main characteristics of these two materials and that of their getting into contact.

The framework of polymers is made up of carbon atoms. These are not arranged in a straight line within the polymer chain. The connecting lines between the atoms give a valence angle of 109.5^{o}. The different elements of the chain may swing by keeping up the value of the valence angle. Due to those mentioned above, polymer chains are rather flexible and in most cases are shaped like a clew. Decrease in temperature causes expansion of the chain, and vice versa. This is because heat-removal decreases the entropy of the polymer chain, and decreased entropy is coupled with a more arranged state, which in our case is the expanded condition. This means that by decrease in temperature the

elastic closing element would expand, if it was not blocked by the closing brim. However, due to the blocking a higher force is developed in it. Glass is an *n*-type semi-conductor, which means that a low number of free electrons can always be seen in it, which can couple with the oxygen atom colliding with the surface. This way, an oxygen layer with a molecular thickness may develop on its surface. However, the potential barrier between the two surfaces is thin. It is known that electrons can penetrate through a thin potential barrier with the tunnel effect. Therefore, it is possible that oxygen atoms within the crystalline region of the polymer may bind the free electrons of the glass, due to their being electron-negative. In this case an application of force develops between the ions of the polymer and the ions of the glass, due to which the two materials create a strong molecular bond along the contact surface.

If force is applied parallel to the contact surface, the ions within the layer move related to each other. In case the maximum shear stress occurring due to symmetry causes is exceeded, the surfaces slide on each other. In this case sliding friction is created. More specifically, the above mentioned concern a local contact surface. The values of $\tau_{\max}$ at the different local contact surfaces may differ according to the degree and extension of the local order. The condition of sliding is that the shear stress values generated at the local contact surfaces should exceed the value of the local $\tau_{\max}$ everywhere.

So, the condition of shear cut of the surfaces is:

$$\sum_i \tau_{\max i} \Delta A_i = F_{ny} \quad , \tag{1}$$

where F_{ny} is the force applied on shearing, ΔA_i is the i^{th} local contact surface size, and $\tau_{\max i}$ is the shear resistance on this surface. The average shear resistance can be defined from this:

$$\tau = \frac{F_{ny}}{A_{val}} = \sum_i \tau_{\max i} \frac{\Delta A_i}{A_{val}} \quad . \tag{2}$$

where A_{val} is the size of the actual contact surface.

Based on the above physical formula it can be stated, that there is an average maximum shear stress, where sliding starts. This apparently corresponds to the shear stress introduced by metallic materials. Let's find out how the size of the actual surface can be defined. The polymer is an elastic material, in our case no plastic deformation is to be taken into calculation. So the actual contact surface is created due to plastic deformation, not in the way as by metallic materials. It is also apparent that it is enough to take the deformation of the polymer into consideration, as the elastic modulus of the glass is much greater. Since the

actual contact surface is created as the resultant of deformations of small peaks, it is assumable that the ratio of the normal force compressing the surfaces and the actual contact surfaces can be given by a function *f(E,G)* made up of the elasticity (*E*) and shearing (*G*) modulus of the polymer:

$$A_{val} = \frac{F_N}{f(E,G)}. \tag{3}$$

Substituting this into formula (2), the shearing component of the friction force is given as

$$F_{nyir} = \tau \; A_{val} = \tau \frac{F_N}{f(E,G)}. \tag{4}$$

The force generated during the sliding of the surfaces on each other is the resultant of this and the cohesion force:

$$F_s = F_{nyir} + F_{koh} = \frac{\tau}{f(E,G)} F_N + F_{koh}. \tag{5}$$

shaped, where F_{koh} is the cohesion force.

In case F_{koh} is negligible by the shear force, the well-known formula

$$F_s = \frac{\tau}{f(E,G)} F_N = \mu F_N \tag{6}$$

is the result for the friction force.

3. Applying theory on the assessment of the degree of tightness

Tightness is total, if the sizes of the above introduced two surfaces are identical, that is, if

$$A_{val} = A \tag{7}$$

It is evident that this state cannot be reached in practice, since extraordinary normal force is necessary for this. Therefore, there is such a surface ratio

$$\eta = \frac{A_{val}}{A} \tag{8}$$

which corresponds to practical requirements. The question is, whether this can be related to friction force. We will show that it can. The actual surface from (8) is actually:

$$A_{val} = \eta A \tag{9}$$

From another point of view, the same from (3):

$$A_{val} = \frac{F_N}{f(E,G)} \tag{10}$$

Normal force can be expressed from (6) this way:

$$A_{val} = \frac{F_N}{f(E,G)} = \frac{F_s}{\mu f(E,G)} = \frac{F_s}{\tau} \propto F_s \tag{11}$$

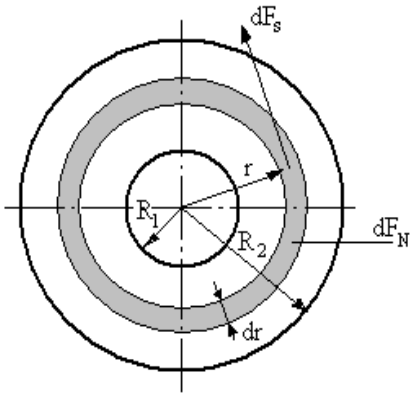

Figure 1. Relationship between the actual surface and the torque

So the measurement of the size of the actual surface can be reduced to the measurement of the friction force. The question is, whether this statement is true on the torque necessary for turning the closure element, since no friction force, but torque is measured. It will be shown that it is.

From the aspect of the generation of friction force and torque it is assumable that the polymer plug and the glass bottle get in contact along a circular ring

(*Figure 1*). dF_N normal compressing force is applied on the *dr*-thick circular ring-shaped contact surface. This force according to (4) generates

$$dF_s = \mu dF_N \tag{12}$$

friction force and

$$dM = \mu dF_N r \tag{13}$$

torque. The resultant torque generated on the sealing surface is:

$$M = \int dM = \int r\mu \, dF_N \tag{14}$$

Let the normal force compressing the surfaces be

$$f_N(r) = \frac{dF_N}{2\pi r dr} \tag{15}$$

its distribution function is known, then the resultant torque can be calculated using the relationship

$$M = \int dM = \int r\mu \, dF_N = \mu \int_{R_1}^{R_2} r \, 2\pi \, r f_N(r) dr \tag{16}$$

At the same time, according to (8) the actual contact surface is in relation with the normal force compressing the surfaces:

$$dA_{val} = \frac{dF_N}{f(E,G)} = \frac{1}{f(E,G)} 2\pi r f_N(r) dr \tag{17}$$

So even the actual surface can be calculated from the distribution function:

$$A_{val} = \int dA_{val} = \frac{dF_N}{f(E,G)} = \frac{1}{f(E,G)} \int_{R_1}^{R_2} 2\pi \, r \, f_N(r) dr \tag{18}$$

Applying the mean value theorem of integral calculus on (16), the result is as follows

$$M = \int dM = \int r\mu \, dF_N = \mu R * \int_{R_1}^{R_2} 2\pi \, r f_N(r) dr \tag{19}$$

where R^* is the defined radius value within the interval (R_1, R_2). Comparing relationships (18) and (19) the following relationship arises

$$M = \int dM = \int r\mu \, dF_N = \mu R^* \int_{R_1}^{R_2} 2\pi \, r f_N(r) dr =$$
$$= \mu R^* f(E,G) A_{val} = \tau R^* A_{val} \propto A_{val} \tag{20}$$

which is the proof for our statement.

4. Rheology and mechanical model of the closing process

Rheology in our case means that the material behaviour of the polymer plug (*Figure 2*) serving as a seal can be described as elastic and viscous behaviour. The resultant stress generated in the polymer plug is the sum of an elastic and a viscous stress:

$$\sigma = \sigma_{rug} + \sigma_{visz} \tag{21}$$

The closing process is assessed according to the mechanical substitute picture shown on *Figure 3*. On the figure, *m* is the mass of the crimping head, on which the crimping force is applied through the spring characterized by spring constant *D*. Due to the crimping force the spring suffers deformation x_1, and the polymer plug substituted with *Poyinting-Thomson*-test suffers deformation x_2.

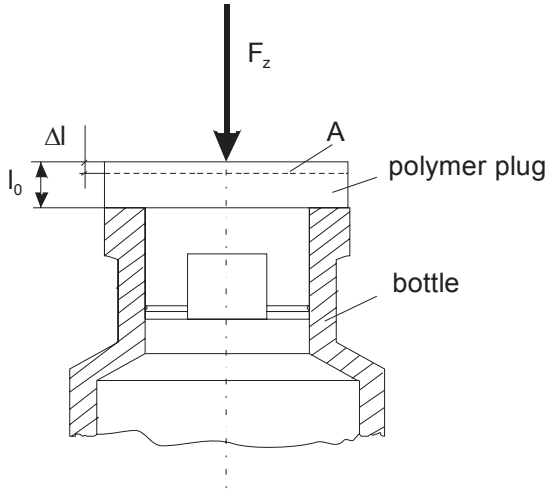

Figure 2. Simplified scheme of the polymer plug and the bottle

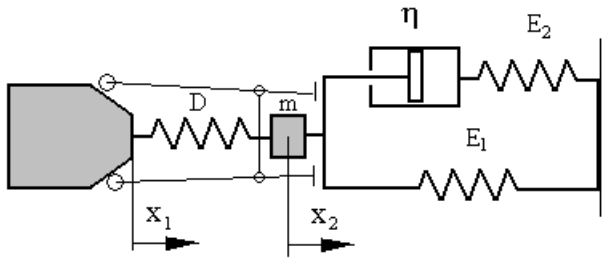

Figure 3. Mechanical model of the closing process

Applying *Newton's* 2nd axiom on the model, the differential equation

$$m\frac{d^2x_2}{dt^2} = -D(x_2 - x_1) - \sigma\ A \tag{22}$$

is given, where σ is the stress generated in the polymer plug, which can be defined from the following equation expressing the relationship between the generated stress and extension.

$$\sigma + T_2\frac{d\,\sigma}{dt} = E_1\varepsilon + E_1T_1\frac{d\,\varepsilon}{dt}, \tag{23}$$

where the time constants are:

$$T_1 = \eta\frac{E_1 + E_2}{E_1E_2},\ T_2 = \frac{\eta}{E_2}. \tag{24}$$

In this case the specific extension of the plug is given, which can be related to the displacement x_2 shown in *Figure 5*:

$$\varepsilon = \frac{x_2}{l_0}. \tag{25}$$

Using relationships (23) and (25) the following differential equation is given

$$\begin{aligned} &\frac{d^2x_2}{dt^2} + \omega_0^2x_2 + \sigma(x_2)\frac{A}{m} = \omega_0^2x_1, \\ &\sigma + T_2\frac{d\,\sigma}{dt} = \frac{E_1}{l_0}x_2 + \frac{E_1T_1}{l_0}\frac{d\,x_2}{dt},\ \omega_0 = \sqrt{\frac{D}{m}} \end{aligned} \tag{26}$$

where the time function of displacement x_1 is the known function given by the parameters of the machine. Assuming that while the machine reaches its greatest displacement, transient effects take place, then the steady displacement of the plug can be defined from the above equations:

$$x_2 = \frac{\omega_0^2}{\beta + \omega_0^2} x_1, \; where \; \beta = \frac{AE_1}{ml_0}. \tag{27}$$

According to this, the steady force generated in the plug is:

$$F_z(\infty) = \frac{AE_1}{l_0} x_2 = \frac{AE_1}{l_0} \frac{\omega_0^2}{\beta + \omega_0^2} x_1. \tag{28}$$

Dynamical behaviour of the system of equations can be tested using the *Laplace* transformation method. Using this method, the *Laplace* transformed displacement of the plug is given as

$$x_2(s) = -\frac{\omega_0^2}{s^2 + \beta \dfrac{1 + sT_1}{1 + sT_2} + \omega_0^2} x_1(s), \; where \; \beta = \frac{AE_1}{ml_0}. \tag{29}$$

5. Instruments elaborated for the measurements

In order to certify the theory introduced in the former points, measuring instruments were elaborated. *Figure 4* shows the instruments used for measuring closing force and torque. Closing force is detected by the transmitter built in the measuring cell, and the measurement sign appears on the display of the force-meter (*Figure 4/a*).

a/ closing force measuring instrument *b*/ sample holding for torque measurement

Figure 4. Instruments measuring closing force and torque

Figure 4/b shows the instrument measuring the closing element torque of the samples crimped with the known closing force. The figure shows the control panel of the torque-meter and the instrument used for clamping the sample. Due to volume causes we do not give measurement results here, but it is to be noted that they support the theoretical concepts described in details.

References

Benkő J. – Vincze Gy.: Peremezett zárások elméleti alapjai. Kutatási jelentés. Gödöllő, 2006.

Bodner, S. R.– Symonds, P. S.: Experimental and theoretical investigation of plasticdeformation of cantilever beams subjected to impulse loading. J. Appl. Mech. 29. 1962. 719-728 p.

Bowden E. P. and Tabor D.: Friction and Lubrication of Solids. Oxford University Press, London 1950.

Hult, J.: Creep in Engineering Structures. Blaisdele Publishing Co. Waltham Massachusetts, Toronto, London, 1966.

Halász L.– Molnár I.– Mondvai I.: A polimerek feldolgozásának reológiai alapjai. Műszaki Könyvkiadó, Budapest, 1978.

Harper, W. R.: How do solid surface charged? Static Electrification, Inst. Phys. Conf Ser. 4. 3-11, 1967.

Kaliszky S.: Képlékenységtan. Akadémia Kiadó, Budapest, 1975.

Lin, T. H.: Theory of Inelastic Structures. J. Wiley & Sons, Inc. New York, London, Sydney, Toronto. 1968.

Nádai, A.: Theory of Flow and Fracture of Solids. Vol. 2. McGraw-Hill Book Co., New York, London, Toronto. 1963.

Odqvist, F. K. G.– Hult, J.: Kriechfestingkeit metallischer Werkstoffe. Sringer Verlag, Berlin, 1962.

Sherwood R. S. : The Mechanism of Dry Friction. Engineering Report No. 6 of the Iowa Eng. Exp. Sta., Ames, Iowa 1951.

Wierzbicki, T.:Impulsive loading of rigid viscoplastic plates. Int. J. Solid Structures 3. 1967. 365-647 p.

Institute for Mechanical Engineering Technology

Professor Dr. Gábor KALÁCSKA
Director of the Institute

Dear Reader,

On behalf of the workers of the Institute for Mechanical Engineering Technology I'd give you a brief summary about our activity, research interests and operational structure.

The Institute for Mechanical Engineering Technology consists of three professional working areas called departments.

- Department of Material and Engineering Technology
- Department of Maintenance of Machinery
- Department of Mechatronics

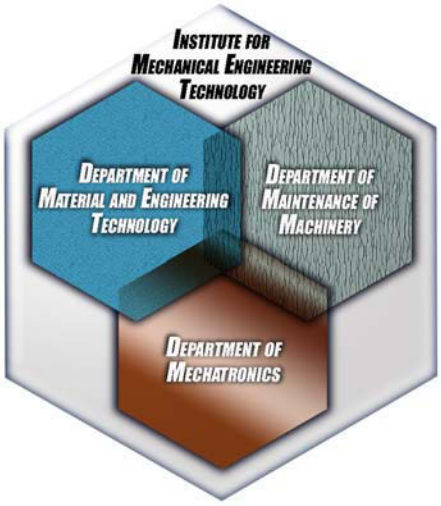

Due to the re-organization carried out some years ago of the Faculty of Mechanical Engineering the most industrial related Institute was formed under our new name.

Our education and research fields start from the material and material science through manufacturing technologies to the maintenance strategies and technologies.

Regarding year 2008 from the material science and manufacturing aspect the following topics were running:

- Topological links in two and three dimensional random structures (glass-metal atomic structure, structure of polycrystalline metals and alloys, domain structure of magnetic materials, granular structures, granulates, cell systems, carbon nano-tubes)
- Symmetry specifications of irregular geometric structures to improve reverse engineering
- Determining machining specifications with minimum lubrication (MMS) based on photon energy (increasing the efficiency of machining and reduction the role of lubricants, which cause pollution)

From the field of maintenance of machinery:

- Friction between polymer/steel gear drives (experimental control of friction during gear mesh along the action line, change of friction and efficiency during running)
- Abrasive wear, tribology of engineering polymers. (Effects of different abrasive media on new polymeric and composite materials)
- Remote maintenance model, system development and reconstructions for small airplanes

From the field of mechatronics:

- Electro-rheological fluids for the hydraulic systems (to achieve higher efficiency of hydraulic systems, new model for calculation ER fluids and experimental control of the model)

The personnel background is characterized by good international co-operation between the academic staff and titular- guest professors, industrial partners supporting the research and education activity.

More details about the Institute for Mechanical Engineering Technology are available at:

www.geti.gek.szie.hu

A New Algorithm of the Symmetry Detection on 2D Figures

Zoltán SZAKÁL, Ibolya ZSOLDOS and Isván PÁLINKÁS
Department of Material and Engineering Technology,
Institute for Mechanical Engineering Technology

Abstract

In this paper a new method is shown for the detection of exact and approximate reflective symmetry. The new algorithm is worked out for 2D case based on the fact that the symmetry axes cross the gravity centre. Accordingly the exact and approximate symmetry axes are selected from the set of the lines crossing the gravity centre. The searching algorithm is based on the definition of the so called symmetry-parameter which is a rate of the symmetry, a number between 0 and 1 without a dimension and its value does not depend on geometrical measures. The value of 1 corresponds to the exact symmetry and a value close to 1 corresponds to an approximate symmetry. A so called shape-diagram is determined from the symmetry-parameters computed for various lines crossing the gravity centre and for points surrounding it. The shape-diagram is applicable to find every exact and approximate symmetry axis. Beside this, the shape-diagram shows an individual shape property of the 2D figures, independently from geometrical measures and so it can be the base of a pattern recognition method being independent from geometrical measures.

1. Introduction

The problem of symmetry detection has been extensively studied in numerous fields including visual perception, computer vision, robotics, computational geometry and reverse engineering. Early methods concentrated on finding perfect symmetries in 2D or 3D point sets. Since the restriction to exact symmetries limits the use of these methods for real-world objects, a method was introduced for computing approximate global symmetries in 3D point sets, but the complexity of the algorithm makes it impractical for large data sets. The notion of approximate symmetry was formalized by expressing symmetry as a continuous feature. The examination of the correlation of the Gaussian image was proposed to recover global reflective and rotational symmetries. A shape descriptor was introduced that concisely encodes global reflective and rotational symmetries . Different applications based on generalized complex moments , grouping feature points, isometric transforms, planar reflective symmetry transform and generalized symmetry transform are used in image processing and mesh processing for detecting exact local and global reflection-symmetry and rotation- symmetry of 2D and 3D images.

The symmetries are often not exactly present, but only approximately present, due to measurement errors in the scanning process, and approximation and numerical errors in model reconstruction during reverse engineering. Beside this, different CAD systems often use different tolerances, and what is symmetric in one CAD system may be only approximately symmetric in another. To solve these problems new algorithms based on the B-rep model were developed to find approximate rotational and translational symmetries of 3D forms built from simple geometric units and complex 3D forms in reverse engineering.

In the most prevalent methods of symmetry detection a number of pixels are aligned to the contour. The perpendicular bisectors of various pixel pairs are regarded as hypothetical symmetry axes. The exact and approximate symmetry axes are searched from the set of the perpendicular bisectors e.g. using a symmetry map created from the parameters of the perpendicular bisectors, or optimizing the gradient orientations of pixel pairs. In this paper a new method is shown for the detection of exact and approximate reflective symmetry. The new method is worked out for 2D case based on the fact that the symmetry axes cross the gravity centre. Accordingly the hypothetical symmetry axes are the lines crossing the gravity centre and the exact and approximate symmetry axes are selected from the set of these lines. The searching algorithm is based on the definition of the so called symmetry-parameter which is a rate of the symmetry, a number between 0 and 1 without a dimension and its value does not depend on geometrical measures. A so called shape-diagram is determined from the symmetry-parameters computed for various lines crossing the gravity centre. The shape-diagram is applicable to find every exact and approximate symmetry axis. Beside this the shape-diagram shows an individual property of the 2D figures, it is independent from geometrical measures but it is characteristic of the shape of the 2D figure.

2. The algorithm

The algorithm consists of several simple steps.

We have proceeded from the fact that the symmetry axes of a 2D figure cross the gravity centre because a symmetry axis divides the figure to two coincident parts therefore a symmetry axis is a median, too. A median has to cross the gravity centre.

The algorithm scans the multitude of the lines crossing the gravity centre and studies how favourable these lines as symmetry axes are. If there is no exact symmetry axis crossing the gravity centre, a best approximate symmetry axis crossing an area surrounding the gravity centre is searched with similar method. Namely, since an exact symmetry axis crosses the gravity centre, an approximate symmetry axis has to cross an area surrounding the gravity centre.

In the followings we detail the steps of the algorithm.

Step 1: Collecting of the input data

The contour of the form is needed for the computation.

The input data set is defined as a set of points aligned to the contour. Such a point set can be created by the use of different tools of electronic image processing e.g. the MatLab. In order to decrease the measure of the point set file and the run time of the algorithm, the point set can be optimized: the points can be fixed rare or thickened depending on the complexity of the geometry. Fewer points are needed at greater curvature and more points are needed at smaller curvature, Figure 1. Such an optimization of the input point set is not required, but if we perform it, it can speed the run of the computer codes. The original contour is approximated with the stretches determined by these points. We name these stretches as perimeter stretches.

The input of the algorithm is the table of the points. The points follow each other in a clockwise direction. Such a table can be created manually and also recorded digitally from a pixel set.

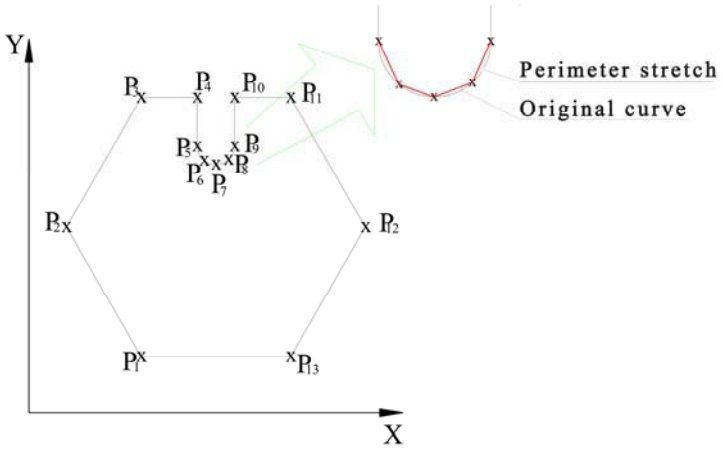

Figure 1. Collecting of points (P_i) on the boundary.

Step 2: Determination of the gravity centre

We determine the gravity centre of the 2D figure with the method used in the geographic information systems. In order to compute the area of the 2D figure trapeziums are defined so that the points aligned to the contour are projected to the horizontal axis of the coordinate system, Figure 2.

The area of the i^{th} trapezium is:

$$A_i = \frac{(x_{i+1} - x_i) \cdot (y_{i+1} + y_i)}{2} \tag{1}$$

where (x_i , y_i) and (x_{i+1} , y_{i+1}) are the end points of the i^{th} perimeter stretch.

The points have to follow each other in a clockwise direction, in contrary case a negative value is derived for the area. The coordinate system is defined so that if the 2D figure is revolved around the gravity centre it always has to remain in the first plane quarter.

The area of the 2D figure is the sum of the areas of the trapeziums:

$$A = \sum_{i=1}^{n} \frac{(x_{i+1} - x_i) \cdot (y_{i+1} + y_i)}{2} \tag{2}$$

where n is the number of the trapeziums.

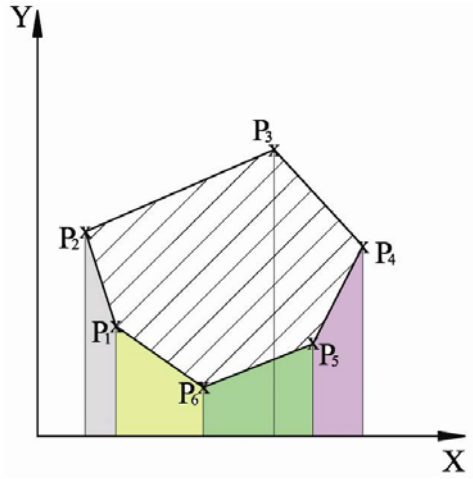

Figure 2. Definition of trapeziums for the computation of the area in the example of a hexagon.

The coordinates of the gravity centre are determined in general case by

$$x_g \cdot A = \int_A x \cdot dA \tag{4}$$

$$y_g \cdot A = \int_A y \cdot dA \tag{5}$$

In our case (because of the trapeziums) the integration reduces itself to a simple summing up:

$$x_g = \sum_{i=1}^{n} \left[(y_i - y_{i+1}) \cdot \frac{\left(x_i^2 + x_i \cdot x_{i+1} - x_{x+1}^2\right)}{6 \cdot A} \right] \tag{5}$$

$$y_g = \sum_{i=1}^{n} \left[\left(x_{i+1} - x_i \right) \cdot \frac{\left(y_i^2 + y_i \cdot y_{i+1} - y_{x+1}^2 \right)}{6 \cdot A} \right] \tag{6}$$

Step 3: Scanning

The vertical line crossing the gravity centre is regarded as symmetry axis in the case of an optional starting orientation of the 2D figure, Figure 2. The algorithm analyses whether the 2D figure is symmetric for this hypothetical symmetry axis. For this purpose the algorithm scans the figure with horizontal lines (so called 'measuring lines') following each other with equal distances, Figure 3. The hypothetical symmetry axis is vertical and the measuring lines corresponding to the scanning levels are perpendicular to the axis namely they are horizontal.

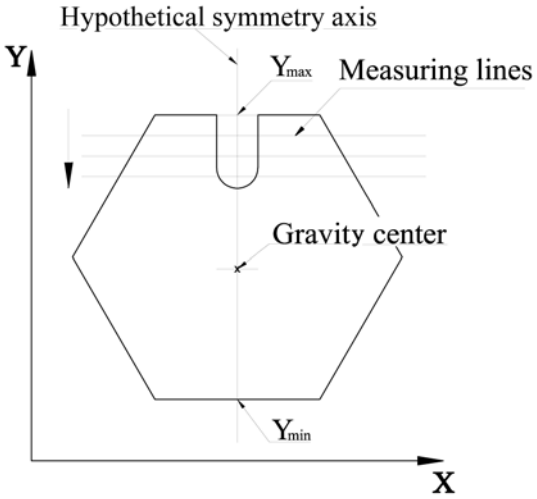

Figure 3. The horizontal measuring lines

In the course of the scanning the so called measuring stretches are determined. A measuring stretch is the distance between the vertical hypothetical symmetry axis and the intersection of a measuring line and a perimeter stretch. In Figure 4 'l' and 'r' are the measuring stretches. In a horizontal scanning level there could be more measuring stretches, as well.

The complete area of the 2D figure is scanned with measuring lines proceeding from up to down, from the maximum (Y_{max}) to the minimum (Y_{min}) vertical coordinate of the points aligned to the contour. The accuracy of the method depends on the distance between the measuring lines: the shorter the distance is the more accurate the result is, however it affects the running time of the computer code as well.

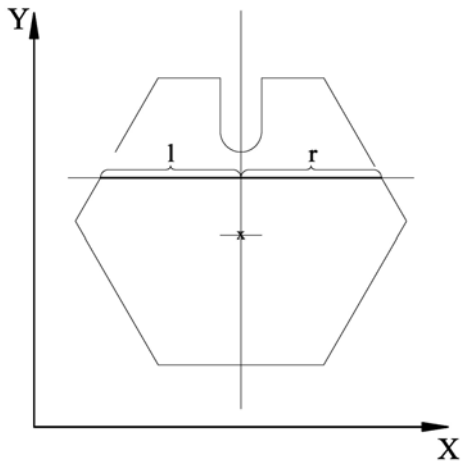

Figure 4. Definition of the measuring stretches in a simple case

Step 4: Computing the symmetry parameter

The symmetry parameter Z shows the deviation from the perfect symmetry numerically. This value between 0 and 1 can be a rate of the symmetry. In order to define it we introduce first a Z_k parameter for the k^{th} scanning level. In the simplest case when there is one measuring stretch on the left and on the right side of the hypothetical symmetry axis, Figure 4, Z_k can be computed simple:

$$Z_k = 1 - \frac{abs(l - r)}{L_{max}} \tag{7}$$

where:
'l' is the measuring stretch on the link side of the symmetry axis,
'r' is the measuring stretch on the right side of the symmetry axis,
L_{max} is the maximum of the measuring stretches in the course of the scanning.
Z_k is defined so that:

- Z_k=1 if l=r when the k^{th} scanning level is symmetrical to the hypothetical symmetry axis,
- Z_k=0 if l=0 and r>0, or r=0 and l>0 when a measuring stretch does not have a pair on the other side of the hypothetical symmetry axis which is the worst case regarding the symmetry,
- $0<Z_k<1$ when l>0 and r>0 and the figure is not symmetrical to the hypothetical symmetry axis, and the closer this value is to 1 the better the k^{th} scanning level approximates the exact symmetry.

Since a ratio of lengths is used in (7) Z_k is a number without a dimension and its value does not depend on the measures.

If there are more than 2 measuring stretches in a scanning level (l_1, l_2, …, l_n on the left side and r_1, r_2, … , r_m on the right side of the hypothetical symmetry axis,

Figure 5) then l_i and r_i are ordered into pairs and Z_k is defined according to (8). Let us assume that there are more measuring stretches on the left side: n>m. In this case the pairs have to be defined so that r_i=0 for every l_i i=m+1, m+2, … , n. In general case Z_k is computed as the average of the expression defined by (7) from the pairs:

$$Z_k = \frac{1}{n}\sum_{i=1}^{n}\left(1 - \frac{abs(l_i - r_i)}{L_{\max}}\right) \tag{8}$$

where n is the number of the pairs in a scanning level.

The symmetry-parameter Z is defined as the average of Z_k:

$$Z = \frac{\sum_{k=1}^{N} Z_k}{N} \tag{9}$$

where N is the number of the scanning levels (measuring lines) from Y_{max} to Y_{min}.

Since Z is defined with averages according to (7), (8) and (9), Z keeps the original properties of Z_k:

- the value of Z can change between 0 and 1,
- Z=1 is the case of an exact symmetry,
- Z=0 is the worst case regarding the symmetry (e.g. the full figure is on the left side of the axis),
- in the case of 0<Z<1 the closer the value is to 1 the better the figure approximates the exact symmetry,
- Z is a number without a dimension, it does not depend on the measures, it depends only on the shape.

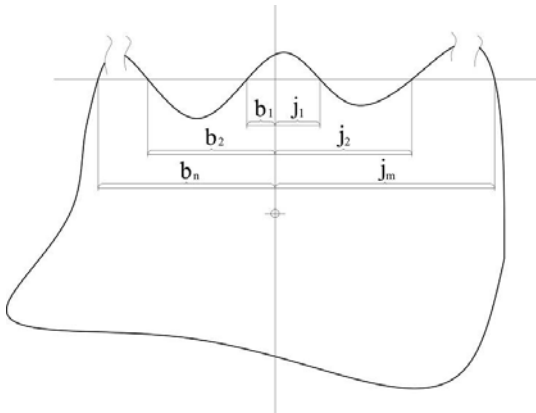

Figure 5. Definition of Z_k in general case

Step 5: Rotation of the geometry
After the determination of the symmetry-parameter for the starting orientation the 2D figure is scanned by rotating the hypothetical symmetry axis, as well. The computation is simpler if the hypothetical symmetry axis is fixed vertically and the figure is rotated with small angles, step by step, Figure 6. The accuracy of the computation depends on the steps (angles) of the rotation. After every step of rotation the symmetry-parameter is computed.

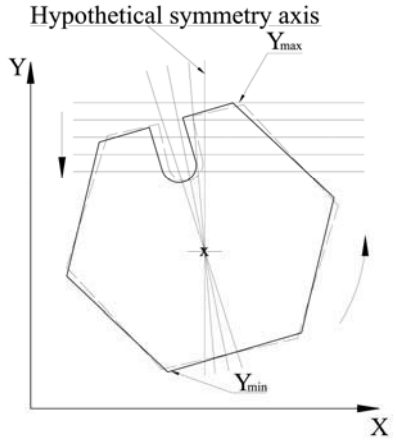

Figure 6. Rotation of the 2D figure with small angles

The method scans the entire 2D figure in such a way that it rotates the examined figure by 180 degrees. Since the algorithm examines the figure both above and below the gravity center, the rotation by 180 degrees means a complete coverage.

Step 5: Evaluation of the results
The symmetry-parameter Z is computed for every rotational step. The values of Z are saved together with the angles of rotation. After the full (180^0) rotation a diagram is drawn where the independent variable is the angle of rotation and the dependent variable is Z. From this diagram the results can be evaluated. Let us name it shape-diagram. Exact symmetry exists where Z=1 and the closer Z is to 1 the better the figure approximates the exact symmetry at a given angle.

The shape-diagram of a square can be seen in Figure 7. The lines signed with numbers (1, 2, 3, 4) are the exact symmetry axes of the square and accordingly these correspond to the angles of rotation where Z=1 ($\alpha=0^0$ or 180^0, $\alpha=45^0$, $\alpha=90^0$ and $\alpha=135^0$).

The shape-diagram shows an individual property of the 2D figures. Since Z is independent of geometrical measures the shape-diagram is a shape parameter of the 2D figures (therefore the name is ‘shape-diagram’). The shape-diagram is the

same for similar 2D figures having different measures. But if there is a smallest change on the shape of the 2D figure the shape-diagram changes, as well.

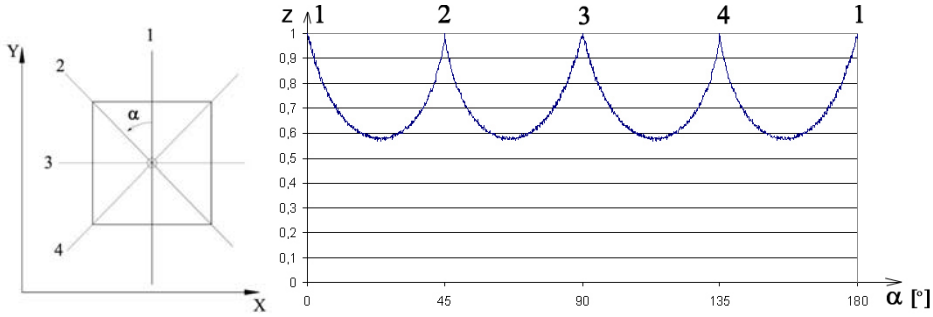

Figure 7. The definition of the shape-diagram

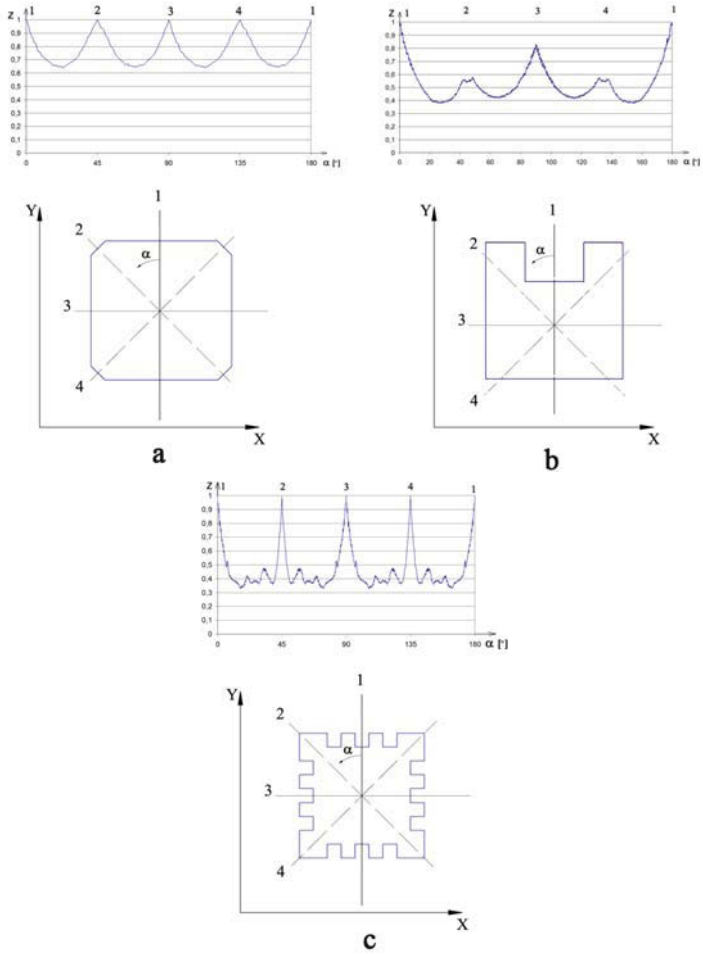

Figure 8. Shape-diagrams for modified squares

We show examples for the individuality of the shape-diagram in Figure 8. Three variously modified squares can be seen and the shape-diagrams are different, as well. In Figure 8a the corners of the square are cut, the number and the place of the original symmetry axes have not changed but the minimum values have increased from Z=0.58 to Z=0.65. In Figure 8b a part of the square is cut out, only 1 symmetry axis has remained and a weakly approximate symmetry axis signed with number 3 can be found at a local maximum of the diagram. The other two local maximums signed with number 2 and 4 correspond to only very weakly approximate symmetry axes. In Figure 8c several small parts are cut out from the square, the exact symmetry axes have not changed but the curve between the maximums is basically other.

The algorithm does not have limits in 2D case. It is applicable even if the contour consists of several closed loops. In Figure 9 a circle with two holes can be seen.

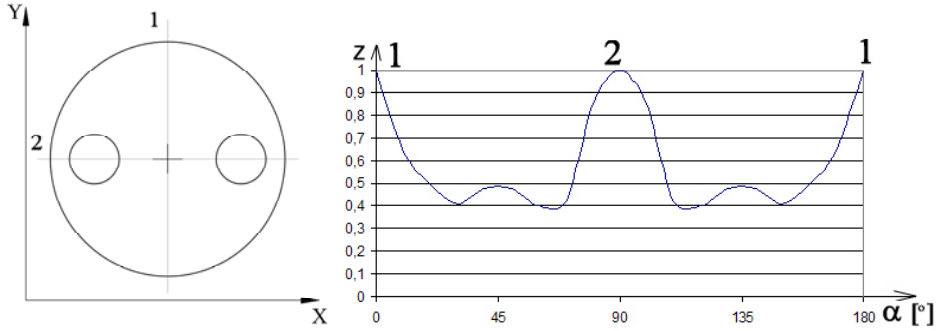

Figure 9. Example of a 2D figure having a contour with several closed loops

It is obvious that the shape-diagram is the constant 1 function in the case of a circle because every line crossing the centre is an exact symmetry axis. Since there are two holes on the circle in Figure 9 accordingly there are only two exact symmetry axes signed with number 1 and 2 where Z=1.

There was an exact symmetry axis in every example shown above, i.e. Z=1 value(s) could be found in every shape-diagram computed for the lines crossing the gravity centre.

But in the case when there is no exact symmetry axis, it is not sure, that the best approximate symmetry axis can be found in the lines crossing the gravity centre. However we can assume that the best approximate symmetry axis has to pass near by the gravity centre in the case of approximate symmetrical 2D forms. In this case it is advisable to repeat the Steps 3-5 so that the shape-diagram is created for the points surrounding the gravity centre, as well. For the best approximate symmetry axis we have to search the shape-diagram where the maximum Z value can be found.

3. Example in the human therapy

We emphasize the significance of the study of symmetry properties on an example in the human therapy.

There are accidents when the skull is injured significantly. In the course of the reparation a prosthesis is designed and manufactured before the operation. During the design the 3D CAD model of the prosthesis is created using the model of the part remained unhurt. The design process can not be performed automatically because every injury is different. A unique design is needed where the symmetry plane (or rather the approximate symmetry plane) needs to known. Knowing the symmetry plane the prosthesis model can be created by a simple reflection.

Since our algorithm works for 2D figures we show the symmetry detection on a plane section of the skull in the following example.

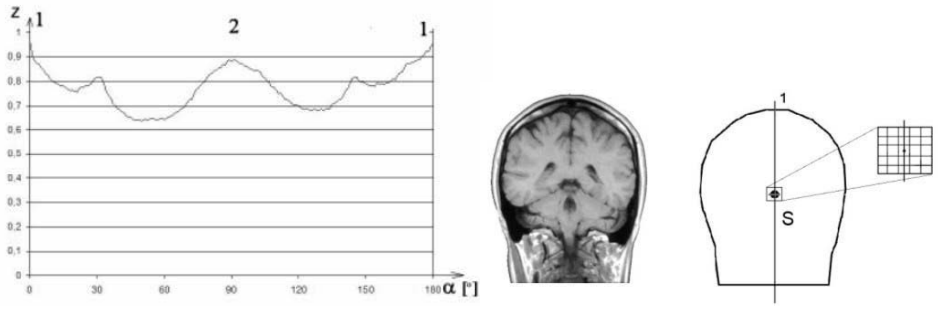

Figure 10. The shape-diagram computed from an MR photograph of the skull

In Figure 11 the study of an MR photograph of the skull can be seen. We have fixed 20 points along the external contour as input data of our algorithm. We have computed the shape-diagram for 6x6 points as a grid around the gravity centre as it can be seen in the enlarged detail in Figure 11. The best approximate symmetry axis (the maximum value of Z) was found in the shape-diagram computed for the gravity centre shown in Figure 11. In this shape-diagram we have got the local maximum in two places. In the position denoted by number 1 Z=0.95, thus, it is close to 1. The corresponding approximate symmetry axis is denoted by number 1. It is remarkable that even in the position denoted by number Z=0.97 which is less considered to be approximate symmetric.

4. Summary

The new algorithm gives a new possibility to detect exact and approximate symmetry axes of 2D figures. Beside the known methods of symmetry detection

the new algorithm define the so called symmetry-parameter which can be a rate for the symmetry using a parameter between 0 and 1.

The shape-diagram created from the values of the symmetry-parameter computed for various lines crossing the gravity centre is independent from geometrical measures and it shows an individual, characteristic shape property of the 2D figures, which can be the base of a pattern recognition independent from geometrical measures.

Acknowledgements

This work was supported by OTKA grants K 73776 in Hungary.

References

Wolter, J.,Woo, T., and Volz, R. 1985. Optimal algorithms for symmetry detection in two and three dimensions. The Visual Computer.

Atallah, M. 1985. On symmetry detection. IEEE Trans. On Computers 34, 7, 663–666. 2004.

Alt, H.,Mehlhorn, K.,Wagener, H., and Welzl, E. 1988. Congruence, similarity and symmetries of geometric objects. Discrete Comput. Geom. 3, 237–256.

Zabrodsky, H., Peleg, S., And Avnir, D. 1995. Symmetry as a continuous feature. IEEE PAMI 17.

Sun C, Sherrah J. 3D symmetry detection using the extended Gaussian image. IEEE Transactions on Pattern Analysis and Machine Intelligence 1997;19(2):164–8.

Kazhdan, M. M., Chazelle, B., Dobkin, D. P., Finkelstein,A., and Funkhouser, T. A. 2002. A reflective symmetry descriptor. In Proceedings of ECCV, 642–656.

Kazhdan, M., Funkhouser, T., and Rusinkiewicz, S.2004. Symmetry descriptors and 3d shape matching. In Symposium on Geometry Processing, 116–125.

Shen D, Ip H, Cheung K, Teoh E. Symmetry detection by generalized complex (GC) moments: A close-form solution. IEEE Transactions on Pattern Analysis and Machine Intelligence 1999;21(5):466–76.

Loy G, Eklundh J. Detecting symmetry and symmetric constellations of features. In: ECCV 2006, Part II. LNCS, vol. 3952. Springer-Verlag; 2006. p. 508–21.

Mitra N, Guibas L, Pauly M. Partial and approximate symmetry detection for 3D geometry. ACM Transactions on Graphics 2006;25(3):560–8.

Mitra N, Guibas L, Pauly M. Symmetrization. ACM Transactions on Graphics 2007. 26(3): Art. No. 63

Martinet A, Soler C, Holzschuch N, Sillion FX. Accurate detection of symmetries in 3D shapes. ACM Transactions on Graphics 2006;25(2): 439–64.

Podolak J, Shilane P, Golovinskiy A, Rusinkiewicz S, Funkhouser T. A planar-reflective symmetry transform for 3D shapes. ACM Transactions on Graphics 2006;25(3):549–59.

Reisfeld D, Wolfson H, Yeshurun Y. Context Free Attentional Operators: the Generalized Symmetry Transform. Int. J. Comput. Vision 1995; 14(2):119-130.

Li W.H, Zhang A.M, Kleeman L. Global reflectional symmetry detection for robotic grasping and visual tracking, ACRA 05, Australasian Conference on Robotics and Automation, 2005.
http://www.visionbib.com/bibliography/journal/acr.html#ACRA05

Varady T, Martin R, Cox J. Reverse engineering of geometric models – an introduction. Computer-Aided Design 1997;29(4):255–68.

Pratt M, Anderson B, Ranger T. Towards the standardized exchange of parameterized feature-based CAD models. Computer-Aided Design 2005; 37(12):1251–65.

Mills B, Langbein F, Marshall A, Martin R. Approximate symmetry detection for reverse engineering. In: Proc. 6th ACM symp. solid and physical modeling. 2001. p. 241–8.

Li M, Langbein F, Martin R. Detecting approximate symmetries of discrete point subsets.

Friction of Polymer/Steel Gear Pairs

Róbert KERESZTES, László ZSIDAI, Gábor KALÁCSKA,
Mátyás ANDÓ and Rajmund LEFÁNTI
Department of Maintenance of Machinery, Institute for Mechanical Engineering Technology

Abstract

Engineering plastics are often applied in tribological systems, where moving parts are subjected to severe friction and wear processes. Compared to metals engineering plastics are used because of their good friction and wear properties together with increased corrosion resistance and vibration damping ability. There are many sorts of technical polymers available of which sliding elements can be produced. To choose proper polymers for a given tribological application is not a simple task owing to many different parameters influencing the performance of a polymer sliding element.

1. Introduction

In many cases investigations on rigs in laboratory have to be used to reveal the tribological properties of different polymer/metal pairs. In our institutes also many investigations on the tribological properties of technical polymer/steel pairs were performed using different tribometers. It was stated that the ranking of polymer/steel pairs alters according to the friction and wear measured on different tribometers, therefore it would be difficult to choose the best polymer/steel pair to make a polymer gear for a given application. We started to approach of gear mesh with a real gear tests. We concluded that the change of the coefficient of friction during the meshing and the misalignment of gears made difficult to evaluate the actual friction coefficient between the teeth of polymer/steel gears. This problem was solved with the following test system.

2. Formulations

The common normal to the tooth profile at the point of contact must always pass through a fixed point called the pitch point in order to maintain a constant angular velocity ratio of the two gears. The involute curve satisfied the law of gearing and is most commonly used for gear teeth profiles in the practice. Data of connecting involute profile gears:

tooth number:	$z_1 = z_2 = 12$
module:	m = 10 mm
pressure angle:	$\alpha = 20\ °$
face width:	b = 5 mm (at polymer segment gear)

We can see from the data, that the used gears are undercut. We chose these gears with large module, because we can measure clearly the changing of force through line of connection. The forces arising from sliding and rolling tooth connection. Therefore we had to modify the addendum circle diameter. The value of maximal addendum circle diameter (d_{fmax}):

$$d_{f\,max} = 2 \cdot \sqrt{\left(a_w \cdot \sin\alpha\right)^2 + \left(\frac{d_o}{2} \cdot \cos\alpha\right)^2} \quad [mm] \tag{1}$$

where:
a_w – applied center distance [mm]
d_o – pitch circle diameter [mm]
α – pressure angle [°]

The calculated engagement factor (ε) with modified addendum circle diameter:

$$\varepsilon = \frac{\overline{AE}}{p_w \cdot \cos\alpha} \tag{2}$$

where:
AE – length of connection section
(A – the first, E - the last connection point) [mm]
p_w – base pitch [mm]

$$\overline{AE} = \rho_{a1} + \rho_{a2} - a_w \cdot \sin\alpha \tag{3}$$

where:
ρ_{a1} – radius of involute curvature of drive gear at E point [mm]
ρ_{a2} – radius of involute curvature of driven gear at A point [mm]
a_w – applied center distance [mm]

$$p_w = \pi \cdot m \tag{4}$$

where:
m – module [mm]

$$\rho_a = \sqrt{r_f^{\,2} - r_a^{\,2}} \tag{5}$$

where:
r_f – addendum radius [mm]
r_a – base radius [mm]

The allowable tangential force F_{tomax} (N) at the pitch circle of polyamide spur gear can be obtained from the Lewis formula. However, the basic equations used are applicable to all other plastic materials if the appropriate values for the factors are applied.

$$F_{to\,max} = m \cdot y \cdot b \cdot \sigma_b \cdot K_v \quad [N] \tag{6}$$

where:
m – module [mm]
y – form factor at pitch point
b – face width [mm]
σ_b – allowable bending stress [N/mm^2]
K_v – speed factor

The values of different factors can be found in the tables.

The surface strength using Hertz contact stress, σ_H, is calculated by this equation

$$\sigma_H = \sqrt{\frac{F_{to}}{b \cdot d_o} \cdot \frac{i+1}{i}} \cdot \sqrt{\frac{1.4}{\left(\frac{1}{E_1} + \frac{1}{E_2}\right) \cdot \sin 2\alpha}} \quad [N/mm^2] \tag{7}$$

where:
F_{to} – tangential force on surface [N]
I – gear ratio
E_1,E_2 – modulus of elasticity of material [N/mm^2]
A – pressure angle [°]

The arising sliding velocity between contact teeth is difference of the tangential velocities (v_t).

The sliding velocity determine the frictional heating and wear of teeth.

The v_s sliding velocity:

$$v_s = v_{t1} - v_{t2} \text{ or } v_s = s \cdot (\omega_1 + \omega_2) \tag{8}$$

where:
s – distance between pitch point and contact point on line of action [mm]
ω_1, ω_2 – angular velocity [rad/s]

Kozma earlier studied the friction phenomena between the gears and found that the forces and torque during the connection changed due to the friction. He distinguished two cases: the change of the teeth-force and torque in case of constant drive torque, and the change of teeth-force and torque in case of constant driven torque. In his theoretical studies he took constant friction between the surfaces, however we know from our previous research projects and from the literature that the friction between a polymer and steel surfaces was nearly never constant.

3. The test systems

We made a new gear connection test rig. The new test method (*Fig. 1.*) using large teeth was developed to measure the influence of friction on the tooth forces. In this method the rotation is limited; the variation of forces is measured during only one meshing cycle of a tooth pair. The three-teethed segments were made of the investigated polymers, but the mating steel gear must be prepared in full size due to balancing reasons.

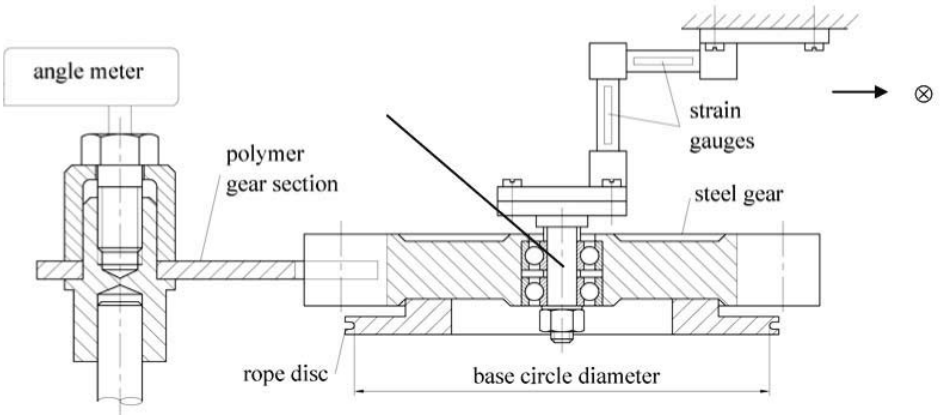

Figure 1. Drawing of test rig

3.1. Measured and calculated forces

The forces on the axe l of steel gear (F_x, F_y) were measured with strain gauges, as it is shown in *Fig. 1.* The normal force (F_N) was equal the applied load force (F_g), because each line of forces were same.

If we consider the effect of friction along the connection section, it's clear that the direction of friction force changes at the pitch point. In this article we focus on this change limiting to the one tooth connection phase.

There are two different section under one tooth connection. The pitch point (C) is in the center position. The value of normal force is equal to load force $F_n=F_g$ [N]. There is a relationship between the friction force and the measured axle force (*Fig. 2.*). The axle force increasing until pitch point and decreasing after it. We can evaluate their relationship using the following equations:

in BD connection section:

$$F_x=F_s \cdot \cos\alpha \tag{9}$$

where:
F_x – measured axel force [N]
α – pressure angle [°]
F_s – friction force [N]

$$F_s = \frac{F_x}{\cos\alpha} \quad [N] \tag{10}$$

In this system we define a coefficient of friction between contact teeth. It is calculated by this equation.

$$\mu = \frac{F_s}{F_n} = \frac{F_x}{F_n \cdot \cos\alpha} \tag{11}$$

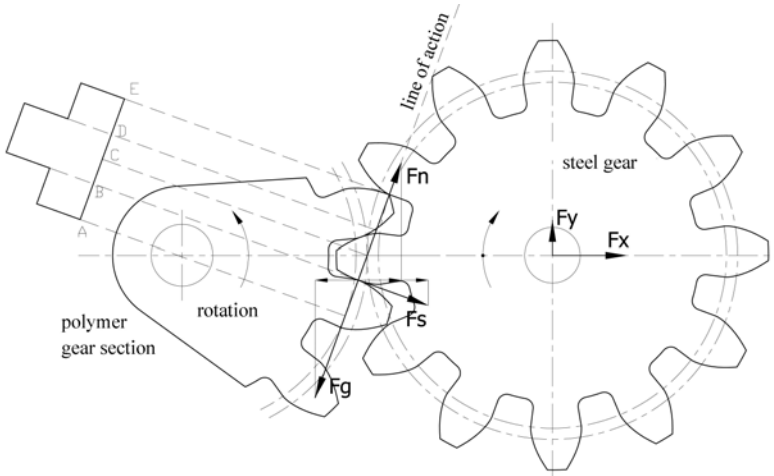

Figure 2. The arising forces at one tooth connection

At the *table 1.* we show the testing conditions.

Table 1. Parameters of the tests

Parameters	Tooth connection model tests
load, M [Nm]	1.1 / 5.5
angular velocity, ω [1/s]	0.1
test time, cycle	1 / 100 / 500 / 1000 / 2000 cycles
ambient temperature, T [°C]	24 °C
Relative humidity, RH [%]	50 %

3.2. Tested materials

The properties of the investigated polymers are presented in the *Table 2.* The gear mating with polymer gears was made of structural steel S355 with a surface finish (CLA) R_a 2,5 μm.

Table 2. Properties of investigated polymers

Polymer	Elongation at rupture A (%)	Young modulus E (MPa)	Rockwell M hardness	Tensile strength R_m (MPa)
PA 6G-Mg	40	3000	86	85
PA 6G-Na	25	3300	88	80
PA 66 GF30	7	5200	98	185
POM C	30	3000	86	70
PETP /PTFE	8	3200	94	75
Bakelite		7000	98	80

4. Results and discussion

Because of the large number of experiments and continuous monitoring of gear mesh friction many different graphs can be drawn about teeth surface processes.

As we have explained earlier in the test system the motion of the measurements were reciprocating (towards – upload, backwards –down load) between the mating teeth and from each cycle the upload process under „one-tooth" connection was grabbed to evaluate.

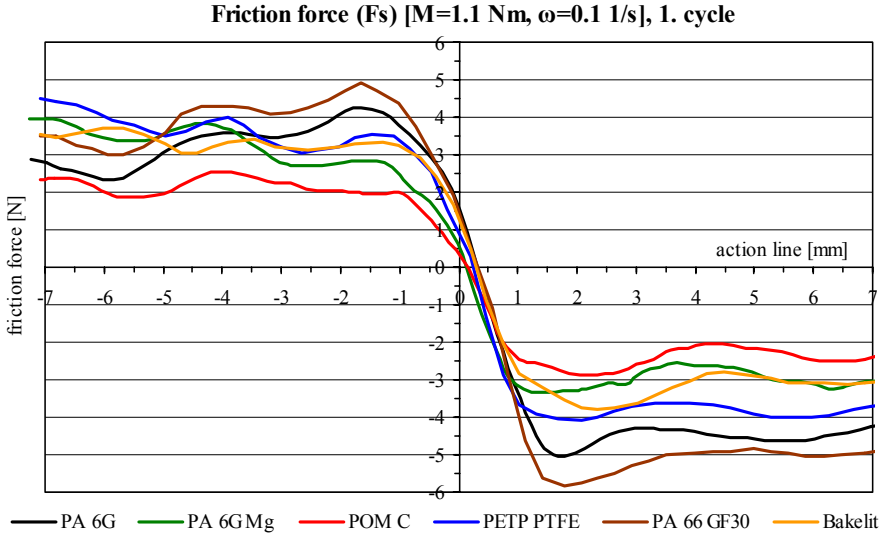

Figure 3. Friction forces during the first test cycle

Fig.3. shows a summary about the measured friction force during the first cycle of drive in case of six different polymer materials mashing with S355 structural steels. The role of pitch point is very spectacular.

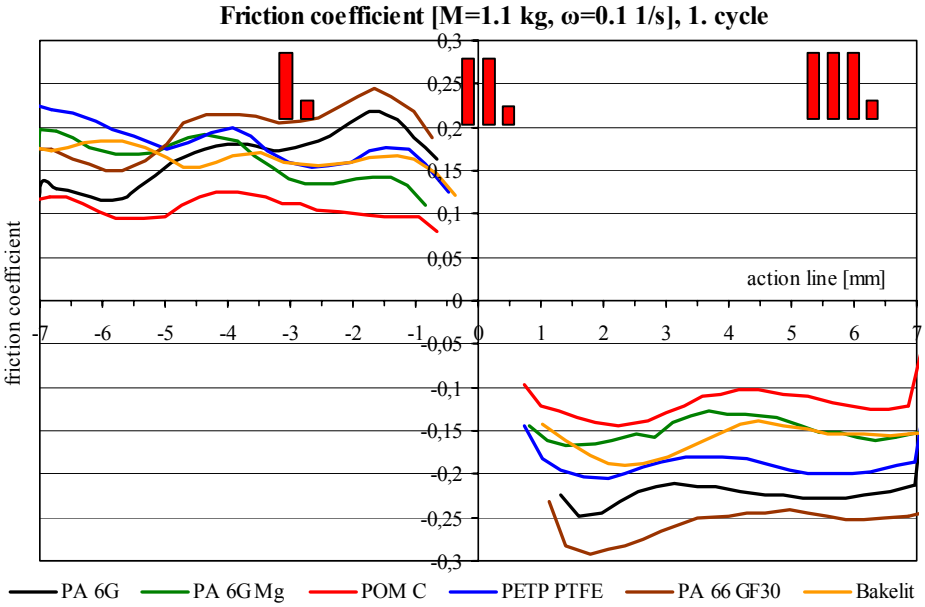

Figure 4. The calculated friction coefficients during the first test cycle

At the beginning of the measurements the POM-C performed the lowest friction and PA 66 GF30 gave relatively high friction force. If we compare the two cast polyamide versions - Na and Mg catalytic types – essential difference can be realized. The Mg catalytic cast polyamide 6 material is better performing much lower friction force.

In Fig.4. the calculated friction coefficients are shown. The main difference between the curves plotted in Fig 3. and Fig.4. is the domain. While friction forces are drawn as continuous functions along action line, curves of friction coefficients are interrupted at pitch point and its transition zone. The reason is the origin of friction movement. At pitch point and its transition zone the dominant form of friction is rolling instead of sliding. Before and after pitch point zone the friction is generated mainly from sliding, the rolling friction effect is much lower.

That means along the action line the friction form van be split to:

I. sliding zone before pitch point with decreasing sliding speed to reach pitch zone
II. pitch transition zone with mainly rolling movement
III. sliding zone after pitch point with increasing sliding speed leaving pitch zone

For further evaluation of gear mesh friction coefficient curves we introduce more values according to Fig. 5.

As an example of the evaluations Fig.6. shows the change with cycle numbers of local maximum friction coefficient values for the different polymer materials.

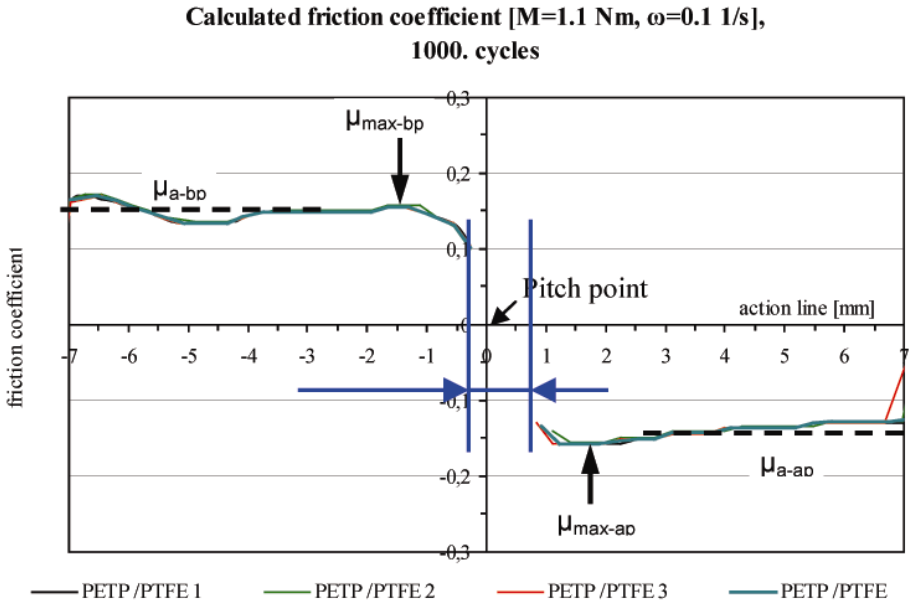

Figure 5. The calculated friction coefficients during the first test cycle
($\mu_{a\text{-}bp}$: average friction coefficient before pitch zone,
$\mu_{max\text{-}bp}$: local maximum of friction before pitch zone,
$\mu_{max\text{-}ap}$: local maximum of friction after pitch zone,
$\mu_{a\text{-}ap}$: average friction coefficient after pitch zone)

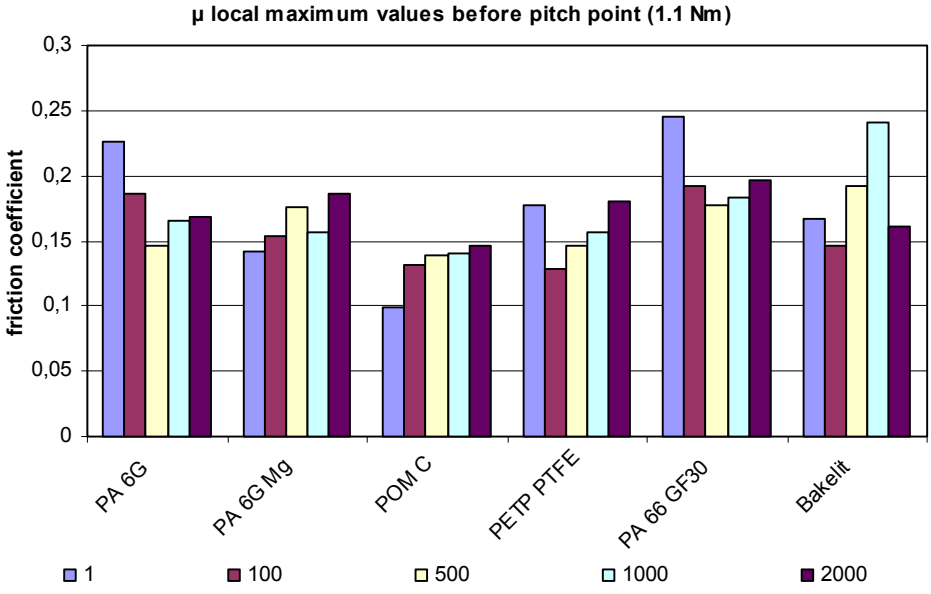

Figure 6. Local maximum values of friction before pitch zone
under different cycle numbers

If we follow the different behaviour of friction values in the function running distance (number test cycles) we can distinguish four different groups.

1. Materials performing basin-like curves or columns (PA 6G, PETP/PTFE, PA 66 GF30, in Fig 6.): with increasing meshing time the friction first decreasing but after a certain running cycle it starts to elevate.
2. Material with continuously increasing friction with increasing meshing time (POM C in Fig 6.): according to the test condition (load and speed) the function of friction increasing with different slopes during the gear mesh.
3. Material with low difference increasing tendency (PA 6G Mg)
4. Stochastic-like friction results with large differences in friction coefficients (bakelite)

Regarding the absolute values of friction coefficient in *Fig 9*. we can find POM C and PETP/PTFE the best ones. Comparing the two cast polyamide types we can state that the Na catalytic cast Pa (PA 6 G) performed higher friction than PA 6 G Mg.

5. Conclusions

- The developed test method is useful to study the friction process along the action line under „one-tooth" connection phase between polymer/steel gears.
- The theoretical friction can be discovered more in depth and described with a given friction pairs.
- The friction changes along the action line.
- The trends also change in the function of load and meshing time (test cycles)
- Different changing trends of friction means different change of efficiency of polymer/gear drive. In our database we set these trends.
- Pitch point rolling effect in the practice means pitch zone. The width of the pitch zone is different with different friction pairs due to the different adhesion and deformation.
- The comparison of local maximum friction and average sliding friction values gives information about „even" or „un-even" running of mesh, the sensitivity for „stick-slip" behaviour of gear drive. Where we find local maximum friction to be much higher to average friction values, that means potential „stick-slip" danger. That is typical for PA 6G under light load.
- Based on our new research method we discovered more material- and system-specific phenomena with polymer/steel gear pair friction and our new database can help to design and maintain such a kind of gear drives.

Acknowledgements

The research was supported by OTKA T42511, OTKA T37244, OTKA NI 62729 and TéT B-1/04 research funds.

References

Antal – Fledrich – Kalácska – Kozma: Műszaki műanyagok gépészeti alapjai, Műszaki műanyagok gépészeti alapjai, Minerva-Sop Bt. Sopron, 1997

Benedict, G.H., and Kelley, B.W.: Instantaneous Coefficients of Gear Tooth Friction. ASLE Transactions, Vol. 4, No. 1, 1961. p. 59–70

Brian Rebbechi, Fred B Oswald, Dennis P. Townsend: Measurement of Gear Tooth Dynamic Friction. NASA Technical memorandum 107279, Army Research Laboratory, 1996

Kozma Mihály: A fogaskerekek súrlódási vesztesége. Gép okt. – nov., 2004

www.quattroplast.hu

Yamaguchi Yukisaburo: Tribology of plastic materials. Amsterdam: Tribology series 16,

Mathematical Analysis of Electro-Rheological Flow Control Valve

László FÖLDI, Eszter SÁRKÖZI and László JÁNOSI
Department of Mechatronics, Institute for Mechanical Engineering Technology

Abstract

Use of intelligent materials has been a more widespread technology in the last ten years in the area of research and development of mechatronic equipments. The main reason is that some problems of the utilization needed such a solution, which couldn't be solved only with new materials produced by material texture modification. In this case, materials must be applied, that changes dynamically its own properties according to the varied ambient parameters. One group of these materials is electro-reologic (ER) liquids that change their shear strength according to the electric field. The main aim of this work is the modification of basic properties of this kind of liquids and specification of its utilization possibilities in mechatronic systems such as hydraulic control equipments. Mathematical model as well as its numerical solution of a flow control valve (ER valve) as an appropriate element of Hydraulic systems has been prepared during this work. Function tests of this unit have been carried out by computer aided simulation of the above mentioned mathematical model.

1. Introduction

The ER phenomenon as a material model is described by the Bingham model related to ER liquids, which is based on the mathematical model describing the non-newton liquids. The Bingham model is a complex viscoplastic rheological model. As a material model it can be divided into an ideally ductile an ideally viscous member. (Fig. 1)

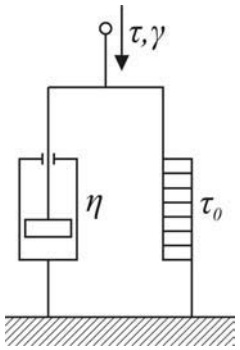

Figure 1. The Bingham model

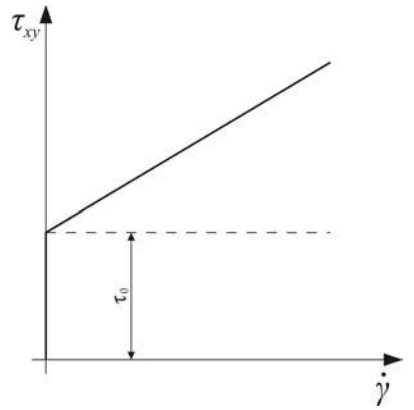

Figure 2. The shearing tension in the function of shearing gradient

1.1. Research Objectives

The aim of testing of the flow properties of the ER liquids is to establish a model, which can be generally applied of testing the behaviours of ER liquids made of different materials considering the physical data of the applied materials. By computer simulation the parameters of this mathematical model can be determined, which can be generated by minimum search. As the first step of the model identification the approximate search of the minimum of the established target function is accomplished by genetic algorithm, then the refinement of the result with the known numerical methods.

2. The Application of the Flow Regulator

During the further material and application tests it is practical to use a device which has application possibilities too. In this consideration for further investigations we need the design of a hydraulic ER valve, which can be operated built in hydraulic circuits.

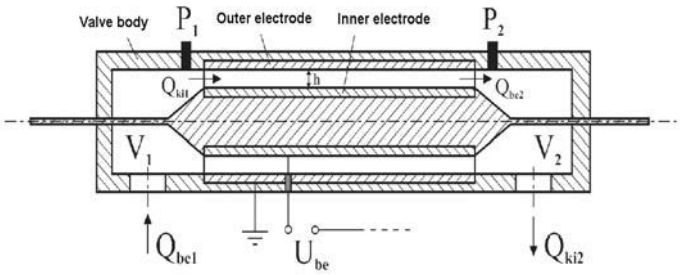

Figure 3. The ER valve

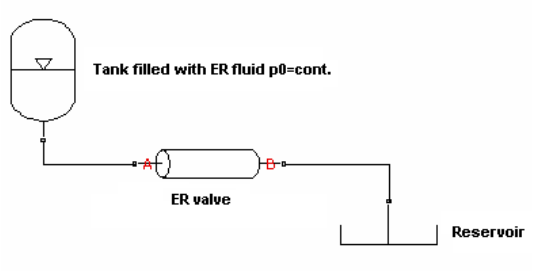

Figure 4. The conceptual diagram of simulation

2.1. Applied Mathematical Model

The flow rates which go in and out the valve can be determined by the following equations:

$$Q_{in1} = \mu \cdot A_1 \cdot \sqrt{\frac{2 \cdot (p_0 - p_1)}{\rho_f}} \tag{1}$$

$$Q_{out2} = \mu \cdot A_2 \cdot \sqrt{\frac{2 \cdot (p_2 - p_3)}{\rho_f}} \tag{2}$$

where

μ is the coefficient of flow loss, p is the pressure and ρ_f is the density of the liquid. On the basis of the incoming and leaving flow rates the balance (differential) equations are the followings:

$$Q_{in1} = \frac{V_1}{E_f} \cdot \frac{dp_1}{dt} + Q_{out1} \tag{3}$$

$$Q_{in2} = \frac{V_2}{E_f} \cdot \frac{dp_2}{dt} + Q_{out2} \tag{4}$$

In equations (3) and (4) the E_f is the bulk modulus of the liquid. The flow rate between the electrodes is:

$$Q_{out1} = Q_{in2} = \frac{L \cdot \Delta p_N}{12 \cdot \eta \cdot b \cdot h^3} \tag{5}$$

In equation (5) L means the length of the electrodes, η is the ER liquid's dynamic viscosity, b is the inside circumference of the electrode, h is the size of

the gap between the electrodes. The pressure drop of the liquid flowing through the ER valve is composed of two parts: the first part is resulted by the liquid's ideal viscid behavior (Δp_N); the second part comes from the electric field (Δp_{ER}). Hence by the right of Bingham-model the pressure drop is:

$$\Delta p_{12} = \frac{12 \cdot \eta \cdot L \cdot Q_{out1}}{b \cdot h^3} + \frac{2 \cdot L \cdot \tau_{ER}}{h}$$

The size of τ_{ER} depends on the ER liquid's physical parameters and the electric field:

$$\tau_{ER}(t) = \alpha \cdot E^{\beta} \cdot \left(1 - e^{-\frac{t}{T}}\right) \tag{6}$$

In the equation (6) the α and the β are parameters, the T is the time constant. The value of the time constant depends on the applied electric field too. With the above equations the behavior of the ER valve can be described.

2.2. The Numerical Solution of the Applied Mathematical Model

The solution of the mathematical model of the ER valve was accomplished by MATLAB with block–oriented method, using Kelvin-Thompson return-circuit principle.

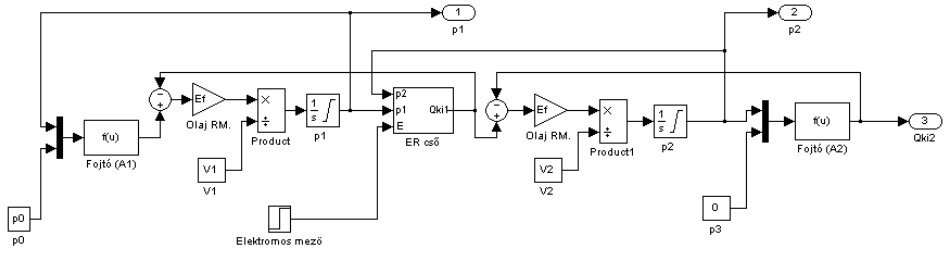

Figure 5. The block diagram of simulation

With this method the volume, which was evolved by the constant pressure difference, put on the ER valve can be measured. In this layout the liquid volume can be controlled by electric field strength. With this we can create a hydraulic valve, which without moving parts, can be controlled by the application of electric field. It can be seen from the measurement data of the professional literature, that for the evolvation of the effect it is enough (2-10) ms, which is a much smaller value that the indication time of the proportional valves applied nowadays.

3. The Results of Operation of the Model

In Chart 6 at making the simulation results we applied 6 bar inlet pressure.

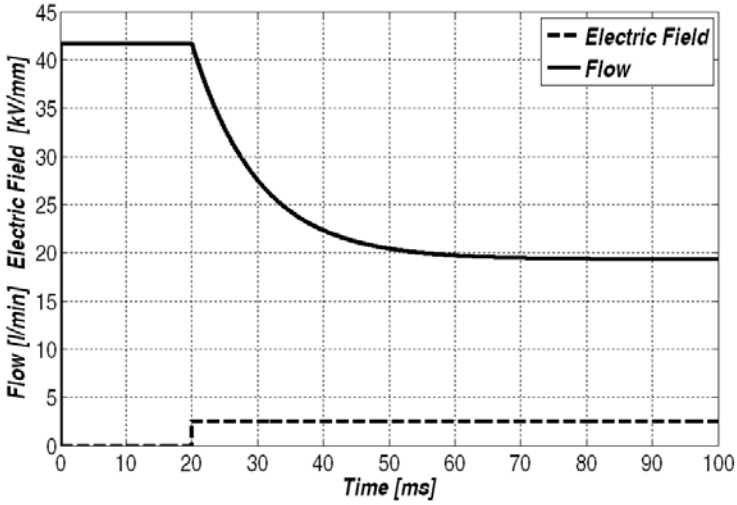

Figure 6. Flow and electric field versus time

As it seems on the figure 6. the flow is 42 l/min up to 20 ms, then by switching 2 kV/mm electric field the streaming flow decreases to 18 l/min in 40ms.

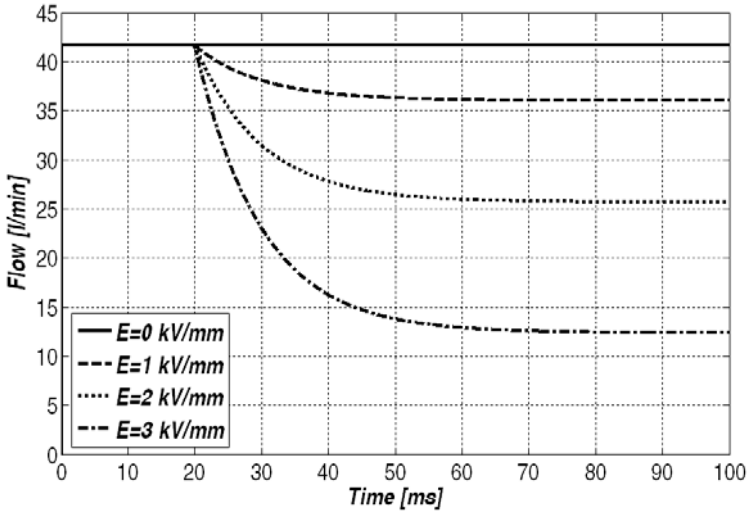

Figure 7. Flow versus time

At the simulation in the figure 7. constant 6 bar inlet pressure (p0) was used. It is shown that how the flow changes at various size electric field.

The expectable behaviour of the flow control valve at different tankpressure and electric field was also calculated (fig.8).

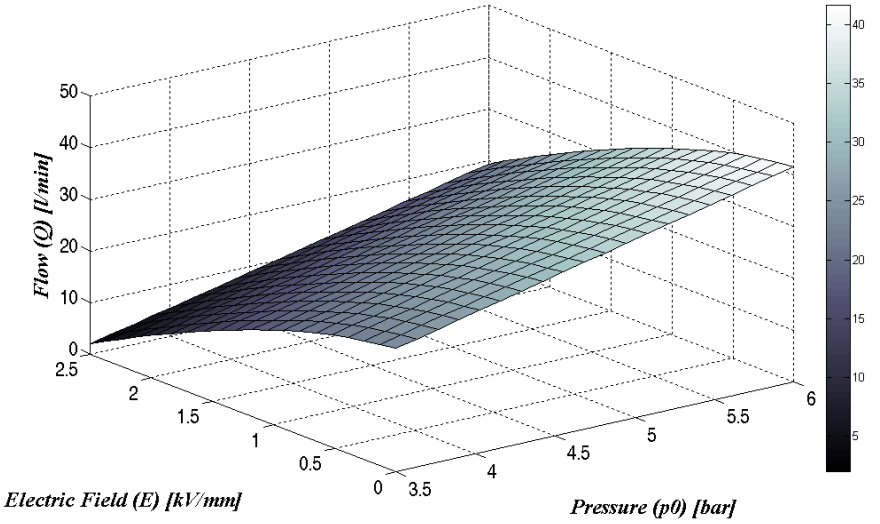

Figure 8. Flow – electric field - pressure

At this simulation the effect of the changes in the input pressure (p0) and the electric field (E) on the flow (Q) is presented.

Beside the simulations a new control equipment is designed for laboratory testing and the construction is being in process.

References

Csizmadia B. – Nándori E. (szerk.): Modellalkotás, Nemzeti Tankönyvkiadó, Budapest, 2003.

Dr. Farkas I.: Számítógépes szimuláció. Gödöllő, 1999.

H. – G. Lee – S.-B. Choi: Dynamic properties of an ER fluid shear and flow modes, In: Materials and Design, 2002., XXIII. évf.

Valasek I. – Auer J. (szerk.): Kenőanyagok és vizsgálataik, Tribotechnik Kft., Budapest, 2003

Institute for Systems Engineering and Management

Professor Dr. István HUSTI
Director of the Institute

Dear Reader,

On behalf of the staff members of the Institute for Systems Engineering and Management I'd like to give you a brief summary about our activities, research interests and operational structure.

Our Institute consists of three professional working areas called departments:

- Department of Engineering Economics and Management
- Department of Machinery Management and Systems Engineering
- Department of Communication Techniques.

Our educational works basically belong to the Engineering Faculty, but our teachers are invited many times to teach for the other Faculties, especially for the Faculty of Economics and Social Sciences.

In the last years, our Institute's most successful educational project was the establishment of the Engineering Manager degree on BSc and MSc level. The first term was started in 2001. We have already more than 100 graduated students, and almost all of them bear a good reputation.

The Department of Engineering Economics and Management has many researches based on the taught subjects:

- Applied Micro-economics, Management, Quality Management, Engineering Economics, Enterprise Management, Economics of Technical Development, Innovation Management, Project Management, Finance, Practice of transaction, Integrated Information and Management Systems, Fundamentals of Trade, Forwarding, Marketing and Market Research, Industrial Marketing, Customer Relationship Management, Law and Quality, Practise of System Development in Quality Management, System of Standards in Quality Management.

The main research and educational fields of Department of Machinery Management and Systems Engineering are:

- Theories of Technologies, Planning of Technologies for Agricultural and Industrial Production, Machinery Management of Agricultural Machines, Diagnostics of Machines and Engines, Planning of Systems.

The most important tasks of the Department of Communication Techniques are to research and teach the following fields:

- Techniques of Presentation and Communication, IT, Techniques of Voices, Studio, Television, Video, 3D Video, Camera-techniques, Multimedia, E-learning.

Due to the high research activity we search constantly for partners from Hungary and abroad. Our Institute brings into focus the international cooperation; therefore our academic staff is able to communicate in English, German Russian and Spanish.

More details about the Institute for Systems Engineering and Management are available at:

http://remi.gek.szie.hu/

Actual Tasks in the Hungarian Agricultural Innovation

István HUSTI, Imre KOVÁCS and Árpád BAK
Department of Engineering Economics and Management,
Institute of Systems Engineering and Management

Abstract

The role of small and medium-size enterprises has increased in the Hungarian agriculture after the transition. In connection with the general problems, most of the Hungarian small and medium-size enterprises (SME's) agricultural enterprises have serious problems in the field of innovation.

I prepared and used some models to examine the exact possibilities of innovation and to determine what needs to be developed. In this publication I am going to present three of them.

- The simplified model of agricultural innovation serves as a theoretical basis for agricultural developments. This model clearly demonstrates the related and dependent works to be done. It shows that the innovation part-works can be systematized into two integrating umbrellas. These are marketing and knowledge. Marketing is important as the success of innovation is decided in the market. The whole innovation process should be guided by the endeavour for market success. Knowledge combines earlier experience and recent information in the entire process.
- The model of the components of technical development shows that technical development serving agricultural production has got a particular bridging role between the production and the previous innovation phases; it integrates several factors at the same time.
- These models that were successful in the past, would be useful today as well, but the small and medium-size enterprises do not have suitable possibilities for applying them. Unfortunately the conditions of cooperation between the actors are missing as well. In our current situation if an enterprise wants to innovate, it has to develop itself with state support. The adaptive innovation can be a possible solution too. This model is going to be presented later.

1. Introduction

We used to say as a slogan: „Innovation is the engine of the development". It's true int he „well-developed" world where the innovative efforts have got more and more important role in the national economy. The situation is absolutely different in our country. There is a serious gap between our innovative practice and the world-level innovative results.

We ought to have much more innovative ideas for developing the competitiveness of our economy, especially int he agricultural small and

medium-size enterprises. (In Hungary: small enterprise is which has max 50 employees and max 10 million euros revenue per year. The same indicators of medium-size enterprise are: 250 employees and 50 million euros.)

The main objective of the research and this publication is to systemise the present innovation tasks of the Hungarian agriculture, especially focusing on the SMS's.

2. Method

Several times during the research I had to create models that represent the typical phenomena of a process or a solution. By doing this I wanted to illustrate the situation as well as to capture the most important characteristics of an innovation related problem, its internal and external relations and to describe the area in which they could be used in. In terms of these I used the possibilities offered by the classical system theory. Including this I could not undertake to come up with customized suggestions which could serve as a base for agricultural enterprises to adopt their own technical development solutions. This is impossible because in practice the combination of the developmental components show such diversity that their overall introduction is impossible and would make no sense.

3. Results and discussion

The present situation and the model of agriculture

There is almost no area in the domestic innovation practice in which we could be compared in an international level. Unfortunately the general observations apply to agriculture as well, which is offending because the sector once being successful has a slight chance to fall into line with Europe.

In the previous decades the Hungarian agriculture has proved several times that it is a favourable area for the innovation efforts.

We can say that innovation made the Hungarian agriculture known and recognized internationally. Between 1960 and 1980 the Hungarian agriculture significantly differed from the sectors of the industry with its own values and system approach. This paradigm brought a dynamic development among countries within the same political systems.

Unfortunately the initial excellent results of the agricultural paradigm striving for priority were accompanied by the deteriorating economical conditions and expenditures exceeding the local optimum, and then the Hungarian economy got into crisis blocking the development of the agriculture. However this does not decrease the value of the Hungarian agricultural innovation – leastwise in the mentioned period.

By the end of the 1980's the Hungarian agriculture's inability to develop was culminated by the problems in connection with the system change. These problems affected the system of innovation and its operation.

The cooperation between the parties interested in innovation is not that strong. The previous mechanisms are no longer, the new ones are not yet functioning. It is disconcerting that the imaginary actors of the agricultural innovation are busy with themselves and their money worries for a long time, and therefore has no energy to coordinate with the innovation partners.

It is sad that most of the times the inclination for coordination is missing as well. In my opinion this is a huge problem because the previously successful period of the Hungarian agriculture was due to the activities of the R+D sector as well as the work of the distributors and processing organizations.

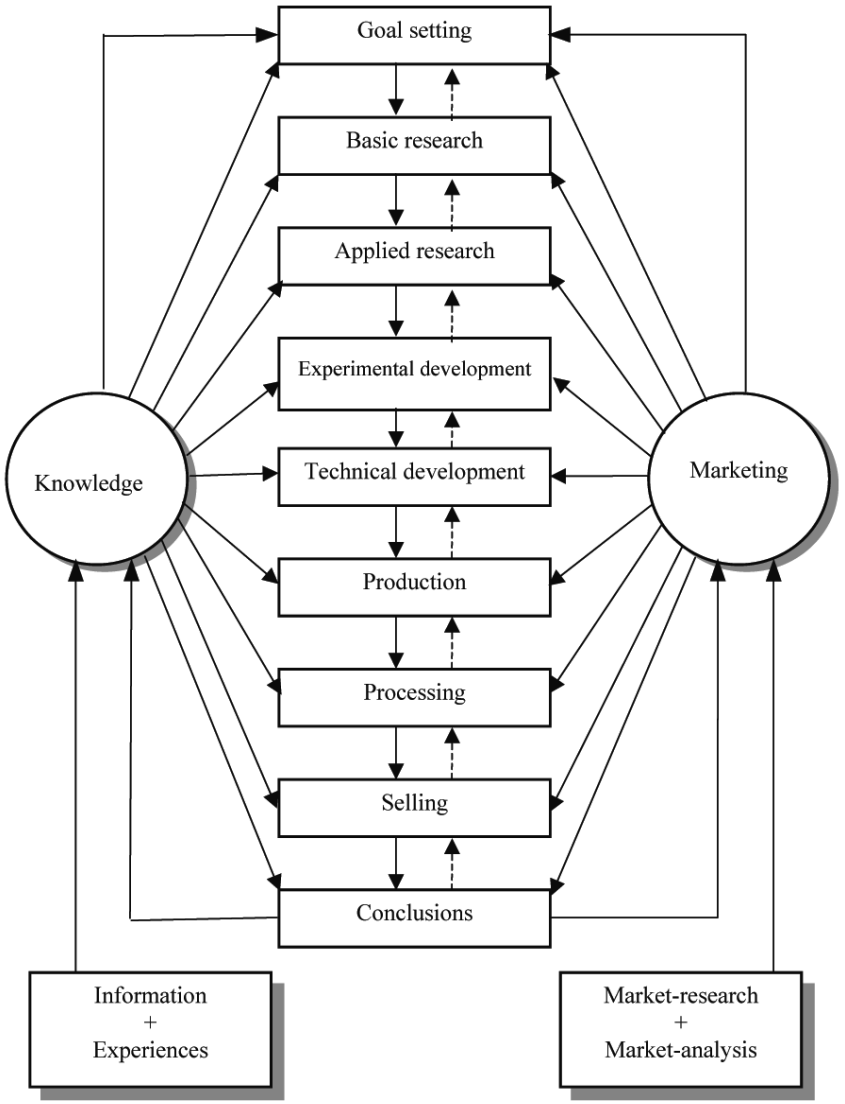

Figure 1. The simplified model of agricultural innovation

It is a mistake to think that with reference to putative or real business interest the activities of the educating-researcing-ennobling-producing-breeding-manufacturing-buying up-processing and distributing organizations interested in the domestic development could split permanently and unpunished. The actors of the Hungarian food economy could already have faced the signs of this regrettable process.

I prepared and used the general model of agricultural innovation (Figure 1.). This model clearly demonstrates related and dependent works to be done. It shows that the innovation part-works can be systematized into two integrating umbrellas. These are marketing and knowledge. Marketing is important as the success of innovation is decided in the market. The whole innovation process should be guided by the endeavour for market success. Knowledge alloys earlier experience and recent information in the entire process.

The functional model is a proper instrument for

- The review of the systematisation of the processes of agricultural innovation
- The introduction of the relation between the part processes
- The analysis of the status of the agricultural innovation
- Defining what to do in the area of development

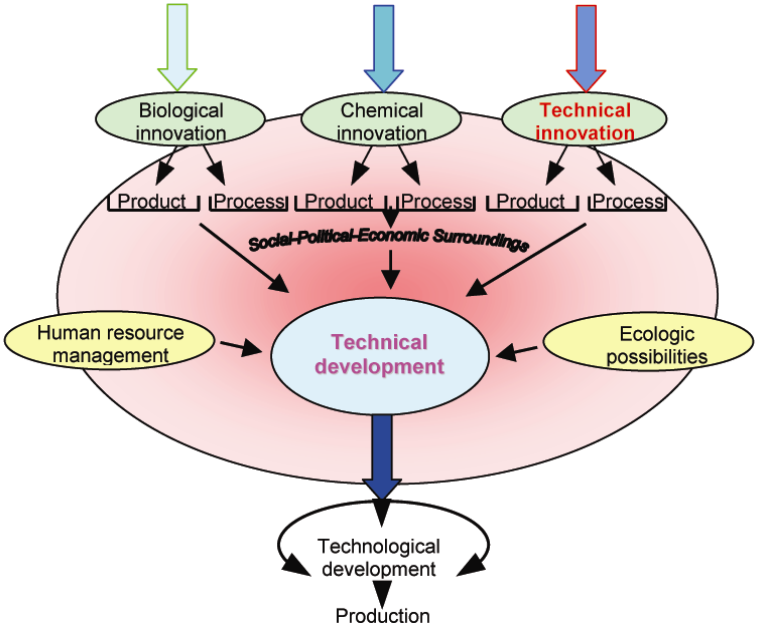

Figure 2. The role and elements of the agricultural technical development

We can say that the Hungarian agriculture was successful till the innovators could do their activities in a harmonized way as represented by the model. The

situation has changed significantly by now. In theory the old practice would be successful, but the SME's do not have the necessary conditions to be able to follow the model. The other problem is that the conditions of a harmonized cooperation between the actors have changed.

The agricultural innovation, the agricultural research and the technical development should be set on new basis in order to improve the competency of the agriculture. It has to be decided which sector should enjoy priority in respect of the sector's competency. We are no longer able to develop every area since our current financial possibilities do not cover it.

Technical development, as a phase of agricultural innovation

The model about the substance of technical development (Figure 2.) shows that technical development serving agricultural production has got a particular bridging role between the production and the previous innovation phases by integrating several factors at the same time. It is important that the marked biological, chemical, human and ecological factors should be in harmony, because otherwise the balance breaks effective factor being in relative minimum as per the minimum-law.

The adaptive innovation and it's model

There are a couple of ways for dividing the innovative solutions. One of them differentiates the original and the adaptive innovation. The original innovation is a result of the organization's own investment, R+D activities and the activities of the co-workers, while the adaptive innovation is built on results already developed by others. (The subject of this takeover can be an idea, an invention, a know-how, a plan documentation etc..)

The revival of the agricultural innovation was the initial intention of my present publication. In accordance with this my attention focused on the adaptive innovation because I do think that the role of the previously ignored SME's should be reconsidered in the whole domestic innovation strategy.

We should not have the illusion that these organizations could finance the R+D's in the long run. Instead their adaptive skills should be improved which is not easy even in the short term. Success requires new challenges in the area of education, consultancy and research.

There are numerous factors influencing the processes of adaptive innovation. In my model I highlighted two of them. (Figure 3.). 'External support' includes all the effects externally influencing the enterprise. The social-political-economical changes could strengthen innovation but could weaken it as well. The pressure of competition could result in mobilizing such dormant energy which would stimulate a sort of 'forward escape'.

The technological push is sensed by producer-distributor organizations interested in agricultural development since their living depends on how well they could force their products and services upon the users/costumers. In this aspect supply push is dominant in our country. The 'demand suck' represents the demands and desires of the buyers, costumers and processors of agricultural

products. In case of manufacturers, satisfying these needs is an evident precondition for competition.

The adventure can be influenced by many factors. The main question is the personality of the entrepreneur, its sensibility to the new and the awareness that development is important otherwise the organization will get to periphery and get off on a slope and do not stop.

It is important to be motivated enough, should it be internal or externally forced. Entrepreneurial knowledge and experience can help a lot. Think of the role of knowledge on Figure 1, which is the integrating component of the main model. In our dynamic world we may frequently encounter the confusion of information-redundancy. It can be crucial for the entrepreneurs to get the relevant information in the right time and in optimal quantity and quality.

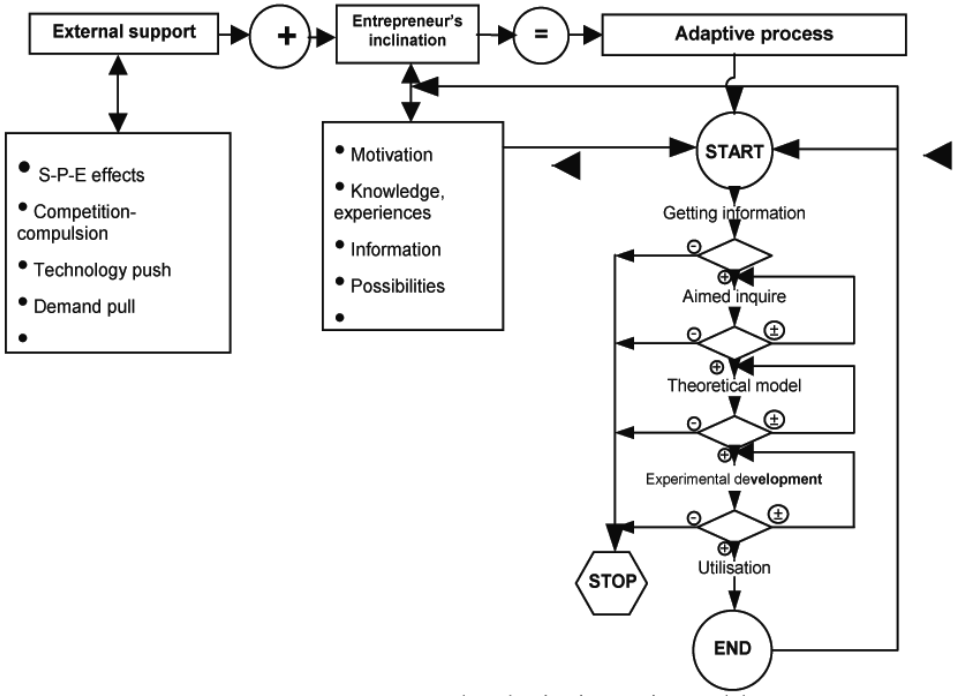

*Figure 3.*The adaptive innovation model

One of the old problems of our consulting system is that the Agricultural Knowledge and Information System (AKIS) is still not operating at an appropriate professional standard.

This operation would be the precondition of a consulting system serving professional objectives.

The enterprise for innovation is also influenced by the capability of an organization.

In case of agricultural enterprises the ecological environment is significantly important as it determines the classical potential of agriculture. Besides these the technological background, production culture, financial status and networks of the enterprise are also relevant.

The enterprise with due external support could start the adaptation process which would then lead to the complete or partial renewal of a product or a process following the principle of the 'considered progress'.

The model illustrates the steps of the adaptation process in a systemized order.

Essential is the first phase, to acquire knowledge, whereby the entrepreneur can be affected by such stimulating impulses that can start the adaptive innovation. Just like in the other phases of the process, the entrepreneur has to consider and evaluate if the new cognition acquired is worth dealing with. If the idea is worth to be improved, then comes the „aimed orientation", whilst additional information and professional details are obtained and discussed. In this phase the idea still can be rejected.

The generally important time factor in the innovation processes appears here as well, the too much speculation is disadvantageous rather than favourable. In case of a positive outcome the next step is to create a 'mental model' in reference to the conception. During this phase the entrepreneur mentally assembles and 'plays' the imagined innovation.

Following the tactics of small steps the next phase is the 'small sample' which is the practical test of the imagination as an experiment or development.

During this- despite of the preparations- problems can arise resulting in the rejection of the imagination. If in this phase our experiences are favourable, the next step could be the complete takeover that is the substantive adaptation, the application of the solutions developed somewhere else.

4. Conclusions

The Hungarian domestic system of the agricultural innovation does not make it possible to follow the model of innovation based on the traditional R+D. Not to mention that the cooperation between the actors of the innovation system in the sector ceased to exist. In this situation it seems to be reasonable to follow the model of adaptive innovation which would be useful especially for the SME's.

In order to make the adaptive innovation faster the external conditions should be improved, and the enterprise enhanced. It would also be important to set up a professional Agricultural Knowledge and Information System (AKIS) which would function accordingly.

References

Edquist, C. (ed.) (1997): Systems of Innovation Technologies, Institutions and Organizations. London: Pinter, Casell Academic.

Hajdú J., Magó L.: (2003) Alternatives of the Domestic Agricultural Machinery Market, Hungarian Agricultural Engineering, Periodical of the Committee of Agricultural Engineering of the Hungarian Academy of Sciences, Vol. 16/2003. p. 41-43.

Hall, A.J., L. Mytzelka, and B. Oyeyinka (2004): Innovation Systems: Concepts and Implications for Agricultural Research Policy and Practice. Maastricht: United Nations University.

Husti, I. (2004): Logistics Problems in Hungarian Agribusiness. =LogInfo. Special Edition for Eurolog 2004. Vol. 14. No. 3. 2004 May - June. p. 20-21.

Husti, I. (2007): Gondolatok az agrárinnováció néhány kritikus területéről. =MAG Kutatás,fejlesztés és környezet, Vol. XXI (6.), No 2, 2007 may, p.: 5-11.

Magó L.: (2007) Survey of the Present Mechanization of Small and Medium Size Plant Production Farms, Proceedings of the 35th International Symposium "Actual Tasks on Agricultural Engineering", Opatija, Croatia, 19-23. February 2007. Proc. p. 497-506.

Spielman D.J. (2005): Innovation Systems Perspectives on Developing-country Agriculture: A Critical

Sustainability in the Technological Development of the Hungarian Agriculture

István HUSTI, Miklós DARÓCZI, Zoltán PESZEKI,
Imre KOVÁCS and Árpád BAK
Department of Engineering Economics and Management,
Institute of Systems Engineering and Management

Abstract

The final outcome of agricultural production basically depends on applied technologies. In a simplified definition technology is the method of production, the chain of logically and rationally connected operations.

The technological development itself has no cease being a self propelling process. The logical development strategy for Hungarian agriculture „here and now" depends on several aspects. The countries in the world can be divided into two major groups; industrialised and developing ones. Hungary would be placed somewhere between the two. The previous „socialist" system has exhausted already, however the new, market-oriented system is not yet established.

The paper is dealing with the Hungarian problems and possibilities of agricultural technological development concerning sustainable production.

1. Development approach

„Development" is a common word, but it has various meanings. In relation to agriculture „development" can be explained best as one among a range of words including „change", „growth", „progress", „advance", „modernisation" and „reconstruction".

The most useful definition of development of agriculture is changes in the biological, chemical, technical, human and farm-economic sub-systems of agriculture and in their relations with the socio-economic system, that are of more than short duration and have more than short-term consequences, and the process that affect these changes or determine their consequences.

Thus some of the changes may prove favourable and some others unfavourable. Some of them may determine now, while others only years later. Some may be fostered or imposed from outside agriculture. Some of them may be natural, rather than the direct result of human decisions. Particular social groups in or outside agriculture may play particular roles in bringing about change. Different groups may be affected differently. The changes may be accelerated or slowed down, or halted.

The definition can be used in all countries, and does not depend on any ideas of „under-development" or poverty. The definition requires logically that those who approve some particular development should state criteria by which they judge. (Reaburn, 1984.)

It is clear that agricultural development, spurred in part by education, the adoption of new technologies, and institutional improvements, can help stimulate broad-based economic development.

Agricultural development can potentially provide a direct increase in rural welfare.

When agricultural development has not been associated with concurrent concern for employment, this development has stimulated less overall economic development than would be possible. Agricultural development has sometimes led to reduced food imports and growing food stocks even though people remain hungry. Mellor has called for an employment-oriented strategy which stresses research, education, rural infrastructure and, most important low-capital intensity industries. A rural sector with growing income can provide a large domestic market for locally produced non-agricultural goods and services.

The logical development strategy for a particular country depends on the available resources, stage of development, and institutional structure of the country. (Norton, Alwang, 1993)

The following guidelines are elements in an alternative approach to development. They form a perspective strategy aimed at building environmental considerations into development planning.

1/ A positive view of the environment needs to be developed, on the basis of present and future livelihood creation: job, incomes and cost-savings. This means a shift towards emphasising the advantages of better environmental practises, including incentives.
2/ There is a need to develop labour and time-saving technology for fuel wood, water, food preparation and post-harvest storage activities.
3/ Wherever possible farm grown inputs should be substituted for market purchases, which make additional calls on scarce finance. This will reduce the external dependence of agricultural producers.
4/ Non-farm sources of income need to be considered together with the measures needed to make farming systems more sustainable. In practice poor household will not employ more sustainable practises if they perceive them as at the cost of income-generation. In some cases efforts at income supplementation may prevent more sustainable practices from being adopted.
5/ Improved livelihood security is required, involving such essential features as land tenure rights and access to common property resources. If extended access to „commons" is leading to increased degradation, other means of bolstering the household's livelihood need to be given emphasis, to provide the essential income supplementation.
6/ Government policies should be directed towards plugging gaps in the food system of critical importance to poor people in low resources areas: for example, post-harvest technology and storage, agro forestry, decentralised marketing, improved transport, better biomass utilisation and alternative sources of income generation. Plugging the „agricultural technology" gap means sharing skills and knowledge in the implementation and adaptation of technology as well as developing appropriate technology.

7/ Poor people's calculations are based on what they know and what they can anticipate. Better environmental monitoring and forecasting are therefore necessary, and the resulting information and predictions should be much more widely disseminated.

The countries in the world can be divided into two major groups; industrialised and developing ones. In the development of agriculture in the industrialised countries, the forces favour specialisation. In most developing countries the respective conditions are the opposite of those in the industrialised countries. Hungary can be placed somewhere between the two, in my opinion. (Table 1.)

Table 1. Conditions for agricultural development:
differences between industrialised and developing countries

Criteria	*Industrialised countries*	*Hungary*	*Developing countries*
Climate-related production risk	lower	lower	higher
Potential negative impact of mechanisation on environment	lower	medium	higher
Population growth	slow	decreasing	rapid
Proportion of population employed in agricultural sector	decreasing	decreasing	constant
Transport and market structure	good	medium	poor
Degree of market involvement	higher	medium	lower
Purchasing power and availability of external inputs	higher	medium	lower
Specialisation and labour productivity	higher	higher	lower

The Hungarian agriculture similarly to the ones in the other „former socialist" countries underwent/goes basic changes in the early nineties. The earlier formed structural features have been blown up and the transformation has shaken the agriculture as a whole. The participants orientate and move more uncertainly among the new markets comparing with the previous system.

The large-scale state farms and co-operatives totally closed down or were basically transformed. During the transformation the private ownership and the small-scale farms had a priority.

2. Technology approach

The final outcome of agricultural production basically depends on the applied technology. Quite simply the technology is the method of production, the chain of logically and rationally connected operations of production.

In a given place and time the applied technologies express well:

- the level of agricultural innovation background
- the ambitions and possibilities of producers
- the different demand and claim of customers
- the agricultural policy of the given state/government.

Basically two approaches to farming development are possible: designing new farming systems or improving existing systems. Here I argue for emphasis on the latter, in such a way that activities of agricultural researchers complement and support the informal R+D efforts of the agricultural enterprises. New, integrated systems of farming are too complex and risky to be readily adopted by farmers.

The Hungarian agricultural producers have better abilities and are more likely to test small changes or new components which fit into their existing production system. Through their informal R+D, they already have experience in observing the effects of small changes within highly complex and interactive agro-ecosystems involving multi-storey cropping, livestock, micro variations in land forms and soils, and highly variable climatic conditions.

A technological development approach is needed which combines the knowledge and skills of farmers to deal with their particular environments and the new ideas and scientific knowledge of researchers about developing agriculture.

The researchers have the tasks of discovering ecologically and economically sound methods practised by the farmers, recognising their attempts to adjust to changing conditions yet retain sustainability of their farming system and, in collaboration with farmers, devising methods to help them adjust.

„Technical innovations which are designed by development organisations at technology centres, for the most part without any knowledge of the prevailing institutional and organisational conditions, and are tested on target groups do not lead to any change in existing farming systems" (Becker,1986.)

A simplified scheme of agricultural technical innovation flow is on the Fig. 1.

The changing agricultural enterprises are in the focus of these activities, for it is primarily on this level that decisions are made to modify productions methods. This means that farming R+D programmes must be highly pragmatic, i.e. related to the realities of the situation. The nature of these realities can be grasped only if technical and scientific questions are viewed in relation to the social, economic and political features of the production system as experienced by the agricultural producers.

New R+D programmes obviously need to be system-oriented and interdisciplinary if they are to address the problems of agricultural enterprises.

The new challenges of the market economy raise a huge amount of questions and problems. Among these tasks the development of production technologies is an important one, because the previously well developed technologies can be

used only limitedly among the new conditions. The development can not be postponed, because the one who wants to stay in competition and goes by the claim of the market has to apply the most suitable technologies.

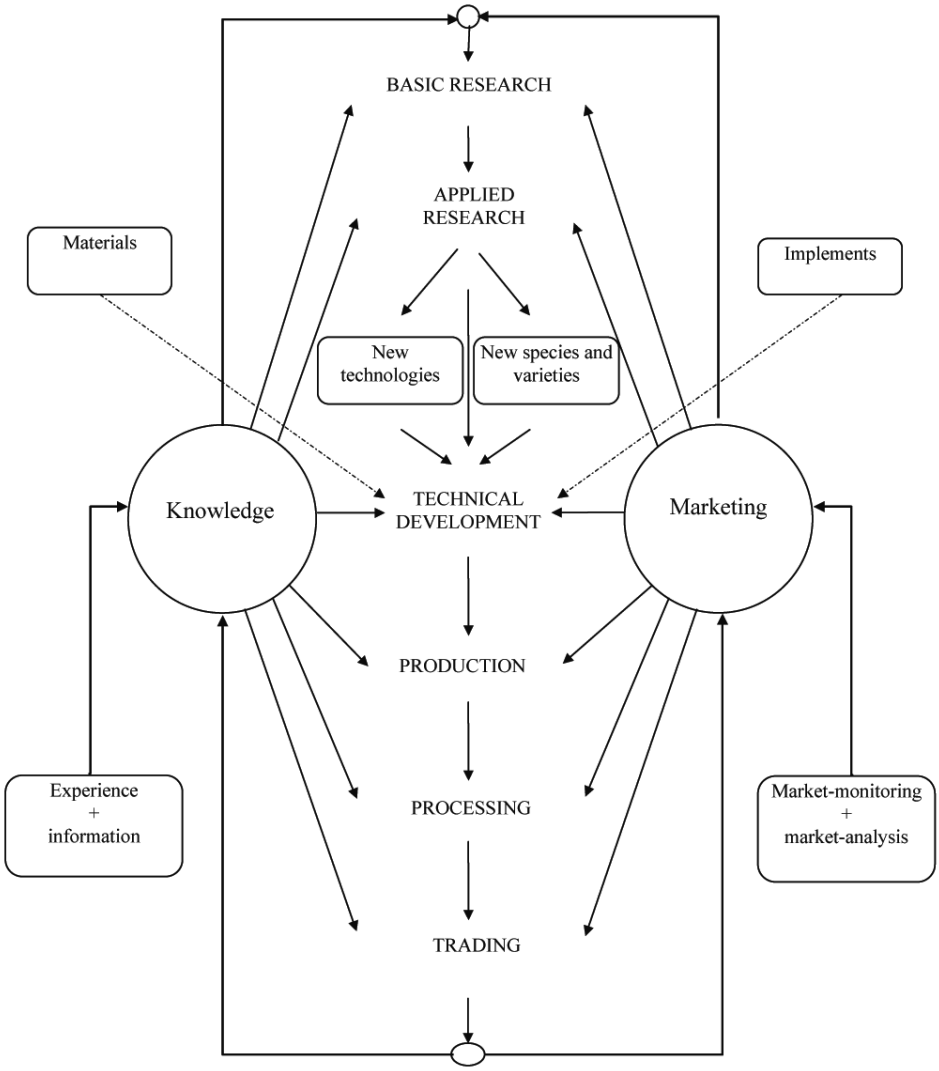

Figure 1. A simplified scheme of agricultural technical innovation flow

The technological development never has an end in itself. When the producers change the method of production they don't do it only to please the others. The rational development has always a reliable objective (or several ones at the same time).

The practical development can be aimed at:

- maximalization of yields (outputs)
- minimalization of inputs
- satisfying special quality requirements
- help the environmental and sanitary protection
- improve profitability or
- reach other particular objectives.

It is easy to see that we can't meet these several requirements, because each time conflicting aspects must be harmonised.

That's why concerning the technological development the rational combination of the different objectives, ambitions and possibilities have to be found. It can be also expressed in a concrete technology or in the different philosophies followed by the producers in different branches.

According to our experiences there are all kinds of ambitions in technological development, but three of them are so characteristic that they need the individual analysis.

They are as follows:

- maximalization of yields
- organic farming
- ecofarming.

The basis of these objectives is the idea that agriculture is an economic activity, which takes place in agricultural enterprises, and which produces high quality and save food products without damaging the physical environment in an irreversible way. Environmental requirements are considered to be integrated parts of the agricultural policy and they will be no longer an external condition (Bruijnen-Speelman**,** 1992.)

The mainstream approach to modernising agriculture has led to dependency on external inputs, e.g. of seed, fertiliser, pesticides, machinery, and fossil fuels.

In recent years, concern with both resource limitations and the ecological repercussions of modern technology has led to a growing awareness of the need for environmental protection and ecologically sound practices in agriculture as well as other forms of research and management. Specifically in agricultural development, the need gradually being recognised to find ways of meeting production requirements without excessive strain on non-renewable natural resources.

3. Sustainability approach (Sustainability as a basic principle of development)

In connection with the development of agriculture the most characteristic feature has been „sustainable" in the last decade. A number of people think all over the world that „sustainable agriculture" is the only possible strategy of agricultural development in the future.

The spread of sustainable agriculture as a development conception is a universal phenomenon! The way how to change and make popular the general

conception is different in the countries, it depends on the state of development of national economy. It is very important because this „sustainable agriculture" gets a rational sense when the general philosophical theories appear in the form of concrete aims and tasks in a given place and time.

That's why technological development is so important in the success of this conception.

From the general conception of „sustainable agriculture" (see some of them in appendix 1.) excel the remarkable areas in connection with the „sustainable technological development". The important ones are as follows:

- soil conservation and rational soil utilisation,
- water conservation, questions of irrigation,
- use of artificial fertiliser and plant-protecting material its quantitative, qualitative and structural characteristics,
- methods of protection against pests, insects and diseases
- problems of productivity and the applied species, their resistance against stress,
- questions of energy production and its efficient use especially the renewable energy sources,
- use of farming systems with regard to their profitability.

Sustainable farming practices vary from farm to farm but commonly include:

1/ Crop rotations that mitigate weeds, disease, insect and other pest problems. Provide alternative sources of soil nitrogen. Reduce soil erosion. Reduce risk of water contamination by agricultural chemicals.
2/ Pest control strategies that are not harmful to natural systems, farmers, their neighbours, or consumers. This includes integrated pest management techniques that reduce the need for pesticides by practices such as scouting, use of resistant cultivars, timing of planting, and biological pest controls.
3/ Increased mechanical/biological weed control, more soil and water conservation practices, and use of animal and green manure.
4/ Use of natural of synthetic inputs in a way that poses no significant hazard to men, animals, or the environment. (O'Connel, 1992.)

3.1. The example of Iowa

The Iowa Groundwater Protection Act defined sustainable agriculture as „the appropriate use of crop and livestock system and agricultural inputs supporting those activities which maintain economic and social variability while preserving the high productivity and quality of Iowa's land."

We can find some messages in this relatively simplified definition which could be useful for the Hungarian practice, too.

The word **„**appropriate**"** in the definition recognises that sustainable agriculture is not a concrete set of practices. Instead, sustainable agriculture is site-specific. The site includes not just the physical location but also the relationship of the location to its surroundings, the farmer and the farm family, their resources, and their goals. The idea is that a sustainable mix of crops,

livestock, and practices in one situation may not be sustainable in another situation.

„Crop and livestock systems**"** in the definition implies that sustainable agriculture includes both farming activities. Furthermore, sustainable agriculture uses „system" approaches which look at all aspects and how they interconnect, as contrasted with „reductionist" approaches which try to isolate single aspects of the production process. The system approach looks at the puzzle rather than at individual pieces.

The use of agricultural „inputs" is another distinguishing feature of the Iowa definition of sustainable agriculture. The agricultural inputs – chemicals, manure, fertiliser, labour, etc. – can be either external or internal to the farm. The question in sustainable agriculture is not how to eliminate inputs but rather how to choose the appropriate mix of resources from all those available.

Economic and social viability are also essential components of any sustainable agriculture scenario. If a farm is not profitable it is not sustainable. Social viability refers to the health and viability of the rural communities in which farmers must live. Social viability also relates to agriculture's ability to produce a safe and adequate food supply at a reasonable cost.

Finally, the Iowa definition refers to preserving the high productivity and quality of the land. While the term „land" is used, this can be taken to mean natural resources as well, including the soil and water. A concern for preserving the quality shows that sustainable agriculture looks not just at the current generation but also at future generations. Although this definition says „Iowa", any other state, country, or institutional unit could be substituted.

4. Some characteristics of the basic options of practical development of technology

A/ In case of maximalization of yields the main objective is to reach the maximum output on the production unit. The technological solutions and the combination of inputs are subordinated to that aim in the frame of the local conditions. The most important advantage is making the best use of potential productivity. The source of the problems at the same time is that the requirements of efficiency and profitability, the aspects of environmental and sanitary protection and some time the quality requirements are pushed into the background.

B/ The organic farming emphasises the environmental and sanitary protection and usually stress the farming totally free from fertilisers and chemicals. The conception has several advantages but there are numerous problems too, first of all at profitability. These are e.g.
   – the yields are lower at most agricultural branches comparing with the ones of traditional technologies and the extra selling price isn't able to compensate it,

- some of the organic products are less market oriented, their appearance is poorer comparing with the traditional ones,
- there is a narrow stratum of customers with solvent demand interested in organic products.

C/ The ecological and cost reduction programme started in the United States became well known as LISA. It means Low Input / Sustainable Agriculture.

The essence of the conception that in contrast with the organic farming it doesn't refuse the chemicals totally but – not just for cost reduction – uses up as little as possible. The same goes for machinery and also for the „outside" resources. At the same time it makes a more efficient use of the on-farm possibilities.

In this sense the German concept of site-appropriate agriculture („Standortgerechter Landbau") builds on a long tradition of location economics and farm management theory. Other countries in various part of the world, and similar concepts are being promoted, e.g. ecologically sound agriculture, organic farming, conservation agriculture, sustainable agriculture. All refers to forms of agricultural land use which depend primarily or almost exclusively on local resources to achieve lasting productivity, i.e. sustainable agriculture with low levels of external inputs. For the sake of brevity, this is often be referred to „ecofarming".

In view of the limited access of most farmers to artificial external inputs, the limited value of these inputs under low-external-inputs agriculture (LEIA) conditions, the ecological and social threats of „green revolution" technology and the dangers of basing production on non-renewable energy sources, the strong emphasis on high-external-inputs agriculture (HEIA) must be questioned. However, it is also open to question whether it will be possible to raise world food production sufficiently without the use of such external inputs. Besides, natural as opposed to artificial inputs can also, have detrimental environmental effects.

Low-external-input sustainable agriculture (LEISA) is an option which is feasible for a large number of farmers and which can complement other forms of agricultural production. As most farmers are not in a position to use artificial inputs or can use them only in small quantities, it is necessary to concentrate on technologies that make efficient use of local resources. Also, those farmers who now practise HEIA could reduce contamination and costs and increase the efficiency of the external inputs by applying some LEISA techniques. It is important that the agroecological knowledge of both scientists and farmers be applied, so that internal and external inputs can be combined in such a way that the natural resources are conserved and enhanced, productivity and security are increased and negative environmental effects are avoided.

LEISA refers to those forms of agriculture that:

- *seek* to optimise the use of locally available resources by combining the different components of the farm system, i.e. plants, animals, soil, water, climate, and people, so that they complement each other and have the greatest possible synergetic effects;

– *seek* ways of using external inputs only to the extent that they are needed to provide elements that are deficient in the ecosystem and to enhance available biological, physical and human resources. In using external inputs, attention is given mainly to maximum recycling and minimum detrimental impact on the environment.

LEISA does not aim at maximum production of short duration but rather at a stable and adequate production level over the long term. LEISA seeks to maintain and, where possible, enhance the natural resources and make maximum use of natural processes. Where part of the production is marketed, opportunities are sought to regain the nutrients brought to the market.

4.1. Strategies for transition to LEISA

Transition is the process of conversion from an unbalanced conventional or traditional farm system to an economically, ecologically and socially balanced (LEISA) one. As regaining an ecological balance may take many years, particularly when this involves growing trees and breeding animals, a transition process can be lengthy. As the conditions for farming will also be changing during transition, the farmers' capacity to adapt to these changes will be crucial for successful transition. However, it must be emphasised that transition is more than just adaptation to change, it is a conscious process to make the farm system more balanced and sustainable.

Transition involves investments in labour, land and/or money and taking risk. To gain an acceptable level of yield increase quickly, to minimise risks and to spread investments, the farm family must find an acceptable transition strategy involving specific combinations of genetic resources, techniques and inputs in a deliberately chosen sequence. The particular technologies involved and the sequence in which they are combined will depend greatly on the biophysical and socio-economic characteristics of the farm, its historical development and present situation, and the needs and preferences of the farm household. Therefore, such strategies will be farm-specific.

The process of building and maintaining LEISA systems requires awareness of and knowledge about feasible technologies, skill in applying them and a constant watch for signs of degradation and destabilisation of the farm system.

As it will not be completely certain what implications the changes will have for the farm household, the strategy for transition should be “undogmatic”, responsive to unexpected results and open-ended. Farmers embarking upon conversion to LEISA need to be highly motivated self-reliant and imaginative.

Sustainable agriculture demands high internal inputs of good farm management.

Under LEIA conditions, where farmers may be particularly wary of the initial investments required and the risks of a temporary decrease in production, it is important that suitable „entry points” to a process of transition have to be found. These are starter techniques, which give good returns in the first season, involve relatively few risks and have positive effects on the ecosystem. Integration of these techniques can then lead to other beneficial changes in the farm system.

Criteria for choosing technologies for human-centred agricultural improvement:

Do the poorest farmers recognise the technology as being successful?
- Does it meet a real need?
- Is it financially advantageous?
- Does it bring recognisable success quickly?
- Does it fit local farming patterns?

Does the technology deal with those factors that most limit production?

Will the technology benefit the poor?
- Does it utilise the resources the poor people already have?
- Is it relatively free of risk?
- Is it culturally acceptable to the poor?
- Is it labour-intensive rather than capital-intensive?
- Is it simple to understand?

Is the technology aimed at adequate markets?
- Are market prices both adequate and reliable?
- Is the market available to small farmers?
- Does the market have sufficient depth?

Is the technology safe for the area 's ecology?

Can the technology be communicated efficiently?
- Does it require a minimum of on-site supervision?
- Is it simple to teach?

Is the principle behind the technology widely applicable?

(Source: Bunch, 1985.)

Legislation, marketing improvement and appropriate pricing policies can give important support to farmers seeking a strategy for transition. Many marginal farmers and enterprises may not be in a position to develop sustainable farm systems unless they have access to additional income, e.g. a kind of starter credit in a revolving found which gives them the financial space to work on their farm instead of working as a farm labourers for others or going elsewhere to look for wage labour. Achieving sustainability is more easily advocated than put into practice and, in the case of many marginal producers, it may not be possible to achieve unless supplementary sources of local, nonfarming income can be found.

5. Conclusions

- The profitability of agriculture both on macro- and micro-level depends on the production technologies at several points. That is why technology development means an evergreen task.
- Concerning the technological development the uniform solutions must be avoided, as it means a dynamic task which must not be treated in isolation of place and time.
- All of the listed 3 options can be viable to reach the certain objectives at given conditions.

- Establishing any of the three options the basic principle can be the criteria-system of sustainability.
- The Hungarian agriculture - in its present situation - has directed its attention more seriously to the rational adaptation of LISA/LEISA-philosophy.
- In the course of this it is suitable to keep to the direction of „precision farming".

References

Bruijnen, F.G.J. – Speelman, L.: The relation between agricultural policy and the development of agricultural mechanisation in the Netherlands.

Wageningen Agricultural University, 1992.

Csete, L.: Strategic concept for the development of the Hungarian agrarian economy.

„Agro-21" Füzetek. 1995. No. 10, p.: 86-102.

Duffy, M.: Current sustainable ag issues.

Newsletter of the Leopold Center for Sustainable Agriculture. Vol. 6 No.4. Winter 1994.

Ecofarming in agricultural development.

Edited by Verlag Josef Margraf. Weikersheim, 1989.

Husti, I.: Tendencies and Priorities in the Development of Agricultural Production Technologies.

Gazdálkodás, XXXVI. (1993). No. 11. p.: 1-8.

Norton, G.W. – Alwang, J.: Introduction to economics of agricultural development.

Mc.Graw-Hill, Inc. 1993.

O'Connel, P. F.: Sustainable Agriculture – A Valid Alternative.

Outlook in Agriculture. Vol. 21. No. 1. p.: 5 -12. (1992.)

Reaburn,J.R.: Agriculture: foundations, principles and development.

John Wiley and Sons Ltd. 1984.

Redclift, M.: The role of agricultural technology in sustainable development. In. Technological change and the rural environment.

Edited by Lowe, Ph.- Marsden,T.- Whatmore, S.

David Fulton Publishers. London, 1990. p.: 81-91.

Reijntjes,C.– Haverkort,B.– Waters-Bayer,A.: Farming for the future. An introduction to Low-External-Input and Sustainable Agriculture.

Macmillan, Ileia. Netherlands. 1993.

Young, T. – M.P. Burton: Agricultural sustainability: definition and implications for agricultural and trade policy.

FAO Economic and Social Development Paper. No. 110. Rome, 1992.

Appendix 1

Some definitions of „sustainable agriculture":

– FAO (Food and Agriculture Organisation of UNO):
„Sustainable development is the management and conservation of the natural resource base and the orientation of technological and institutional change in such a manner as to ensure the attainment and continued satisfaction of human needs for the present and future generations. Such sustainable development (in the agriculture, forestry and fisheries sector) conserves land, water, plant and animal genetic resources, is environmentally non degrading, technically appropriate, economically viable and socially acceptable".

– WCED (World Committee of Environment and Development)
„Development which meets the needs of the present without compromising the ability of future generations to meet their own needs."

– American Society of Agronomy
„A management system that uses inputs, both those available as natural resources on the farm and those purchased externally, in the most efficient manner possible to obtain productivity and profitability from a farming operation while minimising adverse effects on the environment.

A sustainable agriculture is one that, over the long term, (1)enhances environmental quality and the resource base of which agriculture depends, (2) provides for basic human food and fiber needs, (3) is economically viable , and (4) enhances the quality of life for farmers and society as a whole."

– The Brundtland Report („Our common Future")
„Sustainable systems are those that, meet current food requirements without compromising the possibilities for future generations to satisfy their food requirements."

– CGIAR/TAC (Consulting Group of International Agricultural Research / Technical Assistance Committee)
„Sustainable agriculture involves the successful management of resources for agriculture to satisfy changing human needs while maintaining or enhancing the quality of the environment and conserving natural resources."

– *U.S. Congress*

„Integrated system of plant and animal production practices having a site specific application that will, over the long term, satisfy human food needs, enhance environmental quality and the natural resource base upon which the agricultural economy, depends; make the most efficient use of non-renewable resources and on-farm resources and integrate, where appropriate, natural biological cycles and controls; sustain the economic viability of farm operations; and enhance the quality of life for farmers and society as a whole."

Modelling of a Harvesting Process Based on Real Tests

Zoltán BÁRTFAI, Zoltán BLAHUNKA, Péter ILOSVAI and Béla NAGY
Department of Machinery Management and Systems Engineering
Institute of Systems Engineering and Management

Abstract

Changes in the plant cultivating technologies in Hungary revise the cost-proportion toward the harvesting. Therefore planning the harvesting process from the point of view of performance, losses, quality becomes important very much. Because of the complexity of this problem, the computerized stochastical modelling seems to be applicable quite well. On the present occasion we would like to outline the results of a harvesting model based on an instrumental examination under real field conditions.

1. Introduction

According to the characteristic feature of the Hungarian plant cultivation the cereals and maize are growed approximately on the 50 % of the total cultivable land. The changes in the ownerships the deficiency of funds, the problems in disposal will facilitate the closing up to the severe regulations of the EU about the environmental protection and the product quality. At least in the respect of the production technologies, in so far as the cheaper, simpler solutions will be used. In this case the crop capacity naturally will be lower. In the first place from the example of the USA in the countries of the EU, the new technologies started to spread earlier but nowadays in Hungary we also use these technologies in the plant cultivation.

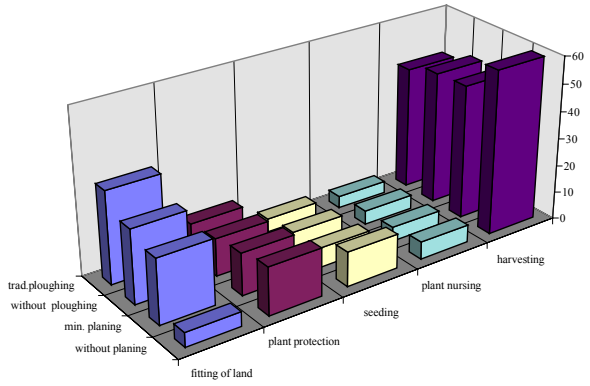

Figure 1. Cost proportions of the maize production in Hungary in different type of soil cultivation systems.

These changes in the technologies have modified the proportions of direct costs of the production circulation. Fundamental changes can be experienced in the preparation of soil, substitution of nutrition and because of the environmental-protection requirements these changes can be experienced in the plant protection too. Figure 1 shows the cost proportions of the maize production in Hungary in different type of soil cultivation systems.

The diagram shows that the costs of the harvesting relativity increased comparing it with the other operation costs. Considering the fact that harvesting is the realization of the production results and also that the possibility of the direct losses is really expressive in this operation, it is calculable with a well organized process the scale of the production process can be influenced advantageously. Figure 2 shows the effect of the harvesting time (regarding to the moisture content) deviating from the optimum on the grain quantity that can be harvested. The main goal is to utilize in the best range the harvesting capacity which claims on the one hand the knowledge of parameters that have an effect on the machine harvesting performance and on the other hand the knowledge of those factors which have effect on the transport capacity.

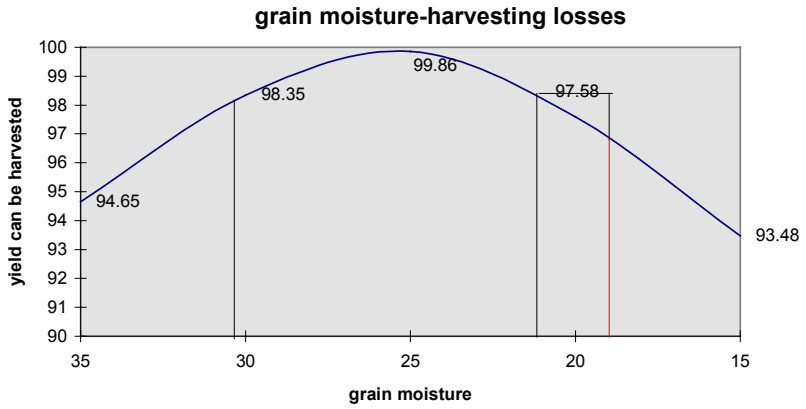

Figure 2. Effect of the moisture content on the grain quantity

2. Discussion

The maize harvesting process can be considered as an assembly in which the elements are in complicated relationship with each other. Another complication in this assembly is the incidence state of the elements can be many variegated. In consequence of this fact the planning possibility of the harvesting process depends on the handling of the harvesting machine (combine)- environment and the combine environment-lorry connections as a complex system. The system approach may ensure a better scientific cognition of the real process through the application of system methods like example modelling.

The model- as a short definition- is a transformation of the system by the aid of the expediently choiced essential features, properties of the system. Thus the model contains those parameters of the examined system which are relevant from the point of the examination. These parameters or features of the system have to be determined by exacting investigations. To determine of the essential parameters of the combines there are international (e.g. ASAE) and national standards which contains and prescribe the topic, the method and also the quality requirements of the scientific investigation. To apply these standards in case of maize combines the next parameters have to be determined through the investigation:

Conditions of the investigation

- configurations of the terrain
- crop- features
  - breed
  - row place
  - distance between plants in the row (average)
  - yield of the grain
  - proportion of the grain-cob
  - grain-moisture

Characteristic features of the examined machine

- energetic features
  - engine revolution per minute
  - fuel consumption
  - travelling speed

Performance features

- time while the grain tank filled up
- emptying time
- revolution of the barrel

Quality features

- grain losses(ear-beating adapter, screen, shaking box, leakages)
- grain cleaners
- grain breaking
- proportion of the grain-stalk

Table 1. summarises data that were taken during a field test of a SAMPO Rosenlow 2075 type combine harvester.

On the basis of the chart the boundary use values determinable for the case of boundary conditions stipulated by the severe standards (Hungarian Standard: 1.5 % losses, ASAE 1 % losses). Making use of the data and altering the harvesting conditions (e.g. yield) fulfilling the modelling the operating parameters of the combine harvester can be determined. The model conditions may deviate from the original field conditions. These parameters generate the

transporting claim (Figure 3.). The transport vehicles have to satisfy all these requirements according to the cost proportions showed by the Figure 1 and 2.

Table 1.

engine	average	fuel	Spec.fuel.	area	grain	masse	grain
revolution	speed	consumpt.	consumpt	capacity	masse		losses
[1/min]	[km/h]	[l/h]	[l/ha]	[ha/h]	[kg/sec]	[kg/sec]	[%]
2242	4.20	21.77	17.14	1.27	4.29	5.81	1.09
2217	5.39	25.13	15.41	1.63	5.51	7.46	1.62
2236	5.49	23.77	14.29	1.66	5.62	7.60	1.71
2194	5.66	23.72	13.84	1.71	5.79	7.83	1.72
2226	6.40	25.25	13.04	1.94	6.54	8.85	2.18
2201	6.41	25.95	13.37	1.94	6.56	8.87	2.23
2214	6.53	25.69	12.99	1.98	6.68	9.04	2.22

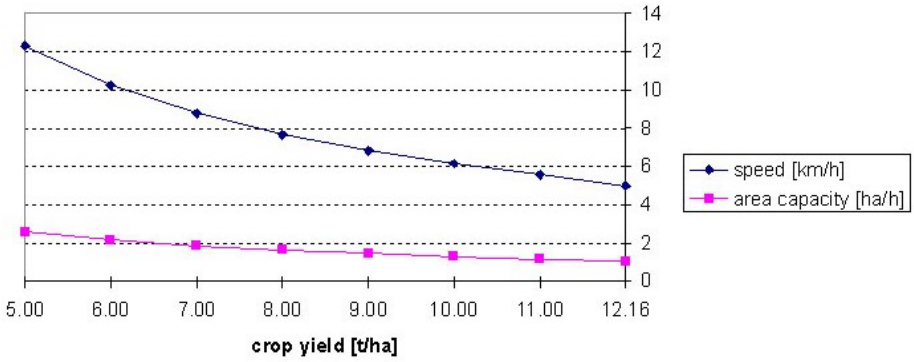

Figure 3. Expectable parameters of the combine harvester SR2075 taken as a function of the crop yield

Namely over the period of harvesting the two processes create the real work-process, and there are two possibilities

- the combine harvester waits for the transport vehicle
- the transport vehicle waits for the combine harvester

These situations can be taken into consideration in the course of simulation and over a period of formation of the computer model.

Going on the analysis of the harvesting process we can make certain that it is a special kind of serving systems really a mass-serving system taking no notice of rejecting the arising claims. Simultaneously the system has several channel if there are two or more transport vehicles at the same time. If we would like to create the model we have to have knowledge about the following data:

- technical working parameters the combine harvester

- number of the machines working in the harvesting process
- technical working parameters of the transport vehicles
- the average yield of the field
- habitat features (size of the yield, soil, relief)
- haul length (transport distance)
- road conditions
- conditions of the receiving and loading.

Studying the connections between the elements, the harvesting process can be described only on the basis of the probability and the active factors have to be handled as random variables.

Let's study the time when raising a claim to serve the combine harvester. Let it be marked by „tj". It is a probability value, that depends on several random time- elements, which are connecting with each other (e.g. previous serving time, time of the filling up of the grain tank, emptying time of the grain tank, failure probability of the attachments of the machines).

Considering only the grain tank filling up time, its value depends on several random variables, like: working width, travelling speed, capacity of the grain tank, crop yield of the examined part of the field, field length and other features of the yield.

3. Conclusion

Table 2

type of the combine harvester:	SR 2075	type of the transport vehicle:	FIAT 180.90+MBP 6.5(2)
capacity of the grain tank:	4.6 m^3	technical reliability factor:	0.991
technical reliability factor:	0.992	load capacity (t):	13
		travelling distance (km):	5
		average speed (km/h):	19

Number of transport vehicle		1	2	3	4
Number of combine			Average waiting time [min]		
1	combine	227	0	0	0
	transp.veh.	0	220	776	1334
2	combine	796	408	113	0
	transp.veh.	0	19	54	428
3	combine	1340	965	589	262
	transp.veh.	0	19	38	80
	Estimated total capacity [t/h]				
1		8.3	12.9	12.9	12.9
2		8.3	15.6	23.0	24.8
3		8.3	15.6	23.0	30.4

The random model, which is created by considering the principles, mentioned above, has peculiarities from them it emerges that we get the results in the form of some distribution. The result will be the value of the distribution. The results of our investigation, which have been taken on the mentioned Sampo combine harvester, can be seen in the Table 2 and in the Figure 4. and 5.

We hope the results of this computer aided modelling will help to make decision of planning and guiding activities in a concrete situation or process.

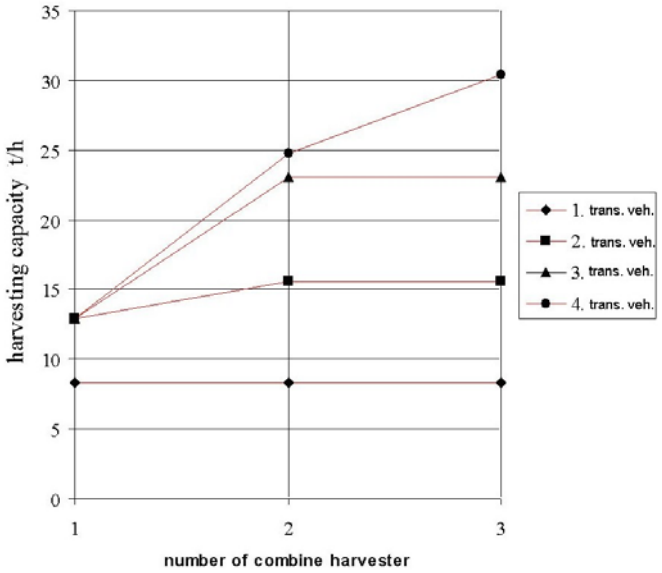

Figure 4. Connection between the harvesting capacity, number of transport vehicle and combine harvesters

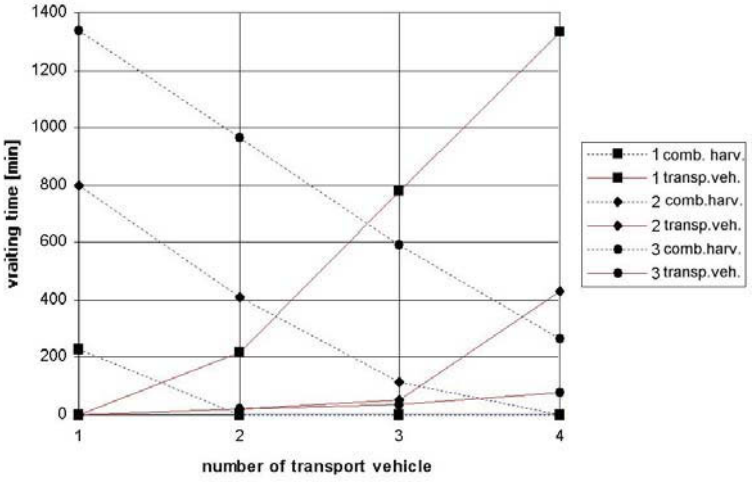

Figure 5. Connection between the waiting time, number of transport vehicle and combine harvesters

References

Stafford, J. V. (ed.): Precision Agriculture ’99, Sheffield Academic Press, Sheffield, 1999.

Gaynor, G.H.: Handbook of technology management, McGraw Hill, New York, 1996.

Liljedahl J.B., Turnquist P.K., Smith D.W., Hoki M.: Tractors and their power units Van Nostrand Reinhold, New York, 1989.

Institute of Mechanics and Machinery

Associate Professor Dr. István SZABÓ,
Director of the Institute

Dear Reader,

The Institute of Mechanics and Machinery (IMM) was established in 2005 with merging two formerly independent educational and research units of the faculty of Mechanical Engineering: the Institute of Machinery and the Department of Mechanics and Technical Drawing. In the new formation scientific and teaching activities are carried out in three departments in close cooperation.

The Department of Mechanics and Technical Drawing is focusing on basic engineering education as well as on advanced theoretical research of different aspects of mechanics of materials. Activities are concentrated around the following key areas:

- Dynamics of Machinery
- Biomechanics
- Design of experiments
- Kinetics and kinematics
- Applied engineering numerical methods (FEM/BEM)
- Statics and structural analyses

The Department of Machine Construction has been known for its work on delivering courses and conducting research in machine design, construction analyses, computer aided engineering, and machine elements etc.

Department of Agricultural and Food-industrial Mechanical Engineering integrates disciplines from wide range of classical biosystems engineering (plant production, soil cultivation, harvesting, animal husbandry, food processing etc.). Among several research areas emphases has been put lately on describing physical properties of chopped plant-structures, biomass energy production and development of new harvesting technologies (sunflower, corn).

One of the outstanding event related to the IMM in 2008 was the official opening of the Center for Engineering Informatics, a laboratory and classroom complex with over 2000 m2 space providing high tech environment for different areas of CAD/CAM/CAE technologies.

Selected papers published in the following section may give an impression on the activities carried out in 2008 by staff member researchers in three characteristic fields of interest. Further information on IMM can be found at www.gek.szie.hu.

Biomechanics of the Human Knee Joint

Béla M. CSIZMADIA and Gusztáv FEKETE
Department of Mechanics and Technical Drawing, Institute of Mechanics and Machinery

Abstract

This paper represents a short summary of the human knee joint modeling. The Biomechanical Team of the Szent István University investigates the motion of the human knee in the case of squatting. In the analysis of the previously mentioned motion the emphasis is laid on the kinematical properties, which is approximated by experimental and numerical ways. Primarily the sliding and rolling properties of the human condyles are examined, especially I in those domains where pure rolling, rolling and sliding jointly, and pure sliding may occur. Since only the two extremities are well known in the theoretical and applied mechanics, this paper wishes to furnish further information to the subject. On the other hand, in order to determine special additional features the global experimental investigations of the knee are also crucial. These results can be essential for further investigations of the phenomena of the combination of rolling and sliding and to show a new path of creating prosthesis.

1. Introduction

The aim of the Biomechanics Team of Szent István University is to reach a deeper understanding of the human knee joint, by carrying out both experimental and theoretical investigations. Different tasks are being explored such as the determination of the axis of revolution, the governing angles of motion of knee, the global determination of the acting forces or the local motions. The team has carried out significant work in this area, and has already presented experimental results. The final aim of the project is to develop a new kind of prosthesis which surface and topography is designed according to the data of multiple cadaver experiments. The steps to successfully carry out this project are the followings:

- Creating a mechanical model to provide initial and boundary conditions,
- Carrying out experimental results in order to determine the acting forces and the governing angles in the knee joint and its surroundings. The results can be useful to verify and even to correct the mechanical model,
- Creating a computational model to ease the calculations and to take into consideration (if necessary) complex geometry. According to the large number of simulations the results can be extended to the level of creating an averaged condyle topology of the human knee.

Worthy of note, there are two governing hypothesizes in the research of the human knee. The first one attributes the importance of the human knee motion properties to the connecting surfaces of the bones (the contact points of the femur and tibia on the condyles), while the function of ligaments remains as a

kind of control of the kinematical trajectory of the knee joint. The second one claims the opposite and hereby it must be mentioned that the SZIE Biomechanical Team follows the first hypothesis. Thus, beside many others, the precise mapping of the condyles geometry is an important issue in our research.

2. Analytical global mechanical model

In the 1st phase, the SZIE Biomechanical Team started using both cadaver and intact living knees in their experimental researches. In order to carry out the experiments a special apparatus was needed which was proper to clutch a cadaver knee, and load the joint as well, in the case of squatting (*Figure 2.1.)*.

Figure 2.1. The SZIE test rig

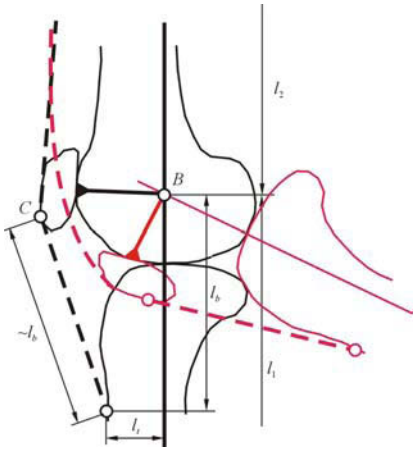

Figure 2.2. The mechanical model

During the load of the test rig, the governing angles are being recorded by the POLARIS system, which can simultaneously determine the tracks of many isolated points while they are in the move. Besides the test rig, the Team created a 2D, global mechanical model to determine the forces in the muscles of the human knee joint (*Figure 2.2 and Figure 2.3)*.

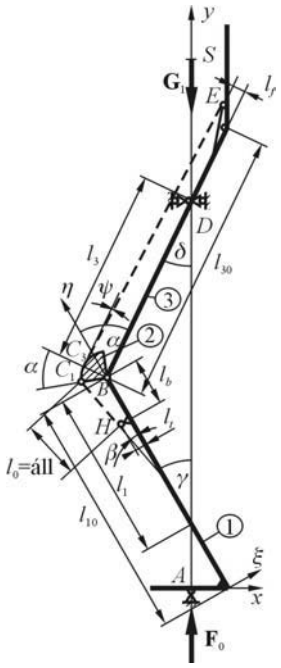

Figure 2.3. The mechanical model

The model provides the evaluation of the forces of the connecting ligaments in the function of an arbitrarily α angle, in the ratio of the load. The main problem of the model was the lack of initial and boundary conditions which are represented as missing functions and constants. These are the following parameters:

- λ_1 (l_1 / l_{10}): Active proportional length of tibia.
- λ_3 (l_3 / l_{30}): Active proportional length of femur.
- λ_b (l_b / l_{10}): Proportional length of ligmentum patellae.
- λ_f (l_f / l_{30}): Proportional thickness of thigh.
- λ_t (l_t / l_{10}): Proportional thickness of shin.
- β: The angle of the ligamentum patellae compared to the tibia.
- ψ (γ / α): The proportional angle of the γ.

Among the parameters, the λ_1, λ_3, ψ, β are the functions of α, while the λ_t, λ_f, λ_b are proportional constants.

3. Experimental methods, results, and validation

3.1. the method

In order to obtain these parameters, experiments were carried out on fourteen human persons. The experimental persons were between in the age of 21 to 27, nine male, and five female in normal physical condition. The aim of the experiment was to measure the center of gravity, and to construct the so-called bone-axes (namely the femur and tibia) so the demanded proportional values could be measured as well. For the experiment, a SPIDER-8 data acquisition system was used, controlled by the Catman Express 3.0 program. Three KALIBER type dynamometers were connected to the SPIDER-8. Before the measurement, certain boundary conditions were given to the experimental persons, such as:

- stretched arms
- straight spine
- heel adapted to the apparatus
- 3 second steady-state in each experimental setting.

The experiments were carried out by having each person stand on to the board shown on the *Figure 3.1*,

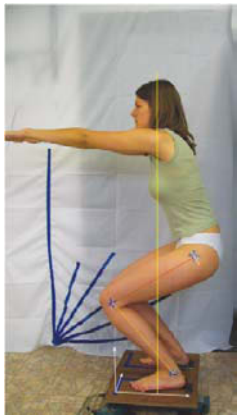

Figure 3.1. Experimental person on the measuring board

while the ’x’ and ’y’ components of center of gravity were measured in seven static positions. The average value and its standard deviation were also determined with the statistical error, calculated by the Student criteria**.** Since the prospective values were available, the bone-axes could be constructed. Markers were put on to the end of the bones, so if they are connected with a line, the theoretical axes will be given in each status. This method was correct in the first status of the squatting, so the axes were constructed, but in the other statuses, the connective tissue was shifted, so the marker did not represent the real position of the end of the bone. The solution of the problem was given by the functional

anatomy. In case of squatting, the posterior muscles of the thigh are in a totally laxed condition, while the same statement is valid to the front muscles of the shin. This fact can be expended as follows: during the motion of squatting the muscles do not act, or the action is not significant in the above mentioned accentuated areas thus the gradient of the volume is zero. So these areas can be modeled as rigid bodies. In the view of this conclusion, two more auxiliary vertices can be taken, and now, with the use of basic construction methods, the demanded vertices can be easily allocated.

3.2. results

When the axes of the bones are constructed in each status, the prospective values of the center of gravity can be plotted as a line, and by the intersections, the unknown values can be appointed. Due to the applied methods, the following results can be reported. All of the constant proportional values have been estimated with their deviation.

$$\lambda_t = 0{,}10 \pm 0{,}037$$

$$\lambda_b = 0{,}158 \pm 0{,}087$$

$$\lambda_f = 0{,}164 \pm 0{,}057$$

In addition, all the proportional functions are given as well. In the case of β function, another result is put in the diagram, given by the Marcus-Wimmer-Adriacchi formula. Unequivocally, it is the segment of the determined domain. Eventually, the results in diagrams are the followings (*Figure 3.2).*

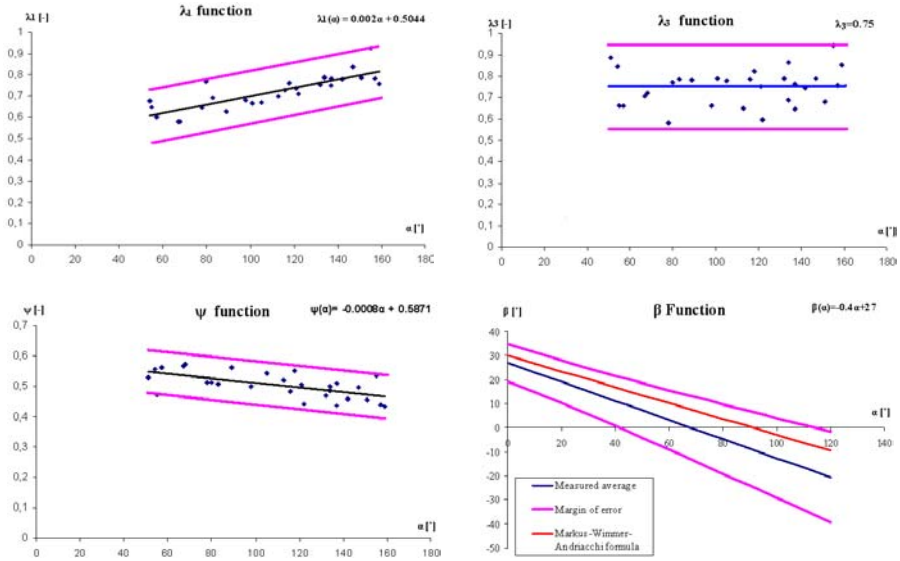

Figure 3.2. Final results of the demanded proportional parameters

With the introduction of these constants and functions, the mechanical model turned to be ready to execute. The solution of the proportional quadriceps force function with the average values of the proportional parameters during flexion is shown on the *Figure 3.3*.

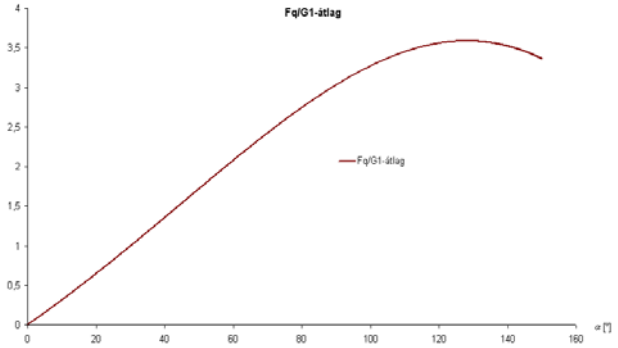

Figure 3.3. The computed quadriceps-force function

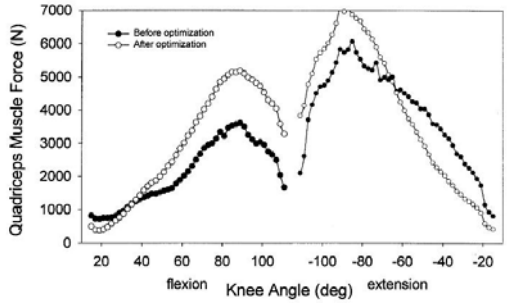

Figure 3.4. The measured quadriceps-force function

Approximately, the function is linear to 80˚, and besides the theoretical result of the SZIE mechanical model, an experimental result is shown carried out by N. Zheng **(***Figure 3.4***)**. Apparently, the character of the model and the experimental result is very similar in the case of flexion.

3.3 comparison of results

Since results derived by pure theoretic models can show great differences between model and reality, in association with the Ghent University verification tests were done on a totally different test rig. The Ghent University set-up is capable to measure the force in the quadriceps, but the proportional parameters can not be adjusted, so the given results are not an entirely appropriate model of the human squatting.

The *Figure 3.5* represents the result of the artificial knee according to the mechanical model, which is only segment to 55˚.

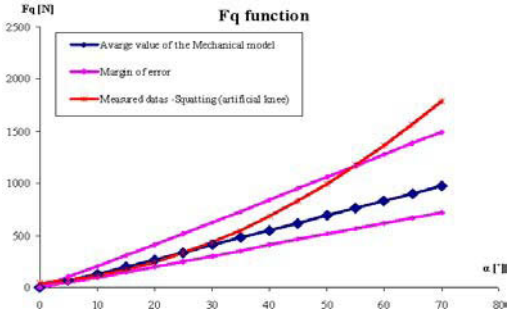

Figure 3.5. Comparison of quadriceps force (artificial knee joint vs. mechanical model)

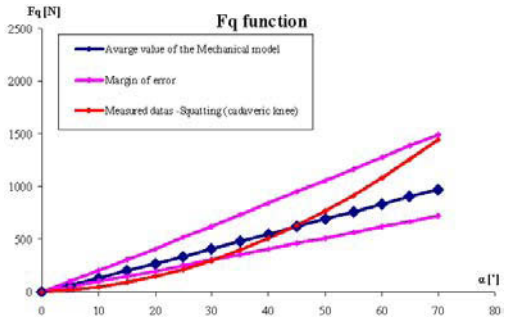

Figure 3.6. Comparison of quadriceps force (cadaver knee joint vs. mechanical model)

With the cadaver knee, the given results are better; the segment goes to 70˚ (*Figure 3.6*). This way the demanded parameters have been estimated with their statistical error, and in the case of the β function, compared with the reference formula. Using the obtained parameters, the solution of the quadriceps force function correlates with the experimental results of the reference. For further use, the functions of the mechanical model can be applied in the computation knee joint model as more realistic and validated boundary conditions, according to the former 'constant loaded' conditions. The applicability of the test rigs is also determined with these calculations and experiments.

4. Computational local mechanical model

4.1 internal motions and their backroud

Since different results about the human knee joint are available, the internal motions and special addition features such as the combination of sliding and rolling must be examined. Two kinds of motions occur inside of the human knee joint during action, which are namely sliding and rolling. Their gradient and proportion is currently unknown. Zuppinger was the first among the medical

researchers who claimed according to X-ray images that the relation between the tibia and femur was basically rolling until 20° of flexion and beyond that point, sliding and rolling jointly occurred. Making a decision about the proportion of movements and the behavior of the phenomena by using only X-ray images is simply impossible. This is the reason why the other aim of the team is to found a new and applicable method to correctly investigate and determined the phenomena of *sliding-roll*. To do so, a special proportional value will be introduced.

4.2 creation of model

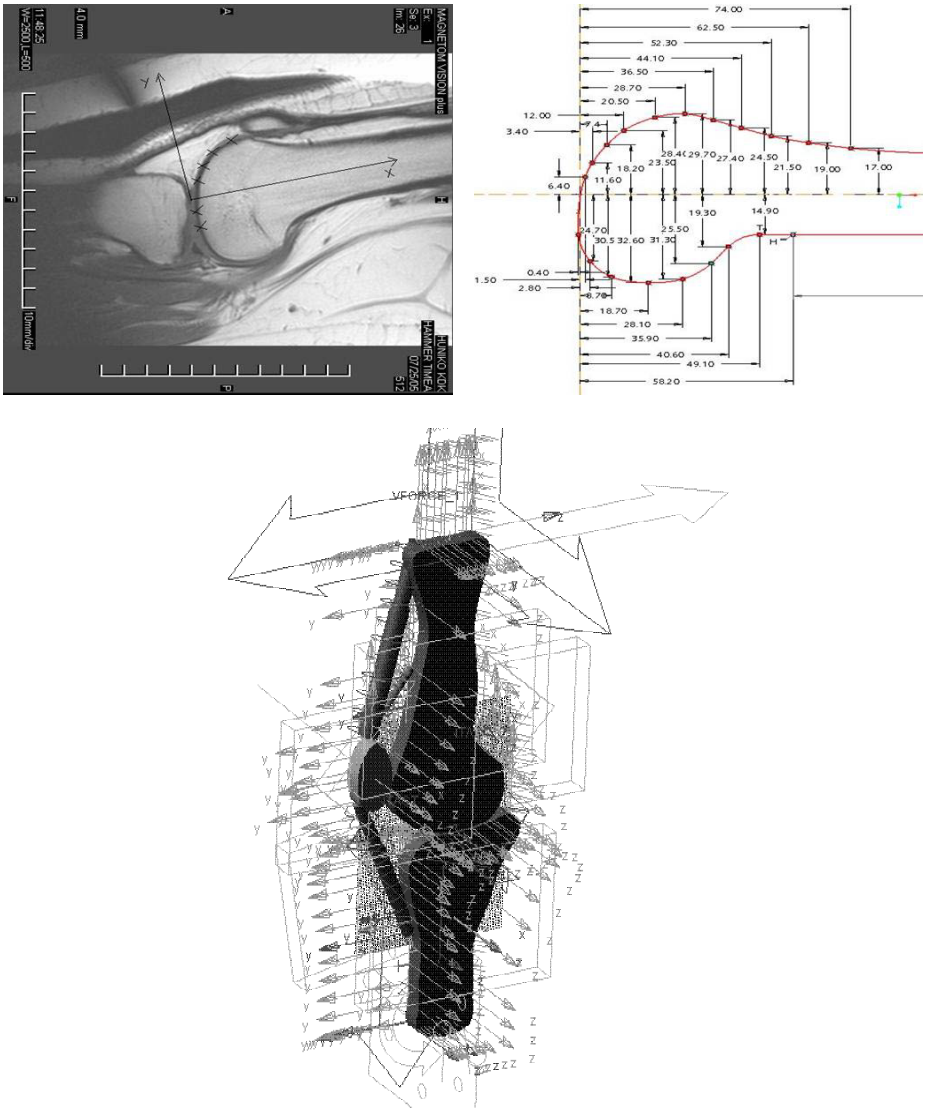

Figure 4.1. Algorithm of knee model creation

In order to correct these hypothesizes and to make further steps in the research the MSC.ADAMS program system was used to carry out computational examination and to build a complex knee model. MR images were taken and a model was mapped from them. With basic CAD methods a geometric model was generated and imported into the ADAMS (*Figure 4.1.)*.

The following simplifications were applied:

- 2.5D model (it involves a third finite extent)
- Bones are considered to be rigid bodies
- The damping and mechanical properties of the meniscuses are neglected but their lubricating behavior is taken into consideration

In the interest of to carry out squatting motion, kinematical constraints must be set to the model elements. The elements such as the femur, tibia and patella must be fixed to each other and to the environment. The following constraints and boundary conditions were applied in the program:

- Tibia, femur and patella can only perform planar motion (PLANAR JOINT),
- The top of the femur is attached to the hip-bone, thus deflection in the 'x' direction is not possible (MOTION JOINT),
- Bodies are attached to each other by springs (SPRING), therefore the muscle model is introduced,
- The tibia is attached to the environment by a hinge, thus the rotation around the 'z' axis is permitted (HINGE),
- The static friction coefficient is 0.11, while according to Wang the dynamic friction coefficient is 0.008,
- One force in the 'y' direction is acting on the femur with a magnitude of 60 N.

4.3 The calculation method

Let a new specific value be introduced, which shall be titled as *sliding-rolling coefficient*, and denoted with χ. Let χ defined as:

$$\chi = \frac{\Delta s_{2i} - \Delta s_{3i}}{\Delta s_{2i}} \tag{1}$$

- $\Delta s_{2i} = s_{2i} - s_{2K}$: Difference of the ith arc length extracted the initiative K arc length of the 2nd body,
- $\Delta s_{3i} = s_{3i} - s_{3K}$: Difference of the ith arc length extracted the initiative K arc length of the 3rd body.

The above-mentioned quantity shows the proportion of the connecting arc lengths in percentages, thus exact conclusions can be drawn to the sliding and rolling feature of the motion. If the value of χ equals to 1, then it is pure sliding, and if it equals to 0, then it is pure rolling.

To carry out this calculation, the arc lengths must be determined. The following kinematic quantities can be calculated by the MSC.ADAMS during the simulation of the motion:

– $\bar{r}_K(t)$ vector-scalar function, which determines the instantaneous position of the connecting points of the two bodies (*Figure 4.2*.),

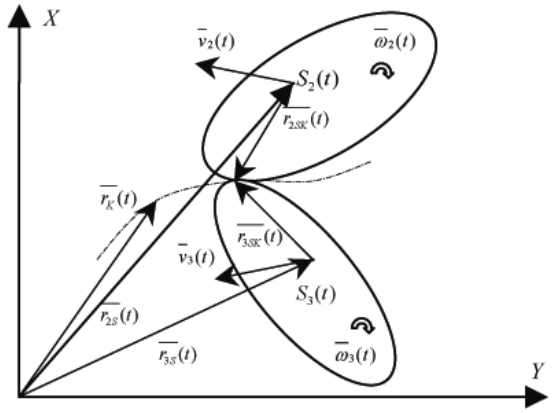

Figure 4.2. Computable displacement vectors defined in the MSC.ADAMS

– $\bar{r}_{2S}(t), \bar{r}_{3S}(t), \bar{v}_{2S}(t), \bar{v}_{3S}(t), \bar{\omega}_2(t), \bar{\omega}_3(t)$ vector-scalar functions, which sequentially determine the instantaneous position of the center of gravity, velocity and angular velocity of the 2nd and 3rd bodies (*Figure 4.3*.).

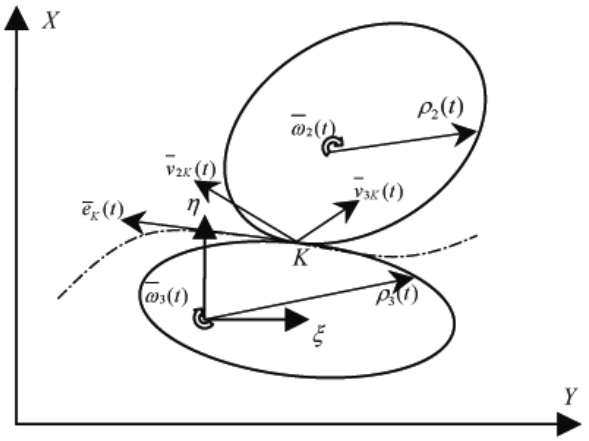

Figure 4.3. Computable velocity vectors defined in the MSC.ADAMS

In addition the following kinematic quantities can be directly estimated:

– Instantaneous values of F_f and F_N, which are the normal and frictional components of the connecting surfaces,

In order to examine the proportion of sliding and rolling, let us consider the following well-known formula from the results given by the MSC.ADAMS:

$$d\bar{r} = \bar{r}_{2SK}(t) = \bar{r}_K(t) - \bar{r}_{2S}(t) \tag{2}$$

Substituting the results of (1) equation into the (2) and (3):

$$\bar{v}_{2K} = \bar{v}_{2S} + \bar{\omega}_2 \times \bar{r}_{2SK}(t) \tag{3}$$

$$\bar{v}_{3K} = \bar{v}_{3S} + \bar{\omega}_3 \times \bar{r}_{3SK}(t) \tag{4}$$

Thus the instantaneous velocity of the connecting points of the bodies can be calculated in the $x-y$ coordinate system. If the instantaneous tangent unit vector of the connecting curvature can be determined:

$$\bar{e}_K(t) = \frac{\dot{\bar{r}}_K(t)}{\left|\dot{\bar{r}}_K(t)\right|} \tag{5}$$

Then by multiplying the velocity vectors with it, the sliding components of the velocities become quantifiable:

$$v_{2N} = \bar{v}_{2K} \cdot \bar{e}_K(t) \text{, and } v_{3N} = \bar{v}_{3K} \cdot \bar{e}_K(t) \tag{6}$$

By these results the sliding components can be calculated:

$$\Delta v_N = v_{3N} - v_{2N} \tag{7}$$

After the execution of the ADAMS program, the following numerical results were produced *(Figure 4.4.)*. The proportion of the Ff/Fn function *(Figure 4.5.)* can be directly plotted.

Figure 4.4. correctly demonstrates that the sliding velocity components turn to be zero at approximately 26º, and by examining Figure 4.5. it shows the peak of the *Ff/Fn* function is also around 26º. That is the threshold where the first sliding occurs, and from that point until cca. 45º, the actions of sliding and rolling are combined. After 45º, the motion is characterized as pure sliding. Unfortunately, the integration of the sliding velocity component is not yet finished, but since the algorithm is already elaborated, the results will be soon presented.

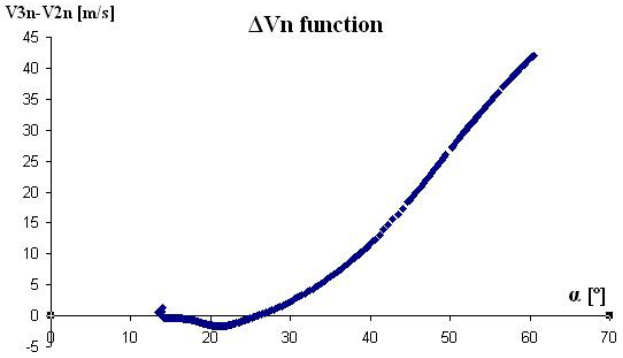

Figure 4.4. Sliding components

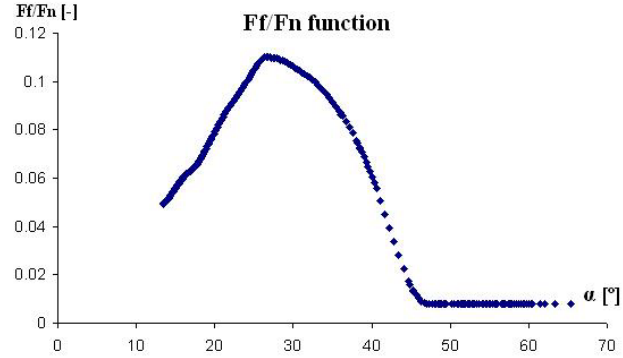

Figure 4.5. The proportion of the Ff/Fn function

5. Further results and applications

The above presented method provides a new way to investigate the phenomena of sliding and rolling in the case of planar motion. The method will be expanded to 3D investigations in the case of the sliding and rolling proportions of the condyles and prothesis. The goal with this method is partly to find the dominant part of the 3D surface, which takes up the majority portion during motion, and partly to investigate these quantities on several human subjects. In this way, by averaging the given results, hopefully a general conclusion will be drawn about the possible domains of the surface where the upcoming wear would be demolishing. In this part of the project, statistical methods will be applied on the set of data in order to determine the sliding-rolling proportions of the human knee. On the other hand, after creating a fairly accurate model, the idea is that according to the measured quantities of angles, the computational model would be adjusted to these statistical results. This can be carried out by an iterative modification of the geometry until the point where the numeric result correctly approximates the result measured by the POLARIS.

References

I. Bíró – B. M. Csizmadia – G. Katona: Determination of instantaneous axis of rotation of tibia and its role in the kinematical investigation of human knee joint, Proceedings of the Third Hungarian Conference on Biomechanics, Budapest, July 4-5, 2008, p. 55-62, ISBN 978 963 06 4307 8

B. M. Csizmadia – G. Katona: Some result on the motion analysis executed on the experimental model of the human knee. 23rd Danubia Adria Symposium on Experimental Methods in Solid Mechanics – Extended abstracts, Podbanské – Zilina, Slovak Republic, 2006.11.26-27.

G. Fekete: Numerical methods for determining local motions of human knee joint, Zilele Tehnice Studentesti - Editia a XII-A, Timisoara, 12-18 Mai (In press), 2008.

B. M. Csizmadia – I. Bíró – G. Katona – Z. Szakál: A térdizület számítógépes megjelenítésén alapuló stereotaxisos navigációs műtéti eljárások (Stereo-taxis navigational methods of surgery, based on computational monitoring of human knee joint). NKFP/1B/0009/2002 pályázat keretében készült kutatási jelentés.

Szentághotai János: Funkcionális Anatómia (Functional anatomy). Medicina Kiadó, Budapest – 1975.

G. Fekete: Experimental methods for determining of mechanical model of human knee, Zilele Tehnice Studentesti - Editia a XI-A,Timisoara, 6-13 Mai, p. 1-8, ISSN 1843 - 1917, 2007.

A. Marcus, Wimmer, T.P. Adriacchi: Tractive forces during rolling motion of the knee: Implications of wear in total knee replacement. Journal of Biomechanics 30 (1997), 131-137.

N. Zheng, G.S. Fleisig, R.F. Escamilla, S.Barrentine: Analytical model of the knee for estimation of internal forces during exercise. Journal of Biomechanics 31 (1998), 963-967.

J.Heegaard, P.F. Leyvraz, A. Curnier, L. Rakotomanana, R. Huiskes: The biomechanics of the human patella during passive knee flexion. Journal of Biomechanics 28 (1995), 1265-1279.

W. Mesfar, A. Shirazi-Adl: Biomechanics of the knee joint in flexion under various quadriceps forces. The Knee 12 (2005), 424-434.

Rheo-Optical Characteristics and the Poynting Thomson Model

Endre GELENCSÉR
Department of Mechanics and Technical Drawing, Institute of Mechanics and Machinery

Abstract

The plastic model materials of photoelasticity are homogenous and isotropic similarly to metals. Against all the stress condition belonging to load and the strain condition related to this is formed with a significant time phase lag. The reason-result relations of this phenomenon were researched using the means of linear rheology.

1. Rheological properties

Rheology is the field that researches the stress and deformation conditions that depend also on time. The rheological models consist of linear elements describe also the time depending changes of stress and deformation conditions.

The time factor is taken into consideration by introducing the stress speed and elongation speed into the material equations. The general form of linear material model containing also time

$$\Phi(\sigma, \varepsilon, \dot{\sigma}, \dot{\varepsilon}) = 0\,,$$

that takes the time dependent creeping and relaxation phenomena into consideration.

One of the possible material equations in single-axle stress condition:

$$\sigma = a\varepsilon + b\dot{\varepsilon} - c\dot{\sigma}$$

where:
σ – stress,
ε – nominal elongation,
$\dot{\sigma}$ – stress speed,
$\dot{\varepsilon}$ – speed of nominal elongation,
a, b, c – material constants.

Assuming that the examined materials behave according to the above relation, their material constants can be determined based on them. The compact, visco-elastic material model appropriate to the equation can be created by connecting basic elements symbolizing flexible, viscous and plastic properties in series or in parallel.

One of the elements has a perfectly flexible characteristic: the force is proportional to the nominal elongation, the other basic element is the speed-proportional damping element representing the viscous liquid, while the plastic element starts operating above a certain stress level.

The solutions of the material equations describing the phenomenon provide the constants typical of the material provided the boundary conditions are appropriate. Applying these equations have very diverse opinions in the literature, even the method for choosing the models is not clarified, in many cases it is random or arbitrary.

It is expedient to examine first the question of model choosing based on other aspects and then carrying out the detailed analysis following this. The basic elements of the model needed to describe the phenomenon can be determined by carrying out some basic, simple experiments and even the proportions of the main characteristics of these can be determined.

Material equations

It is practical to create the solutions of the material equations in the first step in a format valid for single-axle stress condition. In rheological models finding the solution for differential equations describing the phenomenon is not easy. Completing the calculations in case of too complicated models is not possible or it is very difficult. For this reason it is practical to limit the number and type of elements. I have used three basic elements during the analysis: the flexible element, the damping one and the plastic one. The solutions of the *material equations* valid for the optional stress and deformation conditions can be found in the literature.

2. The Poynting Thomson model

The model is actually built of a elastic element parallel connected to a Maxwell model. The force acting on the system in case of elements connected in parallel is the sum of forces in each line parallel to each other. The force this way is the sum of the values of the two basic elements (Fig 1.)

$$F = F_c + F_M = \frac{y}{c} + r\dot{y} - Fcr$$

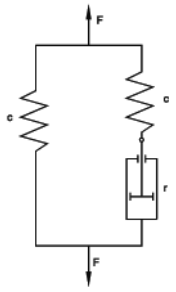

Figure 1. Resulting force

With nominal value

$$\frac{F}{A}=\frac{L}{cA}\frac{y}{L}+\frac{rL}{A}\frac{d}{dt}\left(\frac{y}{L}\right)-\frac{Lr}{AE}\frac{d}{dt}\left(\frac{F}{A}\right)$$

And finally the result is the

$$\sigma = E\varepsilon + \lambda\dot{\varepsilon} - R\dot{\sigma}$$

equation. This is the $\sigma=\sigma_o$=constant and it corresponds the Kelvin model with the $\varepsilon=\varepsilon_o$ initial requirements. So the form of the solution regarding the nominal elongation is

$$\varepsilon = \frac{\sigma_o}{E} + \left(\varepsilon_o - \frac{\sigma_o}{E}\right)\mathrm{e}^{-\frac{E}{\lambda}t}$$

that is the equation of the creep curve (Fig. 2a).

The differential equation in case of $\varepsilon=\varepsilon_o$=constant is

$$\sigma = E\varepsilon_o - R\dot{\sigma}$$

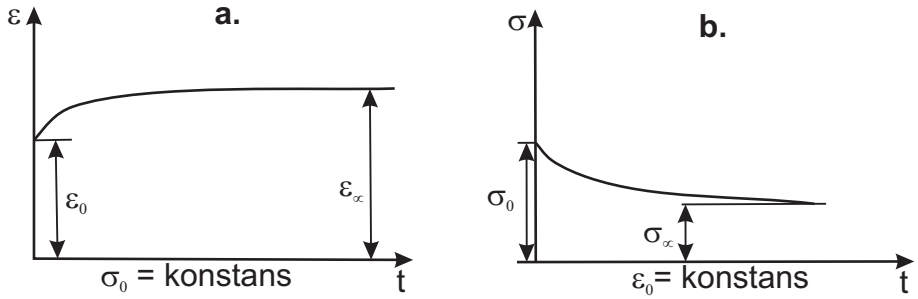

Figure 2. ε and σ in the function of time

That equals to the equation of the Maxwell model, not considering the $E\varepsilon_o$ constant.

The solution of the equation with the given initial conditions is

$$\sigma = E\varepsilon_o + \left(\sigma_o - E\varepsilon_o\right)\mathrm{e}^{-\frac{E}{\lambda}t}$$

that is the equation of the relaxation curve (Fig. 2b.).

3. Optical properties

The optical properties must be determined in polarized light. The principle of the measuring method: the throughput speed of the light through double refracting materials on the effect of stress is in direct proportion to the difference of main stresses.

The light: is a transversal electromagnetic vibration that does not have an indicated vibration direction, that means it is spreading equally into all directions of the space.

Polarization: polarization of the light means choosing components of a special plane.

In mathematical format:

$$\begin{bmatrix} I_x \\ I_y \end{bmatrix} = \begin{bmatrix} 0 \\ I_0 \, \mathrm{e}^{i \cdot \omega \cdot t} \end{bmatrix}$$

The mathematical description of the polariscope (Fig 3.). Since the optical and the mechanical main directions are equivalent, that is $\varphi_O = \varphi_M$ the light vector can be expressed in the format of a complex vector based on the analyzer (this is the Jones-type of notation)

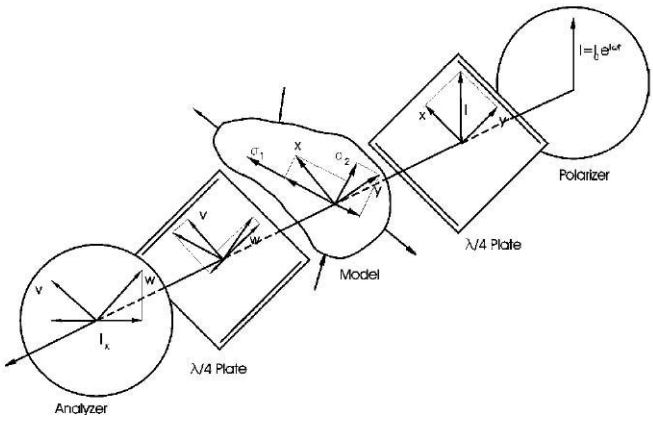

Figure 3. Model of the polariscope

$$\begin{bmatrix} I_x \\ I_y \end{bmatrix} =$$

$$= \begin{bmatrix} 1 & 0 \\ 0 & 0 \end{bmatrix} \frac{1}{\sqrt{2}} \begin{bmatrix} 1 & -i \\ -i & 1 \end{bmatrix} \mathrm{e}^{\frac{i\Delta}{2}} \begin{bmatrix} 1 & 0 \\ 0 & \mathrm{e}^{-i\Delta} \end{bmatrix} \frac{1}{\sqrt{2}} \begin{bmatrix} 1 & i \\ i & 1 \end{bmatrix} \begin{bmatrix} 0 \\ I_0 \, \mathrm{e}^{i\omega t} \end{bmatrix}$$

I_0 – amplitude of the light vector before the polarizer,

I_x – x-component of the light vector after the polarizer,
I_y – y-component of the light vector after the polarizer,
e – base of the natural logarithm (2,71),
i – imaginary unit ($\sqrt{-1}$),
ω – circular frequency of the λ wavelength light,
t – time,
Δ – relative retardation.

The matrixes describing each optical units:

$$\begin{bmatrix} 0 \\ I_0 \mathrm{e}^{i\omega t} \end{bmatrix} \text{ the polarizer,}$$

$$\begin{bmatrix} 1 & i \\ i & 1 \end{bmatrix} \text{ the } \lambda/4 \text{ plate,}$$

$$\begin{bmatrix} 1 & 0 \\ 0 & \mathrm{e}^{-i\Delta} \end{bmatrix} \text{ the model,}$$

$$\begin{bmatrix} 1 & 0 \\ 0 & 1 \end{bmatrix} \text{ the analyzer.}$$

The $\frac{1}{\sqrt{2}}$ in the equation means rotation of the λ/4 plates in π/4 degree.

Following the designated actions

$$\begin{bmatrix} I_x \\ I_y \end{bmatrix} = \frac{I_0 \cdot \mathrm{e}^{i\omega t}}{2} \cdot \begin{bmatrix} 2\sin(\Delta/2) \\ 0 \end{bmatrix}.$$

Sum of squares of the components of the light vector after the analyzer

$$I^2 = I_x^2 + I_y^2 = I_0^2 \cdot \mathrm{e}^{2i\omega t} \cdot \sin^2\left(\frac{\Delta}{2}\right).$$

The intensity of the light vector

$$I_0 \cdot \sin^2\left(\frac{\Delta}{2}\right),$$

is 0, if $\frac{\Delta}{2\pi} = m$, if m is an integer number, and the physical content of m is the phase lag or the ordinal number.

Double refraction and stress condition

The components of the light vector travel through the d thickness double refraction plate at different c_1 and c_2 speed. In accordance with this their wavelengths are different and this is the reason for the phase deviation or the ordinal number

$$m = M_1 - M_2 = d\nu \cdot \left(\frac{1}{c_1} - \frac{1}{c_2} \right) = d\nu \cdot \left(\frac{c_2 - c_1}{c_1 \cdot c_2} \right),$$

ν – the frequency of the monochromatic light.

In case double refraction is small, there is not a big difference between the two speed values, even compared to c_0 the difference is not big so the double refraction

$$m = \frac{d\nu}{c_0^2} \cdot (c_2 - c_1) = \frac{d}{\lambda \cdot c_0} (c_2 - c_1)$$

The phase deviation is caused by the deformation perpendicular to the light vector that depends linearly on the light speed. In plane stress condition the relation between c_1 and c_2 and between ε_1 and ε_2

$$c_1 = c_0 + a \cdot \varepsilon_1 + b \cdot \varepsilon_2, \quad c_2 = c_0 + a \cdot \varepsilon_2 + b \cdot \varepsilon_1,$$

and

$$c_1 - c_2 = (b - a) \cdot (\varepsilon_1 - \varepsilon_2),$$

c_o – speed of the light in an unloaded model,
a, b – material constants.

The Hooke-law is valid for linear flexible conditions

$$\varepsilon_1 = \frac{1}{E} \cdot (\sigma_1 - \mu \cdot \sigma_2), \quad \varepsilon_2 = \frac{1}{E} \cdot (\sigma_2 - \mu \cdot \sigma_1),$$

and

$$\varepsilon_1 - \varepsilon_2 = \frac{1 + \mu}{E} (\sigma_1 - \sigma_2).$$

σ_1 – the larger main stress of the plane stress condition,
σ_2 – the smaller main stress of the plane stress condition.

This way the phase deviation:

$$m = \frac{d \cdot (b-a) \cdot (1+\mu)}{\lambda \cdot c_0 \cdot E} \cdot (\sigma_1 - \sigma_2).$$

Our equation contains the a, b, m, E and c_o constants of what values depend on the material of the model. They can be combined in one, common constant

$$m = \frac{C}{\lambda} \cdot d \cdot (\sigma_1 - \sigma_2).$$

The wavelength of the applied light must always be supplied in optical stress examinations. The equation for a constant wave length light:

$$m = (\sigma_1 - \sigma_2) \cdot k \cdot d\ .$$

4. Measurement of rheological and optical properties

Deformation and double refraction of the model materials happen with phase lag in time compared to an actual stress. The relation between the deformation and the stress and between the double refraction and the deformation in plane stress condition

$$\varepsilon_1 - \varepsilon_2 = \frac{1+\mu}{E}(\sigma_1 - \sigma_2) \qquad m = \frac{d}{D}(\varepsilon_1 - \varepsilon_2),$$

D – elongation optical constant,
ε_1, ε_2 – main elongation,
d – thickness of the model,
m – phase difference or ordinal number,
k – stress optical constant,
E – elastic modulus.

In a single-axle stress condition $\varepsilon_2 \approx 0$ and $\varepsilon = \varepsilon_1$

$$m = \frac{d}{D} \cdot \varepsilon.$$

In time depending, so called rheological experiments the double refraction is determined by stress and elongation together. If the stress is constant (creeping), the double refraction depends only on elongation, that means that is changes in proportion with it

$$m = \beta\varepsilon(t) = m(t).$$

Simultaneous measurement of deformation and double refraction

I used a flat test piece for the experiments. The single axle stress condition was provided by the two load bore-holes.

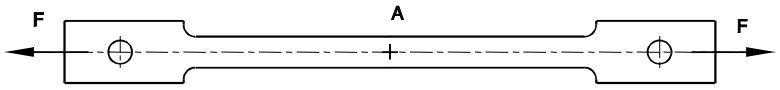

Figure 4. Test specimen

In order to determine the $m = m(t)$ function I applied linearly increasing stress on the test piece ($\dot{\sigma}$ = constant) up to σ_o stress level, then I kept it at a constant level. I read the iso-chromatic ordinal number off accurately at stated intervals using the Tardy-type compensation. The principle of the process is that the intensity of the light traveling through the analyzer does not only depend on the size of the double refraction but also the mutual locations of the polarizer and the analyzer.

The Tardy-type compensation in mathematical format:

$$\begin{bmatrix} I_x \\ I_y \end{bmatrix} = \begin{bmatrix} 1 & 0 \\ 0 & 0 \end{bmatrix} \begin{bmatrix} \cos(-\varphi) & \sin(-\varphi) \\ -\sin(-\varphi) & \cos(-\varphi) \end{bmatrix} \frac{1}{\sqrt{2}} \begin{bmatrix} 1 & -i \\ -i & 1 \end{bmatrix} \mathrm{e}^{\frac{i\cdot\Delta}{2}}$$

$$\begin{bmatrix} 1 & 0 \\ 0 & \mathrm{e}^{-i\Delta} \end{bmatrix} \frac{1}{\sqrt{2}} \begin{bmatrix} 1 & i \\ i & 1 \end{bmatrix} \begin{bmatrix} 0 \\ I_0 \mathrm{e}^{i\cdot\omega\cdot t} \end{bmatrix}.$$

$\begin{bmatrix} \cos(-\varphi) & \sin(-\varphi) \\ -\sin(-\varphi) & \cos(-\varphi) \end{bmatrix}$ the rotating matrix in the $x\ y$ plane, φ the traversing angle of the analyzer.

The basic equation

$$\begin{bmatrix} I_x \\ I_y \end{bmatrix} = I_0 \cdot e^{i\omega t} \cdot \begin{bmatrix} \sin\left(\varphi + \frac{\Delta}{2}\right) \\ 0 \end{bmatrix}.$$

The intensity

$$I_0^2 \sin^2\left(\varphi + \frac{\Delta}{2}\right)$$

will be 0, if $\left(\varphi+\frac{\Delta}{2}\right)=m\cdot\pi$, and m is an integral number, the phase deviation or the ordinal number, so in all cases, if

$$\frac{\Delta}{2\pi}=m-\frac{\varphi}{\pi}.$$

This means that not only the integer (1, 2, 3) double refraction but the fractional ordinal numbers can be measured.

For this reason the traversing angle of the analyzer must be read off. The circumference of the circle is practical to be divided into 100 equal size parts, this way the accuracy will be 1/50. The elongation of the test piece must be measured simultaneously with the double refraction, this results the $\varepsilon=\varepsilon(t)$ function. The appropriate tool for this task is the dual-gauge extensometer. To evaluate the data of the measurement we have the figures $m=m(t)$ of (Fig. 5.) and $\varepsilon=\varepsilon(t)$ of (Fig. 6.) functions in discrete points of time.

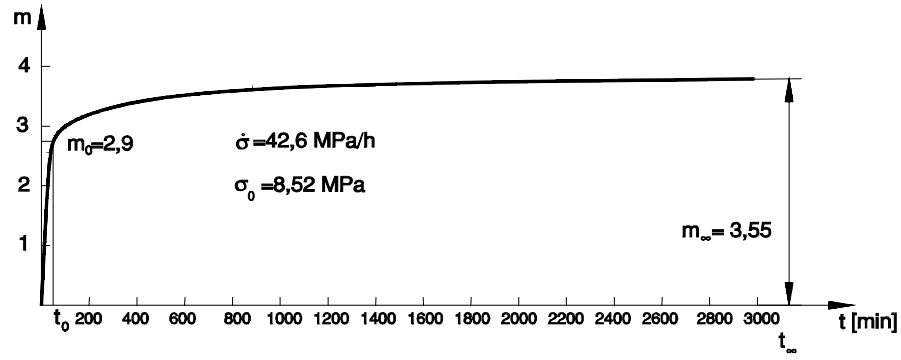

Figure 5. „m" integral number versus time

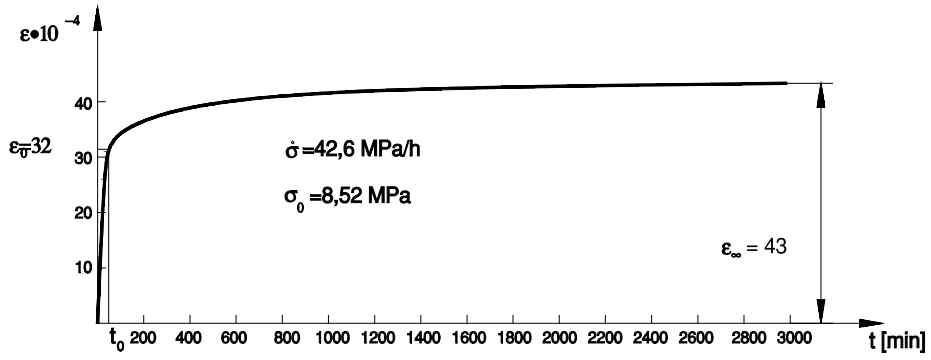

Figure 6. ε versus time

5. Determining material constants

The E, V, R material constants can be determined from the constitutive law based on the measurement data. The measurements were carried out on the model material marked CR-39 (CR = Columbia Resin) by me.
The constitutive law of the Poynting-Thomson model

$$\sigma = E\varepsilon + V\dot{\varepsilon} - R\dot{\sigma}$$

The solution besides $\sigma = \sigma_0 = \text{constant}$ and $\varepsilon = \varepsilon_0$ conditions is

$$\varepsilon = \frac{\sigma_0}{E} + \left(\varepsilon_0 - \frac{\sigma_0}{E}\right)e^{-\frac{E}{V}T}$$

if $t \to t_\infty \to \infty$ and $\varepsilon \to \varepsilon_\infty$ then $\varepsilon_\infty = \dfrac{\sigma_0}{E}$

The elastic modulus

$$E = \frac{\sigma_0}{\varepsilon_\infty}$$

In an optional t_Δ point of time

$$\varepsilon_\Delta = \varepsilon_\infty + (\varepsilon_0 - \varepsilon_\infty)\mathrm{e}^{-\frac{E}{V}T}$$

where
$T = t_\Delta - t_0$
In other format

$$e^{\frac{E}{V}T} = \frac{\varepsilon_\infty - \varepsilon_0}{\varepsilon_\infty - \varepsilon_\Delta} = a\ .$$

The creep coefficient

$$V = \frac{ET}{\ln a} = \frac{\sigma_0}{\varepsilon_\infty}\frac{T}{\ln a}$$

Having the $\sigma = \sigma_0 = \text{constant}$ and $\dot{\sigma} = 0$ initial conditions

$$\varepsilon = \frac{\dot{\sigma}}{E}\left[t - \left(\frac{V}{E} - R\right)\left(1 - \mathrm{e}^{-\frac{E}{V}T}\right)\right]$$

In the t_0 point of time

$$\varepsilon_0 = \frac{\dot{\sigma}}{E}\left[t_0 - \left(\frac{T}{\ln a} - R\right)\left(1 - \mathrm{e}^{-\frac{\ln a}{T}t_0}\right)\right]$$

but $\sigma_0 = \dot{\sigma} t_0$, so

The relaxation time

$$R = \frac{T}{\ln a} + \frac{\varepsilon_0\sigma_0 - \varepsilon_\infty\sigma_0}{b \cdot \varepsilon_\infty \cdot \dot{\sigma}} \quad \text{here} \quad b = 1 - \mathrm{e}^{-\frac{\ln a}{T}\frac{\sigma_0}{\dot{\sigma}}}$$

The changes of *E*, *V*, *R* material constants in relation of the stress speed are summarized in diagrams: (Fig. 7. – Fig. 9.)

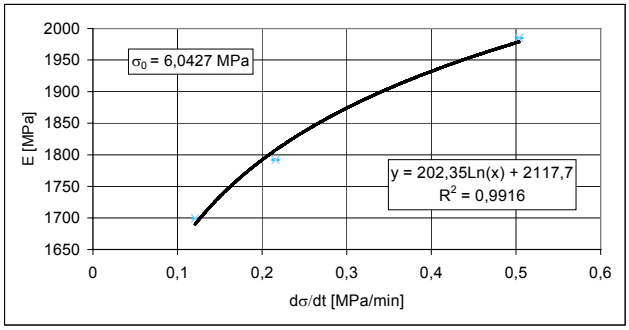

Figure 7. „E" in the function of stress speed

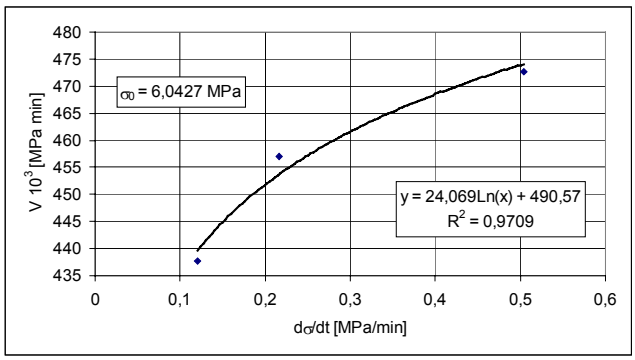

Figure 8. „V" in the function of stress speed

The material equation valid for double refraction

$$\Phi(\sigma, m, \dot{\sigma}, \dot{m}) = 0$$

Transforming this to the Poynting-Thomson model:

$$\sigma = E_{op} m + V_{op} \dot{m} - R_{op} \dot{\sigma}$$

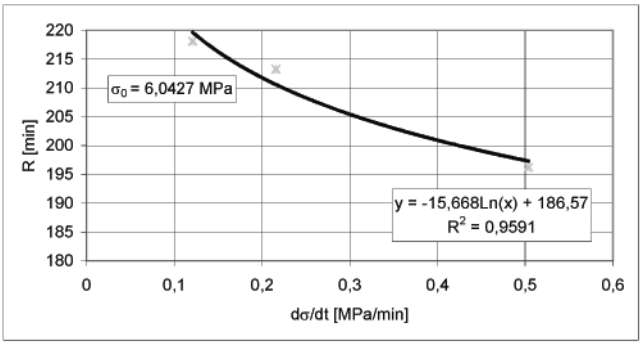

Figure 9. „R" in the function of stress speed

The solution is the $\sigma = \sigma_0 =$ constant and for the case of $m = m_0$

$$m = \frac{\sigma_0}{E_{op}} + \left(m_0 - \frac{\sigma_0}{E_{op}} \right) \mathrm{e}^{-\frac{E_{op}}{V_{op}} T}$$

if $t \to t_\infty \to \infty$ and $m \to m_\infty$, then

$$m_\infty = \frac{\sigma_0}{E_{op}}$$

The elongation modulus is

$$E_{op} = \frac{\sigma_0}{m_\infty}$$

In an optional t_Δ point of time

$$m_\Delta = m_\infty + (m_0 - m_\infty) \mathrm{e}^{-\frac{E_{op}}{V_{op}} T}$$

where $T = t_\Delta - t_0$

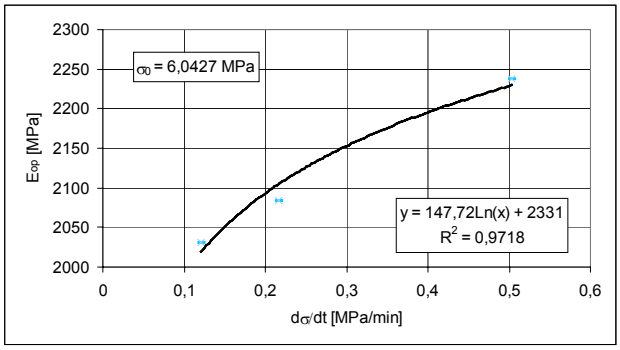

Figure 10. „E_{op}" in the function of stress speed

Following the transformation

$$e^{\frac{E_{op}}{V_{op}}T} = \frac{m_\infty - m_0}{m_\infty - m_\Delta} = a_{op} .$$

The creep coefficient

$$V_{op} = \frac{E_{op}T}{\ln a_{op}} = \frac{\sigma_0}{m_\infty}\frac{T}{\ln a_{op}}$$

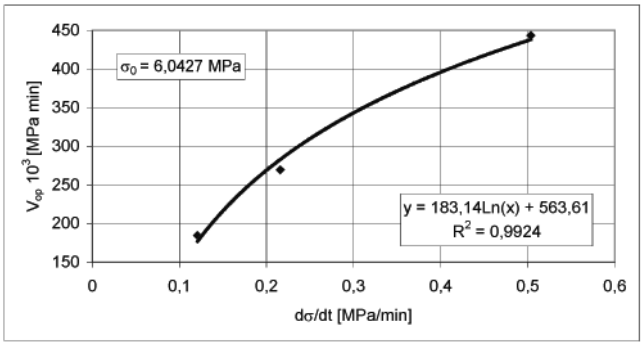

Figure 11. „V_{op}" in the function of stress speed

Let $\sigma = \sigma_0 = \text{constant}$ and $\dot{\sigma} = 0$, this way

$$m = \frac{\dot{\sigma}}{E_{op}}\left[t - \left(\frac{V_{op}}{E_{op}} - R_{op}\right)\left(1 - e^{-\frac{E_{op}}{V_{op}}T}\right)\right]$$

In t_0 time

$$m_0 = \frac{\dot{\sigma}}{E_{op}}\left[t_0 - \left(\frac{T}{\ln a_{op}} - R_{op}\right)\left(1 - \mathrm{e}^{-\frac{\ln a_{op}}{T}t_0}\right)\right]$$

but $\sigma_0 = \dot{\sigma} t_0$, so

The relaxation time

$$R_{op} = \frac{T}{\ln a_{op}} + \frac{m_0\sigma_0 - m_\infty\sigma_0}{b_{op}\cdot m_\infty \cdot \dot{\sigma}} \quad \text{here} \quad b_{op} = 1 - \mathrm{e}^{-\frac{\ln a_{op}}{T}\frac{\sigma_0}{\dot{\sigma}}}$$

Based on the results of the experiments it is obvious that the material constants change in relation to the stress level (σ_0) and the stress speed ($\dot{\sigma} = \mathrm{d}\sigma/\mathrm{d}t$) at constant temperature (τ = constant). The relation among the *E, V, R* mechanical properties and the

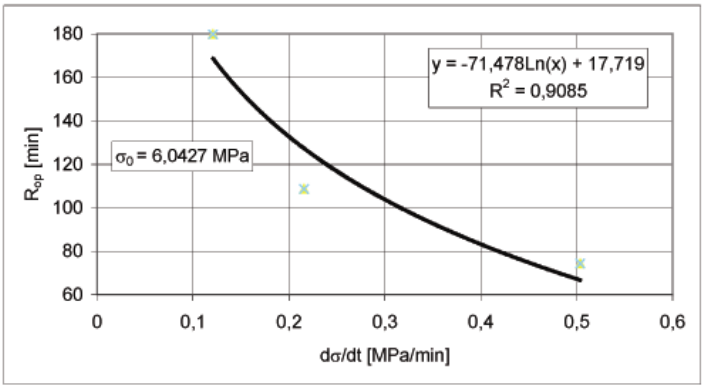

Figure 12. „R_{op}" in the function of stress speed

stress speed at a constant σ_0 stress level

$$E = 202{,}35\ln\dot{\sigma} + 2117{,}7$$
$$V = 24{,}069\ln\dot{\sigma} + 490{,}57$$
$$R = -15{,}668\ln\dot{\sigma} + 186{,}57$$

if $\sigma_0 = 6{,}0427$ MPa and $0{,}1209 \le \dot{\sigma} \le 0{,}5036$ MPa/min.

The relationship among the E_{op}, V_{op}, R_{op} optical material properties and the stress speed:

$$E_{op} = 147{,}72 \ln \dot{\sigma} + 2331$$
$$V_{op} = 183{,}14 \ln \dot{\sigma} + 563{,}61$$
$$R_{op} = -71{,}478 \ln \dot{\sigma} + 17{,}719$$

Here $\sigma_0 = 6{,}0427$ MPa and $0{,}1209 \le \dot{\sigma} \le 0{,}5036$ MPa/min again.

6. References

Huszár I. – Gelencsér E.: Reológiai mérések optikai feszültségvizsgálattal. (Rheological Measurements Completed by Optical Stress Experiments) Gép, 1974. 26. évf. 9. Sz. 332-338. P.

Gelencsér E.: Műanyagtömítés feszültséganalízise. (Stress Analysis of Plastic Sealings) Gép, 1977. 29. évf. 7. sz. 267-271. p.

Gelencsér E.: Az optikai feszültségvizsgálat kísérleti eredményeinek kiértékelése a Laplace egyenlet felhasználásával. (Evaluation of the Results of the Optical Stress Experiments Applying the Laplace-equation). Járművek Mezőgazdasági Gépek, 1978. 25. évf. 4. sz. 145-149. p.

Numerical Modelling of the Impact of the Tow Angle and The Tow Velocity for the Total Drag of Plough

István SZABÓ[*] and András ZACHÁR[**]
[*]Departemnt of Machine Construction, Institute of Mechanics and Machinery,
[**]Department of Informatics, Institute of Mathematics and Informatics

Abstract

The total drag is strongly depends on the tillage velocities and the towing angles in case of plough. Numerical investigations have been carried out to describe the behaviour of a ploughshare and the included plough breast-board. The aim of the study was to analyze the towing efficiency of a plough breast-board. The rheological behaviour of the soil has been considered as a non-Newtonian shear-thinning pseudo-plastic material. Three dimensional, multiphase flow computations have been carried out in Ansys CFX 11 environment. The calculated soil stress and the pressure field in the surface of the plough breast-board have been examined to gain more information about the entire physical processes. The calculated results clearly show that the total induced drag depends upon the towing velocity on a nearly parabolic way.

Nomenclature

c	drag coefficient
c_{pr}	pressure drag coefficient
c_{fr}	friction drag coefficient
F	total drag exerted on the tillage tool (N)
g	acceleration of gravity (m s^{-2})
K	mean viscosity value of the non-Newtonian material model (Pa s)
L	characteristic length (m)
P	total pressure on the surface of the tillage tool (Pa = N m^{-2})
t	time (s)
U, V, W	velocity components x, y, z directions (m s^{-1})
x, y, z	coordinates in the three possible directions (m)

Greek symbols

γ	sheer strain rate of the soil (s^{-1})
η	dynamic viscosity of the fluid (air, soil) (N s m^{-2}, Pa s)
ρ	density of the fluid (air, soil) (kg m^{-3})

1. Introduction

The study of tillage tool interaction on different types of soil is an important phase of tool design and development. Mouldboard ploughing is one of the most important and most energy consuming process of agricultural production. The aim of the presented study is to evaluate the effect of tow angle and towing velocity of plough breast-board geometry to increase the overall tillage efficiency. The total drag of a tillage tool is an important factor of the over all efficiency of soil tillage. The total drag c depends mainly upon the pressure distribution on the tool surface what generates the pressure drag c_{fr}, and the viscous or friction drag c_{pr}.

$$c = c_{fr} + c_{pr} \tag{1}$$

Drag coefficient can be defined by Eqn. 2, where F is the total drag force, V is the velocity into the downstream direction, ρ is the density of the working fluid and A is the characteristic area of the immersed body, in this case the plough.

$$c = \frac{F}{\frac{1}{2}\rho V^2 A} \tag{2}$$

In this study both components of the drag are investigated to gain more detailed information about the behaviour of the plough under different tillage conditions.

2. Literature review

Several studies have been used the method of computational fluid dynamics (CFD) to model soil tillage tool interaction (Formato *et al*., Karmakar *et al.*). Generally three different properties are used to characterize the efficiency of a tillage tool. These are the draught to operate the tillage tool in this case the plough, the soil loosened and the total energy requirement is needed (Karmakar *et al*.). Mechanical behaviour of agricultural soils is an extremely difficult area of research due to the complexity of soil parameters and operating conditions. Many different researches have shown that agricultural soils are approximately showing brittle fracture mechanical behaviour during soil tillage. (Chandler 1984, Aluko and Seig 2000) Several other studies hypothesized different type of soil mechanical behaviour, visco-elastic (Kocher and Sunners, 1985), hypo-elastic (Rosa and Wulfsohn, 1999), elastic- perfectly plastic (Mouazen and Neményi, 1999; Mouazen *et al.* 1999).

3. Theoretical considerations

This section provides the basic equations that must be solved to describe the velocity field and the pressure distribution around the plough. The physical problem is a steady, three dimensional flow of a two component fluid the first one is the air and the other one is the soil component. The momentum equation of the fluid is based on the three dimensional Navier-Stokes equations. A SIMPLE like method is applied to solve the momentum and continuity equations (Patankar 1980, Versteeg and Malalasekera). The dependent variables that describe the present flow situation are the pressure P, the velocity component U in the x direction, velocity component V in the y direction and the velocity component W in the z direction.

3.1. Conservation equations

The following set of partial differential equations for U, V and W as functions of x, y, z describes the flow field around the plough-breast board.

3.1.1. Continuity equation

The continuity equation is formulated in the following manner in Cartesian coordinate system.

$$\frac{\partial}{\partial x}(\rho U)+\frac{\partial}{\partial y}(\rho V)+\frac{\partial}{\partial z}(\rho W)=0\cdot \tag{3}$$

3.1.2. Momentum equations

The following equation system is the representation of the momentum equations where x, y, z means the three different coordinate directions,

$$\frac{\partial}{\partial t}(\rho U)+\frac{\partial}{\partial x}(\rho U^2)+\frac{\partial}{\partial y}(\rho V U)+\frac{\partial}{\partial z}(\rho W U)= \\ =-\frac{\partial P}{\partial x}+\frac{\partial}{\partial x}\left(\eta\frac{\partial U}{\partial x}\right)+\frac{\partial}{\partial y}\left(\eta\frac{\partial U}{\partial y}\right)+\frac{\partial}{\partial z}\left(\eta\frac{\partial U}{\partial z}\right) \tag{4}$$

$$\frac{\partial}{\partial t}(\rho V)+\frac{\partial}{\partial x}(\rho U V)+\frac{\partial}{\partial y}(\rho V^2)+\frac{\partial}{\partial z}(\rho W V)= \\ =-\frac{\partial P}{\partial y}+\frac{\partial}{\partial x}\left(\eta\frac{\partial V}{\partial x}\right)+\frac{\partial}{\partial y}\left(\eta\frac{\partial V}{\partial y}\right)+\frac{\partial}{\partial z}\left(\eta\frac{\partial V}{\partial z}\right) \tag{5}$$

$$\frac{\partial}{\partial t}(\rho W)+\frac{\partial}{\partial x}(\rho UW)+\frac{\partial}{\partial y}(\rho V W)+\frac{\partial}{\partial z}(\rho W^2)= \\ =-\frac{\partial P}{\partial z}+\frac{\partial}{\partial x}\left(\eta\frac{\partial W}{\partial x}\right)+\frac{\partial}{\partial y}\left(\eta\frac{\partial W}{\partial y}\right)+\frac{\partial}{\partial z}\left(\eta\frac{\partial W}{\partial z}\right) \tag{6}$$

where η is the dynamic viscosity of the soil and the air respectively and ρ is the density of the working fluids.

3.1.3. Non-Newtonian material model

Soil is modeled a non-Newtonian pseudo-plastic material to describe the mechanical behaviour of the soil. Dynamic viscosity of a non-Newtonian fluid can be formulated by the following manner where K is the mean viscosity value, n is an exponent specifying the deviation of the material considered from the Newtonian material, and γ is the shear strain rate.

$$\eta = K\gamma^{n-1} \tag{7}$$

3.2. Model validation

It is inevitably important to verify the applicability of the non-Newtonian material model and the CFD approach to simulate the soil plough mouldboard interaction. The value of K and n are specified with the experimental results presented by (Formato *et al*.). Fig. 1 shows the geometrical sizes of the experimentally studied (Formato *et al*.) plough mouldboard. The experimental test has been carried out with 2.86 m/s towing velocity and the working depth was 0.3 m.

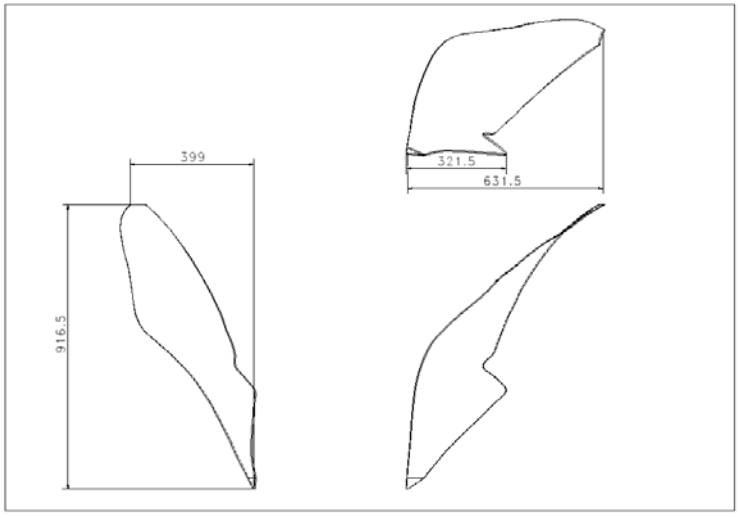

Figure 1. Experimentally tested geometry (Formato *el al*.)

The measured drag force was 4150 N and the total pressure has been monitored at 14 points of the surface of the plough. The calculated drag force with the specified model parameters is 3894 N. The relative error between the measured and the calculated results is

$$\varepsilon = \frac{F_{Measured} - F_{Calculated}}{F_{Measured}} 100 = 0.0661 = 6.61 \quad [\%] \cdot$$

According to the experimental results the applied value for the mean viscosity is K=55 Pa s and the value of the exponent is n=1,5.

Table 1 shows a quantitative comparison of the measured and calculated results with a simple statistical measure.

Geometrical location of the control points can be seen in the second, third and fourth column of Table 1. The following two show the measured and calculated pressure at that points and in the last column the relative error of the calculations is presented. Relative error of the pressure values has been calculated in the following manner $\varepsilon = \frac{P_{Measured} - P_{Calculated}}{P_{Measured}} 100 \quad [\%]$

Table 1. Comparison of the measured and the calculated results

Point	x[m]	y [m]	z [m]	Pressure [Pa]		Relative error [%]
				Measured	Calculated	
1	0.249	0.4	0.17	18000	17466	2.96
2	0.291	0.561	0.299	17000	15820	6.94
3	0.22	0.52	0.37	13000	14220	-9.38

4. Materials and methods

4.1. Domain of discretization and the applied computational grids

Several different geometrical arrangements of the plough-breast board have been studied on different grids. A schematic diagram of the plough indicating one of the applied grids for the computational domain is shown in Fig. 2.

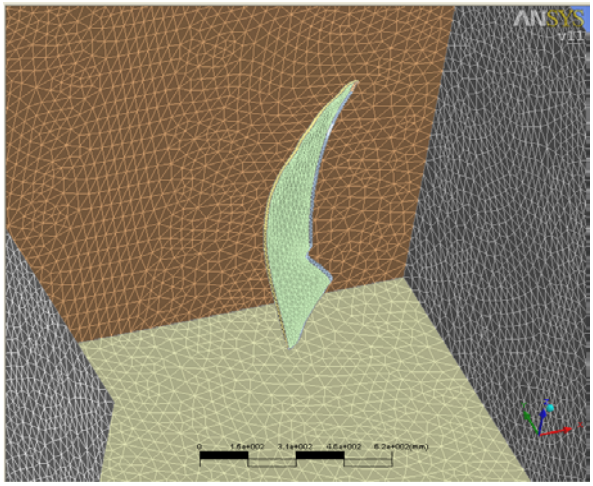

Figure 2. Top view of the generated grid applied for the calculations

The size of the calculation domain is chosen so that the wall effect is negligible and some test calculations have been carried out to check the independency of the numerical result from the horizontal and vertical size of the domain. A careful check for the grid-independence of the numerical solution has been made to ensure the accuracy and validity of the numerical scheme. Four different grids have been used to check the grid independence of the numerical scheme. The total drag of the plough has been applied to test the grid independence of the numerical calculations. The applied grid can be seen in Fig. 3 is much finer near the leading edge of the plough-share than the far field region. Comparison of the results of the calculation on the different grids is shown in Table 2.

Table 2. The induced drag and the relative error of the drag force on the studied grids

Studied grids [Number of cells]	I	II	III	IV
	332 486	391 606	531 722	759 842
Drag force, F [N]	2924.3	2920.5	2912.1	2913.2
Relative error of the drag force $100\left\|\frac{F_{coarser} - F_{finest\ grid}}{F_{finest\ grid}}\right\|$ [%]	0.381	0.25	-0.03	0

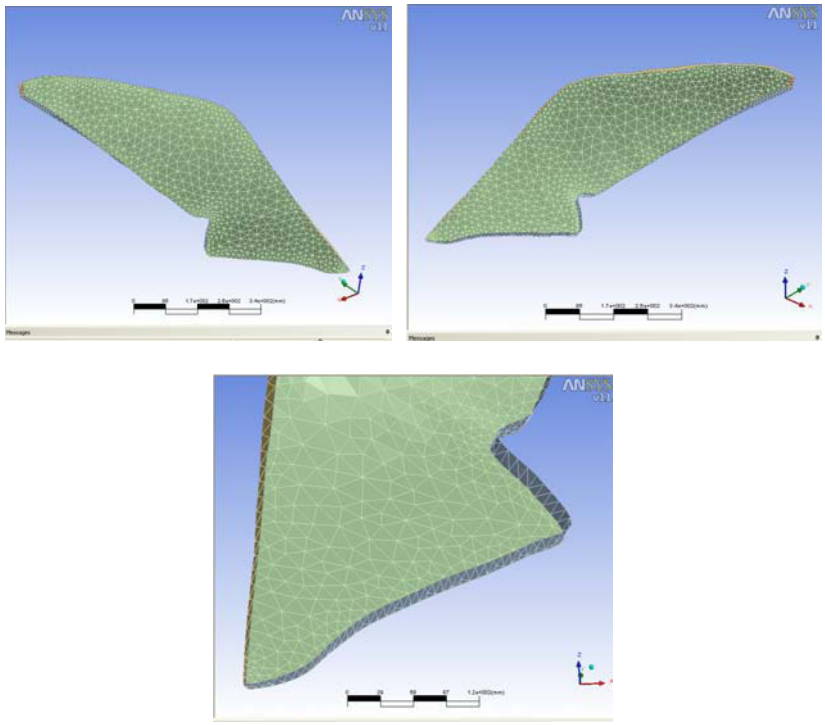

Figure 3. Grid near the plough and the edge of the ploughshare

The induced drag force has been used to test the grid independency of the numerical model. The relative error calculated according to the assumption that the result of the finest grid is approximately ideal. The calculated results show that the difference between the induced drag forces on the finest grids is less than 0.03 %. It means that a grid resolution for the applied calculation domain finer than the third (*III*) grid is acceptable to produce physically realistic calculation results independent from the numerical grid.

4.2. Initial conditions and boundary conditions

The initial velocity field is zero everywhere in the calculation domain. A uniform, constant velocity profile is assumed at the inlet position. The gradient of the velocity profile is assumed to be zero at the end of the outlet location. No-slip boundary conditions have been applied at the bottom, and the left and right wall. At the top of the calculation domain a free-surface boundary condition is specified.

4.3. Numerical solution of the transport equations

Finite volume code has been used in ANSYS CFX environment to solve the transport equations with the specified initial and boundary conditions. A high resolution scheme is used to discretize the convection term in the transport

equations. The resulting large linear set of equations is solved with an efficient linear solver a so-called algebraic multi-grid method.

5. Results

Seven different geometrical arrangements of the plough-breast board have been studied on an adequately fine grid. The total number of cells is 978 995 in the generated grid and this grid resolution is finer than the finest grid applied in the grid independence study. The computational resources make it possible to apply this grid refinement. Fig. 4 shows the applied computational domain to simulate the soil plough mouldboard interaction.

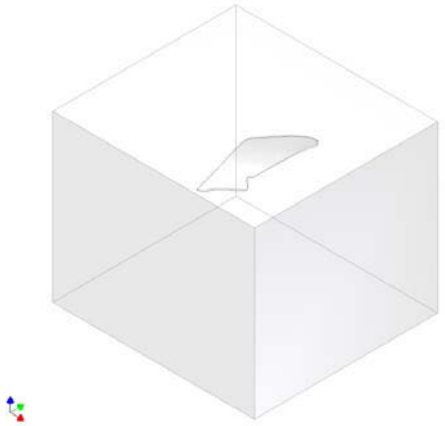

Figure 4. Schematic figure of the computational domain

The geometrical size of the domain and the characteristic sizes of the plough can be seen in Fig. 5. A no-slip boundary condition is applied at the left, right and bottom side of the calculation domain. It means that the velocity components perpendicular and parallel to the wall are specified to zero. $U = 0, V = 0, W = 0$

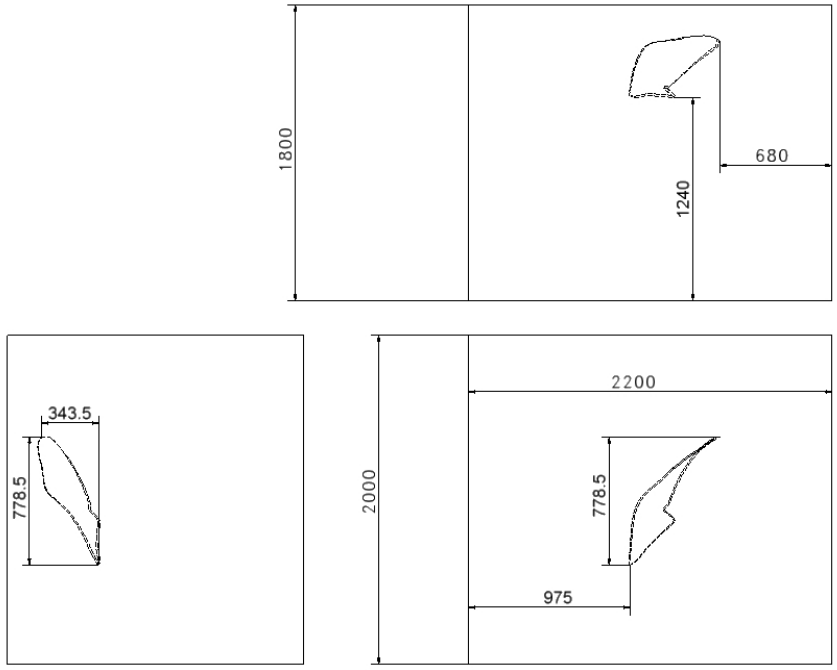

Figure 5. Schematic figure of the studied plough breast-board geometry

Table 3 shows the induced total drag force at different towing angels and towing velocities.

Table 3. Calculated drag force versus towing velocity

Drag force [N]	Towing velocities [m/s]					
Tow angle [^{o}]	2	2.5	3	3.5	4	4.5
-15	1412.03	1793.05	2203.70	2637.80	3118.28	3650.23
-10	1586.12	2012.52	2470.19	2952.34	3484.37	4072.48
-5	1775.99	2256.64	2758.99	3287.61	3892.16	4545.23
0	1970.01	2510.8	3072	3668	4326.1	5052.7
5	2168.79	2776.57	3396.86	4062.25	4798.39	5611.32
10	2351.34	3023.96	3704.26	4442.57	5262.05	6167.35
15	2508.04	3237.99	3975.94	4786.29	5688.97	6687.1

Fig. 6 shows the pressure contours on the surface of the plough breast board at 2.5 m/s towing velocity.

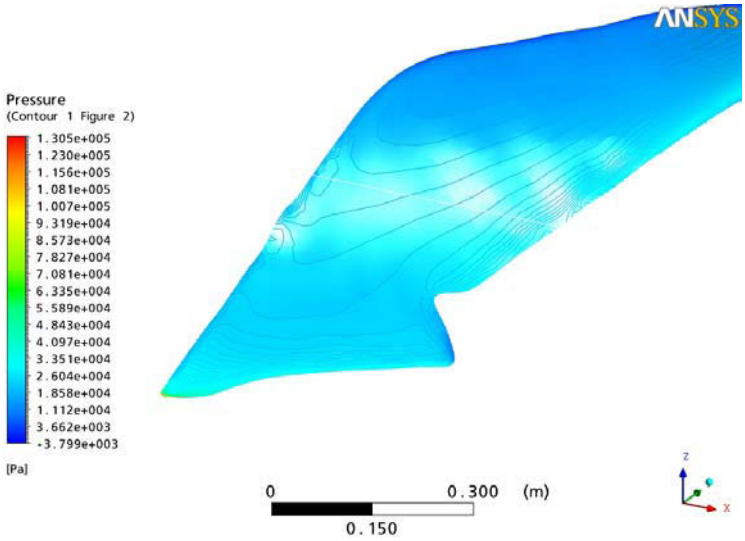

Figure 6. Pressure contours on the surface of the plough breast-board

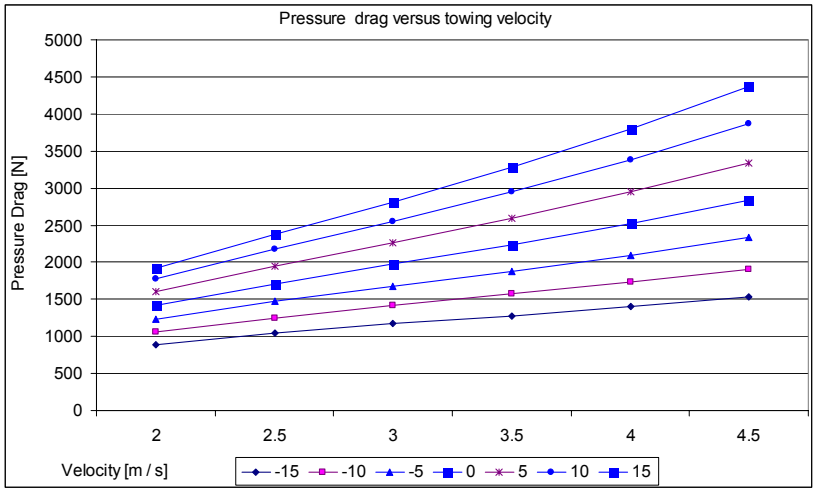

Figure 7. Curves representing the pressure drag at different towing velocities

Extensive study is needed to examine the two different sources of the total drag the first is the pressure component of the drag and the other one is the frictional drag. Fig. 7 shows the dependency of the pressure drag from the towing velocity. It can be concluded from Fig. 7 that the dependency of the pressure drag from the tillage velocity is nearly linear at smaller (-15°, -10°) towing angles and the curves became slightly progressive with increasing tow angles.

The same result can be seen in Fig. 8 where the pressure drag has been depicted at different towing angles and a similar non-linear behaviour can be

noticed. The dependency of the pressure drag from the towing angle is also linear at velocities smaller than 3 m/s.

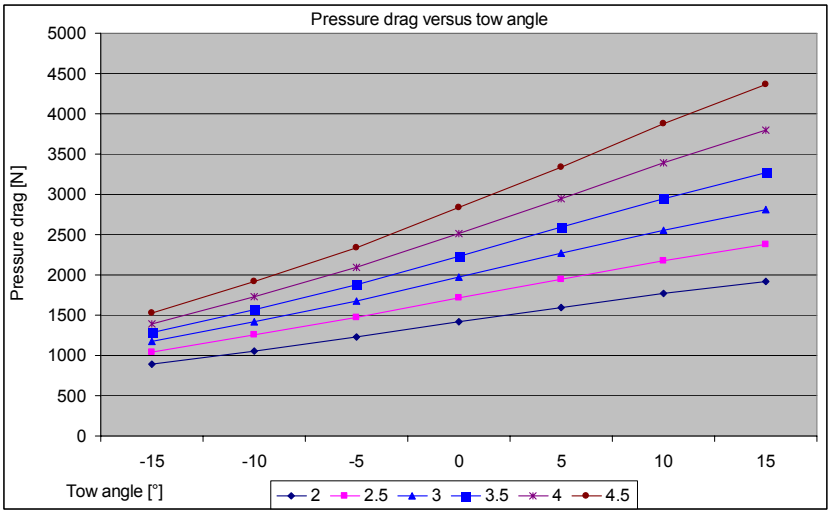

Figure 8. Curves representing the pressure drag at different towing angles

The dependency of the frictional forces from the tillage velocities can be seen in Fig. 9. It is clearly seen that the frictional drag shows the same tendency at different towing angles. The dependency of the

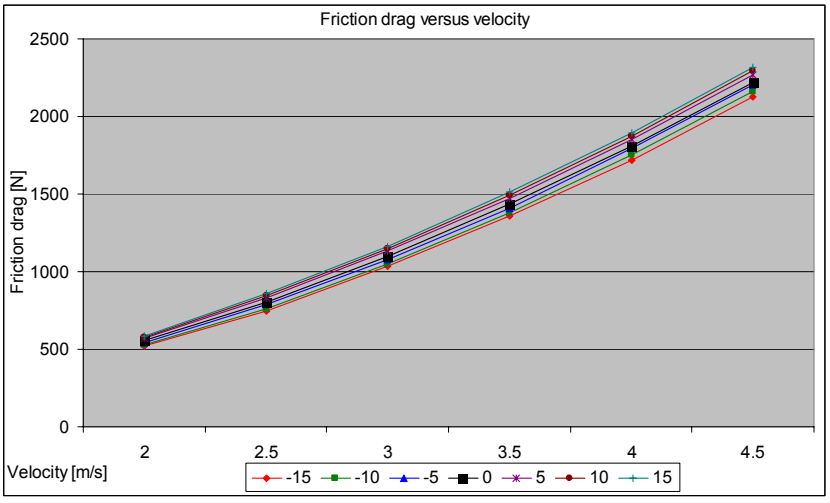

Figure 9. Curves representing the viscose drag at different towing velocities

Fig. 10 shows the dependency of viscose part of the total drag from the towing angles and it can be concluded that the frictional effects almost independent from the towing angles. The functional dependency of the frictional drag is nearly constant or a slightly increasing with the increasing towing angles.

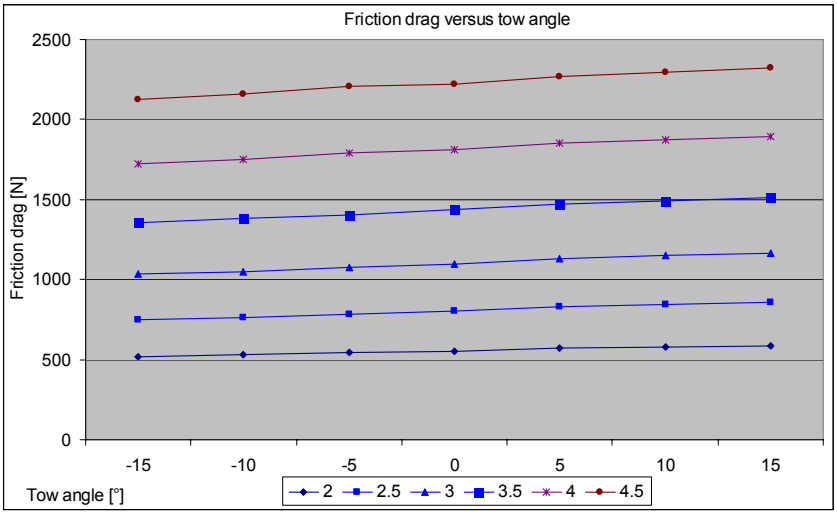

Figure 10. Curves representing the viscose drag at different towing angles

6. Conclusions

An important geometrical parameter of a plough breast-board has been used to study the draught force acting on the tillage tool and the developing pressure field in the surface of the mouldboard plough. The induced drag force strongly depends on the towing angle. The total drag force shows parabolic dependency from the towing velocity. This parabolic behaviour comes mostly from the frictional component of the drag. It is also important to note that the frictional component is almost independent from the towing angle. The pressure component of the drag is linearly dependent from the towing velocities and towing angles at smaller velocities. Further study is needed to examine and proof or modify these results for various soil types. The overall conclusion is that the total drag depends less sensitively from the towing angel than the tillage velocity.

Acknowledgements

The authors thank the valuable help of A. Formato making possible to use their measurements to validate the numerical results of our numerical calculations created by the CFX code.

References

Aluko, O. B., Chandler, H. W., (2004). Biosystems Engineering, 88, (3), 369-381.

Formato, A., Faugno, S., Paolillo, G., (2005). Numerical simulation of soil-plough mouldboard interaction. Biosystems Engineering, 92, (3), 309-316.

Elijah D.L. Weber J.A., (1971), Soil failure and pressure patterns for flat cutting blades, Transactions of the ASAE 14 (4), 781–785.

Karmakar, S., Kushwaha, R. L., Lague, C., (2007). Numerical modeling of soil stress and pressure distribution on a flat tillage tool using computational fluid dynamics. Biosystems Engineering, 97, (3), 407-414.

Karmakar, S., Kushwaha, R. L., (2005). Dynamic modeling of soil-tool interaction: An overview from a fluid flow perspective. Journal of Terramechanics, 43, (4), 411-425.

Mouazen A., Neményi M., (1999). Tillage tool design by the finite element method–part 1: finite element modelling of soil plastic behaviour. Journal of Agricultural Engineering Research, 72, 37-51.

Mouazen A., Neményi M., Schwanghart H., Rempfer M., (1999). Tillage tool design by the finite element method–part 2: experimental validation of the finite element results with soil bin test. Journal of Agricultural Engineering Research, 72, 53-58.

Patankar, S. V., (1980). Numerical heat transfer and fluid flow, Taylor & Francis, New York, 1980.

Versteeg, H. K., Malalasekera, W. (1995). An introduction to computational fluid dynamics, The finite volume method, Addison Wesley Longman Limited, Essex.

Zelenin A N, (1950). Basic Physics of the Theory of Soil Cutting. Kolos, Moscow, Russia.

Invited Papers

1. László FENYVESI:
Interaction Between Vibrating Soil Tillage Tool and Draught Force

The authors's team is research partner of the faculty in the field of bio-systems engineering.

2. Klaus GOTTSCHALK Csaba MÉSZÁROS, Anikó FÖLDI, Bernadett GYARMATI, István FARKAS and Ágnes BÁLINT:
Transient Character of Transport Processes in Binary Mixtures

The authors's team is research partner of the Institute for Environmental Systems in the field of environmental system modelling.

3. Patrick De BAETS, Wouter OST, Stijn TAVERNIER, Simon Van AUTREVE, Jeroen Van WITTENBERGHE, Gábor KALACSKA, László ZSIDAI and Róbert KERESZTES:
Tribotesting With Large Scale Specimens: Luxury or Necessity

The authors's team is research partner of the Institute for Mechanical Engineering Technology in the field of tribology and re-constructional engineering.

Interaction Between Vibrating Soil Tillage Tool and Draught Force

László FENYVESI
Hungarian Institute of Agricultural Engineering

Abstract

Soil tillage is one of the highest energy requiring agricultural operation. Significant part of researches aiming reducing draught force was focusing on utilizing vibration in the process.

There was no energy saving achieved via applying vibrating soil tillage tools operated by external drive. Research results are convincing to use different "self-vibrating" applications (e.g. vibration generated against a spring).

During measurement of draught force while testing soil tillage tool considered solid we learnt that the components of draught force is below 50 Hz in case of undisturbed stubble.

We have created soil tillage tools vibrating against a spring of which self-frequency is adjustable in the 20-25 Hz range even in case of high draught force appearing during ploughing. We assumed that the vibration of one of the components of the tool and the draught force would result in energy saving.

We gained insignificant draught force decrease with each plough version. Significant draught force decrease was achieved using the splay-foot design vibrating cultivator.

1. Introduction

During soil tillage the soil mostly has a periodically, randomly repeating impact on the tool. Compaction, shear and displacement of a specific volume of soil can be observed only separately. Therefore the forces having impacts on the tool are changes but not in a systematic, periodic way (Soehne 1956.).

The internal friction components of soils, that has an impact on the force affecting the tool, is decreasing during vibration load since shearing strength is decreasing (Savchenko 1958).

The vibration characteristics of vibrating soil tillage tools can be harmonized with the characteristics of force working on the tool and as a result of this the draught force is decreasing compared to the rigid tool.

The aim of developing active, vibrating soil tillage tools is to achieve energy saving by harmonizing effects of the tool and soil and by reducing the energy needed for shearing.

Thorough researches carried out in the topic have proven the above advantages in case of using a tool operating on the theory applying a simple blade or chock such as deep-soil loosening tools (Alekszandryan 1963, Totten

and Kauffman 1969, Willardson 1981). This is the reason why vibration is applied in development of medium- and deep-soil loosening tools (Niyamapa at al 1993) and of construction being in trade.

In general draught force can be decreased in case of external energy sourced vibrating soil tillage tools created with proper mechanism but not the energy need (Eggenmüller 1958, Wismer 1968). Jóri (1969) achieved similar results when tested ploughs equipped with springing stems or active drive-discs. Experiments of Sakun (1978) resulted in energy saving in a narrow operating range using self-induced plough structure. Svercek (1992) achieved similar results while testing cultivator-tools.

Harmonizing the self vibration of spring equipped self-induction soil tillage tool and the resistance generated by the soil seems to be a prosperous solution. The soil resistance has to be analyzed using rigid (non vibrated) soil tillage tool in order to develop experimental equipment since this can be considered as induction of the vibrating structure.

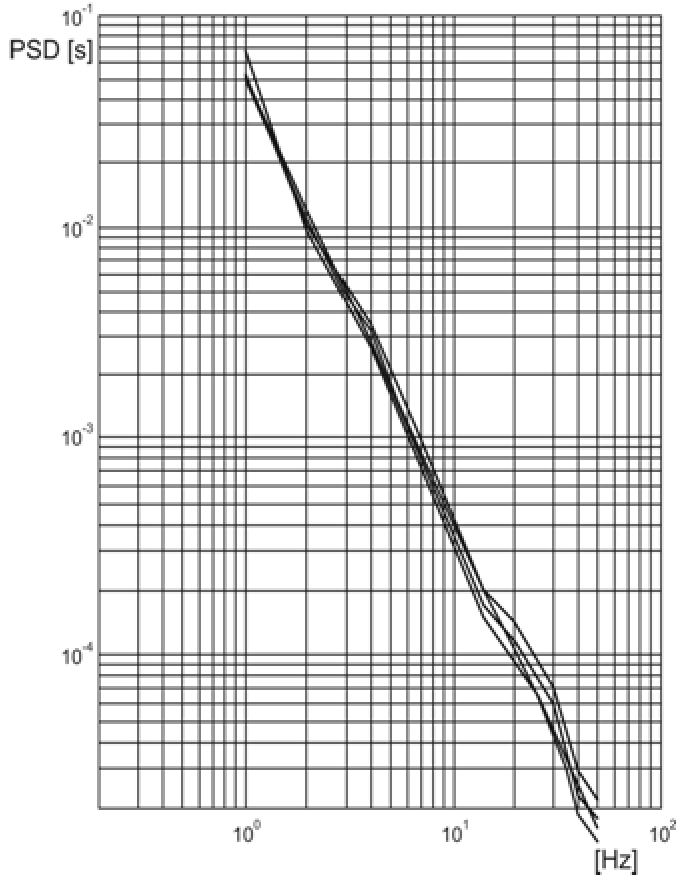

Figure 1. The throughput density- spectrum change on (undisturbed) stubble (Borsa 1991).

Utilizing the measured draught force the power-density-spectrum of the draught force can be determined. Defining the diagram Summers (1984) concluded that the power transmission is the highest at frequency of 9,99 Hz and there are smaller maximum figures at frequencies of 995 Hz and 1187 Hz. Another conclusion of the study was that the power transmission executed via draught force is impacted by several factors: soil type, moisture content and soil condition (Sakai at al 2005). There are only minor local maximum figures in the power-density-spectrum measured on non-disturbed, non-wet soil. Based on experiments completed by rigid medium-depth ploughing, Borsa (1991) found the PSD curve as a monotonously decreasing curve between 0 and 50 Hz (Figure 1)

The spectral characteristics of draught force are changing in parallel with the speed of operation. A speed limit can be determined based on measurements completed in soil bin above which speed the soil displacement is rather a flow-type periodical (Stafford 1984).

2. Methods and Tools

According to Eggenmüller (1958) different structural parts of the soil tillage tool have different impacts on the soil in case of vibration. Prior to creating test soil tillage tools we constructed a plough where there was only the ploughing bar vibrating but not the steering disc. Based on the measurement results completed in the soil bin the vibration perpendicular to the edge of the ploughing bar is more favorable than the edge-directional (Fenyvesi, Mezei, 1996). It is only the ploughing bar vibration that looks advantageous but it is extremely difficult to execute on arable land during normal operation of plough.

Therefore we carried out the alteration of soil tillage tools used in every day practice ensuring the vibration by equipping it with the spring-solution.

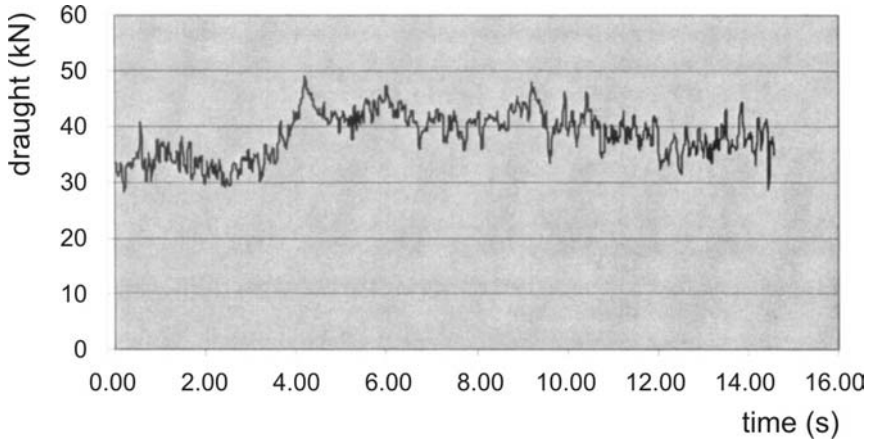

Figure 2. A typical draught force curve during measurement of ploughing

Based on Figure 1 we have to create a tool of which self-frequency is between 0 and 50 Hz, practically around 20-25 Hz. Since the soil tillage was completed on stubble (undisturbed) we can assume that there is no significant frequency in the domain (Figure 1), therefore the tools is vibrating somewhere in the marked region with the proper draught force components. This can result in energy saving.

Nevertheless the tested frequency-range is low therefore we had to apply a relatively soft alleviation. At the same time the mean value of draught force is so high in case of soil tillage (Figure 3) that the vibration is not feasible directly using soft alleviation.

During creating the experimental tools we have to use a mechanism that can reduce the draught force at the spring.

We created three versions for the plough- and one version for cultivator experiments.

The leaf-spring equipped plough was altered in a way that we decreased the number of the leaves in the spring. In this design the plough-head was vibrating against the spring (Figure 3 a).

Altering the plough stem we created a structure that was providing motion directional vibration for the plough-head against spiral spring (Figure 3. b).

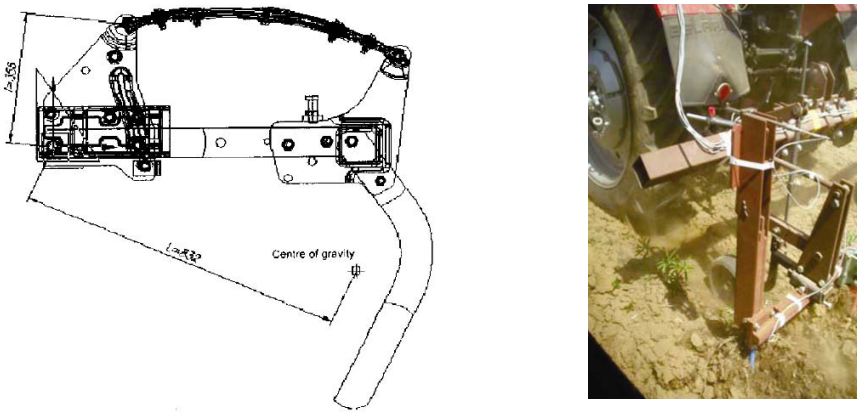

a) b)

Figure 3. Vibration plough alterations: (a) spring-equipped, (b) alternating in the direction of motion (Fenyvesi-Hudoba 2008).

The third plough modification is enabling the plough head to rotate around a joint point against spiral springs (Figure 4 a). The splay-foot design cultivator is a solution similar to the previous version (Figure 4 b).

Modeling self-frequency of the system having relatively huge mass and significant alleviation is a difficult task when also the changing impacts of the soil must be taken into consideration.

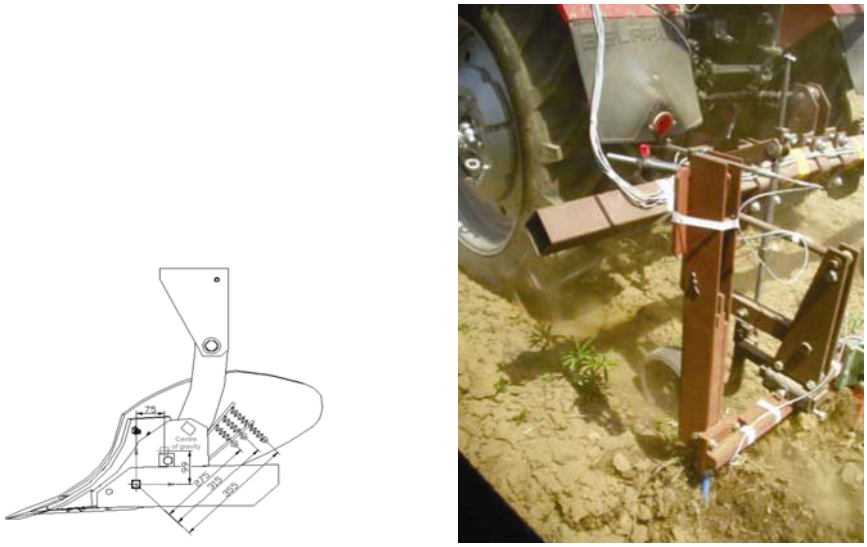

a) b)

Figure 4. Vibration plough (a) and cultivator (b) doing rotating, alternating movement.

We are using a simplified model to the calculations: we assume simple rotating movement for each version and we ignore alleviation and soil impacts. The structure is considered as systems consisting of one degree-of-freedom rigid parts. Condition of system elements can be described by one data: the angle of slew (φ).

Alleviation-free oscillation can be described by the Lagrange-type kinetic equation (using the letters of Figure 3/a):

$$\frac{\mathrm{d}}{\mathrm{d}t}\frac{\partial E_m}{\partial \dot{\varphi}} - \frac{\partial E_m}{\partial \varphi} + \frac{\partial E_h}{\partial \varphi} = 0$$

Where the kinetic energy of the system:

$$E_m = \frac{1}{2}\Theta\dot{\varphi}^2 \text{, } \Theta\text{:}$$

moment of inertia calculated for the rotation point.

Potential energy accumulated in the springs:

$$E_h = \frac{1}{2}\frac{y^2}{c} = \frac{1}{2}\frac{l^2\varphi^2}{c}.$$

y: displacement at the location of the spring,
c: constant of the spring,

l: distance of the spring from the rotation point on the plane of the displacement direction.

The first part of the Lagrange-type kinetic equation: $\frac{\mathrm{d}}{\mathrm{d}t}\frac{\partial E_m}{\partial \dot{\varphi}} = \Theta\ddot{\varphi}$,

Second part: 0,

Third part: $\frac{\partial E_h}{\partial \varphi} = \frac{l^2}{c}\varphi$.

Based on the above the motion equation is the following:

$$\ddot{\varphi} + \frac{l^2}{\Theta c}\varphi = 0 \ ,$$

Out of this the self-frequency of the system is:

$$\alpha = \sqrt{\frac{l^2}{\Theta c}} \ .$$

It is obvious that the moment of inertia of the whole structure calculated to the rotation point, the spring constant and the distance between the spring and the rotation point are neded so as to be able to define the self-frequency of the system. In our case (Figure 3. a) moment of inertia of the whole structure calculated to the rotation point can be replaced by the inertia of the mass-point located into one center of gravity. AutoCAD software capable to define center of gravity of two-dimensional figures and frames therefore the center of gravity of the plough structure and plough stem drawn are available on the plane of the displacement direction following completing the model. Let's mark the distance between the common mass-center point of plough stem and plough structure and the rotation axis with *L* on the vertical plane in the direction of the displacement. The self-circle frequency of the structure having *m* mass:

$$\alpha = \sqrt{\frac{l^2}{mL^2c}}$$

Using the correlation gained for the self-circle frequency we can draw the self-frequency-spring constant curves of each solution (e.g. Figure 5. shows the construction shown on Figure 4/b).

We could define the „theoretical" spring constant figures of each construction by using the correlation achieved and taking the self-frequency into account. Rigidity of the spring was changed to achieve the most favorable vibration, starting from the „theoretical" figure. In general spring rigidity had to be increased.

The measurements could not be completed among well defined circumstances such as in a soil bin since the draught force depends on the soil characteristics, mainly on its mechanical condition as proven earlier. The measurements therefore were completed on arable, non-cultivated land that was covered by flora on the test property of FVM Agricultural Mechanical Institute (MGI).

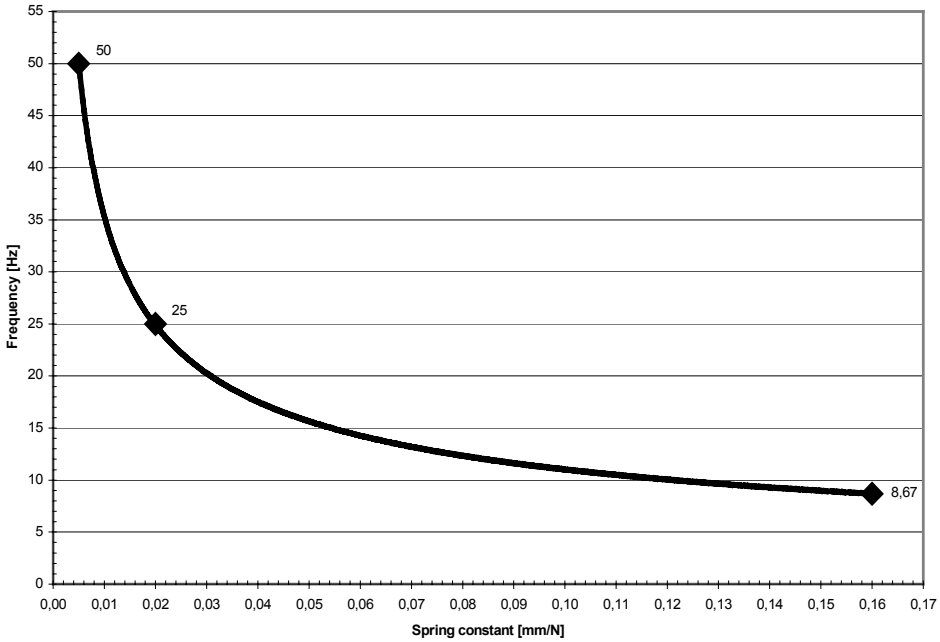

Figure 5. The self-frequency change in relation to the spring constant using vibration plough doing alternating movement in the direction of ploughing

The researches have been carried out with three-iron semi-suspended plough in a way that draught force was measured at the middle plough. Due to the extension measuring testers located on the stem we could constantly record the draught force changes using a Hottinger Spider measuring system.

The displacement detectable at the spring was recoded by an inductive measuring unit. Figure 5 is representing one of the measurement ranges.

The vibrating and the rigid (control) plough structure were identical. This was achieved due to using a spring support.

Measurements were completed for each adjustment on equal length: 150 meters.

The average soil moisture content of medium-compacted sandy-loam soil was the same since the measurements were completed at the same time. The average speed of the operation was 7 km/h, depth of ploughing 36 cm, width 22 cm.

The average tillage width was 16 cm, while the depth 13 cm was using splay-foot design cultivator.

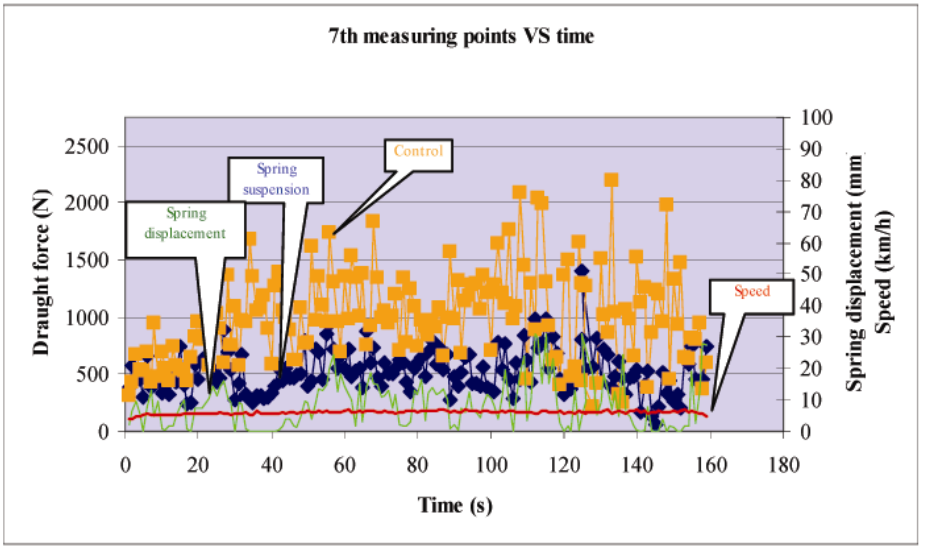

Figure 6. A section of the measurement (vibration cultivator)

3. Test results

We managed to establish adjustments for each plough structure where vibration was finally generated. In these cases we also recorded draught force decrease. The draught force decrease was not significant in case of using rotating-swinging motion providing structures (Figure 7a and b).

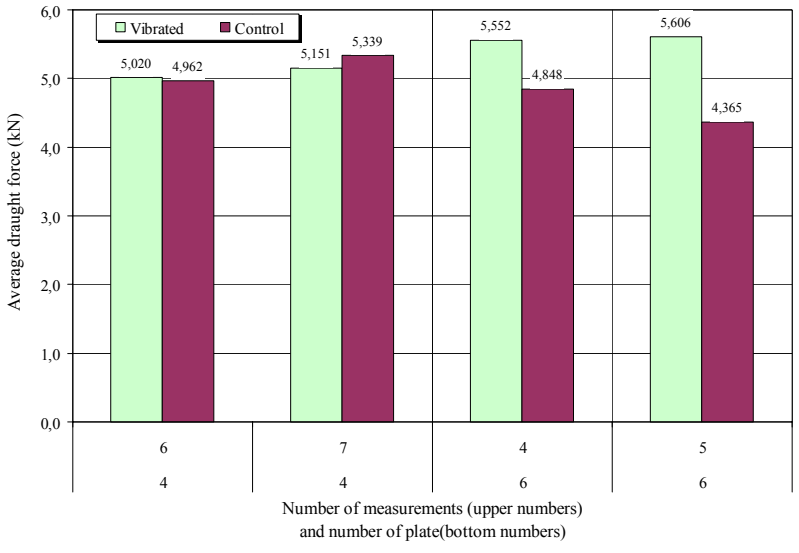

a)

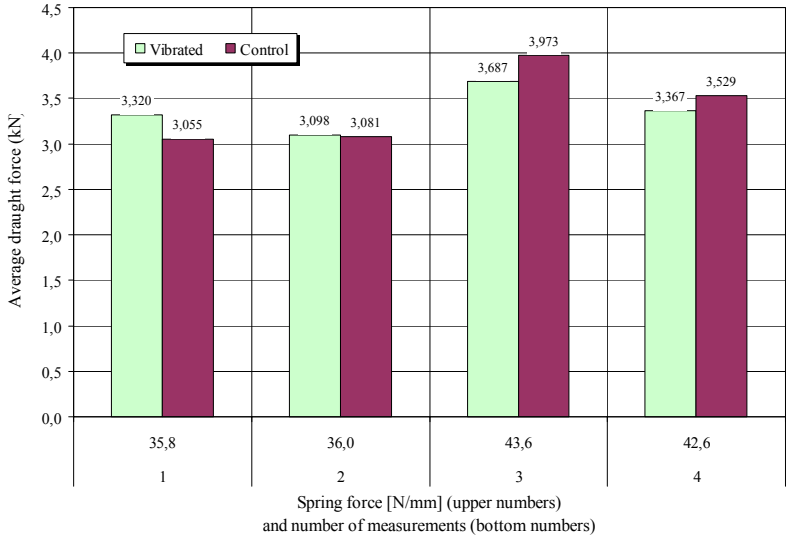

b)

Figure 7. Average draught force at plough structures doing rotating-swinging motion (a., leaf spring-, b., spiral spring design) (Fenyvesi-Hudoba 2008)

We have recorded minor draught force decrease when using the leaf spring structure (Figure 3a) applying 4 leaves (Figure 7a). We achieved the most optimal draught force with the rotating motion (Figure 4.a) structure having spring rigidity at 40-45 N/mm (Figure 7b). Softening the spring moved into the „final-state" when the it was behaving as a rigid structure.

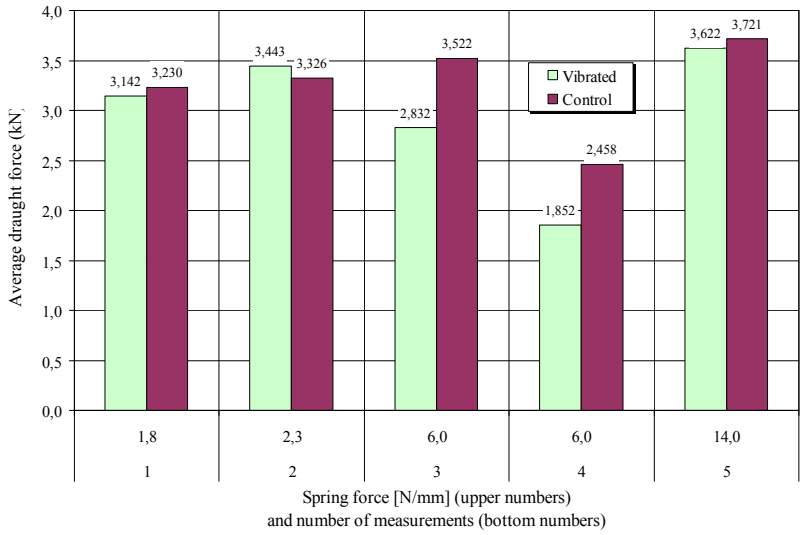

Figure 8. Average draught force changes in case of using alternating and rigid structures driven in parallel with the draught force direction (Fenyvesi-Hudoba 2008)

The highest draught force decrease (Figure 8) was measure when using the structure driven in parallel with the draught force direction (Figure 3b). In this case the optimal figures were around 3-4 N/mm spring rigidity.

There was more obvious result achieved in case of the cultivator-tool (Figure 9). The draught force decrease is significant.

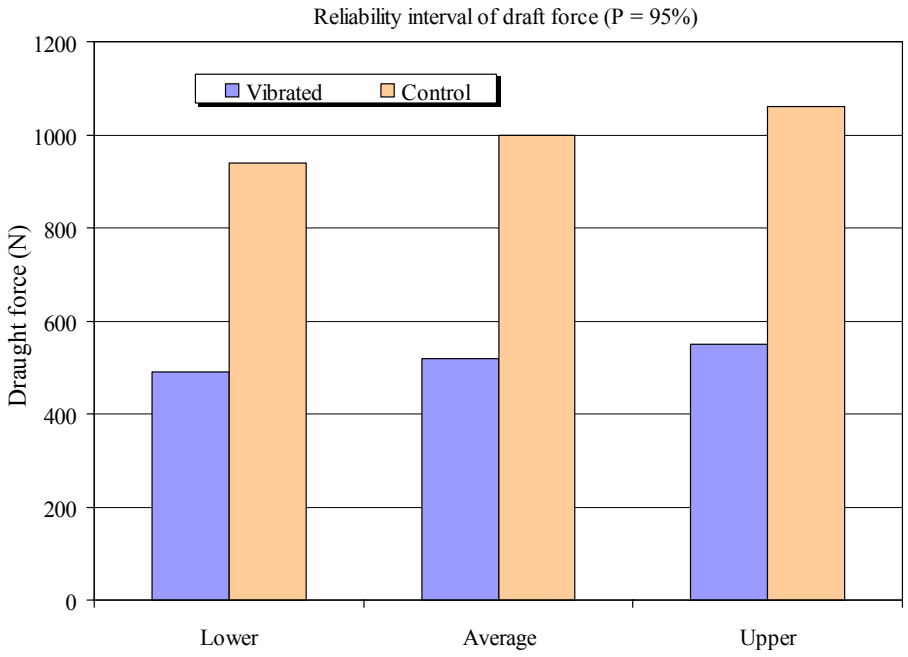

Figure 9. Draught force average changes in case of vibration and rigid cultivator. (Fenyvesi-Hudoba 2008)

Draught force decrease and intense vibration of tool were observed in the total measurement range (Figure 6).

4. Conclusions

Using vibrating soil tillage tools operating on the theory of cutting-rotating movement (e.g. plough, cultivators) there is a range below 50 Hz where draught force decrease and so energy saving can be achieved. Developing a structure that is non-external driven but vibrating against a spring is more promising. The self-frequency of these types of structures should be adjusted below 50 Hz (between 20-25 Hz).

We could not achieve significant draught force decrease with the plough structures vibrating against a spring.

Development of the plough structures vibrating in the direction of the movement can be prosperous. This can be achieved by reducing the alleviation of the system or by creating a mechanism that provides clear horizontal movement.

The cultivator tool is the one where significant draught force decrease can be achieved therefore developing proper constructions in this field is beneficial.

References

Alexandryan, K.V. 1963. The use of vibrations on subsoilers operating in compacted stony soils. Mech. Elektrif. Sel. Hoz.Vol.21, No. 3. 49-55 pp.

Borsa B., 1991. Statistical basic properties of plough resistance. Research of Agricultural Engineering. Hungarian Institute of Agricultural Engineering. Gödöllő

Eggenmüller A. 1958. Field experiments with an oscillation plough body. Grundlagen der Landtechnik, No.10. 85-95 pp.

Eggenmüller A., 1958. Experiments with groups of hoes oscillating in opposite phase. Grandlagen der Landtechnik No.10. 77-88 pp.

Eggenmüller A., 1958. Oscillating implements – Kinetics and experiments with single model tools. Grundlagen der Landtechnik. No.10. 55-69 pp.

Fenyvesi L., Mezei T., 1996. Experiment carried out with active cutting element tillage tool. Hungarian Agricultural Engineering No.9. 52-53 pp.

Fenyvesi L., Hudoba Z., 2008. Vibrated tillage tools, in Springer's series "Soil Biology" (series editor A. Varma), Springer in print.

Jóri J.I. 1969, Comparative tests on plough bodies. Research of Agricultural Engineering. Hungarian Institute of Agricultural Engineering, Gödöllő

Niyamapa T., 1993. Soil failure and its application to vibrating tillage tool, Proc. of the Int. Conf for Agricultural Machinery Seoul, Korea, 1053-1063 pp.

Sakai K., Andrade-Sanchez S., Upadhyaya K., 2005. Periodicity and stochastic hierarchical orders of soil cutting force data detected by an „Auto-Regressive Error Distribution Function" (AREF), Trans ADAE V. 48(6) 2039-2046 pp.

Sakun V.A. 1978. Possibilities of energy saving in soil tillage Veszt. Szlh nauki. 1978/3 118-130 pp.

Savchenko I.A. 1958. The effect of vibrations on inertial friction in sand. Soil Dynamics, Collection of Papers No. 31., State Publishing House on Construction. Moscow.

Sohne, W. 1956. Some basic considerations of soil mechanics as applied to agricultural engineering. Grundlagen der Landtechnik 7. 11-27 pp.

Stafford, J.V. 1984. Force prediction models for brittle and flow failure of soil by draught tillage tools. J. Agric. Eng. Res. 29. 51-60 pp.

Summers, I.D. 1984 Frequency analysis of tillage tool forces. Paper No. 1815 of the Oklahoma Agricultural Experiment Station 377-383 pp.

Totten D.S., Kauffman L.C. 1969. Dynamic response of a clay soil to an oscillating subsoiler. ASAE Paper No. 69.

Wismer, R.D. 1968. Energy applications in tillage and earthmoving. Society of Automative Engineers. Paper No. 680611

Transient Character of Transport Processes in Binary Mixtures

Klaus GOTTSCHALK[*] Csaba MÉSZÁROS[**], Anikó FÖLDI[**],
Bernadett GYARMATI[***], István FARKAS[**] and Ágnes BÁLINT[***]
[*]Leibniz-Institut für Agrartechnik Bornim
[**]Department of Chemistry and Biochemistry, [***]Department of Physics and Process Control

Abstract

A new calculation method is presented for phenomenological description of simultaneous diffusion, convection and wave phenomena in binary systems. A novel type of analysis is performed for connecting the relaxation time constants and deformation phenomena concerning the processes in dissipative macroscopic continua. After their general discussion, the Lagrangian representation of the classical field theories is obtained and the transient character of diffusion is analyzed in detail. The basic convection-diffusion and convection-diffusion-wave equations are presented and solved analytically.

1. Introduction

As the extended irreversible thermodynamics (EIT) shows, (Jou et al., 2001), the classical transport equations (i.e. Fick's relation for diffusion, Fourier's formula for heat conduction, Newton's one for viscous flow, etc.) are not always suitable to give an adequate description of the heat and mass transfer phenomena in many systems. Its reason is that they are implying propagation velocities of infinite value, represented by parabolic type partial differential equations (PDEs), which is incompatible with the basic principles of physics. This problem is usually resolved by introducing of nonzero relaxation time constants (Cattaneo, 1948, 1958), (Vernotte, 1958) in order to ensure presence of inertial phenomena (Maxwell, 1867) in transport processes. The systems which are characterized by long relaxation times are superconductors, low temperature heat and electric conductors, and particularly the polymeric fluids (Jou et al., 2001). The polymer solutions also represent archetypal examples of systems, where non-Fickian diffusion processes are taking place; among them, coating of substrates via deposition and subsequent drying of such solutions play a particularly important role in the relevant engineering practice (Jou et al., 2001). Furthermore, the experimental investigation of thermodynamic cross-effects in the latter type of systems (Wiegand, 2004) is also important from the point of view of the further development of theory, too.

Some of the newest theoretical and modeling results from the field of convective drying of shrinking media (Porras et al., 2007) are about applications of convection-diffusion models in the case of binary liquids. Therefore, the

accurate mathematical modeling of the above described phenomena on the base of the contemporary EIT is of primary interest for further successful studies necessary at understanding of basic properties of such complex condensed matter systems. Finally, it must be emphasized, that examination of the concept of frame-indifference in the case of viscoelastic media is of interest for decades (Jou et al., 2001), since it is acceptable only in the cases, when the inertial effects are not significant (Bird and de Gennes, 1983). This circumstance was exactly the main motivation for our work.

The present study is devoted to description of some basic partial differential equations (PDE-s), whose solutions are necessary for foundations of such modeling procedures. In order to give as general description of these problems as possible, the appearance of deformation phenomena will also be incorporated into mathematical formalism applied here. A convenient description of the transport problems characterized by shrinkage can be given in Lagrangian representation. Although this representation is frequently applied even in numerical calculations (in the form of the so-called Lagrange-Galerkin procedure), it is still far (Knabner and Angermann, 2000) from the fully elaborated state. In order to exploit its characteristics, we at first summarize here concisely the well-known basic types of balance equations related to the problem being investigated, as well as the related balance equations of the non-equilibrium thermodynamics in a unified simple, but novel manner.

2. Analytical solutions of basic partial differential equations of the problem

Solution of the convection-diffusion equation

First of all, we present here the solutions of the basic convection – diffusion PDE (related to the case of constant flow velocity $\vec{v}$ and thermodynamically state-independent conductivity coefficient), and the same equation supplemented by wave term (with relaxation time τ also of constant value). These equations will be written here for one-dimensional case, i.e. for the concentration function *c(x,t)*, which in the case of convection and diffusion obeys:

$$\frac{\partial c}{\partial t} = D\frac{\partial^2 c}{\partial x^2} + v\frac{\partial c}{\partial x}. \tag{1}$$

The (1)-type PDE has been studied many times in the literature e.g. (Pascal, 1993), as well as its applications in numerical mathematics and engineering e.g. (Knabner and Angermann, 2000), (Kirschner et al., 2004). We solve here this PDE directly by use of the MAPLE-10 (MAPLE, 2005) software package, which has made possible novel types of solutions of some fundamental convection problems, too (Kirschner et al., 2007). Then, the relevant (and according to our knowledge: new) solution is

$$c(x,t) = F_1(x) \cdot F_2(t), \tag{2}$$

where the factor functions F_1 and F_2 satisfy the following ordinary differential equations (ODEs):

$$\frac{dF_2(t)}{dt} = K \cdot F_2(t), \frac{d^2F_1(x)}{dx^2} = \frac{K}{D}F_1(x) - \frac{v}{D} \cdot \frac{dF_1(x)}{dx}, \tag{3}$$

where $K = const.$ The solutions of the space- and time-dependent parts have the following explicit form:

$$F_1(x) = K_1 \cdot e^{\frac{(-v+\sqrt{v^2+4KD})}{2D}x} + K_2 \cdot e^{-\frac{(v+\sqrt{v^2+4KD})}{2D}x}, \text{ and } F_2(t) \propto e^{Kt}, \tag{4}$$

where K, K_1 and K_2 are integration constants. The integration constant equating the time-dependent exponential factor with $F_2(t)$ is directly incorporated into K_1 and K_2. Obviously, in the case of solutions with exponentially decaying character in time it must be $K < 0$, if this constant is of real value. We also mention here, that analytical solutions of (1) are known in the literature for decades, but the solution (4), despite of its simplicity - represents a novel solution form. In order to justify this statement, we recall explicit form of the earlier solutions from some confident sources, e.g. from the monograph by (Lee, 1999), where the analytical solution of the PDE (1) is derived by the usual Laplace transformation technique, widely applied in the engineering applications. This explicit solution had the form

$$\frac{e^{\frac{vx}{2D}}}{2}\left\{e^{-\frac{vx}{2D}} \cdot erfc\left(\frac{x-vt}{\sqrt{4Dt}}\right) + e^{+\frac{vx}{2D}} \cdot erfc\left(\frac{x+vt}{\sqrt{4Dt}}\right)\right\},$$

which is more complicated, than (4), particularly, if we compare it to the case of Dirichlet-type boundary conditions, to be specialized below.

Analysis of Dirichlet-type boundary conditions

The boundary condition analysis of the PDE (1) is particularly simple, if we assume, that the convection flow velocity is of constant value. Then, the simple Dirichlet-type boundary conditions (e.g. for a vertical column of height L) are:

$$c(0,0) = c_0, c(L,0) = 0, \tag{5}$$

i.e. c_0 denotes the initial value of the concentration on the top of a column. The first boundary condition from (5) gives immediately $c_0 = K_1 + K_2$. Similarly,

from the second condition (5) we get $e^{\frac{\sqrt{v^2+4KD}}{L}D}=1,$ (if we assume for the sake of generality, that $K_2 \neq 0$). Then, obviously $K=-\frac{v^2}{4D},$ and the general solution (2-5) takes the following particular form:

$$c(x,t)=c_0 \cdot e^{-\frac{2vx+v^2t}{4D}}. \tag{6}$$

This solution, despite of its simple form may represent a useful new formula for examining of the convection-diffusion processes, according to (1)-type PDEs.

Solution of the convection-diffusion-wave equation
Similarly, for the simultaneous presence of convection, diffusion and wave phenomena, we may have:

$$\tau\frac{\partial^2 c}{\partial t^2}+\frac{\partial c}{\partial t}=D\frac{\partial^2 c}{\partial x^2}+v\frac{\partial c}{\partial x}, \tag{7}$$

where, as usual, *D* denotes the diffusion coefficient. In the case of $\tau=0,\vec{v}=0$, (7) reduces to the classical diffusion equation, for $\tau\neq 0,\vec{v}=0$ we get the telegrapher equation (Jou et al., 2001), while for $\tau=0,\vec{v}\neq 0$ we arrive back to (1); therefore, in its initial form, the PDE (7) may serve as a starting point for studying of transport processes of rather general character. For the concrete applications, the PDE (7) may be of interest in hydrology (Ranzi et al., 2002).

Then, application of the MAPLE software package gave us (via transformation $(x,t)\rightarrow(\xi_1,\xi_2)$ of independent variables in the form of $\xi_1=\sqrt{\frac{\tau}{D}}x+t, \xi_2=\frac{1}{2}\left(x-\sqrt{\frac{D}{\tau}}t\right)$) for a new solution of (7) in a separated form:

$$c(x,t)=F_3(\xi_1)F_4(\xi_2), \tag{8}$$

where the factor functions F_3 and F_4 obey the ODEs:

$$\frac{dF_1(\xi_1)}{d\xi_1}=b\cdot F_1(\xi_1), \frac{dF_2(\xi_2)}{d\xi_2}=\frac{b\cdot F_2(\xi_2)\left(D-v\sqrt{D\tau}\right)}{D\left(\frac{2D\tau b}{\sqrt{D\tau}}+\frac{v\sqrt{D\tau}+D}{2\sqrt{D\tau}}\right)}, \tag{9}$$

with $b = const$. The equations (9) can be solved directly and solutions are given in exponential forms, i.e. the expression (8) can be written as:

$$c(x,t) = C \cdot e^{\left(b\left(\sqrt{\frac{\tau}{D}} + \frac{1}{2} \cdot \frac{\sqrt{D} - v\sqrt{\tau}}{\sqrt{D}\left(2b\sqrt{D\tau} + \frac{v\sqrt{\tau} + \sqrt{D}}{2\sqrt{\tau}} \right)} \right) x \right)} \cdot e^{b\left(1 - \frac{\sqrt{D} - v\sqrt{\tau}}{4\tau b\sqrt{D} + v\sqrt{\tau} + \sqrt{D}} \right) t}, \tag{10}$$

where C is an integration constant. This solution implies directly, that the concentration function exhibits exponentially decaying character in time, if the following inequality is satisfied:

$$b < -\frac{v}{2\sqrt{\tau D}}. \tag{11}$$

In the case of complex values of K and expression $b\left(1 - \frac{\sqrt{D} - v\sqrt{\tau}}{4\tau b\sqrt{D} + v\sqrt{\tau} + \sqrt{D}} \right)$ from the exponent of (10), it is necessary to have negative imaginary parts of them, since otherwise we would not have functions of oscillatory character, but also decaying in time, which are necessary for solutions corresponding to stable motions according to the general stability analyses of the viscous fluid flows with respect to always present small perturbations (Landau and Lifshitz, 2000).

3. The balance equations and deformation phenomena in dissipative continua

In general case, the link between the substantial (Lagrange-) and local (Euler-) type balance equations can be demonstrated by the following relation, which connects the relevant substantial and local derivatives, i.e.:

$$\rho \dot{a} = \frac{\partial \rho a}{\partial t} + \nabla \cdot \rho a \vec{v}, \tag{12}$$

where, as usual, $a = \frac{dA}{dM}$ denotes an extensive quantity A per unit mass (Gyarmati, 1970), (Jou et al., 2001). Then, using the identical value of the source density function σ_a in both Lagrange-, and Euler-representations, we may write:

$$\rho \dot{a} + \nabla \cdot \vec{J}_a = \sigma_a = \frac{\partial \rho a}{\partial t} + \nabla \cdot \vec{J}_a^0, \tag{13}$$

which relation, together with the continuity equation $\frac{\partial \rho}{\partial t} + \nabla \cdot \rho \vec{v} = 0$ leads immediately to

$$\frac{\partial a}{\partial t}+\vec{v}\cdot\nabla a=-\frac{1}{\rho}\nabla\cdot\vec{J}_a+\frac{\sigma_a}{\rho} \tag{14}$$

in Lagrangian picture ($\vec{J}_a^0$ is the local-, while $\vec{J}_a$ is the flux according to the substantial representation). Finally, if we take into account the usual method of description of deformations, we will have:

$$\frac{\partial a}{\partial t}+\vec{v}\cdot\nabla a=-\frac{\left|J\right|_{def}}{\rho_0}\nabla\cdot\vec{J}_a+\frac{\sigma_a\left|J\right|_{def}}{\rho_0}, \tag{15}$$

where ρ_0 denotes the density of the continuum before deformation and $\left|J\right|_{def}$ is the Jacobi-determinant of the actual deformation (Gyarmati, 1970), whose explicit form may take rather complicated form at solving of concrete, practical engineering problems (Porras et al., 2007). Despite of this fact, the deformation phenomena may be incorporated into balance equations from the beginning.

Application of the Maxwell – Cattaneo - Vernotte type equations
The modified constitutive equation which is used in this paper is the classical Maxwell-Cattaneo-Vernotte (Maxwell, 1867), (Cattaneo, 1948, 1958), (Vernotte, 1958) equation, whose generalization to coupled transport processes was given by Gyarmati (Gyarmati, 1977). This equation in the case of simple heat conduction has the form of

$$\vec{J}=-\lambda_T\nabla T-\tau_T\frac{\partial\vec{J}}{\partial t}, \tag{16}$$

where the heat conduction coefficient λ_T and relaxation time constant τ_T are assumed to be of constant value, although in general case both of them are thermodynamically state-dependent quantities. Analogous equation is valid in the case of diffusion processes, too. Combination of these equations with the basic (energy- or mass-) balance equations leads directly to hyperbolic heat and mass transfer equations at both fundamental- and applied researches. Among them, we mention here foundation of the hyperbolic formalism (Cattaneo, 1948, 1958), (Vernotte, 1958), (Gyarmati, 1977), examination of the non-Fickian diffusion in binary mixtures at uniform temperature (Depireux and Lebon, 2001), experimental investigation of fast and high-intensity drying processes by pulsed laser technique (Liu et al., 2004), refinements of the Luikov's system of equations e.g. (Luikov and Mikhailov, 1965) by application of the tools of EIT (Mészáros et al., 2004-2007), detailed study of numerical solutions of the convection-diffusion equations based on Cattaneo's law by use of the finite element technique (Gomez et al., 2007). The relevant relaxation time constants will be taken here as genuine constants, although we are aware of the fact, that in

general case they are given by matrix product of the conductivity matrix and matrix, whose elements are identified with the coefficients of the flux-dependent part in the non-equilibrium entropy function (Gyarmati, 1977), (Fekete, 1981).

Connection between deformations and relaxation time constants
In order to set up this connection, we use here a simple description of the problem, supposing a two-component object (where $\rho = \rho_1 + \rho_2$ denotes the density of the complete system, while ρ_1 and ρ_2 denote the densities of its constituents). In this case the choice $\frac{\rho_1}{\rho} = c_1 \to c, \frac{\rho_2}{\rho} = c_2 \to 1 - c$ of relative concentrations is particularly suitable to identify the specific quantity *a* in eqs (12 - 15). Then, we will have:

$$\rho_1 \vec{v}_1 = \vec{J}_1 + \rho_1 \vec{v}, \tag{17}$$

for the balance equation of the first component. The basic constitutive equation will be exchanged as follows according to the Maxwell-Cattaneo-Vernotte theory, i.e.:

$$\vec{J}_1 = -\rho D \nabla c \to \vec{J}_1 + \tau_1 \frac{\partial \vec{J}_1}{\partial t} = -\rho D \nabla c, \tag{18}$$

where the relaxation time constant τ_1 is assumed to have a constant value. Finally, the balance equation expressing the conservation law of the first constituent must also be applied:

$$\frac{\partial \rho_1}{\partial t} + \nabla \cdot \vec{J}_1^0 = 0, \tag{19}$$

if we use local description of fluxes (local fluxes are again indicated by zero upper indices), or:

$$\frac{\partial \rho_1}{\partial t} + \nabla \cdot \vec{J}_1 + \nabla \cdot \rho_1 \vec{v} = 0, \tag{20}$$

if we use substantial description of fluxes, where $\vec{v}$ is the velocity of the convection flow. In the forthcoming calculations we will replace ρ_1 by ρc, and so the direct combination of the eqs. (17), (18) and (20) will give:

$$\frac{\partial (\rho c)}{\partial t} + \tau_1 \frac{\partial^2 (\rho c)}{\partial t^2} + \nabla \cdot (\rho c \vec{v}) + \tau_1 \frac{\partial}{\partial t} \nabla \cdot (\rho c \vec{v}) = \nabla [\rho D \nabla c], \tag{21}$$

i.e. the possible thermodynamic state-dependence of diffusion coefficient will be taken into account during this modeling work A well-known explicit expression for this concentration- and temperature-dependence is given by Arrhenius-type formula $D(c,T) \propto e^{-\frac{A_p}{c}} \cdot e^{-\frac{E_A}{RT}}$, which is applied e.g. in modeling of drying processes of the aqueous polymer solutions e.g. (Jou et al., 2001), where A_p is a constant, E_A is the activation energy and R denotes the universal gas constant). After application of the simple continuity equation $\frac{\partial \rho}{\partial t} + \nabla \cdot \rho \vec{v} = 0$ we obtain directly:

$$\left(\rho + \tau_1 \frac{\partial \rho}{\partial t}\right) \cdot \frac{dc}{dt} + \rho \tau_1 \frac{\partial^2 c}{\partial t^2} + \rho \tau_1 \frac{\partial \vec{v}}{\partial t} \cdot \nabla c + \rho \vec{v} \frac{\partial}{\partial t} \nabla c = \nabla \cdot \left[\rho D \nabla c\right], \qquad (22)$$

from the relation (21), and the notation $\frac{dc}{dt} = \frac{\partial c}{\partial t} + \vec{v} \cdot \nabla c$ has also been used. Finally, from the equation (22) by simple transformation from Eulerian to Lagrangian frame of reference (which is de facto accompanied by $\vec{v} = 0$ value of the convection flow velocity (Gyarmati, 1977)) we obtain:

$$\left(1 + \frac{\tau_1}{\rho} \frac{\partial \rho}{\partial t}\right) \cdot \frac{\partial c}{\partial t} + \tau_1 \frac{\partial^2 c}{\partial t^2} = \frac{1}{\rho} \nabla_L \left(\rho D \nabla_L c\right), \qquad (23)$$

where the lower index „*L*" denotes the Lagrangian representation. Considering one-dimensional case (for which the notation $\nabla_L \to \frac{\partial}{\partial \xi}$ will be used, with ξ as the relevant new space-coordinate) and taking into account method for describing of deformations by Jacobi-determinants $|J|_{def}$, which is also used already in (15), the fully developed form of (23) will be:

$$\left(1 + \frac{\tau_1}{\rho} \cdot \frac{\partial \rho}{\partial t}\right) \cdot \frac{\partial c}{\partial t} + \tau_1 \cdot \frac{\partial^2 c}{\partial t^2} = D(c,T) \cdot \frac{\partial^2 c}{\partial \xi^2} + \frac{\partial c}{\partial \xi} \cdot \frac{\partial}{\partial \xi} \left(\frac{D(c,T)}{|J|_{def}}\right). \qquad (24)$$

When writing PDE (24), the initial density ρ_0 applied in derivation of (15), is assumed to be known and constant quantity. In this way, the limit situation emanating directly from the relation (24), as $\tau_1 \to 0$ leads to the one-dimensional diffusion equation with state-dependent diffusion coefficient in Lagrangian representation. If $\tau_1 \neq 0$, but $\left(1 + \frac{\tau_1}{\rho} \cdot \frac{\partial \rho}{\partial t}\right) \to 0$, it leads to the wave

equation. In this second case, we get directly a simple one-dimensional wave-equation, again with state-dependent diffusion coefficient in Lagrangian representation. Besides, it follows immediately from this wave-equation limit, that the temporal change of the density ρ has an exponentially decaying character, i.e.

$$\rho(\xi,t) = \kappa(\xi) \cdot e^{-\frac{t}{\tau_1}}, \tag{25}$$

where the still unknown function $\kappa(\xi)$ may be determined from the actual boundary conditions. It must also be pointed out here, that the form (25) for density function is not in contradiction with the wave theory of thermodynamics developed for convection-free cases (which predicts constant density) (Gyarmati, 1977), because its exponential decrease in time may be accompanied by increasing character of the function $\kappa(\xi)$.

4. Stochastic refinements

In order to find further possible applications of the modeling methods described above, we combine in the present section results obtained on the base of the non-equilibrium thermodynamics with those based on percolation theory e.g. (Stauffer and Aharony, 1994), which is de facto the genuine mathematical theory of leakage processes through capillary-porous bodies, as it has been demonstrated by numerous important practical examples ranging from e.g. soil columns (taking into account the fractal microstructure of soils, too) (Rieu and Sposito, 1991) till drying processes of thin layers (Tsimpanogiannis et al., 1999). The combination of the methods of non-equilibrium thermodynamics and percolation theory will be performed here in a restricted way: only certain quantities from the conductivity/coupling coefficients will be assumed as percolation-sensitive ones. This approach is justified by some very accurate experimental results from drying engineering practice (Huinink et al., 2002). The *percolation probability p* is the probability that a given conducting edge (or nodes determining it) belongs (belong) to an infinite open cluster. The quantity, which plays a crucial role in this theory is the critical percolation probability, usually denoted by p_c. According to the mathematically strict definitions of the topic, there are two phases in the case of percolation processes (taking place in systems with two or more dimensions). In the so-called subcritical phase (for which $p < p_c$) it is very probable, that every node (or edge) is in a finite open cluster, while in the case of the supercritical phase (i.e. when $p > p_c$), each node (or edge) almost surely belongs to an infinite open cluster. Then, the most important scaling relationships, necessary for this modelling, are explained by the probability difference $\Delta p = p - p_c$. The crucial relation we take over from

this general formalism of the theory of percolative phase transitions is the following one:

$$D(p) \propto (\Delta p)^t , \tag{26}$$

where letter t denotes the critical index, and not the time as usual, having allowed values in the interval between 1.1 and 1.6 (Stauffer and Aharony, 1994). In this paper we assign the dominant percolative behaviour to the diffusion coefficient, and will therefore examine its influence on the solution of the PDE (1) only, although we are aware of the fact, that in general case the coupling constants related to thermodynamic cross-effects and even the relaxation time constants may depend on the actual percolative state of the complex system being examined.

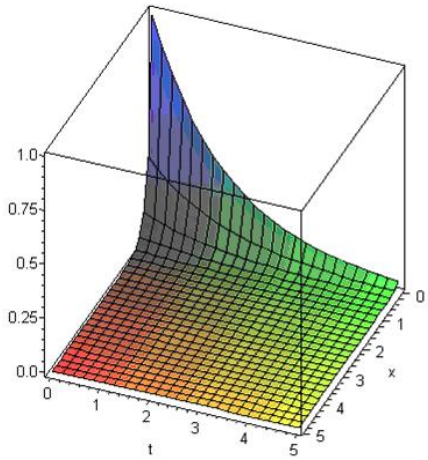

Figure 1. Concentration distribution function for the value Δp = 0.001 of the percolation probability difference (in relative units)

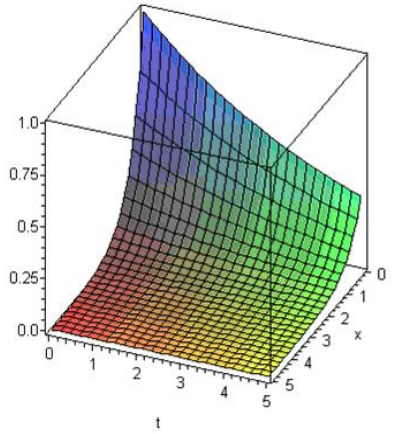

Figure 2. Concentration distribution function for the value Δp = 0.0025 of the percolation probability difference (in relative units)

Some graphical illustrations of these percolative changes for the simplest convection-diffusion systems are given on Figs 1-2. Two different percolation probabilities for the value $t = 1.3$ from the solution (6) result in the following convection-diffusion solution surfaces (after Baksics, 2007):

5. Conclusions

The basic balance equations of the non-equilibrium thermodynamics are studied in their most general form, and it is shown that deformation as well as the relaxation phenomena can be incorporated into general formalism from the beginning. Both Euler and Lagrange representations are used for interconnecting of deformation and relaxation processes in two-component systems in a novel manner. The basic convection-diffusion and convection-diffusion-wave equations are solved analytically in linear approximation for the case of constant convection velocity flow by use of advanced symbolic calculation software packages. Finally, an a posteriori stochastic refinement of solution of the convection-diffusion PDE is given according to the basic scaling relations of the contemporary percolation theory.

References

Baksics E 2007 Diploma Thesis, Szent István University, Gödöllő, Hungary

Bird R B, de Gennes P G 1983 Discussion Physica A 118 43-47

Cattaneo M C 1948 Sulla conduzione de calore Atti dei seminario matematico e fisico delli Universitá di Modena 3 3 – 21

Cattaneo M C 1958 Sur une forme de l'equation de la chaleur liminant le paradoxe d'une propagation instantane Comptes Rendus 247 431- 433

Depireux N and Lebon G 2001 An extended thermodynamics modeling of non-Fickian diffusion Journal of Non-Newtonian Fluid Mechanics 96 105-117

Fekete, D 1981 A systematic application of Gyarmati's Wave Theory of Thermodynamics to thermal waves in solids Physica Status Solidi B 105 161-174

Gomez H, Colominas I, Navarrina F and Casteleiro M 2007 A finite element formulation for a convection–diffusion equation based on Cattaneo's law Computer Methods in Applied Mechanics and Engineering 196 1757–66

Gyarmati I 1970 Non-Equilibrium Thermodynamics (Field Theory and Variational Principles) (Berlin – Heidelberg – New York: Springer-Verlag)

Gyarmati I 1977 On the Wave Approach of Thermodynamics and some Problems of Non-Linear Theories Journal of Non-Equilibrium Thermodynamics 2 (4), 233–60

Huinink H P, Pel L, Michels M A J, Prat M 2002 Drying processes in the presence of temperature gradients- Pore-scale modelling European Physical Journal E 56 487 - 498

Jou D, Casas-Vázquez J and Lebon G 2001 Extended Irreversible Thermodynamics (Third Revised and Enlarged Edition) (Berlin – Heidelberg – New York: Springer-Verlag)

Knabner P and Angermann L 2000 Numerik partieller Differentialgleichungen (Eine anwendungsorientierte Einführung) (Berlin – Heidelberg – New York: Springer-Verlag)

Kirschner I, Mészáros Cs, Bálint Á, Gottschalk K and Farkas I 2004 Surface changes of temperature and matter due to coupled transport processes through porous media Journal of Physics .A: Mathematical and General 37 1193-1202

Kirschner I, Bálint Á, Csikja R, Gyarmati B, Balogh A and Mészáros Cs 2007 An approximate symbolic solution for convective instability flows in vertical cylindrical tubes Journal of Physics A: Mathematical and Theoretical 40 9361–69

Landau L D, Lifshitz E M 2000 Fluid Mechanics (Oxford: Heinemann)

Lee T C 1999 Applied Mathematics in Hydrogeology, CRC Press LLC: Boca Raton

Liu D, Huai X, Hu X and Jiang F 2004 Fundamental research on drying processes in institute of engineering thermophysics Drying Technology 22 (1-2) 145-64

Luikov A V, Mikhailov Yu A 1965 Theory of Energy and Mass Transfer (London: Pergamon Press)

MAPLE 10 2005 Symbolic Computation System Waterloo Maple Inc.

Maxwell J C 1867 On the dynamic theory of gases Philosophical Transactions of the Royal Society London 157 49-88

Mészáros Cs, Farkas I and Bálint Á 2001 A new application of percolation theory for coupled transport phenomena through porous media Mathematics and Computers in Simulation 56 395–404

Mészáros Cs, Farkas I, Bálint Á and Buzás J 2004 Modelling of the coupled heat and mass transfer through porous media on the base of the wave approach Drying Technology 22 (1-2), 71-80

Mészáros Cs, Bálint Á, Kirschner I, Gottschalk K and Farkas I 2007 Mathematical Modeling of Drying Processes Using Methods of the Nonequilibrium Thermodynamics and Percolation Theory Drying Technology 25 1297-304

Pascal H 1993 On a nonlinear convection-diffusion equation Physica A 192 562–568

Porras G O, Couture F and Roques M 2007 A convection-diffusion model for the convective drying of a shrinking medium composed of a binary liquid Drying Technology 25 (7-8) 1215-27

Ranzi, R., Bochicchio, M. and B.Bacchi 2002 Effects on floods of recent afforestation and urbanisation in the Mella River (Italian Alps) Hydrology and Earth System Sciences 6 (2) 239 – 253

Rieu M, Sposito G 1991 Fractal fragmentation, soil porosity, and soil-water properties 1. Theory Soil Science Society of America Journal 55(5), 1231 - 1238

Stauffer D, Aharony, A 1994 Introduction to Percolation Theory (2nd Ed.) (London: Taylor & Francis)

Tsimpanogiannis I N, Yortsos Y C, Poulou S, Kanellopoulos N Stubos AK 1999 Scaling theory of drying in porous media Physical Review E 59 4353-4365

Vernotte P 1958 Les paradoxes de la théorie de l'equation de la chaleur Comptes Rendus 246 31-54

Wiegand S 2004 Thermal diffusion in liquid mixtures and polymer solutions Journal of Physics. Condensed Matter 16 R357–79

Tribotesting With Large Scale Specimens: Luxury or Necessity

Patrick De BAETS[*], Wouter OST[*], Stijn TAVERNIER[*],
Simon Van AUTREVE[*], Jeroen Van WITTENBERGHE[*],
Gábor KALACSKA[**], László ZSIDAI[**] and Róbert KERESZTES[**]
[*]Department of Mechanical Construction and Production, Gent University, Belgium
[**]Department of Mechanical Engineering, Institute for Mechanical Engineering Technology

Abstract

For industrial tribological applications often laboratory simulations are used early in the design process. Generally because of simplicity of testing small scale tribotesters are used and these results are extrapolated to the practical applications. However due to many reasons results obtained with small scale specimens diverge from practical performance. A possibility to reduce extrapolation errors is the use oflaboratory simulations with large scale specimens. In this paper some main influences such as geometrical features, contact pressure distribution and clearance are discussed.

1. Introduction

Since many years Soete Laboratory of Ghent University, Belgium, is specialized in large scale mechanical testing in the research fields of fracture mechanics, fatigue and tribology. It has constructed several large scale set ups capable of testing large specimens (dimension range 10 – 1000 mm) subjected to large loads (kN and MN range). As an example Figure 1 shows a 1200 kN tensile test on a so-called "Curved Wide Plate" taken out of a real steel pipe with diameter over 1m.

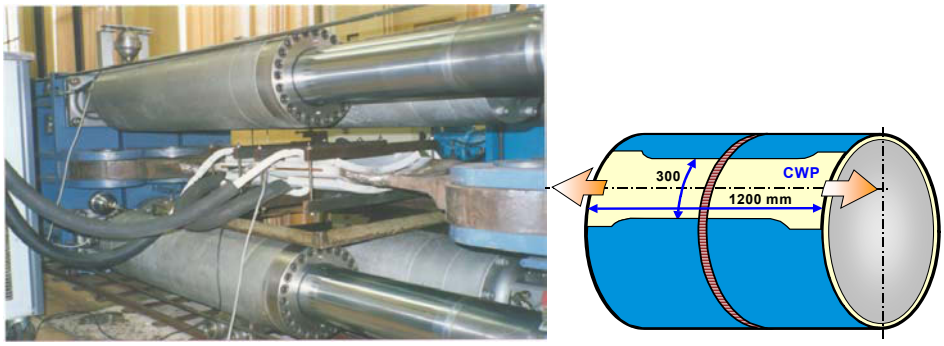

Figure 1. Curved Wide Plate test
(tensile force 1200 kN)

Soete Laboratory has very often been involved in industrial research and development projects where large scale testing was needed. Test results obtained with small scale specimens often revealed to be unreliable and thus not providing the confidence requested by design engineers. This has been true in the different activity fields of the laboratory such as e.g. design of oil and gas pipe lines, dimensioning of welded structures for fatigue applications and design of large and heavily loaded bearing systems. The discrepancy between small and large scale test results practically leads to application of large safety coefficients to cover the uncertainty of small scale data. This approach leads to over dimensioned and consequently expensive constructions. Obviously, the mechanical construction industry is interested in more reliable data. In the present paper some typical tribology cases are described.

Of course the question arises why mechanical testing with small specimens gives different results compared to large specimens and which fundamental mechanisms lie at the base hereof. Today in many research fields important effort is put in place to investigate phenomena at the micro- and nano-scale. The translation of the obtained research results to the macro-scale is far from evident and part of many research projects. Extrapolation to large scale (machinery) situation is even more challenging. It is clear that in tribology the introduction of nanotechnology is very promising, but the question remains how nano modified surfaces will behave in real large scale situations (Figure 2). This knowledge is necessary to extend the applicability of nano-surfaces from nano- and micro-components to large scale structures.

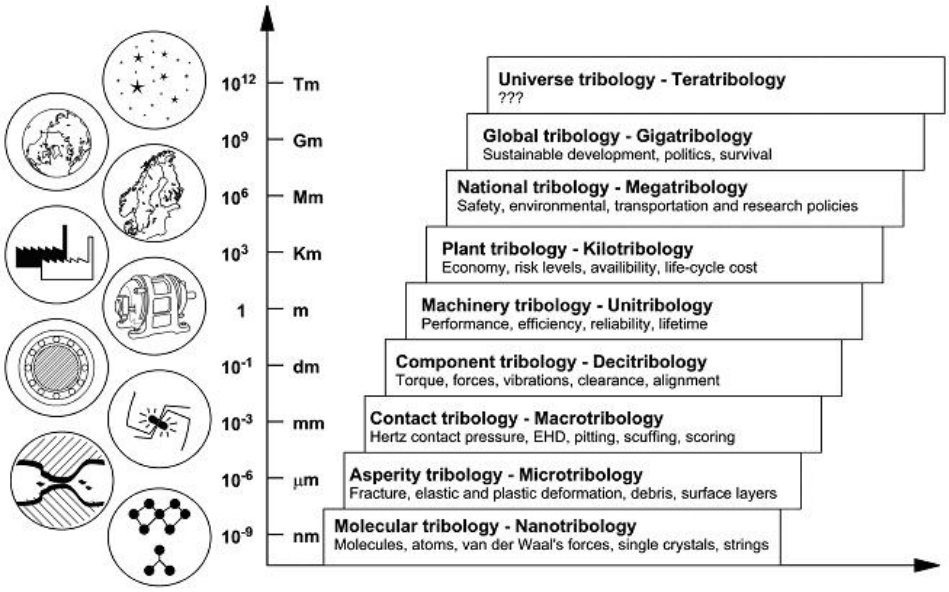

Figure 2. Different scales in tribology

In the next paragraphs different causes leading to the necessity of large scale experiments are treated together with some parameters that can explain the gap between small and large scale results. They are illustrated with practical industrial cases and characteristic results are presented.

2. Geometrical features

Figure 3 shows the Maesland storm surge of Rotterdam in the Netherlands. It was planned in the frame of the important water works decided after the catastrophic flood of 1953 and commissioned in 1997. Figure 3 shows the closed surge, consisting of two circular gates, connected with framework arms to a spherical hinge. A convex and concave segmented spherical component together form the 10 m diameter hinge, designed for a nominal load of 350 MN. Both convex and concave surface are made of cast steel and a 10 μm thin MoS_2-based layer forms a solid lubricant layer between the surfaces. The sliding layer was designed to withstand a nominal contact pressure of 30 MPa and to provide a coefficient of friction lower than 0.15. Despite many research efforts on the sliding material prior to design and construction after two years of operation severe galling between the convex and concave surface was observed (Figure 4).

Figure 3. Storm surge of Rotterdam, the Netherlands
(Courtesy Nederlandse Rijkswaterstaat)

Important and recurrent repair works were necessary and it was expected that safe and reliable operation of the gates could not longer be guaranteed. Consequently redesign of the hinges with an other sliding material was ordered. Especially difficult in the redesign process were the constraints of limited available space for the sliding material and the requested low coefficient of

friction. The sliding layer had to be put in place in the field as dismounting of the hinge was out of question. At some locations a gap of only 30 cm was available to put the sliding material in place. Because of the limited strength of the hinge concrete foundations a friction coefficient below 0.2 was compulsory. It was decided to apply the sliding material as recessed sliding pads in the convex hinge part as shown in Figure 5. By means of a Finite Element calculation taking into account global and local stiffness characteristics it was calculated that the "uniform" contact pressure on a sliding pad could reach 150 MPa or even 190 MPa, taking into account the safety factors. Because it was also explicitly stated that fluid lubricant (oil or grease) had to be avoided, metal sliding pads had to be excluded, but polymers and polymer composites came in sight.

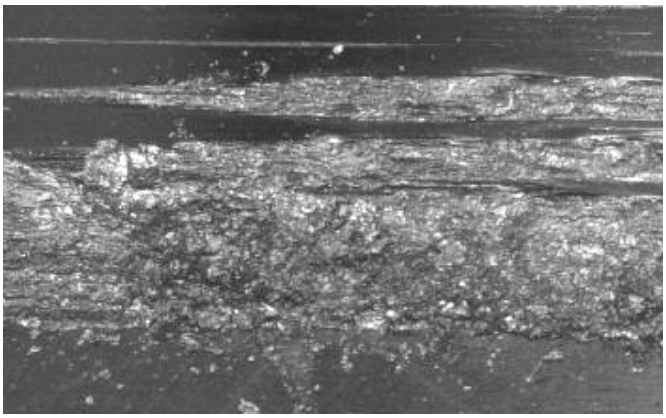

Figure 4. Galling of steel surfaces in Rotterdam surge hinges
(Courtesy Nederlandse Rijkswaterstaat)

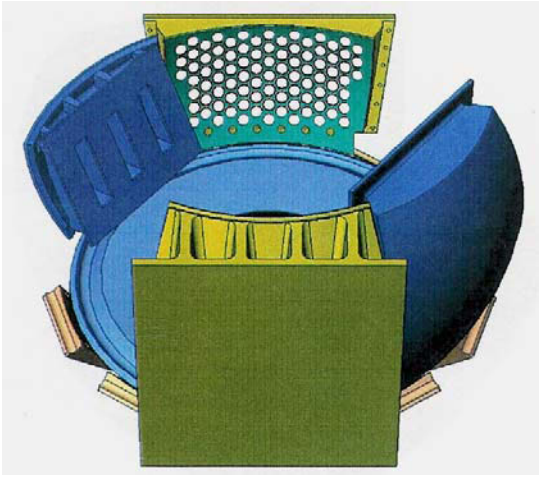

Figure 5. 500 recessed sliding pads as sliding layer
(Courtesy Nederlandse Rijkswaterstaat)

It is clear that pure polymers can not withstand such a high load without any fortification. Commercially available fibre reinforced composites have been investigated but could not provide the necessary bearing load. For this reason a hybrid solution has been worked out, based on a central polymer pad reinforced by a carbon fibre ring at its circumference. A section view of this hybrid sliding pad is shown in Figure 6. It is important to note that the "click" disk is made of a lower and upper part. The upper part covers the carbon ring and prevents it to get into contact with the counter surface. It protects both the counter surface and the carbon ring against wear.

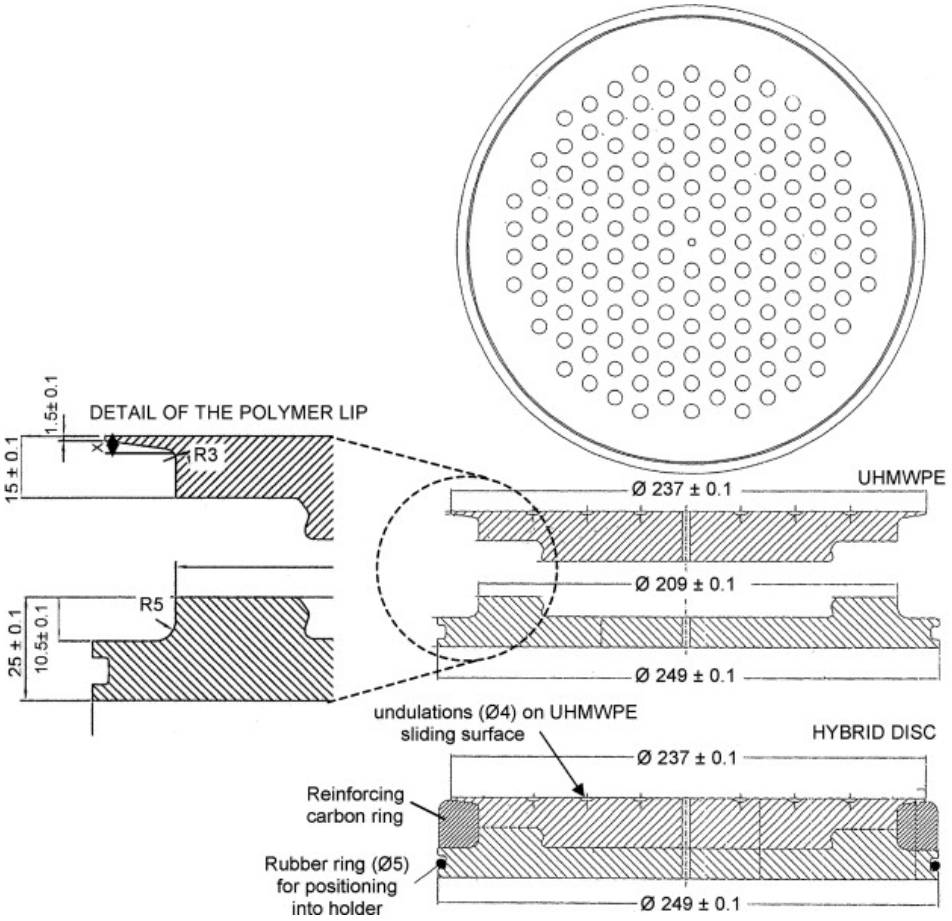

Figure 6. Hybrid sliding pad (Courtesy Solico BV)

It is clear that due to its concept, geometry and size (diameter 300 mm) the hybrid sliding pad can not be tested with standard small scale test equipment and can also not efficiently be scaled down. It has thus been decided to test downscaled specimens with diameter 150 mm on a large scale reciprocating test

rig available at Soete laboratory (Figure 7). This test set up allows for friction and wear testing of specimens with size up to diameter 300 mm with a normal load of maximum 6500 kN, friction force of maximum 2500 kN and a sliding velocity of 5 mm/s. After a literature preselection of the polymer finally Ultra High Molecular Weight Polyethylene (UHMWPE) was chosen because of its low coefficient of friction (0.2 à 0.4 at 3 MPa contact pressure and 0.33 m/s sliding velocity).

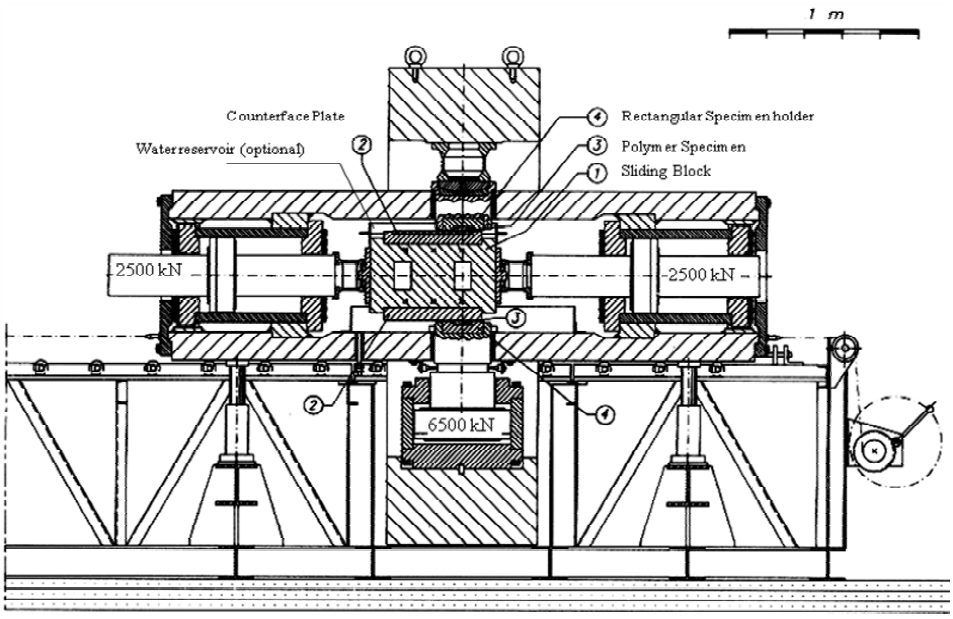

Figure 7. 6500 kN Reciprocating tribometer (6500 kN) of Soete Laboratory

Figure 8 shows a typical friction curve obtained during the first friction cycles in the large scale tribometer for uncovered carbon ring. During the first two cycles the coefficient of friction is relatively high, but it stabilizes to about 0.07 in steady state conditions. The static coefficient of friction remains a little higher at 0.08. Figure 9 shows the much better condition of the carbon ring covered with a polymer lip shown in Figure 6. In this configuration the UHMWPE-disk shows a very low coefficient of friction of 0.04. This is attributed to the very high contact pressure applied (150 MPa) and accompanying high contact temperature (bulk temperature 65 °C, flash temperature 125 °C). Figure 10 shows typical wear and damage of the uncovered carbon ring. Carbon fibres are detached at the surface and debris trapped in the polyethylene surface cause increased damage of the countersurface. The carbon ring also loses its strength due to fibre delamination and fibre breakage. Obviously, contact between the carbon ring and mating steel surface was to be avoided.

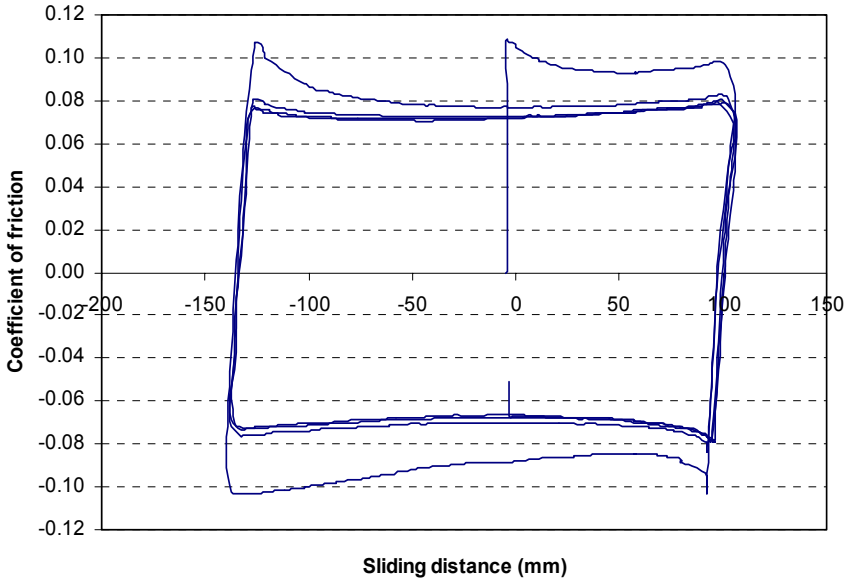

Figure 8. Friction curve of UHMWPE and carbon ring against steel St 37.2

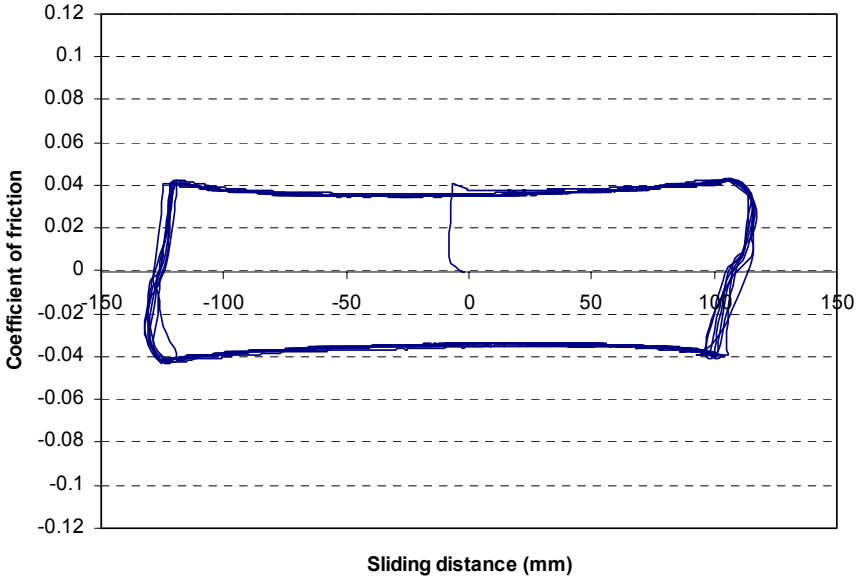

Figure 9. Friction curve of UHMWPE against Steel St 37.2

In this example the reinforcement ring clearly prohibits the specimens to be scaled down to for small scale testing. Other features that are difficult to scale down are particle evacuation groves, lubricant pockets, etc. very often used in sliding bearings.

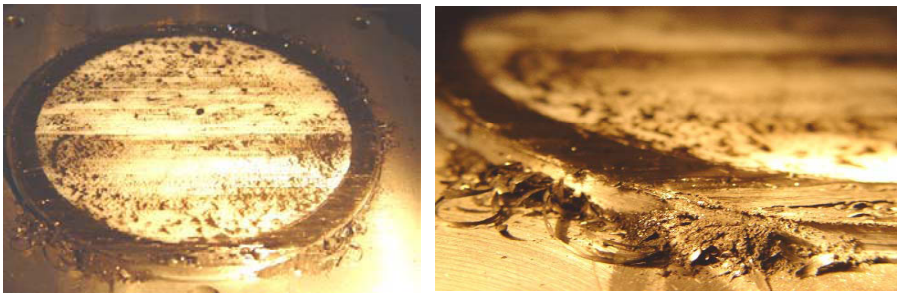

Figure 10. Wear of uncovered carbon ring in contact with steel St 37.2

3. Contact pressure and stress distribution

In the previous example it has been explained that UHMWPE was selected because of its low coefficient of friction at high load. By means of large scale testing the influence of the contact load on the coefficient of friction has been investigated. This investigation is not possible with standard small scale tribometers, due to their limited normal force capability. E.g. a small specimen size with contact surface of 10 x 10 mm, i.e. 100 mm^2, and a uniform contact pressure of 150 MPa, needs a normal load of 15 kN. This fairly high load can not be achieved with traditional small scale tribotesters. Figure 11 shows the coefficient of friction of UHMWPE as a function of the normal load. The coefficient of friction decreases with contact load as is generally the case for polymers. In this particular study the contact pressure is so high that very low coefficient of friction is achieved (about 0.04 at 150 MPa). At these loads the polymer material more or less behaves as a hydrostatically loaded fluid. The carbon ring, however, prevents flow of the polymer material out of the contact area.

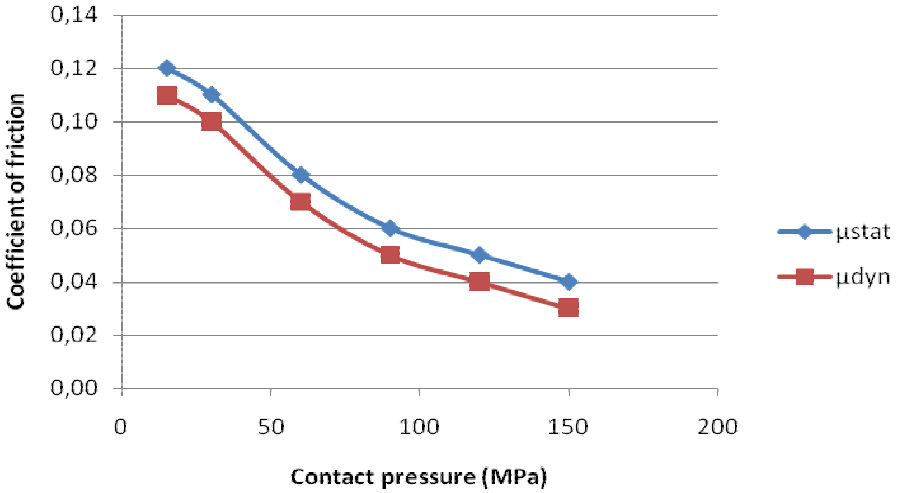

Figure 11. Coefficient of friction of UHMWPE as a function of load

Also very important is the different wear behaviour observed at the edges of bearing materials. As an example the Figure 12 shows the behaviour of polyester fibre reinforced polyester (Orkot TXM ®) loaded at 150 MPa. This material is often used for both radial and linear bearings under dry or water lubricated conditions. Disintegration of the edges of the specimen is observed. This fail mechanism is more pronounced when the ratio contact contour / contact area becomes larger, what is the case for smaller bearing pads. For this reason larger bearing surfaces generally are to be preferred. These large surface areas, however, can not be tested in traditional small scale tribotesters. To avoid exaggerated influence of edge behaviour, large scale specimens must be used. Special attention has to be paid to the mechanical fixation of the bearing material, especially at the materials contour. Free contours tend to fail by seizure.

Figure 12. Failure mechanisms of highly loaded fibre reinforced polyester

4. Heat input

For polymers, often used as self-lubricating material, friction and wear are not solely governed by contact pressure. Also very important is the contact surface temperature that results from the dissipated heat during friction. Figure 12 shows a cast polyamide (PA6) test specimen (size 150 x 150 mm) that has been subjected to 150 MPa contact pressure and 5 mm/s sliding velocity. The calculated pv of 0.75 MPa m/s exceeds the pv-limit reported in literature for this material (e.g. 0.15 MPa m/s according to). As a result excessive flow at the edges is observed, impeding proper functioning of the material under these conditions.

For polyoxymethylene homopolymers (POM-H) an extrapolation model has been developed between friction and wear results obtained with small scale specimens and large scale specimens. A thermal scaling factor S is used to achieve correspondence between sliding temperatures on both small-scale and large-scale equipments. S is defined as

$$S = pvG\sqrt{Pe}$$

with
p: contact pressure
v: sliding velocity
G: geometrical scaling factor
Pe: Péclet number

The dimensionless Péclet number gives the ratio between the velocity of a moving heat source and the velocity of heat transport under the surface.

$$Pe = \frac{v\ell}{\kappa}$$

with
ℓ: contact length
κ: diffusivity, defined as $\kappa = \frac{k}{\rho c_p}$
k: conductivity
ρ: specific mass
c_p: specific heat

The dimensionless geometrical scaling factor G is defined as the ratio of the area of a rectangular apparent contact (length ℓ and width b) and the contour of that contact area.

$$G = \frac{2\ell b}{s(\ell + b)}$$

Figures 14 and 15 show the friction and wear curves as a function of the scaling factor. The corrected pv-value ($pv\sqrt{Pe}G$) is defined in order to obtain similar contact temperature in large scale and small scale conditions (Figure 13). It is observed that friction on large scale test specimens is lower compared to small scale samples. This is attributed to softening of the polymer sliding surface. A relation between friction and normal load is generally known as $\mu = K \cdot F_N^{(n-1)}$, where K and n are constants and 2/3 < n < 1. This equation however does not apply for large-scale results, fitting better to an exponential law $\mu = 0.3 \cdot \exp(-5 \cdot 10^{-7} F_N)$. The discrepancy between both models

results from de deformations under high load changing the contact conditions, as also referred by other workers who suggested that plastic deformation at high loads causes a variation of friction that is less dependent on the normal load. Specific wear (wear rate) using the corrected pv-values is equivalent for large and small scale conditions in the low pv range. At high corrected pv-value the wear curve match thus not hold any more due to the different dominant mechanisms. In large scale conditions the wear at high pv is mainly governed by transfer film formation, while for small scale specimens the transfer film formation is not observed.

Figure 13. Overloaded (p=150 MPa, v= 5 mm/s) PA specimen against steel

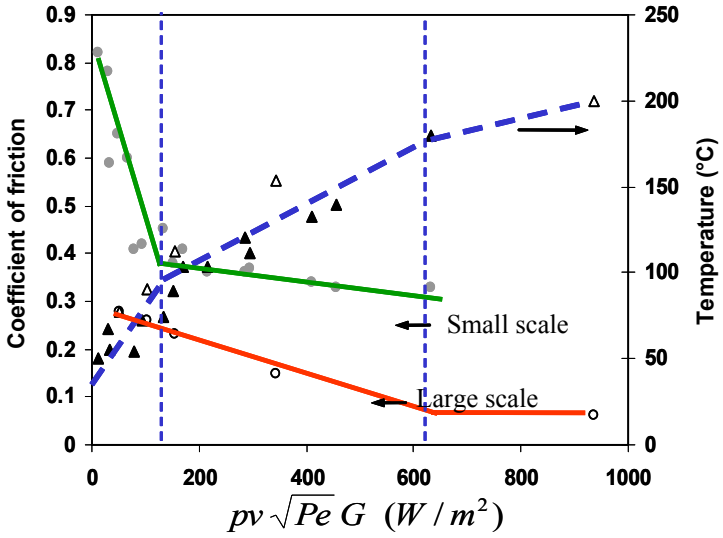

Figure 14. Friction of POM-H as a function of corrected pv
(Δ: large scale, ▲ small scale)

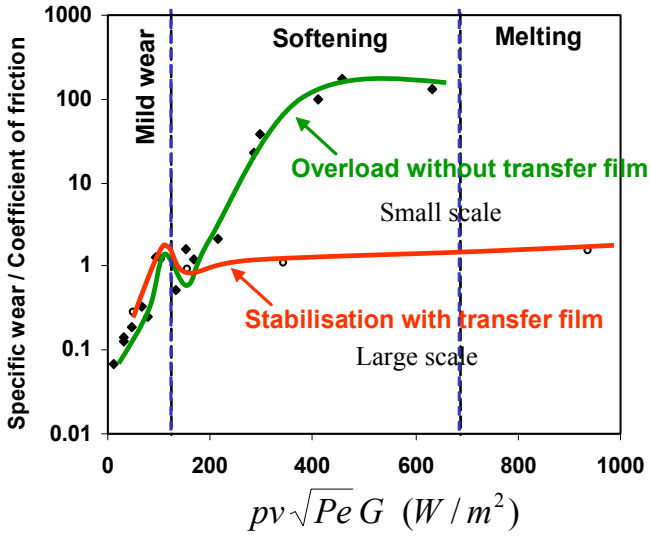

Figure 15. Wear of POM-H as a function of corrected pv

5. Clearance

In radial bearings the play between shaft and bearing are very important for both friction and wear. The influence of clearance is not fully understood and many questions remain on the scalability of play for radial bearing configurations.

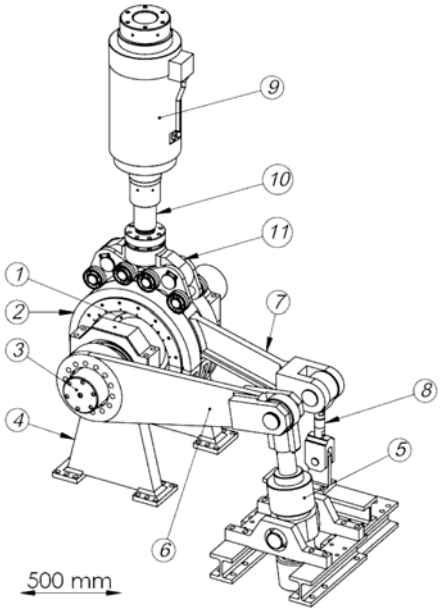

Figure 16. Reciprocating radial bearing tribometer (1350 kN) of Soete Laboratory

Figure 16 shows a large scale radial bearing set-up available at Soete Laboratory. It can handle bearings (1) with diameter 400 mm and width 300 mm. The radial load applied by means of a hydraulic jack (9) maximum equals 1350 kN and a maximum torque of 100 kNm is given by the hydraulic jack (5). In the presented configuration oscillations between +/- 15 deg are possible. The test equipment allows for measuring the driving torque (8), bulk temperature at the shaft surface (integrated thermocouple) and both the vertical and horizontal bearing displacement. In such a configuration special attention must be paid to the calculation of the coefficient of friction that is derived from the torque measurement, with symbols explained in Figure 17. Compared to measuring and calculations methods found in literature in this study the influence of the clearance between shaft and bearing is included. The inner radius R_b of the bearing and the position R_L of the load cell are measured prior to testing. The radial load F_p is controlled during the test and the force F_L is measured by means of the load cell.

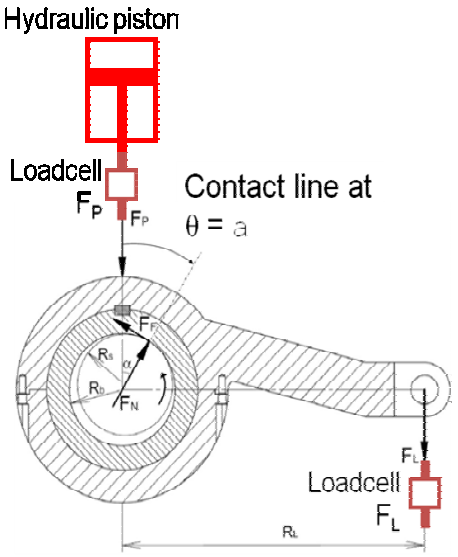

Figure 17. Calculation of coefficient of friction in radial bearing test

$$\mu = \frac{1}{\sqrt{\left(\frac{R_b}{R_L}\right)^2 \left(\frac{F_p + F_L}{F_L}\right)^2 - 1}} = \tan\alpha$$

Figure 18 gives the result of a friction test on filament wound polymer based composite. It is composed of polyester reinforcing fibres embedded in a phenolic

resin matrix filled with polytetrafluoroethylene (PTFE) solid lubricant. The shaft is made of low alloy steel S355J2G3 turned at a surface roughness Ra 0.25 μm. The bearing has a width of 120 mm and an inner diameter of 300 mm. The clearance between bearing and shaft $2(R_b-R_s)$ equals 1.1 mm. In Figure 18 the friction curve is shown together with the drive piston displacement. The latter is computer controlled and follows a linear set point. One friction cycle typically shows two phases. The first phase at onset of the drive piston movement is pure rolling of the shaft against the bearing surface. The "coefficient of friction" typically is lower than the dynamic sliding coefficient of friction (approximately 0.12) and rises until the static coefficient of friction (about 0.14) is reached. At that moment the shaft slips along the bearing and the sliding coefficient of friction is measured. The kinematic behaviour of the shaft and bearing depends on the value of the friction and of the clearance between shaft and bearing as elucidated by Figure 19. In this figure the relation between the angle θ expressing the position of the contact line, and the shaft rotation angle φ is given by

$$\varphi = \theta \cdot \frac{(R_s - R_b)}{R_s}$$

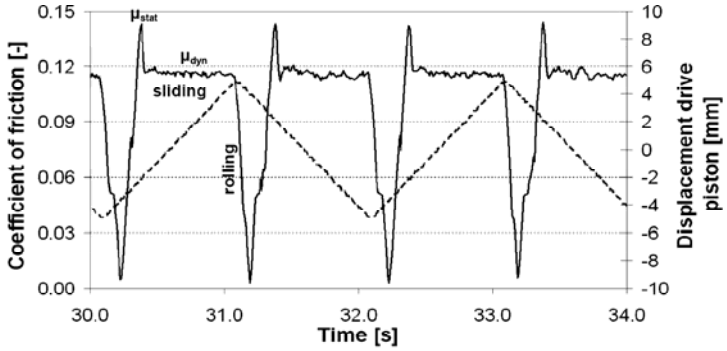

Figure 18. Coefficient of friction of PTFE-filled polyester-phenolic radial bearing, F_p = 100 kN, v = 100 mm/s, A = 10 mm

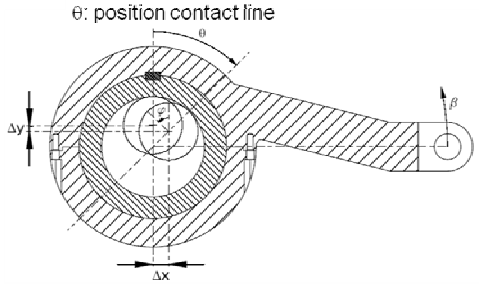

Figure 19. Kinematics of rolling and sliding in a radial bearing

Due to static friction the bearing rolls over the shaft within a small rotation angle $\varphi_{2\alpha}$ of the shaft

$$\varphi_{2\alpha} = \theta \cdot \frac{(R_s - R_b)}{R_s}$$

The curve showed in Figure 20 represents a friction loop with the coefficient of friction as a function of the shaft rotation. During the rolling phase the friction force is build up linearly with the rotation angle. The feature in the curve characterized by constant friction for in(de-)creasing shaft rotation angle is attributed to the play in the loaded connection between torque piston and bearing housing. The gross slipping phase is characterised by a constant coefficient of friction. The static coefficient of friction equals 0.15, while the dynamic coefficient of friction is 0.12.

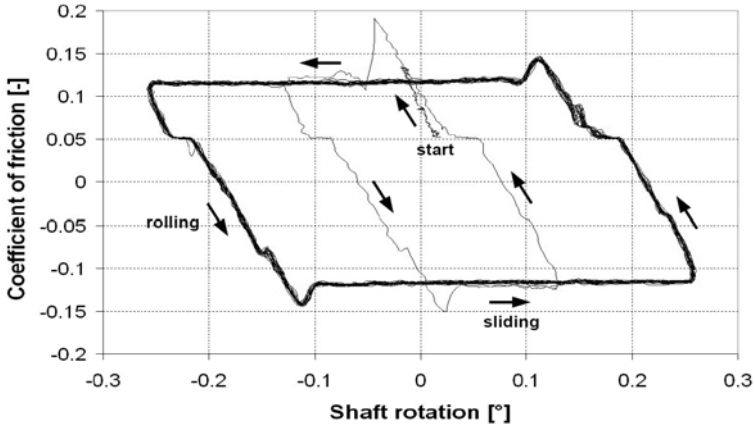

Figure 20. Friction loops of PTFE-filled polyester fibre reinforced phenol radial bearing, F_p = 100 kN, v = 100 mm/s, A = 10 mm

6. Conclusions

The results of tribotests obtained with large scale specimens can significantly differ from results of small scale specimens. Even with basic knowledge on the dominant friction and wear mechanisms it remains very difficult to mathematically convert large scale to small scale results and vice versa. Reliable scale models are still lacking.

Several reasons can be pointed out for the discrepancy between small and large scale results. Very important are geometrical features such as grooves, surface pockets, reinforcements,… that can not easily be scaled. Contact pressure values and contact pressure distribution often differ in large scale conditions compared to small scale. Consequently, friction and wear show

different behaviour. Different heat input for the considered situations also contribute to different tribological results. Finally many questions remain on how to model and take into account relative clearance and stiffness of tribological components.

Acknowledgements

The authors are grateful to Mr. Rudy Desmet and Johan De Clercq for their particular effort in the design and maintenance of large scale test equipment of Soete Laboratory and Mr. Pieter Samyn for his valuable help in the experimental program.

References

Holmberg K., Ronkainen H., Laukkanen A., Wallin K., Friction and wear of coated surfaces – scales modelling and simulation of tribolmechanisms, Surface and coatings Technology 202, Issue 4-7 (2007), p. 1034-1049

Van Paepegem W., Van Schepdel L., Degrieck J., Samyn P., De Baets P., Suister E., Leendertz J.S., Fast characterization of carbon/epoxy rings for use in ball-joints of the Maesland storm surge barrier, Composite Structures 78, Issue 3 (2007), p. 359-367

Samyn P., Van Schepdael L., Leendertz J.S., Gerber A., Van Paepegem W., De Baets P., Degrieck J., Large scale friction and wear tests on a hybrid UHMWPE-pad/primer coating combination used as bearing element in an extremely high-loaded ball-joint, Tribology International 39, Issue 8 (2006), p.796-811

Tevrüz T., Tribological behaviours of carbon filled polytetrafluoroethylene (PTFE) dry journal bearings, Wear 221, Issue 1 (1998), p 61-68

Orkot Marine Bearings – Engineering Manual, version 4.2, Trelleborg Sealing Solutions, Rotherham, UK

Tuszynski R., Friction and Wear Testing, Characterization and Failure Analysis of Plastics, Friction, ASM International - 2003 - Technology & Engineering, p. 259-266.

Samyn P., De Baets P., Friction and wear of acetal: a matter of scale, Wear 259, Issue 1-6 (2005), p. 697-702

Clerico M., A study of friction and wear of nylon against metal, Wear 13, Issue 3 (1969), p. 183-189

Pascoe M.W., Tabor D., The friction and deformation of polymers, Proc Roy Soc London **A235** (1955), pp. 210–224.

Ünlü B.S., Atik E., Determination of friction coefficient in journal bearings, Material & Design 28, Issue 3 (2007), p 973-977

Imado K., Miura A., Kido Y., Influence of testing method on the contact pressure distribution and its effect on coefficient of friction in polymeric bearings, Tribology International 40, Issue 2 (2007), p 390-396

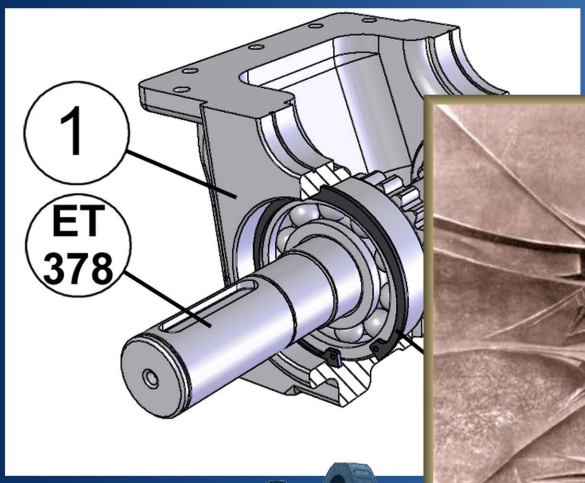
1
ET
378

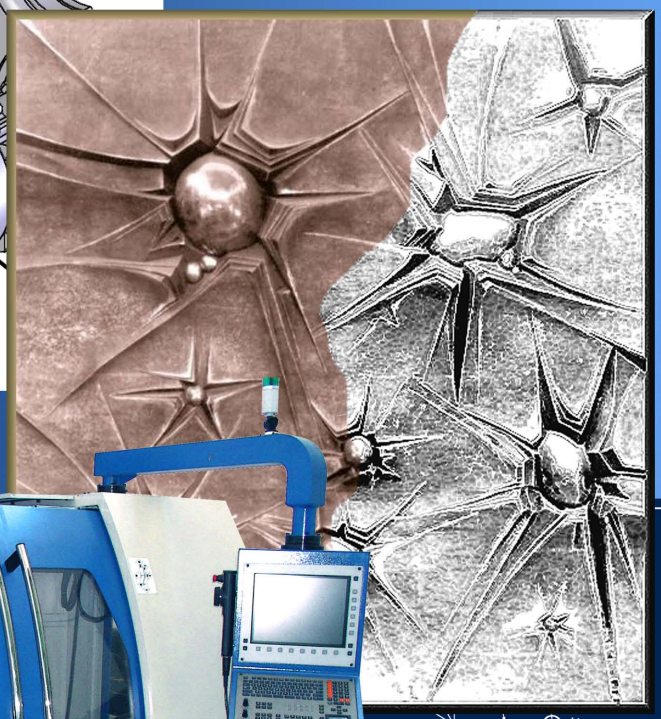

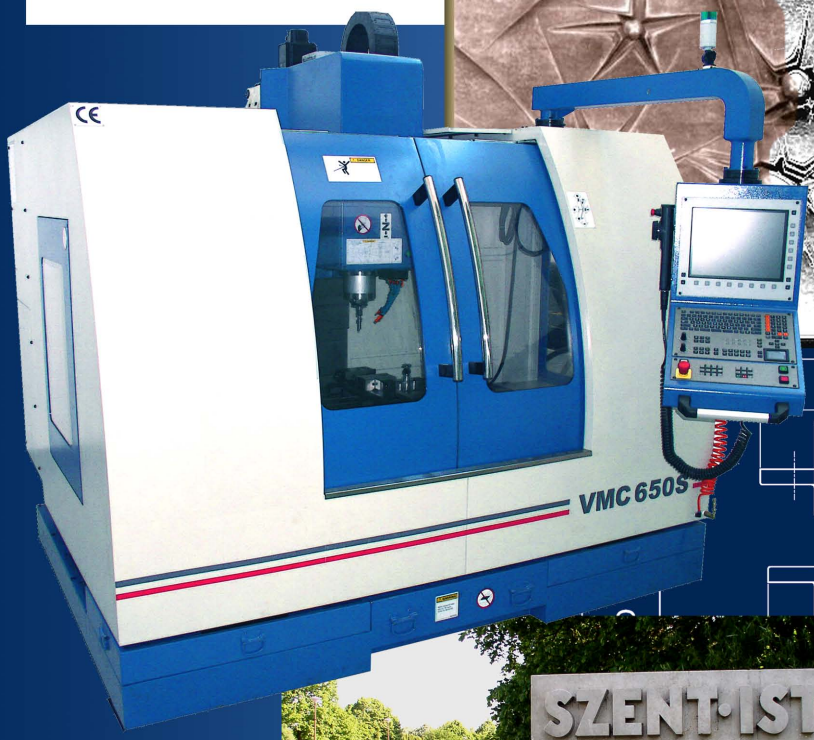
VMC 650S

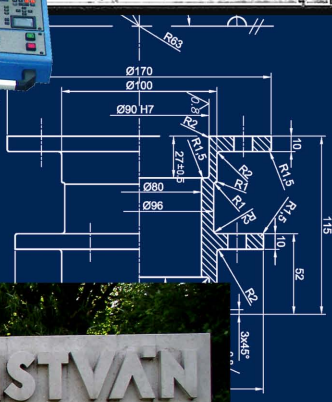
R63
Ø170
Ø100
Ø90 H7
R4
R1,5
27±0,5
Ø80
Ø96
10
R1,5
R2
R1
R2
R1
R2
115
10
52
R2
3x45°


SZENT·ISTVÁN
EGYETEM
GÖDÖLLŐ

6,3